THE ROLE OF THIN FILAMENT SARCOMERIC PROTEINS TROPOMYOSIN 1 AND CARDIAC TROPONIN T IN THE DEVELOPING HEART

Jennifer England, BSc.

Thesis submitted to the University of Nottingham for the degree of Doctor of Philosophy

July 2016

Abstract

The heart is the first functioning organ to develop during embryogenesis to maintain the growing embryo with oxygen and nutrients. However, cardiogenesis is a complex but well-regulated process, and any changes to this regulation can result in detrimental defects of the heart. For many years sarcomeric proteins have been associated with a range of cardiomyopathies and in more recent years are known to been involved in congenital heart defects (CHDs). To date, *tropomyosin 1* (*TPM1*) and *cardiac troponin T* (*TNNT2*) have been associated with cardiomyopathies but never with CHDs. These two genes are important regulatory proteins of the thin filament of the sarcomere and vital for correct contraction and force generation within cardiomyocytes.

To investigate a role for *TPM1* and *TNNT2* in the early developing heart, using the chick as an animal model, antisense oligonucleotide morpholino technology were utilised to manipulate both genes *in ovo*. The gross anatomical structures, ultrastucture and molecular functions of the treated hearts were analysed to determine if the morpholino treatment resulted in any developmental abnormalities. In addition, the *TPM1* gene, including introns, was sequenced in a cohort of 380 patients with a range of congenital heart anomalies.

In the TPM1-morpholino treated hearts, atrial septation and ventricular chamber maturation via the production of trabeculae were affected. Stereological analysis of these hearts revealed a reduction in the proportion of myocardium in the ventricular chamber along with increased luminal size. In addition, TPM1-morpholino treatment had an effect on myofibril maturation *in vitro*, as well as causing increased apoptosis in the developing ventricle and atrial septum. Four genetic variants of *TPM1* were identified in the patient cohort; I130V, S229F, IVS1+2T>C and GATAAA/AATAAA in the polyadenylation signal. *In silico* analysis predicted the missense mutations to be disease causing. *In vitro* functional analyses of the IVS1+2T>C mutation that the IVS1+2T>C mutation resulted in abnormal splicing of the *TPM1* pre-mRNA. TNNT2-morpholino treatment affected the growth of the atrial septum. However, the sarcomere appeared normal in this treatment group. Stereological analysis also revealed normal cardiac proportions except for the atrial chamber, which was reduced in size.

The abnormal phenotypes observed in the TPM1 and TNNT2 treated groups may be a result of altered haemodynamics within the developing heart. Further studies such as *in situ*

hybridisation of markers of haemodynamics may elucidate this role in the future. The abnormal splicing observed in the IVS1+2T>C may be a contributing factor to CHD in man and therefore, indicates that sarcomeric proteins are important for the future screening of potential contributing factors to CHDs.

Acknowledgments

First and foremost, I would like to thank Dr. Siobhan Loughna and Dr. Margaret Pratten for their constant support, advice and guidance over the past five years. You have given me a fantastic foundation, both within research and teaching. Also many thanks to Dr. Deborah Merrick and Dr. Catrin Rutland. You both have been fantastic mentors to me and your never ending encouragement definitely got me to the end of my PhD. It has been a pleasure working with you both and I hope we will work together in the future. I would also like to thank Natasha Russell, Louise Green and all the Anatomy teaching staff. You have given me invaluable advice and teaching guidance over the past five years.

Since I first started at the University of Nottingham, many people have come and gone that have supported me with excellent technical assistance in the laboratory including Maria Isabel Haig, Sue Willington, Dr. Terry Parker and Jamie Webster. In addition, I would like to thank the SLIM team and Liaque Latif for their technical assistance. I would also like to thank Professor David Brook and his laboratory (Kerry Setchfield, Javier Granados-Riveron, Tushar Ghosh, Naveed Malik and Anna Wilson), Dr. Paul Scotting, Dr. Pete Jones and Dr. Sally Wheatley for their excellent advice and helpful discussions for this thesis.

Moving to Nottingham was a daunting experience for me and joining St. Barnabas GAC provided a home away from home. You have given me the opportunity to make friends for life for which I will always be grateful.

Last but not least, I would like to thank my family, Gerard, Carole and Stephanie, and John ‘mo grá’ for your endless support. You have put up with my tears and tantrums, but you got to share many of the highs with me over the past few years. I would not wish to share them with anyone else. Thank you so much for everything.

Declaration

The *de novo* mutations and dHPLC analysis was obtained by Dr. Javier Granados-Riveron, who also aided me in designing the splice-donor site experiment. The electrophysiology data was completed by Dr. Luis Polo-Parada in a collaborative study with our laboratory.

Table of Contents

List of Figures

List of Tables

Abbreviations

ACTC1	alpha cardiac actin
αMHC	alpha myosin heavy chain
ASD	atrial septal defect
AVC	atrioventricular canal
AVN	atrioventricular node
AVSD	atrioventricular septal defect
βMHC	beta myosin heavy chain
cDNA	complementary deoxyribonucleic acid
CHD	congenital heart defect
CRISPR	clustered regularly interspaced short palindromic repeats
cTnT	cardiac troponin T
DAPI	4',6-diamidino-2-phenylindole
dHPLC	denaturing high performance liquid chromatography
ddH_2O	double distilled water
ECG	electrocardiograph
ECM	extracellular matrix
ED	embryonic day
E1I1	exon1-intron1 boundary
E4I4	exon4-intron 4 boundary
GAPDH	Glyceraldehyde 3-phosphate dehydrogenase
GATA	zinc finger transcriptional activator
GFP	green fluorescent protein
LB	Luria broth
HH	Hamburger and Hamilton
MYBPC3	myosin binding protein C
MYH	myosin heavy chain
OFT	outflow tract
PCNA	Proliferating Cell Nuclear Antigen
PCR	Polymerase chain reaction
Poly-A	polyadenylation

qPCR	qualitative polymerase chain reaction
SAN	sinoatrial node
SC	standard control
siRNA	short interfering ribonucleic acid
SOC	Super Optimal broth with Catabolite repression
TALEN	Transcription activator-like effector nucleases
TdT	terminal deoxynucleotidyl transferase
TNN	titin
TNNI	troponin I
TNNT	troponin T
TNNC	troponin C
TPM	tropomyosin
UT	untreated
VSD	ventricular septal defect

Chapter 1 Introduction

1.1 Overview

Cardiogenesis or heart development is a complex early embryological process. It involves the specification and migration of cells from a number of sources that contribute to certain regions of the developing heart. The addition of cells to the developing heart also drives some of the cardiogenic processes such as looping and valvulogenesis. While these events occur early in embryonic development, shortcomings at any stage of cardiogenesis can have serious consequences, ranging from some structural abnormality of the heart, to embryonic lethality. This thesis will discuss some of the early processes of heart development and look at how some important structural proteins are pivotal to a healthy heart.

1.2 Heart Development

The heart is the first organ to function in the developing vertebrate embryo. The initial formation of a contractile tubular heart 22 days after fertilization in the human is followed by complex remodeling processes including looping, chamber septation and specification, the development of its own unique conduction system and valvulogenesis. In this section, formation of the primitive heart and these major remodeling processes involved in cardiogenesis which are of relevance to this thesis will be discussed. These processes have been described in the chick and the mouse and will be referred to in the following sections. A table summarizing some of these processes in different species can be seen in Table 1.1.

	mouse	chick	human	frog	zebrafish
Migration of precardiac cells from epiblast	7 dpc (primitive streak)	HH4 (definitive streak)	15-16 days	stage 10	50% epiboly (5.5 hpf)
First evident assembly of myocardial plate	7 dpc (late primitive streak; just presomite)	HH5 head process (19-22hrs)	18 days	~stage 13	8-10 somites (~13 hpf)
Generation of single heart tube initiated	8 dpc (5-10 somites)	HH9 (7 somites)	22 days (4-10 somites)	stage 28	20 somites (ring) (~19 hpf)
Tubular heart starts contraction	8.5 dpc 8-10 somites)	HH10 10 somites (33-38 hrs)	23 days	~stage 33	26 somites (22 hpf)
Looping	8.5 dpc	HH11 (11-13 somites)	23 days	stage 33-36	33 hpf
Cushions form	9.5 dpc	HH17	28 days (30-38 somites	~stage 41	48 hpf

The mouse data are primarily from DeRuiter et al. (1992) and Kaufman and Navaratnam (1981), the chick from DeHaan (1965), Garcia-Martinez and Schoenwolf (1993), Manasek (1968), Patten (1957), Romanoff (1960) and Viragh et al. (1989), the human from Hamilton and Mossman (1972) and Sissman (1970), the frog from Sater and Jacobson (1990) and the zebrafish from Stainier and Fishman (1992).

Table 1.1 A summary of early heart development in different species.

Table taken from (Fishman and Chien, 1997). dpc indicates days post coitum; HH, hamburger and Hamilton; hpf, hours post fertilisation.

1.2.1 Formation of the primitive heart tube

As mentioned above, the formation of a tubular heart is initiated early in embryonic development; day 22 in humans, embryonic day (ED) 8 in the mouse and 33-38 hrs or Hamburger and Hamilton (HH) 9-10 in the chick. Myocardial cells, a major component of the heart wall, are derived from mesoderm, one of the three germ layers of the early embryo. Prior to heart tube formation in the pregastrula embryo, cardiac precursor cells migrate to the posterior half of the epiblast, bi-lateral to the primitive streak and caudal to Hensen's node (HH3; Figure 1.1a and b) (Buckingham et al., 2005). These myocardial progenitor cells are a small population of about 50 cells (Tam and Behringer, 1997). During gastrulation (formation of a three layered germ disk), the progenitor cardiac cells invaginate through the primitive streak and move cranio-laterally forming a bilateral pre-cardiac mesoderm (HH4; Figure1.1c) (Yang et al., 2002). The pre-cardiac mesodermal cells constitute the primary cardiac field and are surrounded by adjacent endoderm that will play an important role in cardiac specification (HH5-6; Figure 1.1d). The pre-cardiac mesodermal cells form a cardiac crescent at the cranio-lateral border of the mesoderm (HH8-9; Figure1.1e). At this time, the mesoderm of the embryo splits forming two parts; the paraxial mesoderm, which contributes to the limb musculature, and the lateral plate mesoderm, containing the cardiac precursors within a splanchnic mesoderm (Manasek, 1968). Embryonic folding carries the splanchnic mesoderm ventrally and the two cardiac fields meet at the midline, ventral to the developing foregut. Cardiomyocyte differentiation is underway at this time and the cardiac fields fuse forming a tubular heart (HH10; Figure1.1f) (Abu-Issa and Kirby, 2007). This new tubular heart is suspended from the foregut endoderm by the dorsal mesocardium (Männer, 2000). The linear heart is orientated such that the arterial pole of the heart or outflow portion cranial to the inflow portion or venous pole. At this time the heart tube begins to contract, which from the offset is peristaltic, but soon becomes sequential, as ventricular contraction follows atrial (HH10; day 23) (Fishman and Chien, 1997).

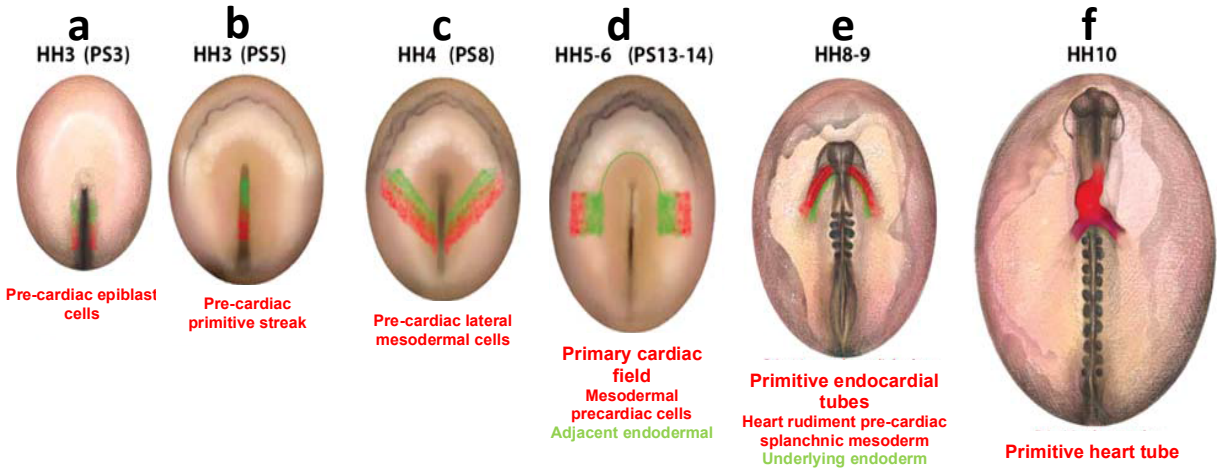

Figure 1.1 A schematic diagram showing the origin and migration of pre-cardiac cells and the formation of the primitive heart tube in the chick.

a and b. In the pregastrula embryo, cardiac precursor cells migrate to the primitive streak. **c.** During gastrulation, the pre-cardiac cells ingress through the primitive streak and move cranio-laterally forming a bilateral pre-cardiac mesoderm. **d.** The pre-cardiac mesodermal cells are positioned in the first cardiac field surrounded by adjacent endoderm. **e.** At the cranio-lateral border of the mesoderm, the pre-cardiac cells form a cardiac crescent. Embryonic folding carries the crescents ventrally and the two cardiac fields meet at the midline, ventral to the developing foregut. **f.** The cardiac fields fuse forming a tubular heart suspended from the foregut endoderm by the dorsal mesocardium. Adapted from (Lopez-Sanchez and Garcia-Martinez, 2011).

1.2.2 Looping of the primitive heart

Fusion of the primary (first) heart fields results in the formation of a tubular, almost symmetrical heart containing a primitive ventricle. Caudally, the primitive heart has paired venous horns' making up the inflow portion of the heart and an aortic sac cranially that drains it. This primitive tube is short-lived as new cardiac cells from a second heart field (discussed below in section 1.2.3) invade, resulting in elongation of the heart. As elongation occurs, the central portion of the dorsal mesocardium disintegrates, but remains at the venous and arterial poles (Männer, 2004). This enables the heart tube to loop to the right. The process of cardiac looping has been well investigated in the chick and, therefore, is discussed in the context of the chick below (see Table 1.1 to refer to other species). Looping can be divided into two phases: c-looping (including dextral looping) occurring from HH10-12 and s-looping occurring at stages HH13-24. C-looping is the transformation of a straight heart tube into a c-shaped tube, caused by ventral bending and dextral (or right-ward) torsion (Figure1.2a and b). This movement results in the left side of the heart tube being repositioned ventrally. Consequently, the original ventral surface becomes the outer curvature of the heart and the dorsal side becomes the inner curvature. This occurs most prominently in the atrioventricular (AV) canal and primitive ventricle. During s-looping, driven by elongation of the heart tube, the primordial atrium moves cranial to the ventricle (Figure 1.2c). Looping determines the approximate topographical locations of the future chambers and great vessels (Sakabe et al., 2005, Taber, 2006).

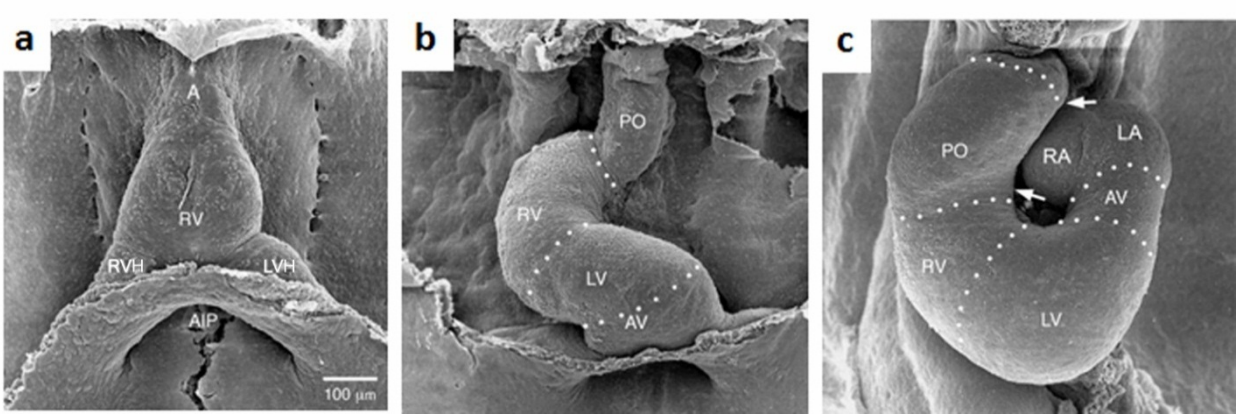

Figure 1.2 Scanning electron micrograph of the developing heart demonstrating looping.

a. A straight tubular heart is formed after embryonic folding and fusion of the two cardiogenic fields (HH10). **b.** As cells migrate to the developing heart and its size increases, dextral c-looping occurs. The heart undergoes ventral bending and rightward torsion, shifting the left side of the heart ventrally (HH12). **c.** During s-looping the ventricles come to lie caudally to the primitive atrium and the future chambers and great vessels lie in their terminal location. A indicates aortic sac; RVH, right venous horn; LVH, left venous horn; AIP, anterior intestinal portal; PO, proximal part of outflow tract; RV, right side of ventricle; LV, left side of ventricle; AV, atrioventricular canal; LA, left half of primitive atrium; RA, right half of primitive atrium; dotted line demarcates different regions of the heart. Taken from (Männer, 2009).

1.2.3 The second heart field

During cardiac looping, a second heart field contributes to the primitive heart tube. This population of cardiac progenitors is located in the medial splanchnic mesoderm known as the pharyngeal mesoderm (Mjaatvedt et al., 2001, Kelly et al., 2001). The cardiac progenitors of the pharyngeal mesoderm are a distinctive lineage from the cells giving rise to the linear heart tube that originated from the epiblast prior to gastrulation. The second heart field cells remain in the medial splanchnic mesoderm, undifferentiated and non-proliferative, as the heart tube forms and come to lie in the dorsal mesocardium with the heart tube situated ventrally (Cai et al., 2003). Once the early heart tube has formed, cells from the second heart field begin to rapidly proliferate and migrate to the arterial and venous poles of the heart tube during looping, driving elongation of the heart (van den Berg et al., 2009). The second heart field contributes to the outflow tract (OFT), right ventricle and the majority of the atrial myocardium (Moorman et al., 2003, Harvey, 2002).

Cells migrating to the arterial and venous poles from the second heart field express different genes from each other suggesting the second heart field is pre-patterned. Therefore, cells contributing to the arterial pole are called the anterior (or secondary) heart field, and contribute to the myocardium of the OFT and right ventricle (Kelly et al., 2001, Xu et al., 2004). Cells contributing to the venous pole are named the posterior heart field and contribute mainly to the common atrium, sinus venosus and atrioventricular canal, with some contributions to the arterial pole of the heart (Domínguez et al., 2012).

1.2.4 Neural crest cells

Neural crest cells are a multipotent group of cells found in the dorsal neural crest of the developing embryo. These cells undergo extensive migration generating a number of differentiated cell types including: neurons and glia of the sympathetic, sensory and parasympathetic nervous system, the medulla of the adrenal gland, melanocytes of the epidermis and skeletal and connective tissue components of the head (Marmigere and Ernfors, 2007, Yoshida et al., 2008, Simões-Costa and Bronner, 2013). In addition, the neural crest can be divided into four functional compartments, which overlap with each

other. These compartments include the cranial, trunk, sacral and vagal, and cardiac neural crest (Simões-Costa and Bronner, 2013).

The cardiac neural crest was first termed by Kirby *et al*., who ablated a portion of the cranial neural crest between the otic placode and somite 3, discovering that the embryonic hearts did not develop an aorticopulmonary septum (septation of the OFT) (Kirby et al., 1983). The importance of the neural crest for OFT septation was confirmed as the migration of neural crest cells into the OFT cushions forming a divide within the OFT (Waldo et al., 1998, Waldo et al., 1999). Cranial and cardiac neural crest cells first migrate from the dorsal neural tube to the 3rd, 4th, and 6th pharyngeal arches. From there, a sub-population migrates to the heart, thus contributing to the aorticopulmonary (or conotruncus) septum of the OFT (Fishman and Chien, 1997). Therefore, ablation of neural crest cells results in persistent truncus arteriosus, or failure of the separation of the OFT (common arterial truck) (Nishibatake et al., 1987). Cardiac neural crest cells also play a role in regulating the addition of cells from the second heart field to the developing OFT. Failure of this addition results in a shortened OFT during looping leading to the misplacement of the developing aorta such as an over-riding aorta seen in double outlet right ventricle (Kirby and Waldo, 1990, Kirby and Waldo, 1995).

1.2.5 Chamber formation and maturation

As a result of looping, the future chambers and great vessels of the heart come to lie *in situ* and constrictions in the heart wall demarcates different regions. These regions are the sinus venosus, primitive atrium, the AV canal separating the primitive atrium and ventricle, the primitive ventricle and the OFT (conus cordis and truncus arteriosus, or proximal and distal OFT, respectively). These are discussed below.

1.2.5.1 Atrioventricular Canal

The AVC connects the primitive atrium and ventricle. Initially, the tubular heart consists of an outer myocardial layer and an inner endocardial layer, separated by an acellular extracellular matrix known as cardiac jelly. As looping occurs and prior to atrial septation, the myocardium of the AV canal begins to secrete extracellular matrix

(ECM) components resulting in the formation of localized ventral and dorsal endocardial cushions (de Vlaming et al., 2012). They first appear as localized swelling in the cardiac jelly, which are then infiltrated by endothelial cells, which have undergone an epithelial to mesenchymal transition. The cushions grow towards each other and eventually fuse, resulting in the separation of the AV canal into right and left (Fishman and Chien, 1997, Anderson et al., 2003a). These cushions are destined to become the aortic leaflet of the mitral valve and the septal leaflet of the tricuspid valve (Snarr et al., 2008). Later in development, lateral mesenchymal swellings appear in the AV canal (de Lange et al., 2004). The right lateral cushion contributes to the antero-superior and inferior leaflets of the tricuspid valve, and the left lateral cushion forms the lateral leaflet of the mitral valve (Snarr et al., 2008).

1.2.5.2 Sinus Venosus and Atria

The venous pole of the primitive heart contains structures that contribute to the mature heart: the primitive atrium, the atrial portion of the atrioventricular canal, the sinus venosus and the dorsal mesocardium. The atrial appendages are formed by expansions (or ballooning) of the right and left side of the primitive atrium. The remnants of the dorsal mesocardium provide the portal for the entry of the pulmonary veins to the left atrium (Anderson et al., 2003a, Webb et al., 1998). While the atrial appendages are expanding, the primitive pulmonary vein becomes canalised in the dorsal mesocardium bringing the venous plexus into continuity with the developing left atrium at the pulmonary pit (Anderson et al., 2002). This left to right remodelling sets the scene for atrial septation.

The primary atrial septum develops as a crescent-shaped muscular growth from the dorso-cranial atrial wall, ensheathed with a mesenchymal cap, that extends towards the AV cushions (i.e. the future valves of the heart located in the AV canal; Figure1.3a) (Moorman and Christoffels, 2003, Fishman and Chien, 1997). As the septum extends towards the AV cushions, a communication remains between the left and right atria, the foramen primum. Eventually the septum fuses with the AV cushions, while at the same time a region of the septum, close to its origin at the atrial roof, develops fenestrations,

forming a foramen secundum (Figure1.3b). This is essential to ensure communication between the systemic venous system and the left side of the heart for the remainder of fetal development (Lamers and Moorman, 2002). The septum secundum forms when the solitary pulmonary vein separates into left and right pulmonary veins. The incorporation of their orifices into the roof of the left atrium causes a deep fold to form, thus forming the septum secundum (Figure1.3c). The septum secundum develops to the right of the septum primum and extends to cover the ostium secundum, hence forming a valve. The opening is now called the foramen ovale (Figure1.3d) (Anderson et al., 2003a).

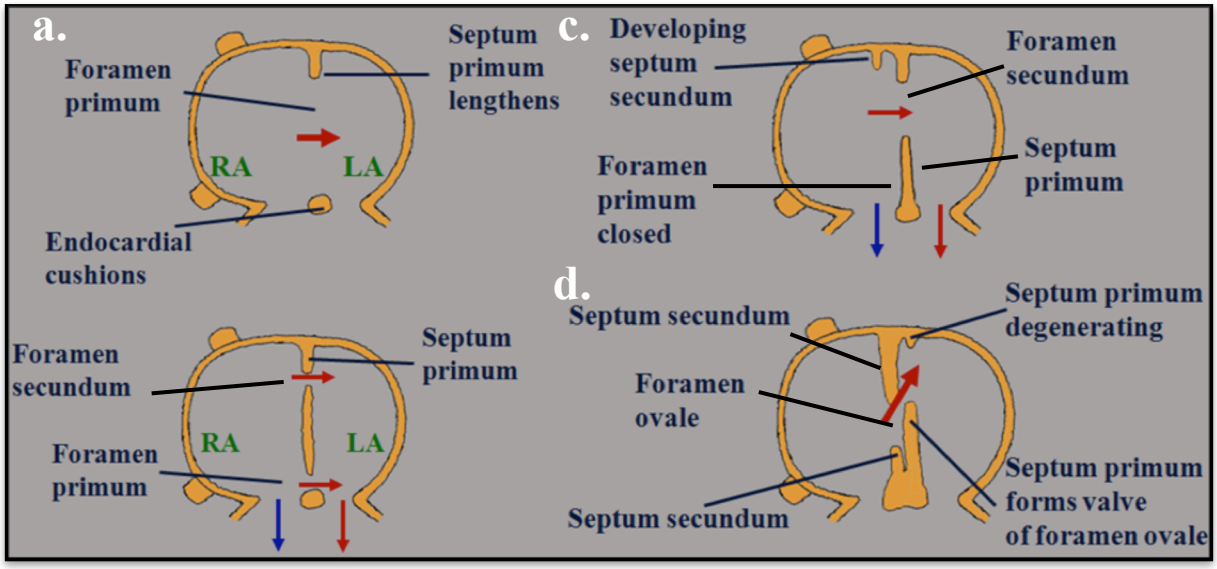

Figure 1.3 A schematic diagram demonstrating atrial septation.

a. The septum primum develops as a muscular outgrowth from the dorso-cranial atrial wall. It extends towards the endocardial cushions of the atrioventricular canal. A communication remains between the left and right atria, the foramen primum. **b.** As the septum primum grows, fenestrations appear in the cranial part of the septum, forming a foramen secundum. **c.** Eventually the septum fuses with the AV cushions, while the septum secundum forms to the right of the septum primum. **d.** The septum secundum extends to cover the foramen secundum, and the free edge of the septum primum forms a valve. The opening is now called the foramen ovale. RA indicates right atrium; LA, left atrium; arrow, blood flow. Image obtained from Dr. Siobhan Loughna.

1.2.5.3 Ventricles

During cardiac looping, the ventricles undergo dextral torsion so that the original left side of the heart tube becomes the ventral portion, while the right side is moved to a dorsal position. This results in the ventricular loop having inlet and outlet components such that the ventricular inlet supports the AV canal and the ventricular outlet supports the OFT (Lamers et al., 1992). The ventricle also has an inner and outer curvature. After looping, ballooning of the apical parts of the ventricle occurs at the outer curvature, resulting in expansion of the ventricle (Christoffels et al., 2000). A constriction, known as the primary interventricular foramen exits between the newly distinguishable right and left ventricle (Moorman et al., 2003). The first heart field contributes mostly to the developing left ventricle, while cells migrating from the second heart field contribute to the right ventricle (Kelly et al., 2001). During ballooning, the proliferating myocardial cells of the outer curvature express genes demarcating them as the new working myocardium of the heart. Myocardium of the inner curvature retains the molecular signals from the linear heart tube myocardium, primary myocardium (Christoffels et al., 2000).

Trabeculae formation in the ventricular chamber is induced by signals from the endocardium to the myocardium (Del Monte et al., 2007, Chen et al., 2013, Grego-Bessa et al., 2007). Changes in the myocardium occur in that it differentiates into an outer compact layer and inner spongy layer, in which the latter contributes to the trabeculae. Groups of spongy myocardial cells separate from each other by ingression of the endocardium, forming trabeculae composed of a myocardial core surrounded by an endocardial sheet (Icardo and Fernandez-Teran, 1987). These trabeculae expand rapidly to produce a dense spongy network in the myocardial wall, which resembles finger-like projections when the heart is sectioned through. Trabeculated myocardium is thought to play a role in oxygenating the myocardium prior to the development of the coronary circulation, as well as contributing to the development of the conduction system, enhancing the direction of blood flow prior to septation, therefore, obtaining optimal contractility (de Jong et al., 1992).

Around the time of the development of the coronary circulation and septation of the ventricle, the compact myocardium grows as the trabeculae begin to compact and

become re-integrated into the ventricular wall (Rychter and Ostadal, 1971). Compacting trabeculae contribute to the interventricular septum (ventricular septation is required to maintain distinct boundaries between the systemic and pulmonary circulation), papillary muscles and the conduction system (Moorman and Lamers, 1994). It is thought that the expansion of the compact myocardium replaces the trabeculae in providing contractile force of the developing heart (Sedmera and Thomas, 1996). As the interventricular septum forms by the coalescence of trabeculae, it extends towards the AV canal and OFT, leaving an opening in the apical ventricle, the interventricular foramen. Closure of the septum occurs by fusion of the proximal OFT cushions (section 1.1.5.4) with the AV cushions, forming the membranous part of the ventricular septum and the interventricular septum contributing to the muscular portion of the septum (Anderson et al., 2003a).

1.2.5.4 Outflow Tract

The OFT is a tubular structure that connects the outflow region of the ventricle to the aortic sac and can be divided into the proximal and distal portions by a distinctive bend in the tube (Ya et al., 1998). It is thought that the proximal part of the OFT will contribute to the future roots of the arterial trunks (pulmonary artery and aorta) as well as to the subarterial outlets. The distal portion will provide the interpericardial portions of the great arteries (Anderson et al., 2003b). As the ventricular myocardium differentiates into a working myocardium, the OFT elongates, while still retaining its myocardial characteristics of the tubular heart (primary myocardium), i.e. slow conduction with long contractions. This characteristic along with the shape of the OFT allow it to act as a sphincter, preventing the regurgitation of blood into the ventricles during ventricular relaxation (de Jong et al., 1992).

Endocardial cushions develop in the proximal and distal OFT, which act to separate blood flow from the ventricular outflow, by forming the ascending aorta and pulmonary trunk, respectively (Webb et al., 2003). Septation occurs by the growth of a spiral mesenchymal septum from the distal to the proximal OFT (van den Hoff et al., 1999).

1.2.6 Development of the conduction system in the embryonic heart and the action potential

Cardiomyocytes are the principal cell type of the cardiac conduction system. Cardiomyocytes contributing to the conduction system possess a distinctive molecular phenotype, morphology and function, such as poorly developed sarcomeres, expression of transcription factors and sarcoplasmic reticulum, which distinguish them from the working myocardium (Eichna and Dehaan, 1961, Hoogaars et al., 2004, Moskowitz et al., 2007, Bakker et al., 2008). As the primary heart tube forms, a repetitive depolarisation impulse is transmitted from the venous pole, through the heart tube to the arterial pole (Hoff et al., 1939). This results in an even peristaltic movement in the muscle across the heart, insuring unidirectional blood flow. An electrocardiograph (ECG) at this stage resembles a sinusoidal conduction phenotype (Figure 1.4A) (Hoff et al., 1939). As the chambers of the developing heart are undergoing septation, the chamber myocardium conducts a faster depolarisation wave than previously seen, while the venous pole, AV canal and OFT retain a conduction seen in the primary heart tube (or primary myocardium) (de Jong et al., 1992). This delay in conduction at the venous pole, AV canal and OFT ensures unidirectional blood flow, as well as preventing backflow. This fast to slow conduction resembles the ECG of the adult heart (Hoff et al., 1939) with just the alteration of cardiomyocyte type (primary and conducting cardiomyocytes) in the absence of specialised conduction cells (such as insulating cells, differentiated nodes or a conduction system).

The conduction system of the mature heart contains a sinoatrial node (SAN), which develops in the main inflow portion of the developing heart. This SAN is the primary pacemaking source for the heart, generating electrical impulses that propagates to the atrioventricular node, rapidly, via the atrial muscle (Flack, 1907, Gourdie et al., 2003). The electrical impulse in the atrioventricular node (AVN), located in the floor of the right atrium, is slowed. This allows the ventricles to remain in diastole during atrial contraction, and also provides protection to the ventricles from arrhythmias triggered by the atria (Dobrzynski et al., 2003). From the AVN, the electrical impulses enter the fast-conducting AV branches and the Purkinje branches in the ventricle, transmitting the impulse to the working myocardium in an apex to base activation. In order for the heart to

transmit electrical impulses at different rates, a number of cardiac gap junctions, called connexins (CX), with variable conductance rates are expressed throughout the heart. The atria and ventricles express CX40 (known as CX42 in chicken) and CX43, both fast conducting gap-junction channels (Christoffels and Moorman, 2009). This provides the fast conductance to these chambers. The slow conducting AV canal is negative for CX40/43 but expresses CX45 and CX30.2, slow conducting gap junctions (Kreuzberg et al., 2006).

It is the generation of an action potential that allows the cardiac cells to contract and is regulated by different ionic gradients present around the cells membrane. The action potential can be divided into 5 phases (see Figure 1.4B). During phase 0, the cell membrane decreases in permeability to potassium, and sodium floods into the cells through fast sodium channels. This influx of sodium results in a rapid depolarisation from -90mV to +10mV. During phase 1 of the action potential, there is partial repolarisation due to the decrease in membrane permeability of sodium. Phase 2 consists of a plateau phase, by which a calcium influx into the cell prolongs the depolarisation and the duration of the action potential. As the membrane becomes less permeable to calcium towards the end of the phase there is an influx of sodium ions via the sodium/calcium exchanger (Pinnell et al., 2007). Calcium channels soon become inactive and there is an inward movement of potassium causing a repolarisation, known as phase 3. This brings the resting membrane potential back to -90mV of phase 4. In the early developing heart, action potentials are usually spontaneous, with a longer duration (Moody, 1995). In contrast, the more mature action potential has a shorter duration and usually triggered by some neuronal input (Spitzer, 1991).

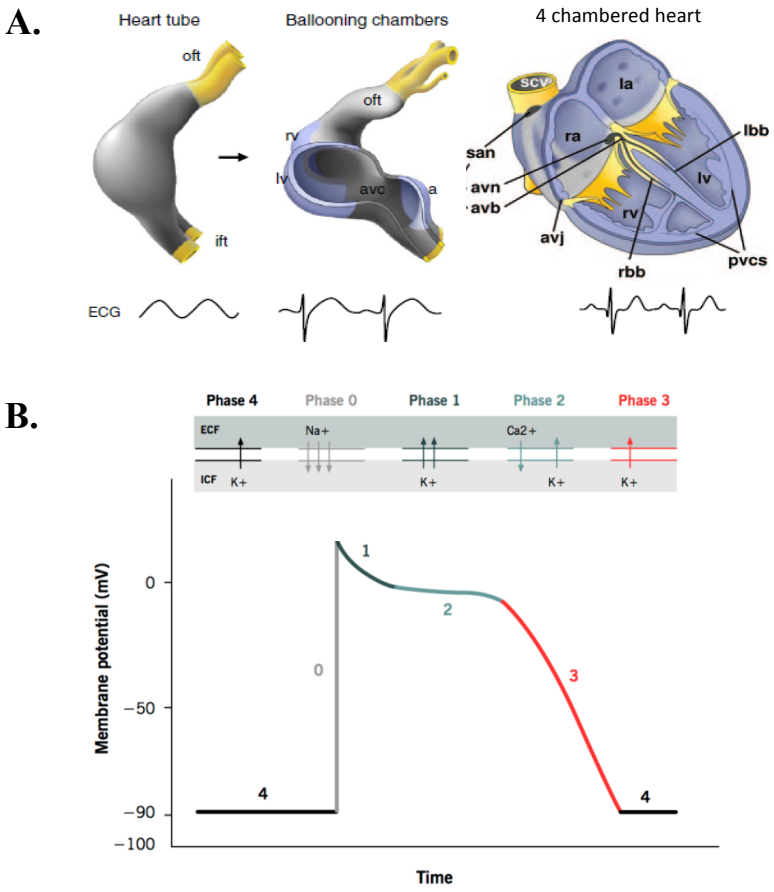

Figure 1.4 Development of the early conduction system and action potential.

A. The heart tube contains primary myocardium which propagates show conduction which has a sinusoidal ECG. As the chambers mature, the myocardium propagate fast conduction though the heart. However, conduction remains slow at the venous pool, AVC and OFT. The ECG in this heart resembles that of the fully formed heart. Grey indicates primordial heart tube, blue indicates the expanding myocardium at the outer curvature of the heart and yellow represents non-myocardial components of the heart. OFT indicates outflow tract; IFT, inflow tract; RV, right ventricle; lv, left ventricle; AVC, atrioventricular canal; r(l)a, right (left) atrium; SVC, superior vena cava; SAN, sinoatrial node; AVN, atrioventricular node; abv, atrioventricular bundle (of His); avj, atrioventricular junction; r(l)bb, right (left) bundle branch; pvcs, peripheral ventricular conduction system. Adapted from (Christoffels et al., 2010). **B.** An illustration of an action potential (AP) in a cardiomyocyte. The AP is divided into 5 phases in which different ions pass in and out of the cell membrane.

1.3 Cardiac muscle and its role in heart development

1.3.1 The sarcomere

Cardiac muscle is a type of striated muscle, which, unlike smooth muscle, contains cross-striations produced by the arrangement of protein filaments. The general structure of striated muscle is composed of muscle fibres made up of many myofibrils arranged into thick and thin filaments. The functional unit of myofibril is called the sarcomere (Figure 1.5) which is defined between two adjacent Z discs. Thin filaments extend from these Z discs, giving rise to I bands, which are terminated by the overlapping of thick and thin filaments. The thick filaments extend the total length of the A bands. It is the I bands that shorten in length during muscle contraction, while the A bands retain a constant length. The H zone is the component of the A band where actin and myosin do not overlap. The M line runs down the centre of the sarcomere (Gregorio and Antin, 2000).

Thick filaments (1.5μm long, 15nm in diameter) are composed of 200-300 myosin II molecules (containing a head and tail region), whereas the thin filaments (1μm long, 7nm diameter) are composed mainly of actin molecules (G-actin) polymerised into filamentous actin (F-actin) (Ross et al., 2003). These two structural proteins are the major components of the contractile apparatus of heart muscle. The head domain of myosin contains an ATP binding site which generates muscle contraction via its binding to the actin filament (Warrick and Spudich, 1987).

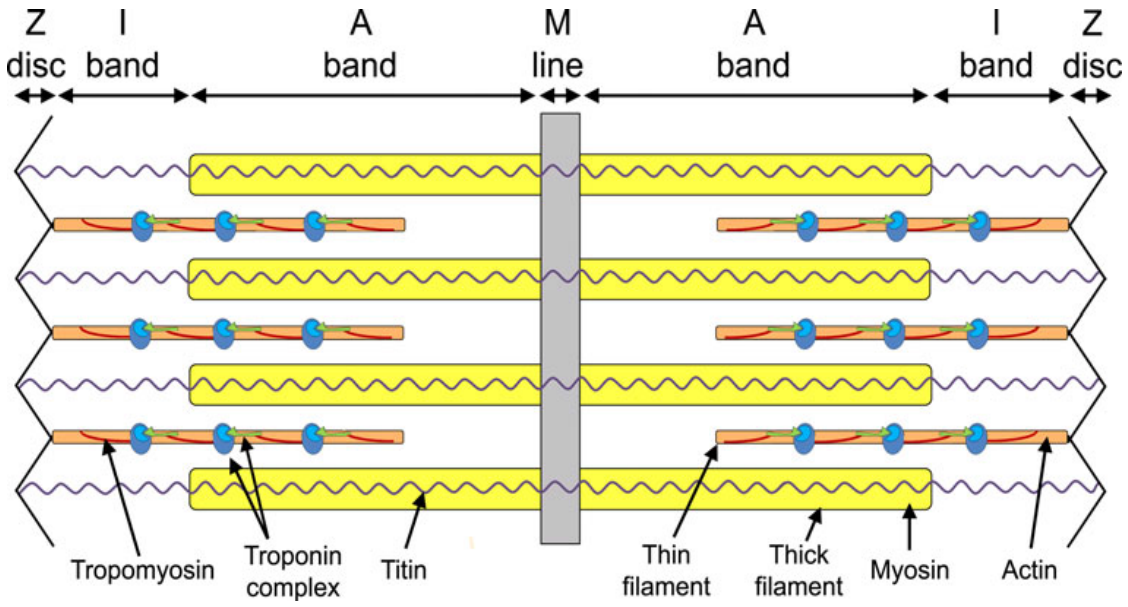

Figure 1.5 A schematic illustration of the sarcomere.

The thick filaments composed of myosin overlaps with the thin filaments (made up of a troponin complex and tropomyosin that interact with actin) in the region called the A-band. The area where the two filaments do not overlap is called the I-band. The thick filaments are anchored at a central point called the M-line, while the thin filaments are attached at the Z-disk. Titin is present along the length of the sarcomere. Taken from (England and Loughna, 2013).

The sarcomere also contains associated proteins that function, generally, to maintain alignment of the thick and thin filaments and to allow efficient muscle contraction. Titin and α-actinin anchor the thick filaments to the Z-discs as well as acting as a ruler for the alignment of the sarcomere during myofibrillogenesis (Tokuyasu and Maher, 1987). Myosin binding protein-C also interacts with titin, as well as myosin, directly binding these thick filament proteins together. Tropomyosin, an alpha helical coiled coil dimer that lies in the groove of the F-actin, masks the myosin-binding site on the actin filament (discussed in Section 1.5). The troponin complex, a tri-globular protein, binds to Ca^{2+} to initiate contraction (troponin-C), anchors tropomyosin (troponin-T; discussed in Section 1.6), and binds to actin, inhibiting its interaction with myosin (Troponin-I). Tropomodulin caps the terminal end of the thin filament, preventing further elongation or depolarisation of proteins with the filament (Ross et al., 2003, Gregorio and Antin, 2000).

Cardiac muscle differs from skeletal muscle in that it contains intercalated discs (Ross et al., 2003). Intercalated discs contain specialised junctions that allow communication between adjacent cells, for example, desmosomes. They function to connect individual cardiomyocytes together and reinforce their attachment during repetitive contractions. Gap junctions are also present in intercalated discs and are a vital component of the conduction system (Ross et al., 2003, Stevens and Lowe, 2005).

1.3.2 Myofibrillogenesis

Sarcomeric proteins are first detected in the cardiac field just before the heart undergoes cranio-caudal fusion and myofibril assembly has initiated by the time the linear heart begins beating (England and Loughna, 2013). Therefore, myofibrillogenesis is a rapid and co-ordinated process. As any impairment of sarcomere assembly leads to potentially detrimental effects to heart development, this process has been investigated greatly. Many studies use the chick as an animal model for myofibrillogenesis and so the following section will be discussed in the context of the chick.

The process of myofibrillogenesis contains three key steps including: 1) the initial formation of premyofibrils (Figure 1.6a), 2) the assembly nascent myofibrils (Figure 1.6b), and the development of mature myofibrils (Figure 1.6c) (Du et al., 2008, Rhee et al.,

1994). Initially, at the periphery of the cells, α-actinin molecules condense to initiate the assembly of Z-body structures, the first marker of premyofibrils (Rhee et al., 1994). Actin monomers begin to incorporate between the Z-bodies at the cell periphery forming actin filaments and continue to do so until the myofibrils reach full maturity (Suzuki et al., 1998). At the same time, nonmuscle myosin IIB can be identified between the assembling Z-bodies. Muscle myosin II is also present in these cells, however, it remains in the perinuclear region of the cardiomyocyte (Du et al., 2008).

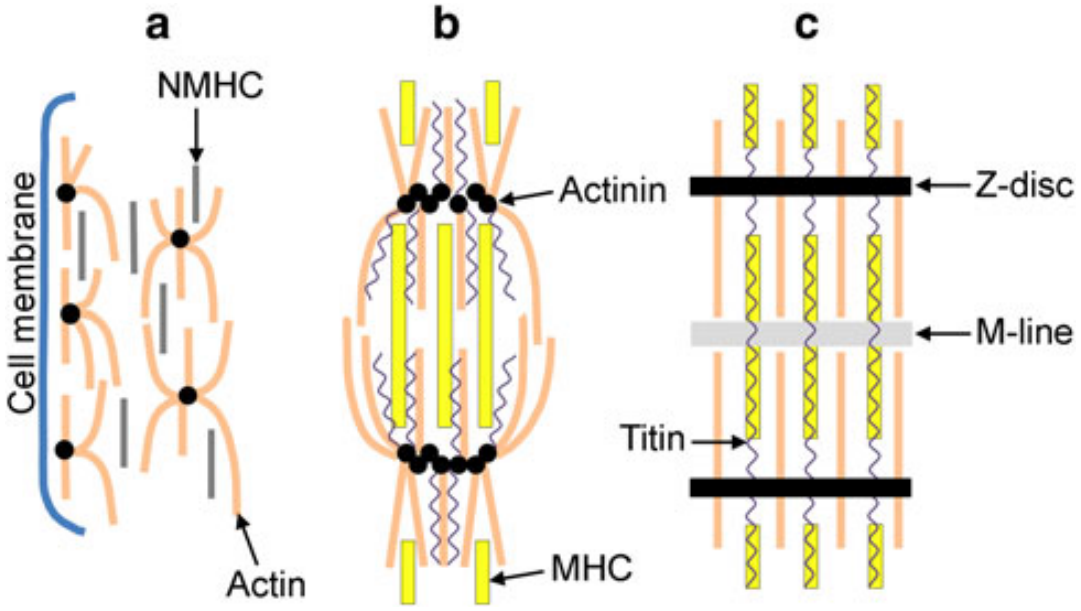

Figure 1.6 The assembly of the sarcomere.

a. Premyofibrils. Sarcomeric protein α-actinin assembles at the periphery of the cell. Actin monomers associate with the α-actinin and assemble into Z-bodies, with nonmuscle myosin (NMHC) scattered between them. **b.** Nascent myofibrils. Muscle-type myosin II isoforms (MHC) replaces the NMHC in the Z-bodies and stabilizing proteins such as titin become incorporated into the myofibrils. **c.** Mature myofibrils. The nascent myofibrils fuse together forming highly organised mature myofibrils. Taken from (England and Loughna, 2013).

Premyofibrils develop into nascent myofibrils by the incorporation of muscle myosin II isoforms and stabilizing proteins, such as titin (Figure 1.6b). In order for the premyofibrils to develop into nascent myofibrils, muscle myosin II must replace the nonmuscle isoform, and distribute itself throughout the myofibril. Titin is also incorporated into the developing myofibril at the Z-disc, thus playing its role in organising and maintaining the structures of the sarcomere and ensuring myosin integration (Turnacioglu et al., 1997, Van Der Ven et al., 1999).

As nascent myofibrils fuse to one another they form mature myofibrils, identifiable by presence of structural sarcomeric proteins, and their highly organized structure of A-bands and Z-discs (Figure 1.6c) (Du et al., 2008). By this stage, the first cardiac contractions are underway.

1.3.3 Sarcomeric contraction

The sarcomere acts to produce muscle contraction and force generation within striated muscle cells. Interactions between actin filaments and the myosin head produces this cyclic contraction, which is fueled by adenosine triphosphate (ATP) and regulated by calcium (Ca^{2+}). ATP binds to myosin via the ATP-binding site on the myosin head (Figure 1.7A). Here it is hydrolysed forming adenosine diphosphate (ADP) and a phosphate (Figure 1.6Ba and b) (Eisenberg and Hill, 1985). Isomerization of the myosin head results in strong bonding of myosin to actin, and extension of the lever arm of the myosin molecule, thus the sliding of the thick and thin filament past each other. ADP is then released and the myosin head dissociates from the actin filament. Rebinding of ATP completes the cycle (Figure 1.7Bd) (Brenner and Yu, 1993, Maughan, 2005).

Ca^{2+} regulates the cycle described above by controlling the movement of tropomyosin on the actin filament. Low levels of Ca^{2+} in the sarcoplasm results in non-binding of Ca^{2+} to troponin (Tn) C, and weak bonding between TnC, TnI and TnT within the troponin complex, while TnI is strongly bound to actin. This means tropomyosin is held in place on the actin filament, blocking the myosin binding sites on the actin filament (i.e. the blocked state) (Lehman et al., 1994). When intracellular concentrations of Ca^{2+} increase, Ca^{2+} binds to TnC, resulting in a conformational change in the troponin complex. TnC

and TnI interactions increase, and interactions between TnT and tropomyosin, TnI and tropomyosin, and TnI and actin decrease (Vibert et al., 1997). TnI is pulled away from the actin filament, resulting in a shift of the tropomyosin molecule, thus exposing the myosin binding sites on the actin filament (Figure 1.7Bc). This allows the actin and myosin interactions in a stereospecific manner (the closed state). As Ca^{2+} concentrations increase tropomyosin is further pushed from its original closed position and allows complete uncovering of the myosin binding sites on the actin filament resulting in the power stroke and generation of force and contraction (Lehrer, 1994).

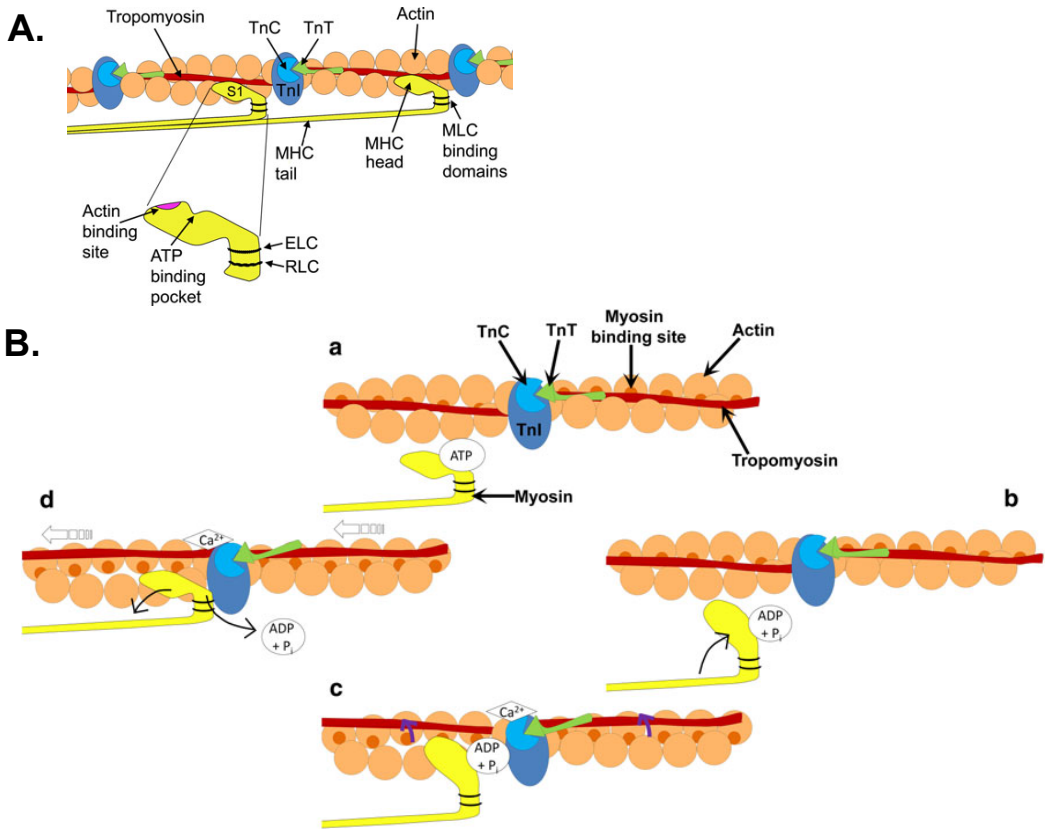

Figure 1.7 Sarcomeric proteins and their involvement in the cross bridge cycle.
A. A schematic representation of the relationship between myosin heavy chain and the actin filament. Tropomyosin, TnC, TnI, and TnT sit in the groove along the actin filament. The globular head of myosin heavy chain contains an actin-binding site, an ATP pocket, and essential light chain (ELC) and regulatory light chain (RLC) binding domains. MHC indicates myosin heavy chain; MLC, myosin light chain; S1, subfragment-1; Tn, Troponin. **B.** A simplified view of the cross-bridge cycle. **a.** An ATP molecule binds to the myosin head via the ATP-binding domain. **b**. When bound, ATP is hydrolysed converting it to ADP and a phosphate. This conversion allows the myosin head to extend towards the actin filament. **c.** Ca^{2+} binds to troponin C (TnC) in the troponin complex resulting in a conformational change of the complex. This pulls the tropomyosin filament around the actin filament (as indicated by the purple arrows) exposing myosin binding sites on the actin filament and the myosin head can bind to actin. **d.** Release of the ADP and phosphate nucleotides from the myosin head results in the extension of the head permitting the sliding of the filaments (open arrows). ATP quickly rebinds the myosin head, causing dissociation of the myosin away from the actin filament, and the cycle is repeated**.** Taken from (England and Loughna, 2013).

1.4 Cardiovascular dysfunction

Myofibrillogenesis is an essential process in early heart development as the assembly of this contractile structure allows for a beating tubular heart and the supply of blood to the developing embryo. Structural proteins of the sarcomere have long been associated with cardiomyopathies (also skeletal myopathies) and more recently with congenital heart defects (CHD). In order to understand the potential role for these sarcomeric proteins in heart development and disease, a brief description of cardiomyopathies and CHDs will be discussed in the following sections.

1.4.1 Cardiomyopathies

Cardiomyopathies are a group of diseases of the heart muscle that contribute to cardiac dysfunction, thus leading to heart failure with a high rate of morbidity and mortality and increased risk of sudden cardiac death (Wexler et al., 2009). According to the American Heart Association, there are five classifications of cardiomyopathy: hypertrophic cardiomyopathy, dilated cardiomyopathy, restrictive cardiomyopathy, arrhythmogenic right ventricular cardiomyopathy and left ventricular non-compaction (Maron et al., 2006). These cardiomyopathies are also further subclassified into inherited and acquired diseases. Genetic mutations in genes involved in cardiac development and muscle contraction contribute to a large proportion of these heterogeneous conditions.

1.4.1.1 Hypertrophic cardiomyopathy

Hypertrophic cardiomyopathy is a cardiovascular disease that is prevalent in 1 in 500 individuals in the general population (Maron et al., 2006). This frequently occurring cardiomyopathy is regularly transmitted as a Mendelian trait (autosomal dominant i.e. 50% chance of passing on the defective gene) (Maron et al., 1995). Although symptoms can be mild, they can vary from asymptomatic to sudden cardiac death (McKenna et al., 1981). In the United States, undetected hypertrophic cardiomyopathy is the leading cause of sudden cardiac death in athletes (Seidman and Seidman, 2001). The general morphology of hypertrophic cardiomyopathy in humans is characterised by left and/or right ventricular wall thickening with non-dilation of the ventricles (Figure 1.8B)

(Maron et al., 2006). Pathophysiological examination of hypertrophic cardiomyopathy reveals myocyte disorganisation, fibrosis, increased calcium sensitivity and cardiac arrhythmias leading to sudden adult death and/or heart failure (Wieczorek et al., 2008). Mutations in sarcomeric, Z-disc and intracellular calcium modulating genes have been linked to hypertrophic cardiomyopathy. Recent clinical guidelines have recommended the comprehensive screening of 5 genes: *MYBPC3, MYH7, TNNI3, TNNT2* and *TPM1* (genes encoding myosin binding protein C, myosin heavy chain 7, cardiac troponin I, cardiac troponin T and tropomyosin 1, respectively) (Towbin, 2014).

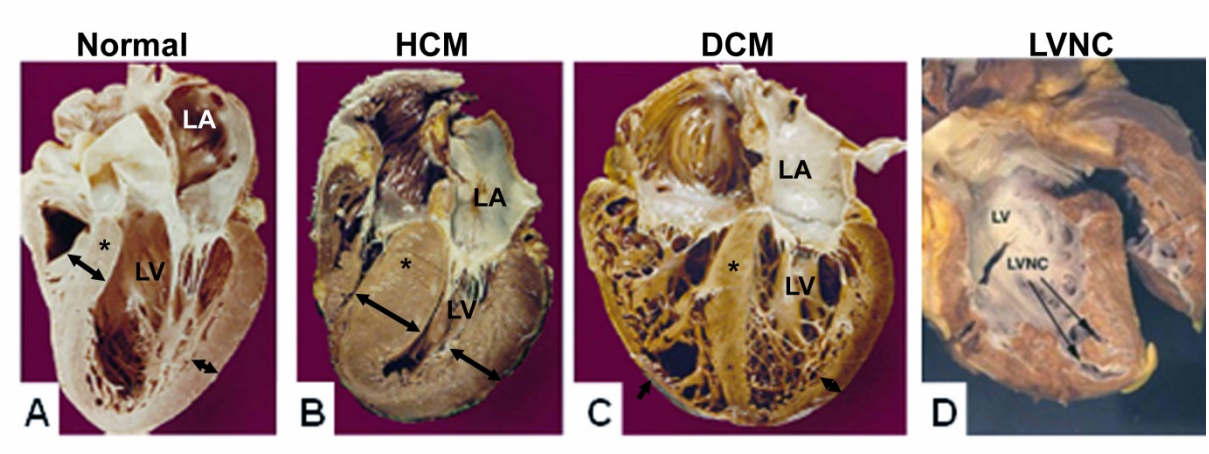

Figure 1.8 Autopsy specimens of hearts showing normal, hypertrophic cardiomyopathy, dilated cardiomyopathy and left ventricular non compaction.

The normal myocardium (A) can be remodelled due to gene mutations. This may result in increased wall thickness (B) as with hypertrophic cardiomyopathy, thinning of the ventricular wall and increased ventricular chamber size (C) seen in dilated cardiomyopathy, or the remnants of trabeculations and deep recesses in the ventricular myocardium as seen in left ventricular noncompaction (D). LA indicates left atrium; LVNC, left ventricular non-compaction; LV, left ventricle; *, ventricular septum; arrows, ventricular wall and septal thickness. Adapted from (Ikeda et al., 2014, Seidman and Seidman, 2001).

1.4.1.2 Dilated cardiomyopathy

Dilated cardiomyopathy has a high incidence of 1 in 2,500 people and is the most common reason for heart transplants (Maron et al., 2006). Dilated cardiomyopathy phenotype includes dilation of one or both ventricles and decreased systolic function, and is usually associated with congestive heart failure (Figure 1.8C) (Towbin and Bowles, 2002, Braunwald, 2008). Dilated cardiomyopathy is associated with a range of causes such as familial, environmental, idiopathic, or related with the progression of other cardiovascular disease, although genetic aetiology accounts for 30-50% of dilated cardiomyopathy cases (Fatkin, 2011). Genetic forms of dilated cardiomyopathy usually result from mutations in genes encoding cytoskeletal and sarcomeric proteins such as *MYH7*, *TNNT2* and *TTN* (gene encoding Titin) (Cahill et al., 2013).

1.4.1.3 Restrictive Cardiomyopathy

Restrictive cardiomyopathy is one of the rarest of the muscle diseases of the heart (Kushwaha et al., 1997). Restrictive cardiomyopathy presents as dilated atria, restricted ventricular filling and reduced diastolic volume in either a single or both ventricles. Systolic function and wall thickness is usually unaffected, although fibrosis of the myocardium may be present. Sudden cardiac death, heart failure and life-threatening cardiac events are commonly associated with restrictive cardiomyopathy and death usually occurs within a few years of diagnosis (Maron et al., 2006). Genetic contributions to restrictive cardiomyopathy are autosomal dominant inheritance and most mutations are found in genes encoding sarcomeric and Z-disc proteins such as *TNNI3*, *MYH7*, *ACTC1* (gene encoding α-cardiac actin), *TNNT2* and *TPM1* (Towbin, 2014).

1.4.1.4 Left ventricular non-compaction

Left ventricular non-compaction is a congenital cardiomyopathy characterized by the presence of prominent trabeculae and deep recesses in the ventricular cavity of the mature heart. Although called left ventricular non-compaction, trabeculae can be present in the left, right or both ventricular chambers (Figure 1.8D) (Towbin, 2010). It

was originally postulated that left ventricular non-compaction resulted in the arrest of ventricular compaction of trabeculae during embryonic development (normal development and maturation of the ventricular chambers is described earlier in Section 1.2.5.3) (Chenard et al., 1965). However, de novo acquired left ventricular non-compaction and noncompaction disappearance have been reported in the literature, bringing into question the abnormal embryogenesis hypothesis (Finsterer et al., 2010, Stollberger et al., 2007). Left ventricular non-compaction can coexist with CHDs such as atrial and ventricular septal defects, aortic stenosis and aortic coarctation (Towbin, 2010). The prevalence of left ventricular non-compaction among the general population is unpublished, however, in a study with children with other cardiomyopathies, 9.2% had left ventricular non-compaction (Andrews et al., 2008). In the adult population, the prevalence of isolated left ventricular non-compaction was 0.01-0.26% (Stöllberger et al., 2006). Mutations in Z-disc and sarcomeric genes in patients with left ventricular non-compaction (such as *ACTC1, MYBPC3, MYH7 and TNNT2*) have been reported (Ichida, 2009). More recently, mutations have also been found in *HCN4*, a gene associated with the SAN and pacemaker activity (Milano et al., 2014).

1.4.1.5 Arrhythmogenic right ventricular cardiomyopathy

Arrhythmogenic right ventricular cardiomyopathy is a less common inheritable heart disease with a prevalence of 1 in 5000, although remains the fifth most common cause of sudden cardiac death (Thiene et al., 1988). Arrhythmogenic right ventricular cardiomyopathy is associated with cardiomyocyte replacement with fibrofatty tissue. This fatty deposition results in obstruction of electrical conduction, thus resulting in arrhythmias (Basso et al., 2009). Although arrhythmogenic right ventricular cardiomyopathy has been linked to 12 genes, none have been identified as sarcomeric genes (Lazzarini et al., 2015).

1.4.2 Congenital heart defects

CHDs are defined as gross anatomical abnormalies of the heart that have or have the potential of becoming functionally significant. In humans, CHDs occur in approximately 12-14/1,000 of live births and remain the leading cause of birth defect mortality in the first year of life (Kodo and Yamagishi, 2011, Hoffman and Kaplan, 2002). Altered cardiac development occurring at various stages of cardiogenesis, such as heart specification, cardiomyocyte differentiation, chamber specification and valvulogenesis, may cause several CHDs. Inherited or sporadic mutations in transcription factor and sarcomeric genes have been linked to CHDs. Chromosomal abnormalities are also commonly association with CHDs (14% of patients with Trisomy 21 or Down's syndrome) (Trevisan et al., 2013). Environmental factors are also associated, for example prenatal exposure to angiotensin converting enzyme inhibitors, although these factors are associated with risk rather than establishing an underlying disease mechanism (Bruneau, 2008).

CHD are classified into three main groups depending on their outcome: 1) septal defects including: atrial septal defects (ASD), atrioventricular septal defects (AVSD) and ventricular septal defects (VSD); 2) left side obstruction defects: including mitral and/or aortic stenosis and aortic coarctation; and 3) cyanotic heart disease, resulting in the mixing of oxygenated and deoxygenated blood including: tetralogy of Fallot, pulmonary atresia, persistent truncus arteriosus, transposition of great arteries and double outlet right ventricle. Bicuspid aortic valve is a CHD that does not fit into any of the above categories (Bruneau, 2008).

The principal CHDs that are underlined in the text above are clinically significant and important in the experimental context of this thesis and are briefly described below.

1.4.2.1 Atrial Septal Defects

Atrial septal defects (ASDs) occur when abnormal cardiogenesis results in a communication between the right and left atria. ASDs account for 7-10% of all CHDs diagnosed in children and 30-33% diagnosed in adults (Kazmouz et al., 2013). The most clinically significant ASD is the foramen secundum defect. It is the result of an inadequately sized septum primum that does not extended to cover the foramen

secundum entirely, or if the septum secundum fails to form fully. Foramen secundum defects often go undetected with the individual having few or no functional limitations. However, larger, more severe foramen secundum defects may lead to right atrial volume overload due to left-to-right shunting of blood between atrial chambers (Briggs et al., 2012). Furthermore, persistence of the defect, which may sporadically close after birth, leads to increased pulmonary resistance causing increased right-sided pressure and result in right-to-left shunting of blood. This in turn leads to decreased systemic oxygenation, as deoxygenated blood from the right side of the heart entered the left side (Engelfriet et al., 2007).

Patent foramen ovale, on the other hand, results in failure of the septum primum and secundum to fuse. The foramen ovale is an important embryonic intra-atrial communication, allowing blood to bypass the underdeveloped pulmonary system, as gas exchange occurs at the placenta. The establishment of pulmonary gas exchange after birth increases intra-atrial pressure pushes the septum primum in contact with the septum secundum, where they fuse together forming a continuous atrial septum. In approximately 25% of the population the septum primum and secundum fail to fuse leaving the foramen ovale patent (Silva, 2014). The patency of the foramen ovale may not result in atrial communication, if left atrial pressure exceeds that of the right atrial chamber. However, if communication does occur due to certain conditions, the patent foramen ovale becomes pathological, resulting in conditions such as cryptogenic stroke, migraine with aura, and decompression illness (Sztajzel et al., 2002, Wilmshurst et al.).

Foramen primum defects are considered as AVSD, in which the septum primum and endocardial cushions do not fuse correctly in the AV canal. Although less common than the foramen secundum defects, foramen primum defects can be more severe. As the septum primum fuses with the endocardial cushions, associated malformations of foramen primum defects include the mitral (more frequent) and tricuspid valves, and the upper portion of the ventricular septum (Blount et al., 1956, Webb and Gatzoulis, 2006).

1.4.2.2 Ventricular septal defects

Ventricular septal defects (VSD) appear to be one of the most prevalent forms of CHD, accounting for 25% of CHDs (Hoffman and Kaplan, 2002). VSDs occur when a component of the ventricular septum fails to align or grow adequately, resulting in the left to right shunting of blood and left ventricular and atrial overload (Minette and Sahn, 2006). VSDs can be classified into groups depending on what part of the ventricular septum is affected: muscular (or trabecular), inlet, infundibular (outlet), and membranous septal defects (Soto et al., 1980).

Muscular defects are likely to occur when the primitive ventricular septum fails to grow adequately. The defect is present within the muscular portion and completely surrounded by a muscular rim (Ramaciotti et al., 1995). Inlet defects occur due to failure of the AV cushions to fuse with each other or with the septum primum of the atrium. This may result in abnormalities of the tricuspid and mitral valves (Soto et al., 1980). Outlet or infundibular defects can result from misalignment or poor development of the OFT cushions and usually the aortic and pulmonary valves are uninterrupted (Minette and Sahn, 2006). Finally, membranous septal defects result from failure of the membranous component of the septum to fuse with the muscular component. True defects of the membranous septum are surrounded entirely by fibrous tissue usually without muscular contribution and identified by a continuous fibrosis between the tricuspid and aortic valves (Penny and Vick, 2011).

The significant impact a VSD can have depends on VSD size, pressure loads in the right and left ventricles and pulmonary resistance (Minette and Sahn, 2006). VSD detection can be missed at birth due to the near equal pressures between the right and left ventricles and therefore, the lack of shunting. When pressure differences change between the ventricular chambers, then shunting increases and the defect becomes clinically apparent. Shunt volume is then determined by the size of the VSD (Minette and Sahn, 2006). Spontaneous closure can occur, usually by prolapse of the right aortic cusp in the case of outlet defect, while muscular defects can undergo spontaneous closure as a result of muscular occlusion (Eroglu et al., 2003).

It is important to note that VSDs are not only isolated, but can be intrinsic to more complex malformations such as Tetralogy of Fallot, transposition of the great arteries and aortic coarctation.

1.4.2.3 Patent Ductus Arteriosus

The ductus arteriosus is a vital structure during embryonic life, where blood can by-pass the fetus's lungs which are not fully functional, while blood oxygenation is obtained from the mother. The ductus arteriosus is located between the pulmonary trunk, ascending from the right ventricle, and the aortic arch. The ductus arteriosus usually closes in the first 48 hours after birth forming the ligamentum arteriousum, although persistence of up to 3 months is not considered abnormal (Cassels, 1973). Failure of the duct to close after 3 months is considered a patent ductus arteriousus (PDA) and has an incidence of 1:2000 babies born at full term and accounts for 10% of CHDs (Mitchell et al., 1971). Surgical intervention would be carried out should the PDA remain open.

1.4.2.4 Pulmonary Atresia

Pulmonary atresia (obstruction of blood flow through the pulmonary trunk) is a rare malformation (occurring 1 in 10,000 live births) that is usually lethal (Shams et al., 1971). Pulmonary atresia is characterized by atretic pulmonary valves, due to hypoplastic development of the pulmonary valve and artery. It is a complex defect and occasionally accompanied by a narrowed right ventricle resulting in obstruction of the pulmonary circulation, VSDs or Tetralogy of Fallot. Pulmonary blood flow in pulmonary atresia is reliant on a patent ductus arteriosus (Maroto Monedero et al., 2001). Treatment options for this cyanotic disease include: valvotomy, shunt operation, heart catheterization and heart-lung transplantation (Januszewska et al., 2009, Dodds et al., 1997).

1.4.2.5 Tetralogy of Fallot

Tetralogy of Fallot occurs in 3 out of 10,000 live births, yet accounts for 7-10% of all CHDs (Bailliard and Anderson, 2009). Before surgical intervention, 50% of patients with Tetralogy of Fallot die in the first few years of life, and it is unusual for a patient to survive past 30 years (Bertranou et al., 1978). Tetralogy of Fallot presents as a number of defects in the heart including: (i) ventricular septal defect, (ii) overriding aorta, (iii) right ventricular outflow obstruction, and (iv) right ventricular hypertrophy (Becker et al., 1975). During embryonic development, misalignment of the outflow portion of the ventricular septum or failure of the outflow cushions to muscularise results in the ventricular septal defects. This misalignment of the muscular septum results in displacement and thus the root of the aorta overrides the muscular septum. Blood shunts from right to left, and deoxygenated blood becomes mixed with oxygenated system blood. Volume overload going to the aorta leads to dilation of the aortic root in adults. The displacement of the aortic root narrows the outflow region to the pulmonary trunk. This in turn can lead to narrowing of the pulmonary trunk and arteries as well as hypoplasia of the pulmonary valves. The associated hypertrophy is associated with the hemodynamic alterations caused by the defects (Bailliard and Anderson, 2009).

1.4.3 Sarcomeric proteins associated with cardiac dysfunction

Mutations in sarcomeric proteins have been associated with cardiomyopathies, while more recently, a subset of these proteins have been associated with CHDs. Studies into dilated and hypertrophic cardiomyopathies have revealed that sarcomeric mutations lead to dysfunction, including changes in Ca^{2+} sensitivity, changes in sarcomeric tension, and alterations in post-translational modifications of proteins, such as phosphorylation (Frazier et al., 2011). Transcription factors such as *TBX5* (Basson et al., 1999), *NKX2.5* (Schott et al., 1998), *TBX20* (Kirk et al., 2007) and *GATA4* (Garg et al., 2003) were more commonly associated with CHDs, although in recent years sarcomeric proteins have been elucidated as candidates for CHDs. However, it is not yet known how mutations in structural proteins

can lead to CHD, but some alteration in haemodynamics may play a crucial role during embryonic development (Granados-Riveron and Brook, 2012).

Mutations in *MYH6* (encoding α myosin heavy chain or αMHC) were the first to be associated with CHDs in 2005 (Ching et al., 2005), and found in patients with ASDs (see Table 1.2 for summary of sarcomeric proteins associated with CHDs). Yet, relatively few mutations in *MYH6* have been linked to cardiomyopathies (Niimura et al., 2002, Carniel et al., 2005). Since then, numerous missense, splice site and nonsense mutations have been discovered in *MYH6* causing a variety of CHDs, such as patent truncus arteriosus, patent foramen ovale, tricuspid atresia and VSD (England and Loughna, 2013). Knockdown of αMHC in the chick showed that atria septation was compromised, although atrial chamber formation was unaffected (Ching et al., 2005, Rutland et al., 2009).

Numerous mutations have been reported in *MYH7* (encoding βMHC) associated with cardiomyopathies (Walsh et al., 2010), and in more recent years CHDs (Table 1.2). A family with left ventricular non-compaction carried a mutation in *MYH7*, and 4 members were also afflicted with ASD and Epstein's anomaly (malformed tricuspid valve) (Budde et al., 2007). Interestingly, knockdown of βMHC in the chick showed a structurally normal developed heart, although the hearts appeared enlarged and displayed abnormal calcium transients in atrial and ventricular cells (Rutland et al., 2011).

Mutations associated with *MYBPC3* and *ACTC1* have also been identified in CHDs. Both genes were linked to ASDs and VSDs that were either isolated or in patients with left ventricular non-compaction or hypertrophic cardiomyopathy (Wessels et al., 2015, Matsson et al., 2008).

H252Q	Transposition of great arteries, patent foramen ovale	
E501Stop	Tricuspid atresia, VSD, hypoplastic right ventricle	
V700M	patent foramen ovale	
R1116S	ASD	
A1366D	Aortic valve stenosis, subaortic ridge, patent foramen ovale, septal diskynesia	
A1443D	Secundum ASD	
R1865Q	Secundum ASD, VSD and dilated inferior vena cava	
IVS37-2A>G	Truncus arteriosus	
R17H	AVSD, ASD	(Posch et al., 2011)
C539R	ASD	
K543R	ASD	
A1004S	ASD	
I820N	ASD	(Ching et al., 2005)
Y283D	Ebstein anomaly and secundum ASD; perimembranous VSD	(Postma et al., 2011)
N1918K	Ebstein anomaly; coarctation of the aorta, bicuspid aortic valve	
	Ebstein anomaly and perimembranous VSD	
E1573K	Ebstein anomaly, pulmonary artery hypoplasia and secundum	
Y283D	ASD	
	Ebstein anomaly and patent foramen ovale	(Bettinelli et al., 2013)
L390P	Ebstein anomaly and VSD	
E1220del		

Table 1.1 A summary of cardiac sarcomeric proteins associated with congenital heart defects.

1.5 Tropomyosin

Tropomyosins (TPM) are a diverse group of proteins with distinct isoforms found in muscle and non-muscle cells (Gunning et al., 2005). Four *TPM* genes have been identified in vertebrates (excluding zebrafish which has 6 *TPM* genes): *TPM1, TPM2, TPM3,* and *TPM4*. Of these four genes, over 40 isoforms are expressed by alternating promoter regions or RNA processing and are highly conserved (Perry, 2001, Lees-Miller and Helfman, 1991). *TPM* gene organisation varies from species to species and is discussed below in relation to *TPM1*.

1.5.1 TPM1 Structure and Function

TPM1 is a parallel double-stranded α-helical coiled-coil that is composed of 284 amino acid residues. It binds to the long grooves of the helical filaments of actin, and is crucial in regulating and stabilising actin functions. It is also associated with the troponins in a contractile role in response to Ca^{2+} in striated muscle (discussed in section 1.2.3). The N-terminus and C-terminus of tropomyosin required for high actin affinity are encoded by alternative exons (exon 2a/b and 9a/b). Both the general features of an α-helical coiled-coil structure and the special features of the TPM1 molecule give TPM1 its regulatory role in muscle contraction. The amino acid sequence of the molecule contains a number of features (Figure 1.9). Firstly, it has a so-called short range repeat made up of 40 continuous seven-residue repeats labelled *a-b-c-d-e-f-g* (known as heptads). The *a* and *d* residues are apolar resulting in them interlocking with one another by the winding of the α-helices around one another, thus producing the coiled-coil structure (Crick, 1953). In addition, the *e* and *g* residues on chains are joined by salt links that increase stability of the coiled-coil and favours the parallel arrangement of the two-chained molecule (Parry, 1975, Cohen and Parry, 1990). Residues at the *b*, *c,* and *f* position are present on the surface and are, therefore, available for binding of other molecules. Secondly, there are the long range repeats/periods composed of 7 alternating charged and apolar surface side chains that correspond the actin-binding sites, depending on which state of contraction is active (Phillips et al., 1986).

TPM1 molecules bond head-to-tail with short overlaps of about nine-eleven residues. This forms a long, unbroken filament that wraps around the actin filament, where each TPM1

molecule spans seven actin monomers (Phillips et al., 1986, Palm et al., 2003). This joining allows for cooperative interactions along the actin filament. Troponin-T binds to TPM1 at the C-terminus, encoded by exon 9a, and spans the overlapping site of two TPM1 molecules, thus strengthening this head-to-tail joint (Hill et al., 1992). The amino acid sequence for TPM1 also contains a repeat of core alanine residues that generate seven bends in the molecule's axis (Brown et al., 2001). This promotes winding of the molecule around the actin filament.

In cardiac muscle, TPM functions to regulate the interaction of actin and myosin in response to Ca^{2+} (Ebashi et al., 1969). Under resting intracellular Ca^{2+} concentrations, TPM interacts with troponins to inhibit ATPase activity of the actin and myosin. After Ca^{2+} release in a muscle cell (from the sarcoplasmic reticulum) triggered by an action potential, Ca^{2+} binds to troponin-C, inducing conformational changes between the TPM-troponin complex. This induces ATPase activity, allowing actin and myosin binding, resulting in contraction (Gordon et al., 2001). Unlike in striated muscle, the biological function of TPMs in smooth muscle and non-muscle cells is poorly understood, as these cells do not contain the troponin complex. These variations of TPM between different tissues may account for the large number of isoforms which are structurally and functionally different from each other (Lees-Miller and Helfman, 1991).

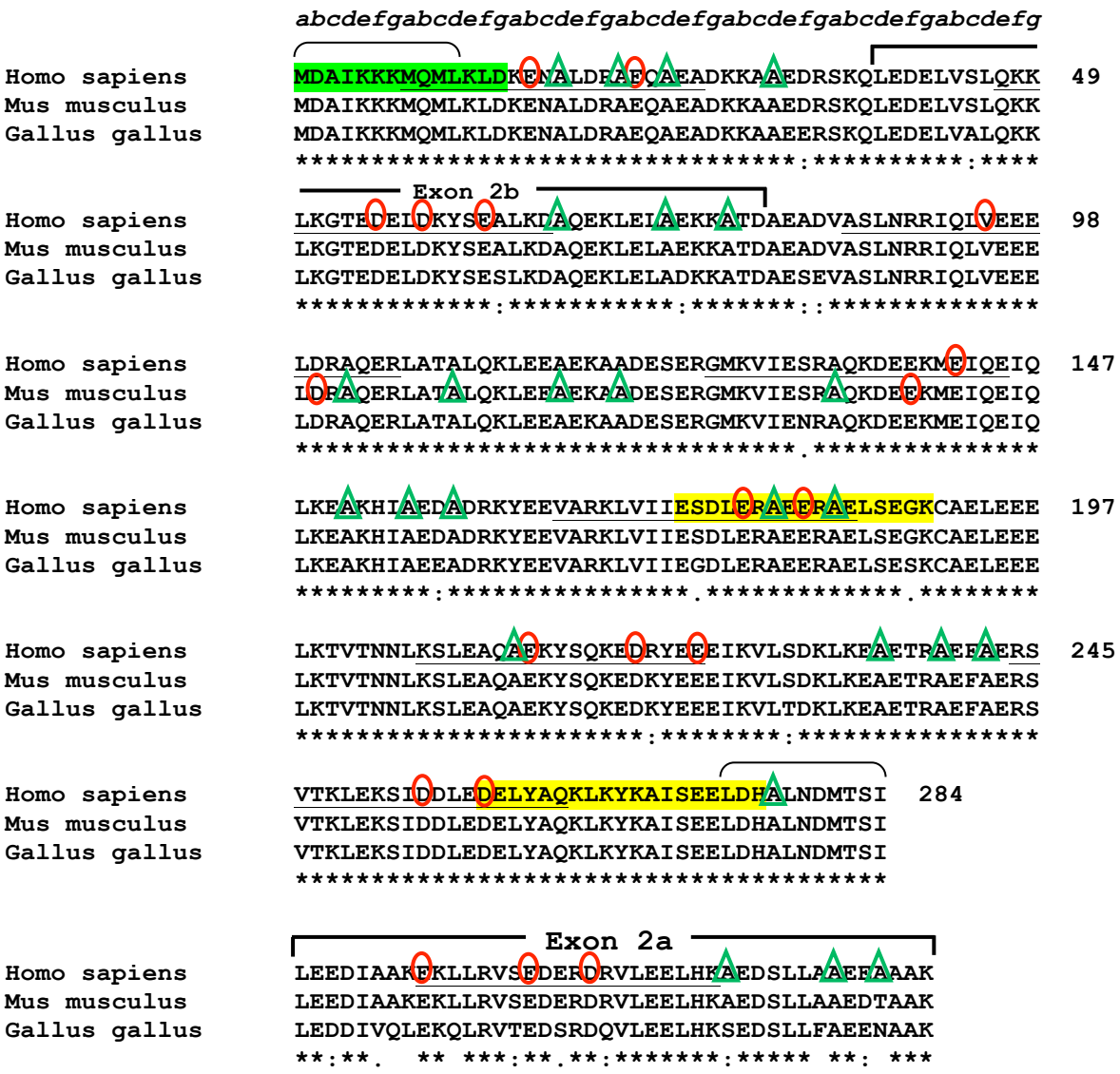

Figure 1.9 Comparison of human, mouse and chicken TPM1 protein sequence.
The human TPM1α and TPM1κ protein sequences (TPM1α: NP_001018005.1, TPM1κ: AY640414.1) are compared to the mouse (TPM1α: NM_024427.4, TPM1κ: NP_001157721.1) and chicken (TPM1α: AY150210.1, TPM1κ: NP_990732) with various structural domains indicated on the human sequence (Brown et al., 2001). The sequences were aligned in ClustalW2 (Larkin et al., 2007). TPM1 is highly conserved within the 3 species, although with slightly more variation in exon 2a corresponding to the TPM1κ isoform. The amino-acid residues have 40 continuous seven-residue repeats (*a-b-c-d-e-f-g;* highlighted in grey), the heptad repeats. The α-zones are the actin-binding regions are outlined (underlined). TPM1 molecules join in a head-to-tail fashion so that the first and last

11 residues overlap with adjacent molecules (rounded brackets). The Troponin-T binding sites are highlighted yellow (Hitchcock-DeGregori et al., 2002). The Tropomodulin binding site is located at the N-terminus (highlighted in green) (Sung and Lin, 1994, Kostyukova et al., 2001). The 7 core alanine groups are responsible for generating seven bends in the axis of the TPM1 molecule so that is wraps around actin (green triangles). The negatively charged α-zones correspond to the actin-binding regions (red circles) (Brown et al., 2001).

1.5.2 *TPM1* expression in the developing heart

In human (*Homo sapiens*), *TPM1* (chromosome 15) contains 15 exons, 5 of which are expressed in all isoforms. For these isoforms, alternative splice sites are found at exons 2a/2b, 6a/6b, and 9a, 9b, 9c and 9d. Two isoforms of *TPM1* have been shown to be predominantly expressed in the developing, neonatal and adult human heart. These isoforms are *TPM1α* and *TPM1κ*, and differ in that *TPM1α* contains exon 2b (an exon associated with striated muscle isoforms), whereas *TPM1κ* contains exon 2a (an exon associated with smooth muscle isoforms) (Denz et al., 2004, Zajdel et al., 2003). Recent studies have shown that mRNA levels of both *TPM1α* and *TPM1κ* are expressed in equal amount and are present in the 6 week old human fetal heart. Expression of *TPM1* increases 3-fold in the adult heart (Rajan et al., 2010). *TPM2α* is expressed at equivalent levels in both the fetal and adult heart. Interestingly, protein levels in the adult heart revealed that ~92% of the total TPM was TPM1α, with the remainder being TPM1κ and TPM2α (Rajan et al., 2010).

TPM2 (chromosome 9) encodes various isoforms from alternative splicing of 11 exons. These include the skeletal muscle isoform (*TPM2α*), which is also found to be expressed in the heart (Gunning et al., 2005). No cardiac muscle isoforms have been identified in the human heart for *TPM3* and *TPM4*, however they do play an important role in embryonic stem cells in early embryogenesis and in fibroblasts, respectively (Gunning et al., 2005, Hook et al., 2004).

In the developing mouse (*Mus muscularis*) heart, *Tpm1α* and *Tpm2* are expressed (5:1 ratio, respectively), while *Tpm1α* is expressed mainly expressed in the adult murine heart (60:1 ratio) (Muthuchamy et al., 1993). *TPM1κ* has been detected in the adult mouse heart but at lower levels than TPM1α (Dube et al., 2014).

TPM1 expression has also been shown in the developing chicken (*Gallus gallus*) heart. *TPM1α* and *κ* are expressed as early as stage HH12 and up to day 15 in development. However, in the adult avian heart, both *TPM1* isoforms are absent (Zajdel et al., 2003, Wang et al., 2008). Instead a striated muscle isoform of *TPM4*, *TPM4α*, is the only isoform to be expressed (Fleenor et al., 1992). *TPM4* encodes 3 distinct isoforms by alternative splicing of 11 exons in avians. These tissue specific isoforms include the

cardiac muscle isoform (*TPM4α*), the cytoskeletal isoform and the smooth muscle isoform (Fleenor et al., 1992, Forry-Schaudies et al., 1990). This expression is not evident in human or other mammals. Nevertheless, because *TPM1* is expressed in the developing chicken heart, it provides a good animal model for studying the role of TPM1 in cardiac development.

The axolotl heart (*Ambystoma mexicanum*) also expressed the *Tpm4α* transcripts, as well as *Tpm1α* and *Tpm1κ*, in both the developing and adult heart (Zajdel et al., 2013).

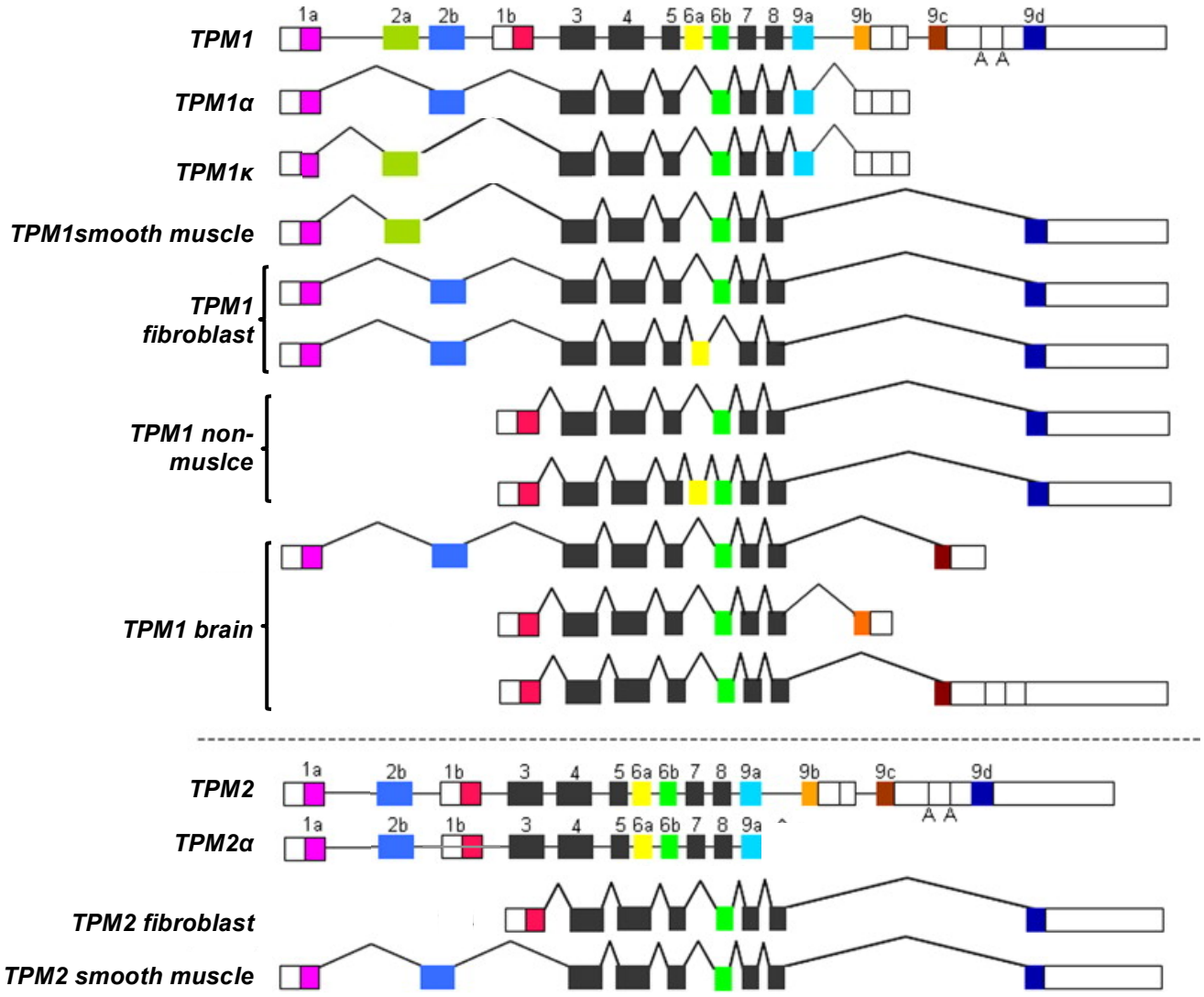

Figure 1.10 An illustration of the multiple genes and isoforms of tropomyosin.
There are four tropomyosin genes, three of which are illustrated above. *TPM1* gives rise to 10 isoforms, 2 of which are expressed in cardiomyocytes, *TPM1α* and *TPM1κ*. *TPM2α* is known to be expressed in the human and mouse heart. The TPM4 gene has one isoform, *TPM4α,* which is expressed in the chick and axolotl heart.

1.5.3 TPM1 and cardiac dysfunction

TPM1 has long been associated with cardiomyopathies (Braunwald, 2008). 35 amino acid substitutions have been found associated with TPM1 and cardiomyopathies. 18 mutations have been found in hypertrophic cardiomyopathy patients (Karibe et al., 2001, Thierfelder et al., 1994, Chang et al., 2005, Yamauchi-Takihara et al., 1996, Otsuka et al., 2012, Frisso et al., 2009, Van Driest et al., 2003, Regitz-Zagrosek et al., 2000, Morita et al., 2008, Fokstuen et al., 2011, Olivotto et al., 2008), 12 in dilated cardiomyopathy (Hershberger et al., 2010, Olson et al., 2001, Lakdawala et al., 2010, van de Meerakker et al., 2013, Lakdawala et al., 2012), six in left ventricular non-compaction (Chang et al., 2011, Hoedemaekers et al., 2010, Probst et al., 2011) and one associated with restrictive cardiomyopathy (Caleshu et al., 2011). A summary of mutations can be seen in Table 1.3. To date *TPM1* has not been linked to CHDs, although much evidence suggests a critical role for *TPM1* in cardiogenesis.

The utilisation of the transgenic mouse as a model to study the developing heart has been used to elucidate the role for TPM. The *Tpm1* heterozygous (+/-) knockout mouse was first described in 1997 by Rethinasamy *et al*. (Rethinasamy et al., 1997). A 50% reduction of *Tpm1* mRNA was achieved. However, at the protein level there was no change in Tpm1 expression, and no transcriptional upregulation of other TPM transcripts was seen. The authors suggested that the normal protein levels were maintained through increased translatability of *Tpm1* transcripts. Nonetheless, the +/- mice appeared normal, with no abnormal cardiac morphology and lived a full lifespan (Rethinasamy et al., 1997). Conversely, mating of the heterozygous litters to produce homozygous (-/-) knockouts resulted in non-viable offspring that died in utero between embryonic day E8 to 11.5 (Rethinasamy et al., 1997). Upon further analysis of these embryos at E9.5, it was found that the hearts were non-beating and had an abnormally thin ventricular wall with reduced trabeculae. In addition, myofibrils did not form in the cardiomyocytes with aberrant F-actin filaments dispersed.

TPMs have also been acknowledged for their role in myofibrillogenesis. In the axolotl *cardiac* (*c*) mutant heart, the hearts do not beat, TPMs are greatly reduced and the

cardiomyocytes lack sarcomeric myofibrils (Moore and Lemanski, 1982, Starr et al., 1989). The lack of myofibrils was rescued by the delivery of murine *Tpm1* cDNA to stage 36-39 mutant hearts (equivalent to HH11-12 in the chick heart) (Rugh, 1962) and the heart beat resumed in over half of these mutants (Zajdel et al., 1998).

Cardiomyopathy	Amino acid location	reference
Hypertrophic cardiomyopathy	V95A	(Karibe et al., 2001)
	D175N	(Thierfelder et al., 1994)
	E180G	(Thierfelder et al., 1994)
	E180V	(Regitz-Zagrosek et al., 2000)
	E62Q	(Jongbloed et al., 2003)
	L185R	(Van Driest et al., 2003)
	A63V	(Yamauchi-Takihara et al., 1996)
	K70T	(Yamauchi-Takihara et al., 1996)
	R21H	(Fokstuen et al., 2011)
	A22T	(Otsuka et al., 2012)
	A107T	(Otsuka et al., 2012)
	M281T	(Van Driest et al., 2003)
	D58H	(Frisso et al., 2009)
	I172T	(Van Driest et al., 2003)
	E192K	(Morita et al., 2008)
	S215L	(Morita et al., 2008)
	I284V	(Olivotto et al., 2008)
	D230N	(Lakdawala et al., 2010)
Dilated cardiomyopathy	K15N	(Hershberger et al., 2010)
	E23Q	(Hershberger et al., 2010)
	S16I	(Hershberger et al., 2010)
	I92T	(Hershberger et al., 2010)
	A239T	(Hershberger et al., 2010)
	A277V	(Hershberger et al., 2010)
	E40K	(Olson et al., 2001)
	E54K	(Olson et al., 2001)
	D230N	(Lakdawala et al., 2012)
	M8R	(Lakdawala et al., 2012)

	D84N	(van de Meerakker et al., 2013)
	A211G	(Lakdawala et al., 2012)
Left ventricular non-compaction	K37E	(Chang et al., 2011)
	R160H	(Hoedemaekers et al., 2010)
	K248E	(Probst et al., 2011)
	c.241-12_241-11delinsTG	(Hoedemaekers et al., 2010)
	D84N	(van de Meerakker et al., 2013)
	E192K	(Probst et al., 2011)
Restrictive cardiomyopathy	N279H	(Caleshu et al., 2011)

Table 1.3 A summary of *TPM1* mutations found in patients with cardiomyopathies.

1.6 Troponin T

The troponin complex, a multipart protein found in the thin filament, is made up of three components: troponins (Tn) C, I and T (Greaser and Gergely, 1971). TnC, as discussed in section 1.2.1, binds Ca^{2+} during muscle contraction, TnI is an inhibitory component of contraction and TnT is the TPM binding component (England and Loughna, 2013). Of the TnTs, three *TNNT* genes exist in the human, *slow skeletal TNNT* (*TNNT1*), *cardiac TNNT* (*TNNT2*) and *fast skeletal TNNT* (*TNNT3*). In addition, alternative RNA splicing adds another dimension of generating multiple isoforms of *TNNT*.

1.6.1 TnT Structure and Function

The role of TnT is to bind the troponin complex to TPM and actin, therefore acting as the glue, holding the thin filaments in contact. TnT is a 30–35-kDa protein that ranges from 223 to 305 amino acids in length due to varying isoforms. It is a comma in shape, located in the groove of the actin filament extending along it (Ohtsuki and Nagano, 1982). The N-terminal region of the protein varies in size between different isoforms and the first 1-59 amino acid residues of the N-terminus are enriched with negatively charged residues glutamine and aspartate (Figure 1.10) (Jin et al., 2008). Conversely, the C-terminus and middle portion of the protein are highly conserved and enriched with positively charged residues (Jin et al., 2008). There are two TPM binding domains, one of which is present at the N-terminus (known as T1 fragment) within residues 98-138 (Jin and Chong, 2010). The T1-subfragment is thought to bind to the C-terminus of the TPM in the region where TPM overlaps head to tail to form a continuous TPM filament (Pearlstone and Smillie, 1982). Residues 183-200 act as a flexible linker between the T1-fragment and the C-terminus (Takeda et al., 2003). The C-terminus of TnT is composed of α-helical rings at residues 204-220 (H1 which interacts with TnI) and 227-271 (H2 which interacts with TnC) (Takeda et al., 2003, Stefancsik et al., 1998). A second TPM binding domain (T2) is located closes to the C-terminus but controversy remains as to where it is located (either at residues 197-239 or the last 16 residues of the TnT sequence) (Pearlstone and Smillie, 1983, Jin and Chong, 2010, Morris and Lehrer, 1984, Franklin et al., 2012).

Figure 1.11 Comparison of human, mouse and chicken cTnT protein sequence.

The human cTnT protein sequence (NM_000364) was compared to the mouse (AB052890) and chicken (M10013) with various structural domains indicated on the human sequence. The sequences were aligned in Clustal W2 (Larkin et al., 2007, Goujon et al., 2010). cTnT is highly conserved within the 3 species, although with slightly more variation at the N-terminal end of the protein. The T1 domain, that binds the tail of tropomyosin is found at residues 98-136, while the T2 domain binding is thought to exist at the last 16 residues of the cTnT protein (highlighted grey) (Jin and Chong, 2010, Franklin et al., 2012). Underlined is a region known as the flexible linker of cTnT (Manning et al., 2011). The α-helical H1 and H2 domains are found in the C-terminus portion of the protein are are thought to interact with TnI and TnC, respectively (highlighted yellow) (Takeda et al., 2003, Stefancsik et al., 1998).

1.6.2 *TNNT2* expression in the developing heart

The human *TNNT2* gene, which encodes cardiac TnT protein (cTnT) is located on chromosome 1 and contains 17 exons, some of which can be alternatively spliced, leading to the creation of 4 different isoforms ($cTnT_1$, $cTnT_2$, $cTnT_3$ and $cTnT_4$). The differential splicing for some *TNNT2* exons is developmentally regulated, where cTnT isoforms 1, 2 and 4 are expressed in the human fetal heart, while isoform 3 is predominantly expressed in the adult heart (Anderson et al., 1991). Thus, some isoforms are present only in specific stages of development.

Expression of *Tnnt2* in the mouse is detected at ED7.5 in the cardiogenic field of the lateral plate mesoderm (Wang et al., 2001). As the heart tube forms, *Tnnt2* is expressed and restricted to the myocardium until ED16.5 (the latest embryonic stage investigated). Four isoforms of cTnt ($cTnt_{1-4}$) are expressed in the developing mouse heart by the alternate splicing of exons 2, 3a, 4 and 12 (Jin et al., 1996). $cTnt_1$ and $cTnt_2$ are initially expressed, however, a switch occurs at ED13.5, and $cTnt_4$ (and some $cTnt_3$) is expressed and persists in the neonatal and adult heart (Siedner et al., 2003).

Using whole mount *in situ* hybridisation, mRNA transcripts of *TNNT2* isoforms were first detected in the chick at HH4 in the region of the primitive streak (Antin et al., 2002). Expression of *TNNT2* was then observed in the pre-cardiac fields at HH5-6. By HH9, when cardiomyocyte differentiation is underway, *TNNT2* expression was present in the region of the heart tube and expression becomes restricted to the myocardium at HH12. However, when whole embryo homogenates (from stages HH4 to HH12) were analysed for cTnT protein expression by western blot, cTnT was not detected until HH9 at the onset of cardiomyocyte differentiation (Antin et al., 2002). As with the human and mouse, there is also an isoformal shift of *TNNT2* in the chick. Using 2D SDS-PAGE, the high molecular weight isoform of cTnT is expressed in the HH30-45 heart (day 7 to day 19 in the embryo) (Yonemura et al., 2002). However, in the neonatal and adult chick heart, the low molecular weight isoform of cTnT is predominantly expressed (Yonemura et al., 2002).

1.6.3 Troponin and cardiac dysfunction

In heart undergoing heart failure, the fetal isoforms ($cTnt_1$ and $cTnt_2$) are re-expressed at the mRNA and protein level (Anderson et al., 1995, Solaro et al., 1993). It has been suggested that this alternate splicing is important because different cTnT isoforms respond differently to cytosolic Ca^{2+} concentrations within the cell, and thus force development in the sarcomere (Gomes et al., 2002). They may also play a role in the inhibitory activity of the troponin complex in the absence of Ca^{2+} (Gomes et al., 2002). These data suggest not just a structural role for cTnT, but also a functional one.

Mutations in *TNNT* are said to be responsible for some cardiomyopathies in human. Although mutations of *TNNT2* commonly result in mild hypertrophy, they can cause sudden cardiac death (Watkins et al., 1995). Currently, over 90 mutations have been identified in troponin subunits associated with hypertrophic cardiomyopathy, dilated cardiomyopathy, left ventricular non-compaction and restrictive cardiomyopathy (Murakami et al., 2010, Parvatiyar et al., 2012), with over 50 of those found in the *TNNT2* gene. Mutations associated with hypertrophic cardiomyopathy and restrictive cardiomyopathy generally lead to increased Ca^{2+} sensitivity in the thin filament, while the mutations associated with dilated cardiomyopathy mainly decrease the Ca^{2+} sensitivity of the filament (Murakami et al., 2010). See Table 1.4 for a list of *TNNT2* mutations that play a role in cardiomyopathy.

Cardiomyopathy	Mutation	Reference
Hypertrophic cardiomyopathy	A27V	(Rani et al., 2008)
	A28V	(Curila et al., 2009)
	K66Q	(Olivotto et al., 2008)
	S69F	(Varnava et al., 2001)
	F70L	(Richard et al., 2003)
	P77L	(Varnava et al., 2001)
	I79N	(Thierfelder et al., 1994, Watkins et al., 1995)
	V85L	(Konno et al., 2004)
	D86A	(Van Driest et al., 2003)
	F87L	(Gimeno et al., 2009)
	I90M	(Xu et al., 2008)
	R92W	(Varnava et al., 2001, Van Driest et al., 2003, Moolman et al., 1997)
	R92Q	(Thierfelder et al., 1994, Watkins et al., 1995, Marian et al., 1997)
	R92L	(Varnava et al., 2001)
	R94C	(D'Cruz et al., 2000)
	R94H	(Ho et al., 2009)
	R94L	(Varnava et al., 2001, Varnava et al., 1999)
	K97K	(Gimeno et al., 2009)
	R102L	(Forissier et al., 1996, Richard et al., 2003)
	A104V	(Nakajima-Taniguchi et al., 1997)
	F110I	(Watkins et al., 1995)
	F110V	(Richard et al., 2003)
	F110L	(Olivotto et al., 2008, Torricelli et al., 2003)
	P120V	(Richard et al., 2003)
	K124N	(An et al., 2004)
	R130C	(Torricelli et al., 2003)
	ΔE160	(Watkins et al., 1995, Richard et al., 2003, Torricelli et al., 2003)
	E163K	(Watkins et al., 1995)
	E244D	(Watkins et al., 1995, Hershberger et al., 2008)
	N262S	(Ho et al., 2009)
	D271I	(Gimeno et al., 2009, Richard et al., 2003, Brito et al., 2012)
	K273E	(Konno et al., 2004)
	R278C	(Gimeno et al., 2009, Ho et al., 2009, Torricelli et al., 2003, Erdmann et al., 2003)

	R278P	(Erdmann et al., 2003, Miliou et al., 2005)
	R286H	(Van Driest et al., 2003)
	W287ter	(Richard et al., 2003, Brito et al., 2012)
	R293C	(Richard et al., 2003)
	W294ter	http://www.ncbi.nlm.nih.gov/clinvar/variation/177636/
	IVS15+1G>A	(Varnava et al., 2001)
Dilated cardiomyopathy	E96K	(Zeller et al., 2006)
	R131W	(Mogensen et al., 2004)
	R134G	(Hershberger et al., 2008)
	R139H	(Morales et al., 2010)
	R141W	(Li et al., 2001)
	R141Q	(Rani et al., 2008)
	R144W	(Rani et al., 2014)
	R151C	(Hershberger et al., 2008)
	R159Q	(Hershberger et al., 2008)
	R205W	(Hershberger et al., 2008)
	R205L	(Mogensen et al., 2004)
	ΔK210	(Daehmlow et al., 2002, Kamisago et al., 2000)
	D270N	(Mogensen et al., 2004)
Restrictive cardiomyopathy	ΔE96	(Peddy et al., 2006)
	E136K	(Kaski et al., 2008)
Left ventricular non-compaction	R131W	(Klaassen et al., 2008)

Table 1.4 A summary of *TNNT2* mutations found in patients with cardiomyopathies.

In the mouse, *Tnnt2* was ablated using homologous recombination gene targeting. The heterozygous mouse (*Tnnt2*$^{+/-}$) showed a mild decrease in *Tnnt2* mRNA, with no decrease in cTnt protein. A normal cardiac phenotype was also observed (Ahmad et al., 2008). The homozygous knockout mouse (*Tnnt2*$^{-/-}$) was not viable beyond ED 10.5. The study showed although cardiac looping occurred normally, there was no contractile activity in the heart, the ventricular myocardium was thin and the cardiomyocytes lacked sarcomeric organisation (Ahmad et al., 2008). In another model of gene knockout of *Tnnt2* using homologous recombination gene targeting, the heterozygous *Tnnt2*$^{+/-}$ mouse had a normal cardiac structure and function; normal life-span; although there was a moderate decrease in the amount of cTnt protein expressed. However this decrease was not statistically significant (Nishii et al., 2008). The *Tnnt2*$^{-/-}$ mouse also lacked a heartbeat and were embryonic lethal at ED10 and the heart appeared enlarged (Nishii et al., 2008). However, with this model there was defective looping of the heart. Internally, the endocardial cushions also failed to develop. At the ultrastructural level, myofibril disassembly was evident and likely caused by the lack of a heartbeat. Thin filament proteins (such as α-actinin, actin and TPM) were colocalised into Z disc like structures, indicating no role for cTnt in the formation of the thin filament (Nishii et al., 2008). However, the thin filament proteins failed to form sarcomeric structures with the thick filament (Nishii et al., 2008). Knockout animals are usually developed to evaluate phenotypic similarities to the human disease. However, homozygous knockout, as described above, can result in severe cardiac dysfunction resulting in lethality. In addition, heterozygous knockout models results in a 50% reduction of the targeted gene, rarely resulting in impaired cardiac dysfunction (Delic et al., 2008). Therefore, other methods of gene manipulation, such as antisense oligonucleotides (discussed in Section 1.8), should be investigated, rather than relying on knockout methods alone to investigate the role of genes during cardiac development.

Transgenic mice expressing low levels (<10%) of the R92Q mutation, which causes hypertrophic cardiomyopathy in human's, results in induced cardiac myocyte disarray, increased myocardial interstitial collagen content, and diastolic dysfunction (Tardiff et al., 1999). These phenotypes observed were almost identical to that seen in humans with the mutation (Maron et al., 1979), although the hypertrophic cardiomyopathy phenotype was absent. At higher levels of expression (30-92%), the hearts were significantly smaller, and

cellular disarray and fibrosis was evident compared to their control counterparts (Tardiff et al., 1999). They also demonstrate enhanced systolic function in the presence of diastolic dysfunction, resulting in hypercontractility of the heart, a common finding in patients with hypertrophic cardiomyopathy (Maron et al., 1979). Although no myofibril disarray was observed, sarcomeric shortening was apparent. In addition, alterations in mitochondrial morphology and increased mitochondrial numbers were seen (Tardiff et al., 1999). Transgenic mice expressing <10% of truncated *Tnnt2* at the C-terminus also display a small heart phenotype with diastolic dysfunction, however, the mice die within a few hours of birth (Tardiff et al., 1998).

A knockin mouse model of a dilated cardiomyopathy causing mutation, deletion mutation ΔK210, was used to determine the cause of pathogenesis in human (Du et al., 2007). The phenotype presents as early onset dilation of the ventricle with a high incidence of sudden cardiac death (Mogensen et al., 2004, Kamisago et al., 2000, Hanson et al., 2002). In this model, the mice developed enlarged hearts and heart failure with a high incidence of premature sudden cardiac death, just like the phenotype from human patients. In addition, there was a decrease in myofilament Ca^{2+} sensitivity of force generation, with no change in maximum force generation capability because of the increase in peak amplitude of Ca^{2+} transient in cardiomyocytes (Du et al., 2007).

A role for *Tnnt* in the Mexican axolotl (*Ambystoma mexicanum*; salamander) has also been investigated. The axolotl carries a recessive mutation in gene *c*, and in its homozygous recessive condition results in abnormal cardiac development (Humphrey, 1972). Phenotypically, these recessive mutant hearts fail to beat due to disorganised myofibrils and do not survive beyond stage 42 (20 days) (Fransen and Lemanski, 1989). TPM and TnT protein expression were dramatically decreased in the mutant hearts (Erginel-Unaltuna et al., 1995), as well as decreased total RNA levels compared to normal hearts due to aberrant splicing (Sferrazza et al., 2007).

Tnnt2 morpholino treatment in the Zebrafish did not affect the formation of Z-bodies, the initial structure for myofibrillogenesis, however, the Z-bodies never assembled further into pre-myofibrils (Huang et al., 2009).

The animal models discussed above have elucidated the importance of *TNNT2* in both the structure and function of the developing heart. However, the importance of *TNNT2* in the developing chick heart has not been investigated and may reveal some important aspects in relation to its role in the heart at very early stages of development and the important processes that are occurring, such as atrial septation, trabeculation of the ventricular chamber and myofibrillogenesis.

1.7 Chick as an animal model for cardiac development

In this thesis, embryonic domestic fowl (*Gallus gallus*) was used as an animal model. The embryonic chick holds the longest record in history as an experimental model for studying developmental biology (Table 1.5). Dating back to the ancient Egyptians, they have been used to observe the progression of embryonic development after different lengths of incubation. Hippocrates's and Aristotle's work on embryonic morphology (300BC) has been referred to up until the 19th century (Needham, 1959).

These animals have many advantages for their use. Firstly, they are cheap and readily available all year round. In addition, many eggs can be incubated together so that they are all the same stage at the same time and are still part of the same experimental group. Secondly, chick development is well documented throughout the literature. Therefore, if a specific stage of development is required it can easily be obtained in the lab (Hamburger and Hamilton, 1951). The extrauterine development of the chick allows for easy access to the embryo for *in ovo* manipulation rather than *in vivo*. Thirdly, with the development of approaches such as spatial and temporal gain and loss-of-function techniques (such as siRNAs and morpholinos) the chick can be genetically manipulated *in ovo*. For example, if a knockdown is being carried out using a morpholino, then the morpholino can be applied on top of the chick embryo once it has been exposed, with reasonable knowledge of the concentration being added to the embryo. Knockdown *in vivo* is difficult in the mouse as the morpholino cannot be applied directly to the embryos individually, and the morpholino can become diluted by the maternal vasculature (Siddall et al., 2002, Kanzler et al., 2003). Finally, the chick genome has been sequenced and is highly conserved to that of mammals (Wallis et al., 2004).

There are some disadvantages of using the chick as a model for human development. Although basic anatomical organisation is similar between the chick and the human during early embryogenesis, there remain some anatomical peculiarities. In the developing heart, during atrial septation, a septum primum develops from the cranio-dorsal wall of the atrium. However, the chick does not develop a septum secundum and the septum primum matures to form the atrial septum which closes within two days after hatching (Martinsen, 2005). The use of chick embryos for procedures such as gene editing, CRISPR (clustered regularly interspaced short palindromic repeats) or TALEN (Transcription activator-like effector nucleases) technology has not yet reached fruition. It is hoped that strategies for using these tools for genetic analysis will become available in the future.

Date	Concept	Discoverer(s)
1628	function of arteries and veins, proposed existence of capillaries	Harvey
1672–1675	neural tube, somites, capillaries	Malpighi
1817–1828	germ layers (ectoderm, mesoderm, endoderm)	Pander, von Baer
1868	the neural crest	His
1911	viruses cause cancer (Rous Sarcoma Virus)	Rous
1929	gastrulation cell movements (Polonaise)	Gräper, Wetzel
1932	extraembryonic endoderm (hypoblast) regulates embryo polarity/mesoderm induction	Waddington
1932	hemangioblast proposed (common precursor of endothelium and blood cells)	Murray
1932–1937	Hensen's node is the amniote organizer	Waddington
1936	first genetic map for the chicken	Hutt
1948–1968	Apical Ectodermal Ridge controls limb outgrowth	Saunders
1953	gut endoderm is derived from the epiblast via the primitive streak	Bellairs
1956	Zone of Polarizing Activity patterns the A/P axis of the limb	Zwilling, Saunders
1960–1968	T- and B-lymphocytes	Miller, Good, Glick, Claman
1964–1970	provirus hypothesis and reverse transcriptase	Temin
1967	contact inhibition	Abercrombie
1970	importance of extraembryonic endoderm (hypoblast) in head development	Eyal-Giladi and Wolk
1975 onwards	hemangioblast demonstrated	Dieterlen-Lièvre, Le Douarin
1976	first cellular oncogene (*c-src*)	Bishop and Varmus
1984	somites control segmentation of peripheral nervous system	Keynes and Stern
1985–1987	retinoic acid as a limb morphogen	Tickle, Eichele
1988	the notochord patterns the dorsoventral axis of the spinal cord	Van Straaten
1989	rhombomeres are embryologically and functionally important	Lumsden and Keynes
1991	DT40 cells undergo frequent homologous recombination	Buerstedde
1993	Sonic hedgehog patterns the spinal cord (D/V) and specifies motor neurons	Jessell
1993	Sonic hedgehog is the ZPA morphogen	Tabin
1995	a genetic cascade patterns the dorsoventral axis of the limb	Tabin
1995	a genetic cascade regulating left-right asymmetry	Tabin, Kuehn, Stern
1997	oscillating gene expression during somitogenesis	Pourquié

Table 1.5 Some major concepts discovered by work completed in the chick embryo. Taken from Stern, 2005 (Stern, 2005).

1.8 Anti-sense oligonucleotides 'Morpholinos' in vertebrate development

Oligonucleotides are sequence specific binding polymers that are capable of blocking translation of a mRNAs sense strand, thus, antisense oligonucleotides, resulting in a targeted inactivation. Initially, these oligonucleotides were developed for drug therapy in which a pathogen or disease could be targeted and inactivated. Many challenges remained for their therapeutic potential such as: good efficacy to attain an effective concentration within the cell; specificity so no other sequences were targeted by the oligonucleotide; the need to be stable within extracellular tissues, cell surface and intracellular proteins; deliverable; soluble in aqueous solutions; non-toxic at the therapeutic concentration and affordable (Summerton and Weller, 1997). First generation oligonucleotides contained natural genetic material with cross-linking agents ensuring irreversible binding to their targets (Zamecnik and Stephenson, 1978). However, the stability, efficacy and delivery of these were poor.

Summerton developed the morpholino structural type oligonucleotide which overcame these limiting properties of the early type oligonucleotides (Summerton, 1989, Summerton and Weller, 1993). Morpholinos differ from other antisense oligonucleotides such as Phosphorothioate-linked DNA (S-DNA) and short interfering RNA (siRNA), as these oligonucleotides rely on cellular RNase-H or the RNA induced silencing complex (RISC) to degrade the targeted RNA (Cohen, 1993, Saxena et al., 2003). On the other hand, morpholinos bind so strongly to the targeted RNA, preventing translation or post-transcriptional modifications, such as splicing, in a nuclease independent fashion. This is known as steric block (Summerton, 2007). Morpholinos are capable of knocking down gene expression, can modify RNA splicing (by the antisense sequence being designed to an exon-intron boundary) or can inhibit miRNA activity and maturation.

Morpholinos are composed of a 6-membered morpholino ring, which replaces the 5-membered-ring sugar backbone of naturally occurring nucleic acids. In addition, the negatively charged phosphate intersubunit linkages of nucleic acids is replaced with a non-ionic phosphorodiamidate intersubunit linkage (Figure 1.11) (Summerton and Weller, 1997).

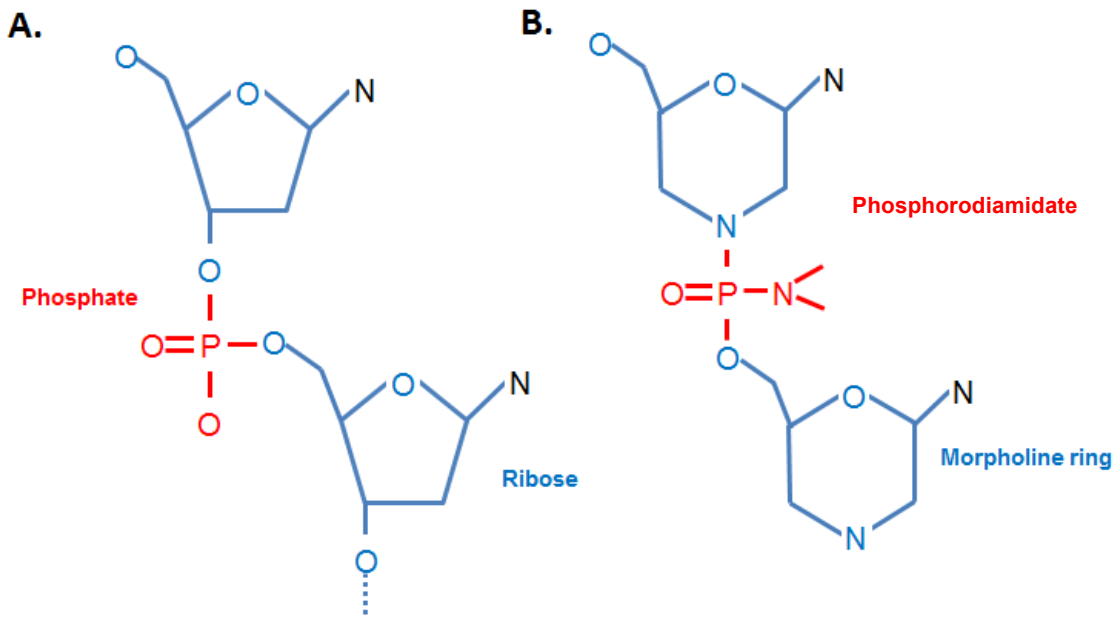

Figure 1.12 The structure of a morpholino.

A. The structure of DNA, with the ribose subunits linked together with a negatively charged phosphate (P). **B.** Morpholinos are composed of a morpholine rings linked together by a non-ionic phosphorodiamidate (P) intersubunit. N indicates the nucleic acid base (Adenine, Cytosine, Guanine or Thymine). Adapted from (Summerton, 2007).

1.9 Aims and Objectives of this study

A number of sarcomeric proteins have been shown to play a critical role in heart development. In addition, mutations in these proteins have led to abnormal cardiogenesis and CHDs (Ching et al., 2005, Budde et al., 2007, Matsson et al., 2008). Sarcomeric proteins TPM1 and cTnT have not been linked to CHDs. The primary aim of this project was to investigate a role for TPM1 and cTnT in the early developing heart. Antisense oligonucleotide morpholinos were used to down regulate expression of both proteins in the developing heart in a temporal manner, with the morpholino being applied once the heart tube has already formed. External and internal phenotypic examination and stereological analysis of embryos treated with morpholino were performed to determine if any gross morphological effects had occurred. From there, the ultrastructural and cellular effect of the morpholino treatment was investigated.

This project aims to provide greater insight into the role of TPM1 and cTnT in the developing chick embryonic heart.

Sequencing of the *TPM1* gene in a group of patients with a variety of CHDs revealed four novel mutations (work completed by Javier Granados-Riveron). This project aims to investigate the functional effect of these mutations in the developing heart using *in silico* and *in vitro* techniques.

It is hypothesised that reduced expression of TPM1 and cTnT leads to abnormal cardiac development and gross morphological abnormalities in the developing chick heart. Furthermore, a novel mutations discovered in *TPM1* is detrimental to normal *TPM1* mRNA modification.

Chapter 2 Materials and Methods

2.1 Animal husbandry

White fertile chicken eggs (*Gallus gallus*; Dekalb White strain; Henry Stewart, UK) were incubated at 38^{o}C in a humidified atmosphere and underwent constant rotation prior to opening (Bellairs and Osmond, 2005). The Hamburger and Hamilton (HH) staging system was used to age developing chicks (Hamburger and Hamilton, 1992). The eggs were incubated, unopened, until they reached the required age for each experiment. Once the incubation time was complete, a small window was made in the egg shell. 3-5ml of albumin was removed from around the embryo, avoiding the yolk and chorioallantois. This allowed the embryo to separate from all extra-embryonic membranes, which were removed, thus, exposing the embryo. This allowed for clear visualisation of the embryo so that it could be staged. Animal work was completed within national (UK home office) and institutional regulations and ethical guidelines.

2.2 Morpholino design

Antisense oligonucleotide morpholinos were designed against *TPM1* (ENSGALT00000039589; ATG start-site morpholino 5'TCCCGCGAGAAGTACAGCCGAAATC3'; exon1-intron 1 (E1I1) splice-site morpholino 5'GAGCAAGCAGGTCTGCACTGAGAGC3'; and exon4-intron 4 (E4I4) splice-site morpholino 5'TTCCCTGTGTCCCAAAACTGACCTC3'; GeneTools LLC, USA). An ATG start-site morpholino was designed to *TNNT2* (ENSGALT00000000401); 5' ACGACCTCTTCAGAGTCCGACATGC3'. In addition, a standard control (SC) morpholino was designed to mutated human *β-globin* (5'CCTCTTACCTCAGTTACAATTTATA3') (GeneTools). Morpholinos were tagged with fluorescein fluorescent tag. All morpholinos designed tested for sequence similarity using BLAST (http://blast.ncbi.nlm.nih.gov/) to ensure gene specificity.

2.3 Morpholino application and confirmation of uptake

Morpholino application was completed at either stage HH10/11 (referred to as HH11; approximately 47-50 hours of incubation) or HH19 (TPM1 ATG morpholino only; 78-82 hours of incubation; TPM1-morpholino treated hearts n=296 eggs; TNNT2-morpholino treated hearts n= 123 eggs; Untreated and standard controls n=429) (Bellairs and Osmond, 2005). Morpholino was applied to embryos at a concentration of 500μM suspended in 30% F127 pluronic gel (BASF Corp., Germany) and HBSS. For the TNNT2 study, morpholino was also applied at 250μM concentration for optimization of the morpholino concentration. This experiment had already been conducted in the laboratory for the TPM1 ATG morpholino (MRes student Diji Kuriakose). During this procedure, all pipette tips, pluronic gel and morpholinos were stored on ice to prevent thermogelation of the pluronic gel during application. Once the pluronic gel was applied, the eggs were resealed using masking tape and were reincubated with no rotation until they reached the age required (a further 28-30 hours for HH19 or 62-66 hours for HH24). Untreated controls (UT) were also included, in which the embryos underwent the same treatment as the experimental and SC groups, except morpholino/pluronic gel mix was not applied.

Once at the desired age, the embryos were harvested by cutting around the chorioallantois and placed into a petri dish with ice cold phosphate buffered saline (PBS). The chorioallantois and amnion were removed from the embryo as these membranes fluoresce due to the morpholino application technique. Morpholino uptake was confirmed for each embryo by detection of the fluorescein tag within the embryonic tissue using a SV11 stereomicroscope (Zeiss, Germany). Embryos positive for morpholino uptake were graded from one, not very positive, to five, very bright fluorescence, depending on how bright the fluorescein was. Only embryos that graded at three or above were used for further experiments, along with the UT controls.

2.4 Embryo tissue collection and processing

2.4.1 Embryo processing for phenotypic work

All embryos were externally examined at the time of harvesting. The overall gross morphology, structure and size of the heart was observed as well as the embryo as a

whole. Images were taken using Stemi SV11 stereomicroscope and camera (Zeiss). Embryos harvested and externally analysed were fixed at room temperature in 4% paraformaldehyde (PFA) in PBS for 1.5 hours for HH19 and 3.5 hours for HH24. Embryos were washed and stored in PBS overnight. The following day, embryos were washed with double distilled water (ddH_2O) to remove salts and dehydrated in 70-100% series of ethanol and cleared with xylene. Embryos were embedded in paraffin wax in a transverse orientation for sectioning. Each embryo was sectioned at 8μm using a Leica DSC1 microtome (Leica Microsystems, Germany) and serial sections were floated onto 42^{o}C ddH_2O for collection on glass slides. The glass slides used were 3-Aminopropyltriethoxysilane treated to ensure adhesion of the sections to the slides. Sections were dewaxed in xylene, rehydrated in a graded ethanol series, and stained with nuclear stain Mayer's Haemalum (Raymond Lamb, UK). Internal features such as atrial septa, endocardial cushions, cardiac jelly and ventricular trabeculae were examined. Analysis was performed blinded (unaware of the treatment the embryo received) using a Nikon Eclipse microscope (Nikon Instruments Inc., UK).

2.4.2 Immunohistochemistry on serially sectioned embryos

Immunohistochemistry was completed on non-morpholino treated embryos to show expression of TPM1 in the myocardium. Sections were deparaffinised and rehydrated in xylene and graded alcohol solutions, respectively. Antigen retrieval was performed by microwaving samples in 10mM sodium citrate (pH6) for 10 minutes. The sections were blocked with 5% goat serum and incubated with CH1 primary antibody (1:200) at room temperature for 1hour for the indirect immunohistochemistry method. After washing, an avidin-biotin phosphatase amplification kit was used to label the primary antibody with an avidin-biotin complex (StreptABComplex duet kit; Dako, Denmark). Slides were then incubated in 3,3`-diaminobenzidine reagent to develop the peroxidise bound to the avidin-biotin complex. Sections were counter-stained with Mayer's Haemalum (Raymond Lamb), dehydrated in graded ethanol and xylene, and mounted with DPX mounting media. Analysis was performed using a Nikon Eclipse microscope (Nikon).

2.4.3 Transmission electron microscopy

Chicks treated with TPM1 ATG-start site morpholino at HH11 and harvested at HH19 had the hearts dissected out and immediately fixed in 3% glutaraldehyde in Cacodylate buffer (TPM1 n=9, SC n=3, UT n=3). Hearts were post-fixed in 1% osmium tetroxide for 1 hour. The tissue was dehydrated in a graded ethanol series and incubated in 100% propylene oxide. Fresh resin was made up on the day of use consisting of 25ml Araldite CY212 resin (TAAB, UK), 15ml Agar 100 resin (Agar Scientific, UK) and 55ml of Dodecenyl Succinic Anhydride (hardening agent; TAAB). 2ml of Dibutyl phthalate was added to the resin mix to act as a softner (palsticizer; Agar Scientific). Each heart was infiltrated with the resin, orientated and polymerised for 48 hours at 60^{o}C. Samples were firstly sectioned semi-thin (0.5µm) using a glass knife to find a region of interest. The sections were collected onto glass slides and allowed to dry. The sections were stained with one drop of 1% toluidine blue for 1 minute on a hot plate at 90^{o}C and sections were washed with ddH_2O.

Once in a region of interest, samples were then sectioned ultra-thin (90nm) using a diamond knife (DiATOME, USA) in that region of interest. Ultra-thin sections were collected on copper grids and stained. Ultra-thin sections were stained using 50% methanolic uranyl acetate made up in 100% methanol for 10 minutes in the dark (stains proteins, nucleic acids and phospholipids). After rinsing the copper grids with the sections attached in 50% methanol and ultrapure water the grids were placed in a drop of Reynold's lead citrate for 30 seconds (increases the contrast of the uranyl acetate) (Bozzola and Russell, 1992). Sections were dried and visualised using the Tecnai 12 Biotwin TEM at magnifications 6000X-21000X (FEI, USA).

2.4.4 Proliferation and apoptosis study

ATG start site TPM1 morpholino or SC morpholino was applied to HH10/11 chick embryos, which were harvested at HH19 (n=7; described above in Section 2.3). UT and SC embryos were also included in the study (n=3, respectively). Embryos were fixed in 10% neutral buffered formalin (NBF) overnight at 4^{o}C, washed, dehydrated in graded series of ethanol and embedded in paraffin wax. Embryos were sectioned at 5µm using DSC1 microtome (Leica), where every 8th section was collected on poly-L-lysine slides

(Sigma-Aldrich). Sections were de-paraffinised by immersing the slides in xylene for 5 minutes twice, then rehydrated through graded alcohols. The sections were washed in ddH_2O and allowed to equilibrate in PBS for 5 minutes.

Proliferation study

Antigen retrieval was completed by heating the slides in sodium citrate buffer (pH6) for 1 minute below boiling. Cell proliferation was detected using Zymed's Proliferating Cell Nuclear Antigen (PCNA) staining kit according to manufacturer's instructions (Zymed Laboratories, USA) and all steps were completed at room temperature. In short, the slides were blocked using the blocking solution for 10 minutes. 100µl of the biotinylated mouse anti-PCNA primary antibody was added to each slide and incubated for 30 minutes in a humidified chamber. The slides were rinsed in PBS and 100µl of streptavidin peroxidase was added for 10 minutes. The slides were again rinsed in PBS and 100µl of 3,3`-diaminobenzidine chromagen was added for 3.5 minutes. Slides were immediately immersed in ddH_2O to stop the reaction. Slides were mounted in 100µl of VECTASHIELD HardSet Mounting Media with nuclear stain 4',6-diamidino-2-phenylindole (DAPI; Vector laboratories Inc., USA) and stored at 4^oC. As a negative control anti-PCNA antibody was replaced with PBS, while all other steps remained the same. Positive control slides of mouse ilium were supplied with the kit and stained alongside experimental chick sections.

Apoptosis study

Once tissue sections were rehydrated, they were digested in 20µg/ml of proteinase K for 20 minutes (Thermo Fisher Scientific). Sections were washed twice with dH_2O to remove the enzyme and then further pretreated in 3% H_2O_2 to quench endogenous peroxidase. The slides were again washed in dH_2O and then in PBS for 5 minutes. The following reagents were supplied by the ApopTag® Peroxidase *In Situ* Apoptosis Detection Kit (Millipore, USA). The sections were equilibriated in 75µl of equilibriation buffer for 1 minute and without rinsing, 55µl of working strength terminal deoxynucleotidyl transferase (TdT) enzyme was added to the sections. To spread the solution throughout the slide, a coverslip

of parafilm was gently applied on top of the liquid which allows to liquid to cover the entire slide by capillary action. The slides were placed in a humidified chamber and incubated at 37^{o}C for 1 hour. After the TdT incubation, the slides were transferred to stop/wash buffer to inactivate the TdT enzyme for 10 minutes. Slides were washed three times in PBS for 1 minute and 75µl of anti-digoxigenin peroxidase was added to the slides. Again, coverslips were mounted to the slides, and they were placed in a humidified chamber for 30 minutes at room temperature. The specimens were again washed three times in PBS for 2 minutes. 100µl of 3,3`-diaminobenzidine chromagen was added for 3.5 minutes and the specimen was immediately immersed in H_2O for 5 minutes. Slides were mounted in 100µl of VECTASHIELD HardSet Mounting Media with DAPI (Vector laboratories) and stored at 4^{o}C. As a negative control, TdT enzyme was replaced with PBS, while all other steps were followed. For a positive control, heart tissue was pre-treated with DNase I (3000U/ml; Qiagen).

Analysis of apoptosis and proliferation

Tissue sections were imaged using the Axioskop 2 mot plus (Zeiss) and Openlab (PerkinElmer, USA). Two images were taken in the ventricles and in the atria for each section, and one of the atrial septum when present. The total number of non-proliferating and non-apoptotic cells in each section was counted using the DAPI counterstain. This was also completed for the brown (3,3`-diaminobenzidine reactive) proliferating and apoptotic cells. A total of 47,747 and 44,297 cells were counted for the proliferation and apoptosis studies, respectively. The DAPI and 3,3`-diaminobenzidine reactive cells were added together to get a total cell number and the ratio of proliferating/apoptotic cells to total cell number was obtained for each heart. A test for significance was also conducted (Section 2.13).

2.5 Systematic Random Sampling of TPM1 and TNNT2 morpholino treated embryos

Systematic random sampling was used to quantify cardiac tissue proportions (HH11/19) and was completed on embryos processed in Section 2.4.1. Three groups were analysed; UT (TPM1 n=6; TNNT2 n=3), SC (TPM1 n=5; TNNT2 n=4) and TPM1/TNNT2-treated (TPM1

n=13; TNNT2 n=9). A 96 point grid was placed over every third section through the heart, and the tissue region and type on each point was identified (12,225 points counted for TPM1 study; 7,900 points counted for TNNT2 study). Contributions of the outflow tract (OFT), atrium and ventricle to the total heart size were initially measured by dividing the number of points counted in that region by the total number of counts for that heart. These were tested for statistical significance (Section 2.13).

Tissue contributions to OFT, atrium and ventricle were also examined. These tissues included: atrial wall, ECM, lumen and septum; ventricular wall, ECM and lumen; and OFT wall, ECM and lumen. The average tissue proportions were calculated by dividing the number of points counted for that tissue type divided by the number of points counted in that region. These proportions were also tested for statistical significance (Section 2.13).

2.6 Western blot

2.6.1 Protein quantification using pooled hearts

HH11 hearts were treated with TPM1 ATG morpholino as per section2.3. At harvesting, hearts were quickly checked for morpholino uptake, and three hearts from each treatment group (TPM1-treated n=9, SC n=9 and UT n=9) were pooled and snap frozen and stored at -80^{o}C until use. 250µl of 10mMTris/EDTA buffer was added to each sample and sonicated. Protein was quantified using a BCA Protein Quantification Kit (Abcam, UK). 50µl of loading buffer was added and samples were heated to 95^{o}C for 5 minutes. 15µg of protein was loaded on a 12% sodium dodecyl sulphate polyacrylamide gel and resolved at 60mA. Protein was transfer to a Hybond-C Extra nitrocellulose membrane (Amersham Biosciences, UK) via semi-dry transfer at 15Volts (V) in tris-glycine solution. Membranes were stained with ponceau-S stain (Sigma-Aldrich) to ensure transfer of the protein. Each membrane was blocked in 5% marvel semi-skimmed milk powder in 1X TBS with 0.1% Tween-20 (TBST) for 1h at room temperature. CH1 antibody was diluted in marvel/TBS in a 1:500 ratio (CH1 anti-mouse; detects striated muscle isoforms of tropomyosin; Developmental Studies Hybridoma Bank, USA) for 1h at room temperature followed by 1:1000 rabbit anti-mouse horseradish peroxidase conjegated secondary antibody (Dako). Membranes were washed in TBST and then incubated with enhanced Chemiluminescence

(Thermo Fisher Scientific). The membranes were placed against X-ray fim (Fugifilm, Japan) for 1 minute, and was then developed (Ilford, UK). To remove the bound antibody, the membranes were again washed in TBST to get rid of the enhanced chemiluminescence and then incubated with stripping buffer for 10 minutes (7.5g glycine, 0.5g SDS and 5ml Tween-20, made up to 500µl and at pH2.2). Membranes were neutralised in PBS and washed in TBST. Enhanced chemiluminescence was again added to the blots to ensure the bound antibody was removed and no signal was detected. Membranes were rinsed in TBST and blocked again in 5% marvel semi-skimmed milk powder in TBST and incubated in 1:2500 dilution of Glyceraldehyde 3-phosphate dehydrogenase (GAPDH; Abcam) over night at 4^{o}C and the following day incubated in 1:1000 rabbit anti-mouse horseradish peroxidase secondary antibody for 1h. Three 10 minute washes in TBST were carried out, and the protein bands were again detected by enhanced chemiluminescence detection method. All immunoblots were loaded with TPM1-treated, SC and UT samples (n=4 for all samples) and all experiments were carried out in triplicate.

2.6.2 Protein quantification of TPM1 ATG start-site or TNNT2 ATG start-site morpholino treatment in single hearts

Individual embryonic hearts from TPM1-treated (n=9), TNNT2-treated (n=4), SC (n=7) and UT (n=7) groups were isolated and snap frozen following treatment at HH11 and harvesting at HH19. Each individual heart was lysed in 60µl 10mM Tris/EDTA buffer containing protease inhibitors and using a syringe. 15µl of 6X loading buffer was added and samples were heart to 95^{o}C for 5 minutes. Samples were resolved by sodium dodecyl sulphate polyacrylamide gel in a 4-12% precast gel (Bio-Rad) at 175V along with Precision Plus Protein Dual Color Standards (Bio-Rad). Gels were transferred onto nitrocellulose membrane at 100V for 1 hour.

For the TPM1 study, the membranes were blocked for 1 hour at room temperature in 5% marvel semi-skimmed milk powder in TBST. Blots were incubated in CH1 mouse antibody (DSHB) at a concentration of 1:200 overnight at 4^{o}C and 1hour at room temperature. As a loading control, blots were incubated with 1:500 rabbit monoclonal Histone H3 (Cell Signalling Technology Inc., Massachusetts) overnight at 4^{o}C.

For the TNNT2 study, nitrocellulose membranes were blocked in 10% bovine serum albumin TBST for 1 hour at room temperature, followed by overnight incubation with CT3 anti-mouse antibody (1:10 dilution; DSHB) at 4^{o}C and 1 hour at 37^{o}C. As a loading control, blots were incubated with 1:2000 rabbit polyclonal GAPDH (Abcam) for 1 hour at room temperature.

For both studies, two secondary antibodies with different infrared properties were used. IRDye® 680RD was used to detect CH1 or CT3 and IRDye® 800CW was used to detect Histone H3 or GAPDH (LI-COR biosciences, Germany). All immunoblots contained TPM1-treated or TNNT2-treated samples, SC samples and UT samples, which were carried out in triplicate. The immunoreactive bands were visualised using an Odyssey infrared imaging system (LI-COR biosciences) and fluorescent intensities of the bands were gathered for statistical analysis.

2.7 RNA work

2.7.1 Tissue isolated for RNA

The chorioallantoic membrane (chorioallantois) was cut around the embryos using autoclaved scissors. The embryos were placed in ice cold DEPC treated PBS and the hearts were removed from the embryo using sterile autoclaved forceps. Hearts were removed from the chicks at HH12, 14, 19, 22, 24, 26, 34, neonatal (day 1) atrium and ventricle, and adult atrium and ventricle and placed in RNase free micro-centrifuge tubes. Neonatal and adult tissue was obtained from Dr. Siobhan Loughna according to national and institutional guidelines. The heart tissue was snap frozen in liquid nitrogen and stored at -80^{o}C.

2.7.2 RNA Extraction

RNA was extracted using an RNeasy Micro kit (Qiagen, UK) for HH12-HH26 hearts following manufacturer's protocol. 150µl of buffer RT with β-mercaptoethanol was added to <5 mg of tissue and homogenize using a 1ml syringe (Becton Dickinson, USA) with a 0.5mm x 16mm Microlance needle (Becton Dickinson). 295µl of RNase-free water was

added to the homogenate with 5µl Proteinase K solution (100µg/ml; Qiagen) and mix thoroughly. Each lysate was incubated at 55°C for 10 minutes and then centrifuged for 3 minutes at 10,000g at room temperature to obtain a pellet of cell debris and unlysed material. The supernatant was removed and placed in a new RNase-free tube avoiding the pellet. 0.5 volumes of ice cold 100% ethanol was added to the lysate, and the lysate mixture was transferred to a RNeasy MinElute spin column placed in a 2ml collection tube that was supplied with the kit. The tube was centrifuged for 15sec at 8000g (same for all centrifugations unless otherwise stated) and the flow-through was discarded. 350µl of the Buffer RW1 was added to the spin column and centrifuged to wash the spin column membrane.

All lysates were DNase treated at this stage. 10µl of *DNaseI* (1500 Kunitz Units; Qiagen) was added to 70µl of Buffer RDD to make the DNaseI incubation mix and was directly added to the RNeasy MinElute spin column membrane. The lysates were left to incubate on the benchtop for 15 minutes. Another 350µl of Buffer RW1 was added to the RNeasy MinElute spin column and centrifuged. The flow-through was discarded along with the collection tube. After placing the spin column into a new collection tube, 500µl of Buffer RPE was added and centrifuged to wash the spin column membrane. 500µl of 80% ethanol was then added to the spin column and centrifuged for 2 minutes. The flow-through was again discarded along with the collection tube. The spin column was place in a new collection tube, and centrifuged at 13,000g for 5 minutes with the lids open to get rid of residual ethanol. The spin column was then transferred to a 1.5ml collection tube and 14µl RNase-free water was added directly to the centre of the membrane and centrifuge for 1 minute at 13,000g to elute the RNA. The concentration of the RNA was measured using NanoDrop 2000c UV/IV spectrophotometer at 260nm absorbance (Thermo Fisher Scientific, USA).

HH34, neonatal and adult heart tissue was homogenised in 1ml ice-cold Tri-reagent (Sigma-Aldrich, USA). The homogenates were incubated for 5 minutes at room temperature to permit complete dissociation of nucleoprotein complexes. 0.2ml of 1-bromo-3-chloro-propane (BCP; Sigma-Aldrich) was added to the homogenates and vigorously mixed. Homogenates were centrifuged at 10,000g for 15 minutes at 4^{o}C in order to separate the mixture into two phases. The upper (aqueous) phase was carefully

transferred to a fresh tube, while avoiding contamination within the interphase and lower phase containing DNA and proteins, respectively. The RNA was precipitated out of the upper phase by adding 0.25ml 2M sodium acetate (pH 4) and 0.7ml of 100% isopropanol (Fisher Scientific UK Ltd., UK), and storing at -20^{o}C for 30 minutes.

The precipitate was collected by centrifugation for 10 minutes at 10,000g at 4^{o}C. The RNA pellet was washed twice with 70% ethanol and resuspended in 87.5µl of DEPC-treated H_2O. 2.5µl of *DNaseI* and 10µl RDD buffer per sample (Qiagen) was added to the RNA and incubated for 10 minutes at room temperature. 300µl of DEPC-treated H_2O was added along with 400µl of phenol/chloroform/isoamyl alcohol (Sigma-Aldrich). The mixture was centrifuged at 10,000g for 10 minutes at 4°C. Again, the upper phase was removed and transferred to a fresh tube. The RNA was precipitated by the addition of 1/10 volume of 3M sodium acetate (pH 5.2) and 2 volumes of absolute ethanol. The lysate was incubate at -20°C for 20 minutes. The precipitated RNA was pelleted by centrifugation at maximum speed for 10 minutes, washed with 70% ethanol and resuspended in 50µl DEPC-treated H_2O (ddH_2O). The concentration of the RNA was measured using NanoDrop 2000c UV/IV spectrophotometer at 260nm absorbance (Thermo Fisher Scientific).

2.7.3 Reverse Transcription of mRNA

Reverse transcription (RT) reactions were performed using SuperScript® III Reverse Transcriptase (Invitrogen, UK) following manufacturer's instructions. An RT mixture was made by mixing 200ng of Hexamer solution, 1µg total RNA, 10mM dNTPs and 13µl of ddH_2O in an RNase-free tube. The mixture was heated to 65^{o}C for 5 minutes and cooled on ice. 1X reverse transcriptase buffer, DTT, RNase OUT and 1µl superscript III enzyme (200U/µl) was added to the RT mixture to give a total volume of 20µl. The reaction was heated to 25^{o}C for 5 minutes and then to 50^{o}C for 1h. The mixture was finally heated to 70^{o}C for 15 minutes to deactivate the enzyme and store at -20^{o}C.

2.8 Primer Design and Polymerase Chain Reaction Protocols

2.8.1 *TPM1* and *TNNT2* expression profiles and polymerase chain reaction

Primers were designed to all *TPM1* isoforms (ENSGALT00000039589 Table 2.1). Primers were designed to specific isoforms of chick *TPM1* (*TPM1α*: ENSGALT00000039589; *TPM1κ*: substituting in exon 2 of ENSGALT00000006394) (see Table 2.1 for primer pairs and PCR conditions) using the online website Primer3 (http://primer3.ut.ee/) (Untergasser et al., 2012, Koressaar and Remm, 2007). Primers were also designed to chick *TPM4* using a sequence available from (Fleenor et al., 1992).

Primer pairs were designed to *TNNT2* gene (ENSGALT00000000401; Table 2.1) utilising the presence/absence of exon 5 in the embryonic and postnatal chick heart. The RT control used was *GAPDH*.

Polymerase chain reaction (PCR) was performed using Red Taq® DNA polymerase (Sigma-Aldrich). PCR reactions were conducted in 20µl reaction mixtures comprising of 1X PCR buffer, 1.5mM $MgCl_2$, 0.5mM deoxynucleotide mix (dNTPs), 0.5µM of forward and reverse primer, 0.05U of DNA polymerase, 10ng of cDNA made up to a 20µl volume with ddH_20.The PCR reaction was carried out using a T100 thermal cycler (Bio-Rad laboratories Inc., USA). The cycling program began at 94^oC for 2 minutes to heat activate the DNA polymerase. This was followed by 35 cycles of 94^oC for 30 seconds, and annealing temperature cycle specific to each primer set (see Table 2.1), a 72^oC extension time, and a final single extension time of 8 minutes. All PCR cycling conditions for each primer pair can be seen in Table 2.1.

b-	GGCTCTGCAAAAGAAGCTGA	CATGGAAGTCATATCGTTGAGAG	721	57	2.0
a-	TTGTGCAATTGGAAAAGCAA	CATGGAAGTCATATCGTTGAGAG	725	57	1.5
wn	AGAGCAGAGCAGGCTGAGAC	TTTCACTTCGGACACCTC	507	56	-
-	CGGACTCTGAAGAGGTCGTT	GAAGGTGAATCAAAGCCCAA	235/178	58	-
-6	CCTCTCTGGCAAAGTCCAAG	CATCCACCGTCTTCTGTGTG	500	58	-

Table 2.1 A list of primer pairs and annealing temperatures used for expression profiles.

2.8.2 Splice donor-site mutation

Gene specific primers were designed to the 5'upstream region and exon 2a of *TPM1* (ENST00000403994; forward primer 5'gggggcaggagaaaaaag3'; and reverse primer 5'TTGGCGGCGGCCTCTTC3'). The forward and reverse primers also contained additional *NheI* and *KpnI* linkers, respectively. Genomic DNA was obtained from the affected patient, with a heterozygous splice-donor site mutation at the exon1-intron1 boundary and a *tgt* insertion within intron1 on the opposite strand (see Figure 2.1). DNA was also obtained from an ethnically matched control. Consent was attained from all participants and work was approved by local ethics committees. A PCR product was obtained using the following PCR reaction: 1µl of each primer, 50ng of DNA, 15µl of Extensor Long Range PCR Enzyme mastermix (a proofreading polymerase; Thermo Fisher Scientific) and made up to 30µl ddH_2O. The PCR was run at 95^{o}C for 5 minutes, and then 95^{o}C 30 sec, 59.7^{o}C 45sec and 72^{o}C for 3 minutes for 30 cycles.

ıgram illustrating the alternate splicing of *TPM1*, giving rise to *TPM1α* and *TPM1κ* isoforms (full ectively).

within intron 1-2a: c.116+2T>C (indicated as T>C) and a *tgt* insert. Primers were designed to amplify the ient containing these mutations (PR1 in the 5' upstream region and PR2 in exon 2a). Five stop codons are S72, S204, S348, S357 and S366) in the 1st open reading frame. The ATG start-site and the untranslated . E indicates exon.

2.8.3 Gel Electrophoresis

PCR products were run on 2% agarose gels (Sigma-Aldrich), prepared with 1X Tris-acetate-ethylenediaminetetraacetic acid buffer and 1X ethidium bromide. 8µl of PCR product was loaded onto the gel, with 5µl of 1Kb plus ladder (Invitrogen) and were run at 150V for 40 minutes. The gels were visualized under UV light using GeneGenius Bioimaging System (Syngene, UK) and photographed.

2.8.4 PCR clean up

PCR reactions were purified using the GenElute™ PCR Clean-Up Kit (Sigma-Aldrich). The PCR products were loaded on a spin column containing a silica membrane. DNA from the PCR product binds to the membrane, where it is washed and cleaned. The concentrated DNA was eluted in 30µl ddH_2O. Purified PCR products were sent for sequencing analysis (Biopolymer Synthesis and Analysis Unit, University of Nottingham).

2.9 Preparation of constructs for mutational analysis

2.9.1 Ligation and Transformation

Splice-site mutation

Once amplicons containing the splice donor-site mutation, the *tgt* insertion and wild-type were obtained (Section 2.8), they were ligated into pGEM-T Easy vector (Promega, UK) at a 3:1 molar ratio of PCR product:vector and left at 4^{o}C overnight. 2µl of the ligation mixture was added to 30µl of DH5α competent cells. The tube was gently flicked to mix the two components and left on ice for 30 minutes. The mixture was incubated at 42^{o}C for exactly 2 minutes and returned to ice. 950µl of Super Optimal broth with Catabolite repression (SOC) media was added and the reaction was incubated at 37^{o}C for 1 hour. The reaction was spun for 1 minute to generate a cell pellet, which was resuspended in 200µl of SOC and plated out on Luria broth (LB) with 100µg/µl of Ampicillin agar plates. The plates were incubated upside down overnight at 37^{o}C.

The following day, colonies were picked and inoculated in 5ml of LB (with 100ng/ml ampicillin). Cultures were grown overnight at 37^{o}C at 200 rotations per minute (RPM).

Cultures were minipreped using the GeneElute Miniprep Kit (Sigma-Aldrich) and sent for sequencing (Source Bioscience) to check we had vectors containing the splice donor-site mutation, the *tgt* insertion and that the wild-type had the correct sequence.

2.9.2 Digest of inserts and expression vectors

Splice site mutation

To obtain an expression vector containing the TPM1 inserts, pcDNA3.1(-) was singly digested with two enzymes (Figure 2.2). Firstly, pcDNA was digested with *KpnI* in the following reaction: 2µl of the pcDNA vector, 3µl of NEB buffer 1, 3µl of 10X bovine serum albumin, 2µl of *KpnI* (15 U/µl; NEB, UK) made up to 30µl with ddH_2O. The reaction was incubated at 37^oC for 3 hours. It was loaded on a 0.8% agarose gel and run at 150V for 40 minutes. The band was cut out under minimal UV light to visualize the band. The band was extracted from the gel and purified using GeneElute Gel Extraction Kit (Sigma-Aldrich) and eluted in 30µl ddH_2O. For the second digest, 22µl of the eluted vector was mixed with 3µl of NEB buffer 2, 3µl of 10X bovine serum albumin, 2µl of *NheI* (15U/µl) made up to 30µl with ddH_2O. The reaction was incubated at 37^oC for 3h. The reaction was, again, run on a 0.8% agarose gel. The band was extracted and purified using the gel extraction kit and eluted in 30µl ddH_2O. T-vector containing the TPM1 inserts with the splice-site mutation, *tgt* insertion and wild-type were double digested with 1µl of *NheI*, 1µl *KpnI*, 2µl NEB buffer 1 and 2µl of 10X bovine serum albumin in a 20µl reaction. This reaction was incubated for 3 hours at 37^oC. Similarly to the pcDNA digestion, the reactions were run out on a 0.8% agarose gel and purified.

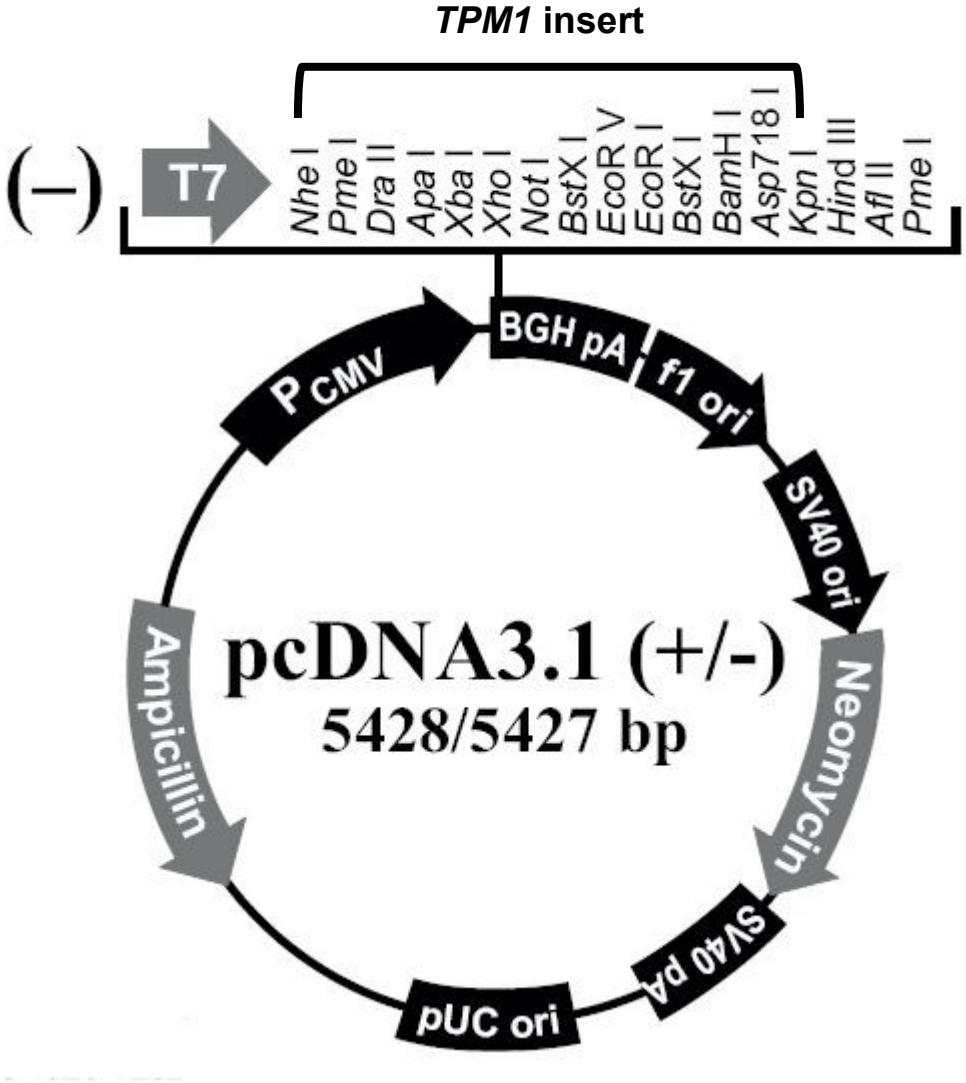

Figure 2.2 pcDNA3.1 (-) with either: TPM1-WT, TPM1-tgt or TPM1-T>C inserted at the *NheI* and *KpnI* sites.

2.9.3 Ligations and transformations

Once the inserts and vectors were digested, they were ligated using 1µl of T4 DNA ligase (40U/µl; NEB), 2µl of DNA ligase buffer, 3µl of vector and 14µl of the insert. For a negative control, the insert was replaced with ddH_2O. The reactions were left on the bench for 30 minutes and transferred to 16^{o}C overnight.

The following day, 2µl of the ligation was added to 30µl of DH5α competent cells. The mixture was left on ice for 30 minutes and heat shocked at 42^{o}C for exactly 2 minutes. The mixture was returned to ice and 950µl of SOC was added. The cells were left in a water bath at 37^{o}C for 2 hours. The DH5α mixture was plated on LB-Ampicillin (100ng/µl) agar plates. The plates were incubated upside down for 16 hours at 37^{o}C.

After overnight growth, colonies were individually picked and inoculated in 5µl of LB broth containing Ampicillin. The cultures were grown overnight at 37^{o}C rotation at 200 rotations per minute (RPM). Cultures were minipreped using the GeneElute Plasmid Miniprep Kit (Sigma-Aldrich) and and each miniprep was digested using the enzymes above to check and see if an insert 'fell out' from the vector. Constructs containing the correct insert size were sequenced to check inserts were correct (Source Bioscience). Glycerol stocks were made from the remaining cultures at a 1:1 ration of glycerol:culture and stored at -80^{o}C.

2.9.4 Maxiprep

Using the glycerol stocks from section 2.9.3, cultures were streaked out on LB-Ampicillin plates and incubated overnight at 37^{o}C. The following day, colonies were picked and inoculated in 5ml LB broth with Ampicillin. The cultures were grown at 200RPM at 37^{o}C for 10 hours. 1ml of this culture was then added to 100ml of fresh LB broth and grown overnight at 200RPM. Each culture was centrifuged at 4000g for 10 minutes to pellet the cells. Using the GeneElute Endotoxin-free Plasmid Maxiprep Kit (Sigma-Aldrich), the plasmid was isolated from the cells and eluted in 2ml of ddH_2O.

2.10 Cell lines and tissue culture

2.10.1 Cardiac cell micromass

Isolation of cell micromass from embryonic chick hearts

White fertile chicken eggs were incubated for 6 days (HH26) at 38^{o}C in a humidified atmosphere and underwent constant rotation prior to opening. Six eggs were washed with trigene (Tristel Solutions Ltd, UK) and swabbed with IMS and placed in a clean and sterilised class II Laminar flow hood. Forceps, scissors, ice box and necessary tools were also sprayed with IMS and transferred to the hood. A window was opened in the egg exposing the developing embryo. 3-5ml of albumin was removed from the egg allowing the embryo to separate from extra-embryonic membranes. An incision was made around the chorioallantoic membrane of the embryo so the embryo could be picked up and transferred to a 90mm petri dish containing ice cold Hank's Balanced Salt Solution (HBSS). The heart was immediately removed from the embryo using straight forceps and placed in prepared 1:1 horse serum/HBSS in a 15ml falcon tube, which was then placed on ice. This method was repeated for 40 hearts. Once explanted, they were washed twice with 5ml HBSS to remove the horse serum and placed in 500µl warm trypsin/EDTA. The mixture was incubated at 37^{0}C, 5% CO_2 for 20 minutes, with gently agitation for five minutes. During this time, the micromass embryonic cardiomyocytes culture medium was prepared. 10% heat inactivated fetal bovine serum (FBS), 2mM L-glutamine and 50uU/ml penicillin/50µg/ml streptomycin was added to 500ml Dulbecco's Modified Eagles Medium (DMEM) and nutrient mixture F-12 HAM. This medium can be kept in at 4^{0}C

and utilised for no more than two weeks. The hearts were triturated several times until they disappeared and a homogenous suspension was obtained. To neutralise the trypsin, 8 ml of culture media were added to 2ml trypsinised hearts suspension. The suspension was centrifuged for 5 minutes at 1500rpm. The supernatant was aspirated and the packed cells pellet was resuspended with 2ml of warm culture media. Using a haemocytometer to count the cells, the cells density was determined to be 4×10^5 cells/ml. The cell suspension was pipetted at the middle of the well of a 24 well plate containing glass coverslips. The cells were left in the 5% humidified CO_2 incubator at 37^{o}C for 2 hours to allow attachment to the coverslips before adding 500µl of warm culture medium.

In-vitro morpholino application to cardiomyocyte micromass

TPM1 ATG start-site or TNNT2 ATG start-site morpholinos (Section 2.2) was pre-heated to 65^{o}C for 5 minutes to ensure morpholino was completely suspended in HBSS. 2.5µl of the morpholino was added to 250µl of pre-warmed micromass embryonic cardiomyocytes culture medium. 3µl of Endo-Porter (GeneTools) was added to the mixture and the solution was mixed by pipetting. SC morpholino and no treatment were used as controls. The culture media was removed from the cardiomyocyte micromass and 250µl of the morpholino mixture was added to the well. Another 250µl of fresh pre-heated culture media was also added to the well leaving a 10mM morpholino concentration in each well. Cells were left for 48 hours in a 5% CO_2 humidified incubator at 37^{o}C.

Immunofluorescence and visualization of cell micromass

Culture media was removed from the cardiac cell micromass and were washed twice with 500µl PBS. The cells were fixed for 10 minutes in 4% PFA at room temperature and washed again with PBS. Cells were permeabilised with 200µl of 0.2% Triton-X 100 in PBS for 10 minutes at room temperature and washed with PBS. The cells were blocked for 1 hour at room temperature with 5% goat serum. The CH1 (anti-TPM1 antibody; used in TNNT2 study) and CT3 (anti-TNNT2 antibody; used in the TPM1 study) polyclonal mouse primary antibodies (Developmental Studies Hybridoma Bank, USA) were prepared at a 1:50 dilution in 0.1% bovine serum albumin in PBS. 200µl of the antibody mixture

was added to the wells and incubated overnight at 4^{o}C. The antibody was removed by washing the cells three times with PBS. The goat anti-mouse secondary antibody, Alexafluor 594 (Thermo Fisher Scientific) was also prepared in 0.1% bovine serum albumin in PBS at a dilution of 1:1000 and 200µl of the mixture was added to each well and left for 40 minutes at room temperature. Cells were also stained with Hoechst to indicate nuclei. The cells were finally rinsed with PBS and the coverslips were mounted on glass slides with 2µl of Fluorogel Mounting Medium (GeneTex, USA). Cells were protected from light at all times during the procedure and stored at 4^{o}C in slide box. Examination of the cells was completed within two weeks. Cells were visualised using the DMIRE2 inverted microscope (Leica) and imaged using the Velocity^{TM} 6.3 (PerkinElmer).

Analysis of morpholino treated cells *in vitro*

After cardiac micromass cells treated with morpholino were imaged, cells positive for CH1 or CT3 antibody were considered as cardiomyocytes. Cardiomyocytes positive for morpholino uptake were included in the study. The assembly of the sarcomere was divided into four stages. Stage one consisted of cells with positive staining around the periphery of the cell but no sarcomeric structures can be clearly seen, especially around the nucleus. Stage 2 cardiomyocytes contain assembled sarcomeres, however, they appear thin and disorganised. Stage 3 cardiomyocytes present with organised sarcomeres that appear thin but are organised and run parallel to one-another. Finally, stage 4 cardiomyocytes contain mature cardiomyocytes with thick bands running through the cell.

2.10.2 COS-7 cells

COS-7 cells were cultured in Dulbecco's Modified Eagle's Medium (Invitrogen) supplemented with 10% Foetal bovine serum (FBS) and 1% Penicillin-Streptomycin (Invitrogen). Cells were grown at 37^{o}C in a 5% CO_2 humidified atmosphere and were passaged every 4 days by detaching the cells from the flask with 0.05% 1X Trypsin/EDTA (Invitrogen) and reseeded at a ratio of 1:10.

COS-7 cells were seeded at $1.6x10^6$ in 100mm culture dishes (Corning, USA) 24h prior to transfection. Cells were approximately 70% confluent when transfected. To each dish, 6µg of plasmid DNA was added to 220µl of media (without FBS and Penicillin-Streptomycin) and 40µl of Polyfect transfection reagent (Qiagen). The cells were incubated for 10 minutes at room temperature and then added to the cells along with 8ml of DMEM growth media. Cells were incubated for 48h with transfection mixture. For each construct, three transfection experiments were carried out. As a positive control, COS-7 cultures were transfected with 'empty' pcDNA vector.

The cells were harvested after 48h post-transfection, washed in PBS and stored at -80^oC. RNA was extracted using Tri-reagent (Sigma-Aldrich) and RT was performed as described in Section 2.7. Primers were designed to the 5'upstream region and exon 2a of *TPM1* (Forward primer 5'gtattggctgtcttgaggaatg3'; reverse primer 5'GAGAAGTTGCTGCGGGTGT3') to indicate whether transcription of the genomic insert had occurred in the cells. β-actin primers were designed as a control (forward primer 5'ACTCCATCATGAAGTGTGACG3'; reverse primer 5'CATACTCCTGCTTGCTGATCC3'). PCR reactions were set up as follows: 4µl of GoTaq buffer (5X), 0.5mM dNTPs, 0.5µM of forward and reverse primer, 0.05U GoTaq® DNA polymerase (Promega), 1µl DNA made up to 20µl with ddH_2O. The first PCR was carried out at 94^oC for 2 minutes followed by 94^oC 30 seconds, 58.5^oC for 30 seconds, 72^oC 80 seconds for 27 cycles with a final extension time at 72^oC for 8 minutes. As there was genomic contamination, the extension time was decreased to 50 seconds for each cycle. Products were resolved on 2% agarose gels against Hyperladder I (Bioline) and visualized on the GeneGenius Bioimaging System (Syngene).

2.11 Microinjection of embryonic chick hearts

2.11.1 Optimization of the microinjecting

White fertile chick eggs were incubated at 38^oC in a humidified incubator as described in Section 2.1 until they reached HH11, HH14 and HH19. A window was opened in the eggs to expose the embryo and albumin was removed to separate the embryo from the extra-embryonic membranes. The HH19 embryos were left out of the incubator for 2 hours prior

to injection to slow down the heartbeat. Following a published protocol (Ishii et al., 2010), a transfection mixture was prepared as follows: 4µg pEGFP-C1 vector (Clontech Laboratories Inc., USA), 10µl Lipofectamine in 50µl OptiMEM, (Life Technologies Inc., UK), and 0.5µl Fast Green. 4µl of the transfection mixture was loaded into a glass needle that was prepared by heating the centre of the borosilicate glass capillary tubes under a Bunsen burner and pulling the ends apart while the glass is molten. The glass needle was attached to a picospritzer (Parker Hannifin, USA).

Once the tip of the needle was visualised under the SMZ1500 stereomicroscope (Nikon) at 8X magnification, the sealed tip of the needle was broken using a forceps and the drop size was optimised to 3nl per injection using a graticule. The transfection reagent was injected into the pericardial sac of the HH11, HH14 and HH19 embryos. The HH19 embryos received 15, 20 or 25 injections to see if increasing the amount of reagent results in increased transfection. The amount of Lipofectamine was also optimised at 10, 15 and 20µl. Embryos were placed in the humidified incubator at 38^{o}C for 24 hours.

When embryos were harvested, they were checked for positive GFP fluorescence using a SV11 stereomicroscope (Zeiss). GFP fluorescence was graded for 1-5 stars, 1 being low transfection efficiency and 5 the highest efficiency.

2.11.2 Whole mount immunohistochemistry of microinjected embryos

Once the embryos had been checked for GFP, they were fixed for 1.5 hours in 4% PFA. The embryos were transferred to a 96 well plate to limit the amount of reagent used. The embryos were washed three times for 30 minutes in PBS containing 1% Triton-X. Embryos were blocked twice for 1 hour in 10% normal goat serum and 1% Triton-X in PBS. An anti-GFP antibody (GFP-12A6; Developmental Studies Hybridoma Bank) was made up at 1:50 in blocking buffer and the embryo was incubated for 3 days at 4^{o}C undergoing gentle rotation. Embryos were washed for 1 hour 3 times in blocking buffer, and a further 3 times for 10 minutes in PBS with 1% Triton-X. The secondary antibody, polyclonal goat anti-mouse immunoglobulins/ horseradish peroxidase (Dako), was made up at 1:100 in blocking buffer and incubated with the embryo for 2 days at 4^{o}C under gentle rotation. After washing the embryos in PBS, 1% 3,3`-diaminobenzidine was added

to 0.3% H_2O_2 PBS. This 3,3`-diaminobenzidine reaction was added to the embryos until a colour reaction was seen. The 3,3`-diaminobenzidine solution was then quickly removed and embryos were rinsed in PBS. Embryos were imaged using a SV11 stereomicroscope (Zeiss).

2.11.3 Harvesting and fixing embryos for cryosectioning to check GFP location in a transfected heart

24 hours post transfection, the embryos were removed from the egg by cutting around the chorioallantois and placed in ice cold PBS. The membranes were removed under a SV11 stereomicroscope to visualise the embryo and embryos were checked for fluorescence of the GFP. Embryos that tested positive for transfection were scored according to their level of fluorescence on a scale of 1-5 stars.

To check the location of the fluorescence inside the cell, embryos were fixed in 4% PFA for 30 minutes, washes with PBS and transferred to 30% sucrose until the embryos sank to the bottom of the solution. The embryos were transferred to individual 1cm moulds and orientated so that the right side of the embryo was facing down. The mould was filled with Optimum Cutting Temperature Compound to embed the embryo and placed on dry ice until the compound set. The moulds were transferred and stored in a -80^{o}C freezer. Embryos were sectioned at 10µm using a cryostat (Leica) and sections containing the heart were collected and stored at -20^{o}C.

Sections were rehydrated in PBS and mounted in 100µl of VECTASHIELD HardSet Mounting Media with DAPI (Vector laboratories). Sections were stored in the dark at 4^{o}C. The transfected embryonic hearts were visualised using the DMIRE2 inverted microscope (Leica).

2.11.4 Quantification of GFP by immunohistochemistry on microinjected hearts

Microinjected embryos with a fluorescent score of 5 were fixed and processed according to Section 2.4.1. The embryos were sectioned at 8µm (see Section 2.6) and every third section was collected. The slides were left to dry at 42^{o}C overnight. Sections were deparaffinised in xylene, re-hydrated in a graded series of ethanol and rinsed in dH_2O.

Tissue sections were permeabilised with 0.1% Triton-X 100 in PBS for 30 minutess and rinsed with dH_2O. Sections were blocked with 10% normal goat serum with 1% bovine serum albumin for 1 hour at room temperate. Without rinsing the sections, GFP-12A6 monoclonal anti-mouse antibody was added to the sections made up with 1% bovine serum albumin in PBS at a 1:10 dilution and incubated for 1 hour at 37^{o}C. Sections were rinsed with PBS and incubated for 1 hour at room temperature with Alexa Fluor 448 at 1:100 dilution in 1% bovine serum albumin in PBS. All incubations were completed in in a humidified chamber. Sections were rinsed with dH_2O and mounted with VECTASHIELD heard-set mounting media with DAPI (Vector Laboratories).

Images were taken of 3 areas of the ventricular chamber and 3 parts of the atrial chamber throughout the heart. The total number of DAPI cells and GFP positive cells were counted and divided to obtain the percentage of GFP positive cells (5,919 cell nuclei counted).

2.12 In silico analysis of novel mutations found for *TPM1*

In silico analysis of the four novel mutations of TPM1 was carried out to investigate the potential damaging effects these mutations may have. This was done using three online mutation-predicting programs; Polyphen-2 (http://genetics.bwh.harvard.edu/pph2/), SIFT (Sorting Intolerant From Tolerant; http://sift.jcvi.org/) and MutationTaster (http://www.mutationtaster.org/). Polyphen-2 and SIFT programs were used to predict whether or not the non-synonymous substitutions were likely to affect protein structure, and in turn, function. MutationTaster on the other hand, predicts mutational affects from the DNA sequence of the gene.

2.13 Statistics

Levene's test for equality of variances was used followed by a t-test for equality of means on SPSS V21.0 (SPSS Inc, USA). Where appropriate, the mean ± standard error of the mean was calculated.

Chapter 3 Investigating a role for *TPM1* in the developing chick heart

3.1 Overview

The use of developing chick embryos has the potential to give insight on how the dynamic heart develops, and the effect genetic manipulation has on development. This chapter describes the *in ovo* manipulation of *TPM1* and the phenotypic and structural outcomes of this manipulation. The aims of the experiments were to:

- show the overall expression of *TPM* isoforms in the developing and post-hatch chick heart
- determine if *in ovo* delivery of TPM1 specific morpholinos resulted in an abnormal morphology in the developing heart
- assess functionally the consequence of TPM1 morpholino application leading to an abnormal phenotype using apoptosis and proliferation studies
- investigate at the cellular level the consequence of TPM1 morpholino application to cardiomyocytes in culture
- to develop a protocol by which *in ovo* gene rescue can be achieved using microinjection

Three morpholinos were designed to *TPM1*, one targeting translation via the ATG start-site, while the remaining two targeting splicing via exon1-intron1 (E1I1) and exon4-intron4 (E4I4) boundaries. Morpholinos were applied *in ovo* to the developing embryo. Phenotypic and structural analyses were conducted after serial sectioning of the treated hearts. Potential mechanisms resulting in the abnormal morphology were investigated.

Recently, *in ovo* over-expression of genes in the developing heart was achieved using a microinjection technique (Ishii et al., 2010). Using this method, this technique was optimised with the intention to achieve a rescue after morpholino treatment.

3.2 mRNA expression of *TPM1* and *TPM4*

RT-PCR expression profiling was performed for all isoforms of *tropomyosin 1* (*TPM1*), and more specifically for *TPM1α* and *TPM1κ* isoforms, during critical stages of cardiogenesis (HH12, HH14, HH19, HH22, HH24, HH26 and HH34) and in the neonatal and adult heart. Primer pairs were first optimised using HH24 whole embryo cDNA. A primer pair was designed that was specific to all isoforms of *TPM1*, including; striated muscle, smooth muscle, fibroblast, non-muscle and brain (Table2.1). PCR revealed expression of *TPM1* throughout embryonic development and in the neonatal and adult heart (221 base pairs; Figure 3.1Ba). Due to the alternate spicing of *TPM1*, *TPM1α* and *TPM1κ* were identified separately using primers specific to each isoform (see Figure 3.1A for the alternate spicing of *TPM1* striated muscle isoforms). When looking more specifically at striated muscle isoforms of *TPM1*, *TPM1α* and *TPM1κ* were present at all stages analysed in the embryonic chick (721 and 725 base pairs, respectively); conversely, expression was absent in the neonatal and adult atria and ventricles (Figure 3.1Bb and c). RT (-) and PCR (H_2O) controls were negative and *Glyceraldehyde 3-phosphate dehydrogenase* (*GAPDH*) was utilised as a loading control (500 base pairs; Figure 3.1Be).

TPM4 expression was also examined as it is known to be expressed in the adult chick heart (Fleenor et al., 1992). Primers were designed to *TPM4* from a published sequence on ENSEMBL (www.ensembl.org; accession number ENSGALT00000039281; Table 2.1) The sequences obtained from the PCR product were aligned with the published sequence for *TPM4* and sequences were homologous (Figure 3.2). These results show that *TPM4* is also expressed in the chick heart. An expression profile of *TPM4* was then conducted for the developing and postnatal chick heart. *TPM4* is expressed at the early stages of heart development (HH12) and is continuously expressed throughout development as well as in the neonatal and adult chick heart (507 base pairs; Figure 3.1Bd). In addition, *TPM4* was also aligned against *TPM1* to compare homology in the sequences (Figure 3.3). *TPM1* and *TPM4* are 82% homologous, showing the similarity of the two mRNA transcripts produced by two separate genes.

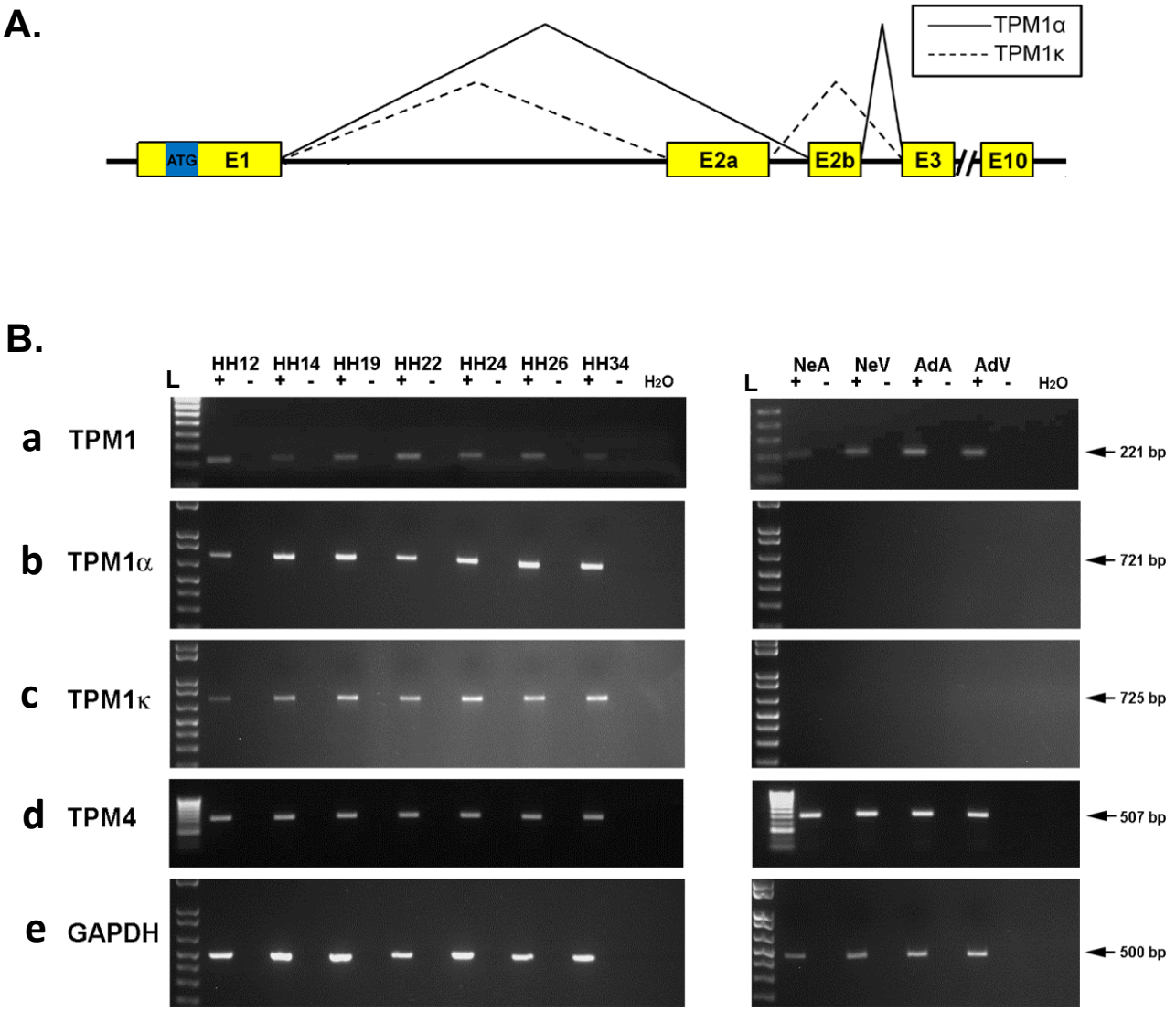

Figure 3.1 Figure 3.1 Expression profile of Tropomyosin in the chick heart.

A. A schematic diagram of *TPM1*, where exons 2a and 2b are alternatively spliced in *TPM1α* and *TPM1κ*. **B.** Primers designed to all isoforms of TPM1 showed expression in the embryonic stages of development as well as in the neonatal and adult atrium and ventricle (a). Primers designed specifically to striated muscle isoforms TPM1α and κ showed expression in the embryonic heart, but not the neonatal and adult (b and c). TPM4 is expressed in the embryonic chick heart as well as in the neonatal and adult (d). *GAPDH* was used as a loading control (e). L indicates ladder; +, RT; -, no RT; Ne, neonatal; AD, adult; A, atrium; V, ventricle; H_2O, water control; bp, base pair.

```
ENSGALT00000039281      AGAGCAGAGCAGGCTGAAACGGATAAGAAGGCAGCTGAGGACAAATGCAAACAGGTCGAG
TPM4_primer2            AGAGCAGAGCAGGCTGAGACGGATAAGAAGGCAGCTGAGGACAAATGCAAACAGGTCGAG
TPM4_primer1            ------------------------------------------------------------

ENSGALT00000039281      GATGAGCTGGTAGCTCTGCAGAAGAAGTTGAAAGGAACTGAAGATGAGCTGGATAAATAC
TPM4_primer2            GATGAGCTGGTAGCTCTGCAGAAGAAGTTGAAAGGAACTGAAGATGAGCTGGATAAATAC
TPM4_primer1            ----------------------------------------GAAGATGAGCTGGATAAATAC
                                                                  ********************

ENSGALT00000039281      TCTGAGGCTCTGAAAGATGCCCAGGAAAAGCTGGAGCAGGCTGAAAAGAAGGCCACGGAT
TPM4_primer2            TCTGAGGCTCTGAAAGATGCCCAGGAAAAGCTGGAGCAGGCTGAAAAGAAGGCCACGGAT
TPM4_primer1            TCTGAGGCTCTGAAAGATGCCCAGGAAAAGCTGGAGCAGGCTGAAAAGAAGGCCACGGAT
                        ************************************************************

ENSGALT00000039281      GCAGAAGGTGAGGTGGCGGCGCTCAACAGACGCATCCAGCTGGTGGAAGAGGAGCTGGAT
TPM4_primer2            GCAGAAGGTGAGGTGGCGGCGCTCAACAGACGCATCCAGCTGGTGGAAGAGGAGCTGGAT
TPM4_primer1            GCAGAAGGTGAGGTGGCGGCGCTCAACAGACGCATCCAGCTGGTGGAAGAGGAGCTGGAT
                        ************************************************************

ENSGALT00000039281      CGGGCCCAGGAGCGGCTGGCCACAGCCCTGCAGAAGCTGGAAGAGGCCGAAAAAGCGGCG
TPM4_primer2            CGGGCCCAGGAGCGGCTGGCCACAGCCCTGCAGAAGCTGGAAGAGGCCGAAAAAGCGGCG
TPM4_primer1            CGGGCCCAGGAGCGGCTGGCCACAGCCCTGCAGAAGCTGGAAGAGGCCGAAAAAGCGGCG
                        ************************************************************

ENSGALT00000039281      GATGAGAGTGAGAGAGGAATGAAAGTCATTGAGAACAGAGCAATGAAAGATGAAGAAAAA
TPM4_primer2            GATGAGAGTGAGAGAGGAATGAAAGTCATTGAGAACAGAGCAATGAAAGATGAAGAAAAA
TPM4_primer1            GATGAGAGTGAGAGAGGAATGAAAGTCATTGAGAACAGAGCAATGAAAGATGAAGAAAAA
                        ************************************************************

ENSGALT00000039281      ATGGAAATTCAGGAAATGCAGCTGAAGGAGGCCAAGCACATCGCTGAGGAGGCCGACCGC
TPM4_primer2            ATGGAAATTCAGGAAATGCAGCTGAAGGAGGCCAAGCACATCGCTGAGGAGGCCGACCGC
TPM4_primer1            ATGGAAATTCAGGAAATGCAGCTGAAGGAGGCCAAGCACATCGCTGAGGAGGCCGACCGC
                        ************************************************************

ENSGALT00000039281      AAATACGAAGAGGTTGCCCGCAAGTTGGTGATTTTGGAGGGGGAGCTGGAAAGAGCTGAA
TPM4_primer2            AAATACGAAGAGGTTGCCCGCAAGTTGGTGATTT-GGAGGGGGAGCTGAAAAGGGG----
TPM4_primer1            AAATACGAAGAGGTTGCCCGCAAGTTGGTGATTTTGGAGGGGGAGCTGGAAAGAGCTGAA
                        ********************************* ************.****.*

ENSGALT00000039281      GAGCGCGCAGAGGTGTCCGAAGTGAAATGCAGTGACCTTGAAGAGGAGTTGAAGAATGTC
TPM4_primer2            ------------------------------------------------------------
TPM4_primer1            GAGCGCGCAGAGGTGTCCGAAGTGAAA----------------------------------
```

Figure 3.2 Alignment of PCR product sequences from primers 1 and 2 with *TPM4* transcript available on ENSEMBL .

The sequence obtained from the PCR product was aligned with a *TPM4* transcript published on ENSEMBL (ENSGALT00000039281). There is 100% homology between the sequences. The primer pair used to obtain the PCR products are underlined.

Figure 3.3 Alignment of TPM1 and TPM4 to show homology.

TPM1 and TPM4 sequence are highly homologous (82%). Base pairs highlighted in yellow indicate primers designed for all isoforms of TPM1. The grey base pairs indicate the TPM4 primer pairs and the underlined primers are designed specifically to TPM1α.

3.3 Protein expression of TPM1

To look at the protein expression of TPM in the chick heart at different ages, an antibody designed to TPM1 cardiac and skeletal muscle (CH1) was used. However, the epitope of this antibody is unknown, but is thought to target exon 9a of TPM1. Since the homology of TPM1 is known to be similar to TPM4 (Figure 3.3), there is a possibility CH1 antibody can detect both TPM1 and TPM4. Therefore, the following results investigate the expression of both TPM1 and TPM4 in the chick heart at different developmental ages

Immunohistochemical staining with CH1 antibody showed positive staining throughout the myocardial wall of the early heart tube at HH12 and HH14 (Figure 3.4a and b). Positive staining was also seen in the atrial (including septum), atrio-ventricular canal, ventricular (including trabeculae) and OFT myocardium in stage HH19, 24, 26, and 34 embryos as well as in the neonatal atrium and ventricles (Figure 3.4c-h). No staining was seen in the cardiac jelly, endocardium or endocardial cushions other than the haemalum counterstain. Non-specific binding was not seen in the negative control heart where the primary antibody was omitted (Figure 3.4i).

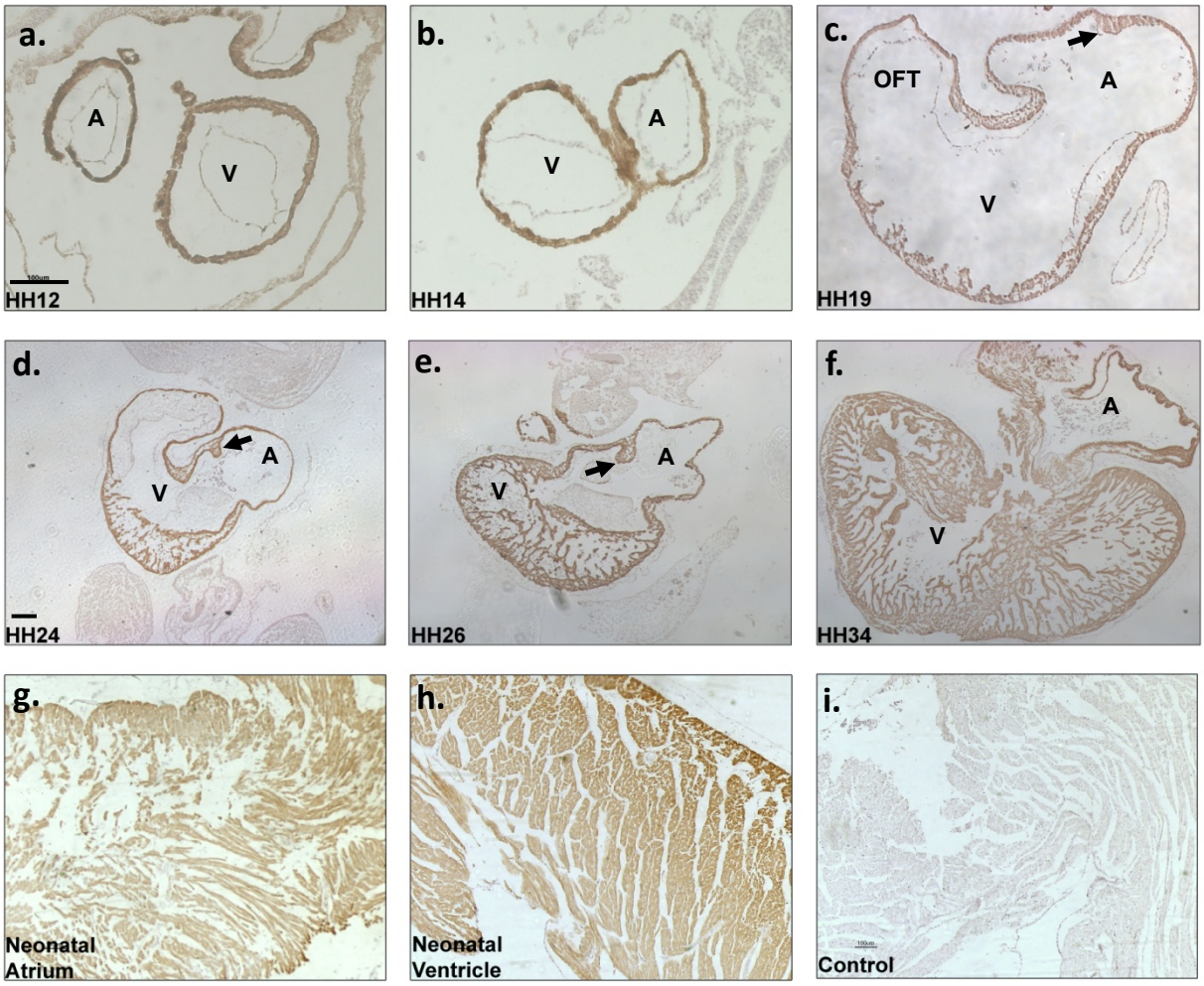

Figure 3.4 Expression of TPM in the chick heart.

The CH1 antibody was used to detect TPM expression in the heart. TPM expression is brown, while the counterstain, Mayer's Haemalum stains light purple. Expression was seen at all stages including HH12, HH14, HH19, HH24, HH26, HH34, neonatal atrium and neonatal ventricle (a-h). Antibody reactivity was restricted to the myocardium of the hearts and no expression was seen in surrounding tissue including the endocardium, endocardial cushions and cardiac jelly. No reactivity was seen in the negative control (i). A indicates atrium; V, ventricle; OFT, outflow tract; arrow, atrial septum. Scale bars indicate 100μm; scale bar in a is same for b and c and scale bar in d is same for e-i.

3.4 Embryo grouping, survival and morpholino uptake

TPM1-morpholino delivery was completed at two ages: 1) delivery at HH10/HH11 and harvested at HH19 (HH11/19), or 2) delivery at HH19 and harvesting at HH24 (HH19/24). The HH11/19 embryos were analysed for survival and uptake of each morpholino used. Survival rates for untreated (UT) chick embryos (n=81), standard control (SC) group (n=92) and TPM1-morpholino treated group (ATG n=52; E1I1 n=36; E4I4 n=35) were 91.4%, 89.1% and 88.6%, respectively (*P*=0.98, no significant differences). Surviving embryos were examined for 'morpholino uptake' determined by the degree of fluorescence. 68.3% of the SC and 88.1% of the TPM1-treated embryos were considered positive (*P*=0.76, no significant difference).

In the HH19/24 study, embryos were treated with the ATG morpholino only. The survival rate was 100% for the embryos receiving TPM1 morpholino (n=14), 87.1% for SC embryos (n=31), and 71.4% for UT embryos (n=21; *P*=0.236, no significant difference). Embryos were again examined for morpholino uptake. Morpholino uptake was 64.3% for TPM1-morpholino embryos, and 66.7% for SC embryos.

3.5 Looping defects were present upon TPM1-treatment

At the time of harvesting, all embryos were observed at high and low magnifications, to ensure they had developed correctly. Images were taken of the heart at high and low magnifications, with photos being taken on the left and right hand sides of the embryo. Particular features studied were atrium and ventricle size, cardiac looping, length of the OFT, and any misplacement of the heart components. The UT and SC groups all appeared normal (n=137; Table3.1; Figure3.5Aa and b). Upon application of TPM1 morpholino at HH10/11 and harvesting at HH19 (HH11/19), the external phenotype of the embryonic hearts appeared normal for the majority of embryos (92/96, 96%; Figure 3.5Ac and d). However, of the 4% that appeared abnormal (2/36 ATG, 1/31 E4I4 and 1/29 E1I1; Table 3.1) the hearts appeared to be distorted dextrally, indicating a looping defect (Table 3.1; Figure 3.5Ae and f). Nevertheless, the overall size of the OFT, ventricle and atrium looked normal in these hearts.

For the HH19/24 study, all control and TPM1-treated embryos appeared to have a normal external phenotype (SC n=18, UT n=15, and TPM1-treated n=9; Figure 3.5Ba-c).

ype†	looping		ext						int
ontrol	-	137	137	-	-	60	-	-	60	60
PM1 .TG	2	34	36	1	11	17	1	12	16	29
PM1 4I4	1	30	31	-	7	7	-	8	6	14
PM1 1I1	1	28	29	-	9	17	-	5	21	26
ontrol		33	33						10	10
PM1 .TG		9	9						8	8

Table 3.1Summary of phenotypic analysis after treatment with TPM1 morpholinos.

Assessment of heart shape based on qualitative analysis of gross morphological features.
Qualitative assessment of atrial septa and degree of trabeculation obtained from serial histological sections.
* Stage of development when treatment/harvesting performed.
† Control embryos include standard control and untreated; TPM1 denotes embryos treated with tropomyosin 1 ATG or splice site morpholino.
‡ Total number of embryos analysed externally and internally.
Ab, abnormal; ext, externally; int, internally.

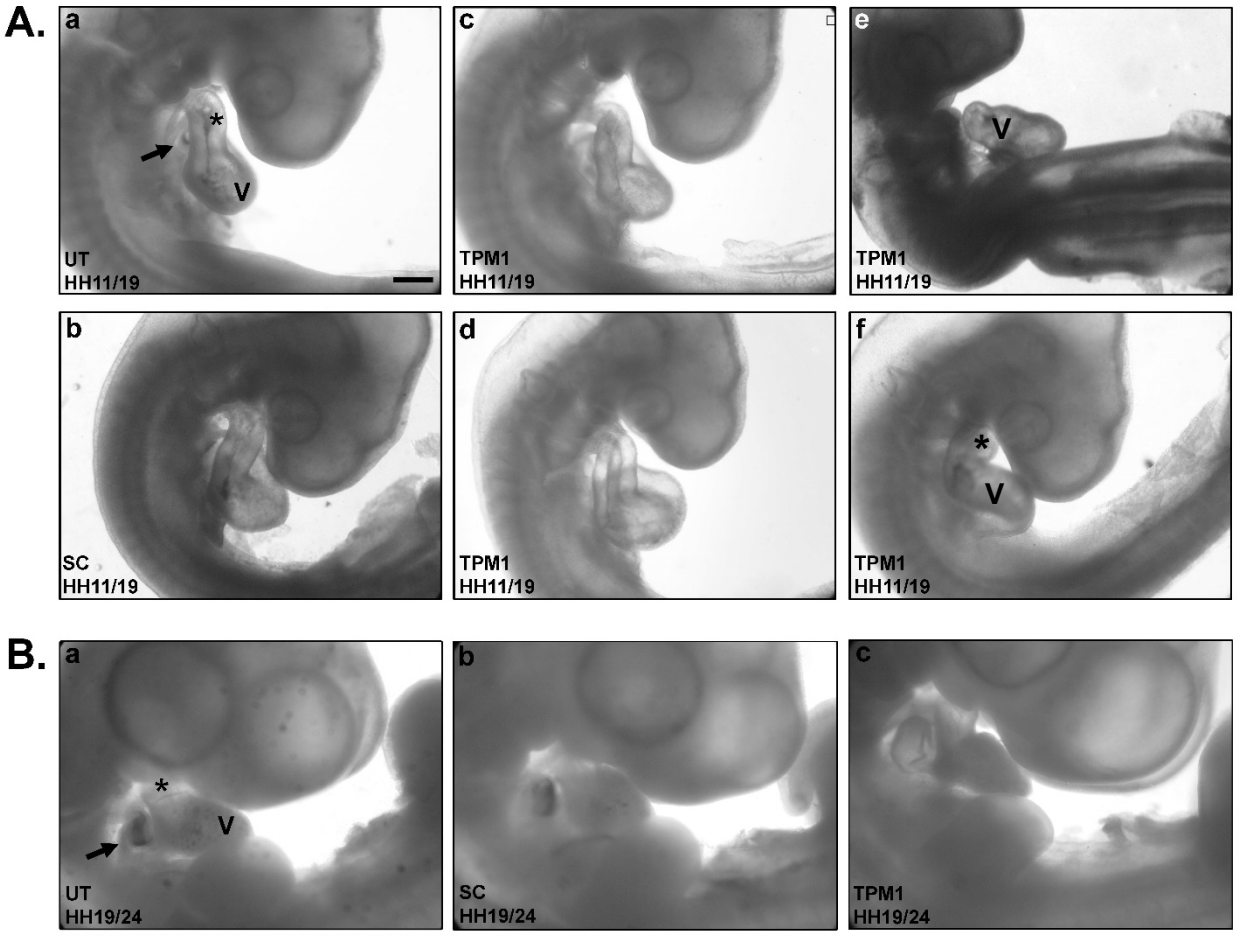

Figure 3.5 External analysis of TPM1 treated embryos at HH11/19 and HH19/24.
A. HH11/19 embryos that are untreated or SC treated display normal external phenotype (a and b). This is true for the majority of TPM1-morpholino treated embryos (c and d). In a small proportion of TPM1 morpholino treated embryos the external heart appears to be abnormally looped with the ventricle appearing dextrally (e and f). **B.** HH19/24 embryos all appear to have a normal external appearance (a-c). * indicates outflow tract; V, ventricle; arrow, atrium; UT, untreated; SC, standard control; TPM1, TPM1-morpholino treated.

3.6 TPM1-treatment results in abnormal atrial septa in the HH11/19 heart

HH11/19 embryos were serially sectioned in a transverse orientation to observe internal structures. The septum emerges from the roof of the atrial wall, extending into the atrial chamber towards the atrioventricular canal. The atrial septa appear to develop normally in all the controls (n=60; Table 3.1; Figure 3.6a and b). However, in 41% of the morpholino treated embryos, the septum appeared small and resembled a knuckle shaped outgrowth from the atrial myocardium (ATG n=11/29, E1I1 n=9/26, and E4I4 n=7/14; Table 3.1; Figure 3.6c). The septum can be observed at higher magnification in Figure 3.6d-f.

One ATG morpholino-treated embryonic heart displayed a remarkable septal phenotype with the initiation of a second atrial septum from the dorso-cranial wall of the atrium (1.4%; Figure 3.7). Firstly, there was the appearance of the septum proper (Figure 3.7a); soon after, a second septum appeared to the right (Figure 3.7b). These septa progressed in size, achieving close to normal septal length, however, both still appeared slightly smaller than usual (Figure 3.7c and d). Finally, the septa fused towards the posterior heart wall of the atrium (Figure 3.7e and f).

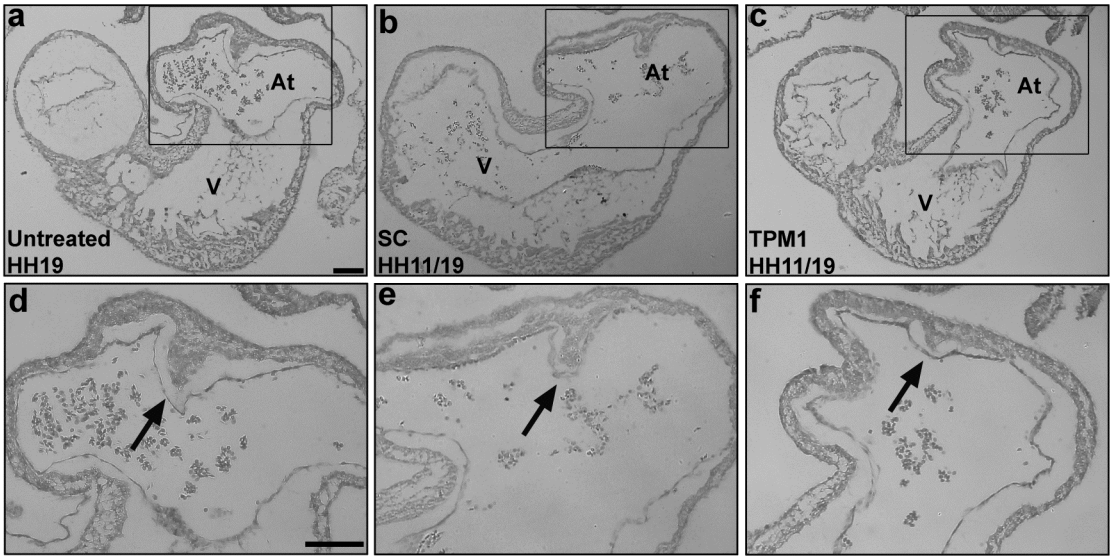

Figure 3.6 TPM1-morpholino treatment at HH11 results in reduced atrial septum size. Normal septation initiation and growth can be seen in the untreated and standard control embryos (a,b,d and e). TPM1-treated embryos have reduced atrial septa size (c and f). At indicates atrium; V, ventricle; arrow, septum. Mag bars indicate 100µm in a-c and d-f.

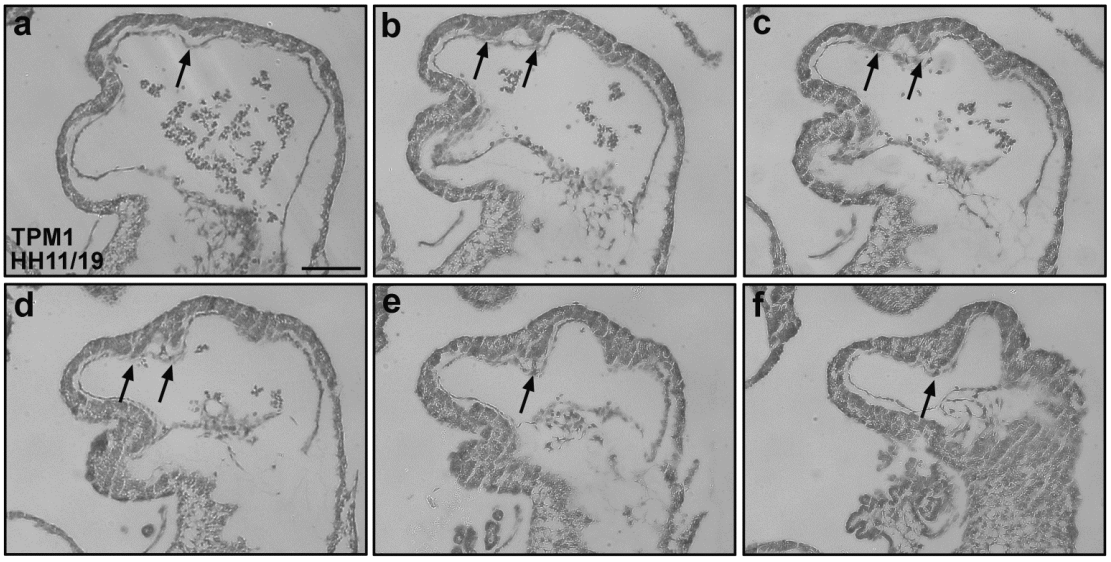

Figure 3.7 Initiation of a double atrium septum was seen in a TPM1-treated embryo. The atrial septum grows from the dorso-cranial wall of the atrium (a). Soon, the appearance of a second septum can be seen emerging to the right of the original septum (b). Both septa continue to grow as (c and d) until they both fuse at the posterior aspect of the atrial chamber (e and f). Arrow indicates septum. Mag bar indicates 100µm.

3.7 Abnormal ventricular trabeculation is observed in HH11/19

During normal cardiac development, trabeculae form a vibrant sponge-like meshwork within the myocardium, which appear as finger-like projections in the transverse orientation of the ventricular cavity. These projections appeared normal in the UT and SC groups (n=60; Table 3.1; Figure 3.8a and b). In morpholino treated embryos, 38% of the hearts appeared to have abnormal trabeculae development, with most hearts having a severe reduction in number and size of trabeculae (n=13/29 for the ATG, 5/26 for the E1I1 morpholino and 8/14 for the E4I4 splice site morpholino; Table 3.1; Figure 3.8d), with one heart completely lacking defined trabeculae, and apparent thinning of the ventricular wall (Figure 3.8c).

In total, of the 4 embryos with an abnormal external looping phenotype, each had an internal abnormal phenotype. With regards internal phenotypes to the developing atrial septa and trabeculae, 55% of hearts (38/69) had at least one defect (in either the atrium or ventricle) and 23% (16/69) had both internal phenotypes.

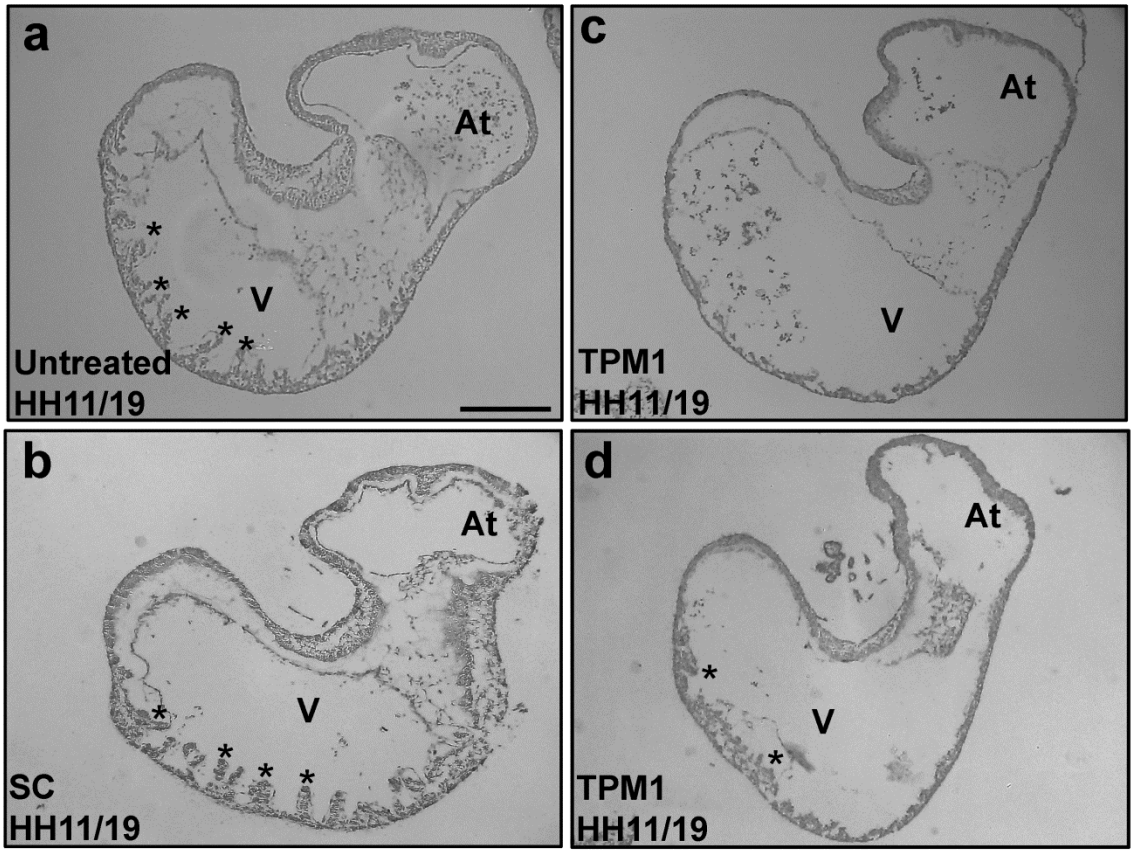

Figure 3.8 TPM1-treatment at HH11/19 results in reduced trabeculation in the ventricle.

Trabeculae grow from the caudal surface of the ventricular chamber in the untreated and standard control embryos (a and b). In the TPM1-treated embryos these trabeculae are reduced in both number and size (c and d). * indicates trabeculae; V, ventricle; At, atrium; SC, standard control. Mag bar=100μm.

3.8 TPM1-treatment at HH19 does not result in an abnormal internal phenotype

Internal analysis was conducted on embryos treated with TPM1 morpholino at HH19 and harvested at HH24 (HH19/24). No abnormalities were observed upon internal analysis of TPM1-treated (n=8), SC (n=5), or UT embryos (n=5) (Table 3.1). Serial sectioning through the HH19/24 hearts revealed normal atrial septation when comparing the controls to the TPM1-treated hearts. In the atria, an inter-atrial septum is present and is fully extended and fused with the dorsal and ventral endocardial cushions obliterating the foramen primum, thus dividing the atria in two (Fig. 3.9Aa-c). No abnormalities in the mesenchymal cap of the septum were seen.

In the ventricular chamber, numerous trabeculae can be seen protruding into the ventricular lumen (Fig. 3.9Ba-c). Major trabecular bundles can be seen inside the un-septated ventricle in the region of the ventricular groove (Fig 3.9Bd-f). However, at this stage no solid muscular septum can be seen.

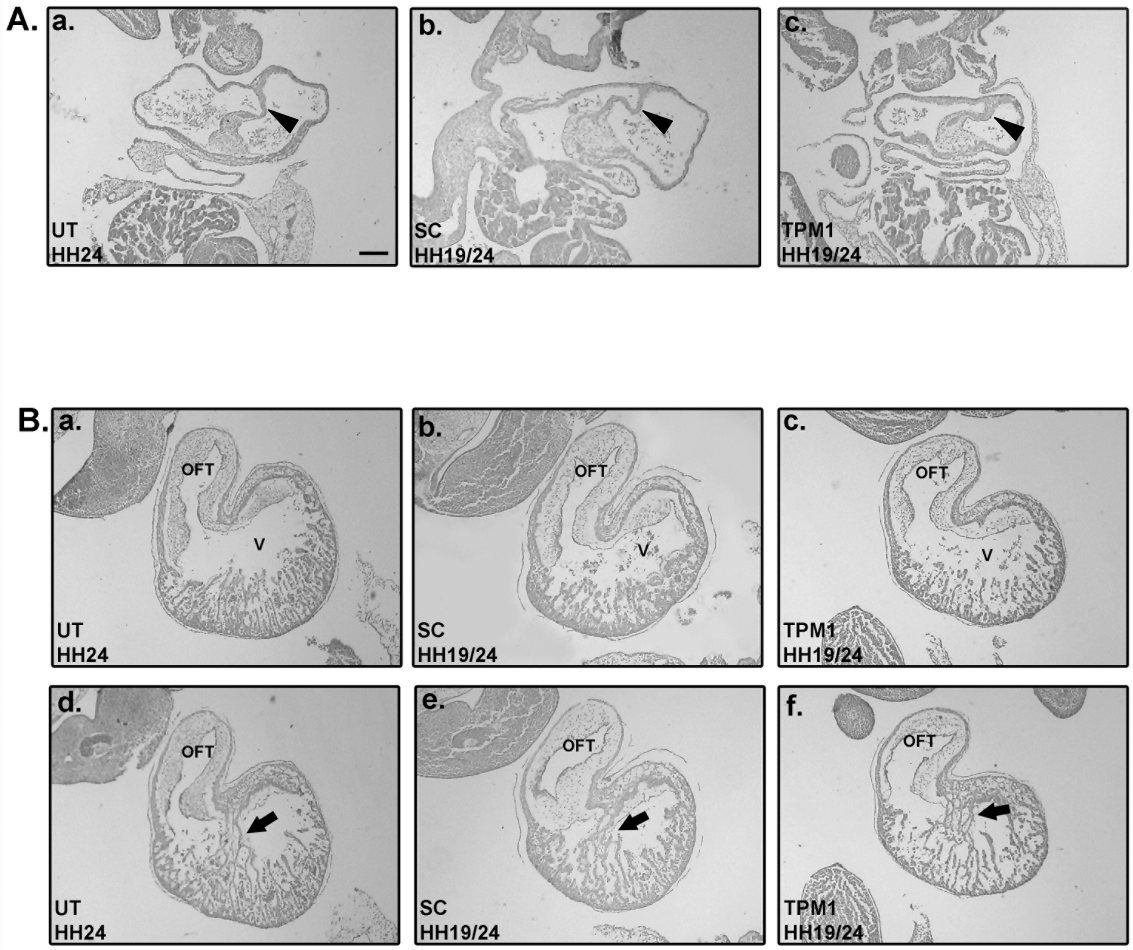

Figure 3.9 TPM1 morpholino treatment at HH19/24 results in normal atrial and ventricular development.

A. The atrial septum has fused to the endocardium cushions in the atrioventricular canal at HH24 (arrowhead). Normal atrial septation can be seen in all groups (a-c). **B.** By HH24 trabeculae are protruding into the ventricular lumen in all groups (a-c) and begin to coalesce to form the ventricular septum (arrow; d-f). OFT indicates outflow tract; V, ventricle; UT, untreated control; SC, standard control; TPM1, TPM1-morpholino treated. Mag bar=100μm.

3.9 Stereological analysis reveals normal total heart proportions

For stereological analysis, a 96-point grid was placed over every third 8μm section through the HH11/19 embryonic heart. Each point at which the grid hit a specific region (atrium, ventricle or OFT) of tissue (or lumen) was counted for that specific region. For the control hearts (SC and UT; n=5 and n=6, respectively) 5842 points in total were counted, and 6383 points were counted for the TPM1-treated hearts (n=13). The TPM1-treated group included hearts with normal atrial or ventricular phenotype (no phenotype; n=3), hearts with an atrial septal phenotype only (n=6) and hearts with an abnormal ventricular phenotype (n=4). Once all points were counted, the total number of counts per region was divided by the total number of counts for that heart, giving a percentage proportion that each region contributed to the heart.

The percentage proportion of atrium, ventricle and OFT was not significantly different between the UT and SC hearts so these were pooled into one group (P=0.662 atrium, P=0.889 ventricle and P=0.656 OFT). The normal, abnormal ventricular and abnormal atrial septal phenotyped TPM1-treated groups were also not significantly different and were pooled together into one TPM1-treated group (P>0.253). When compared to the control group, the TPM1-treated groups showed no significant difference (P=0.693, 0.318 and 0.489 for the atrium, ventricle and OFT, respectively; Figure 3.10).

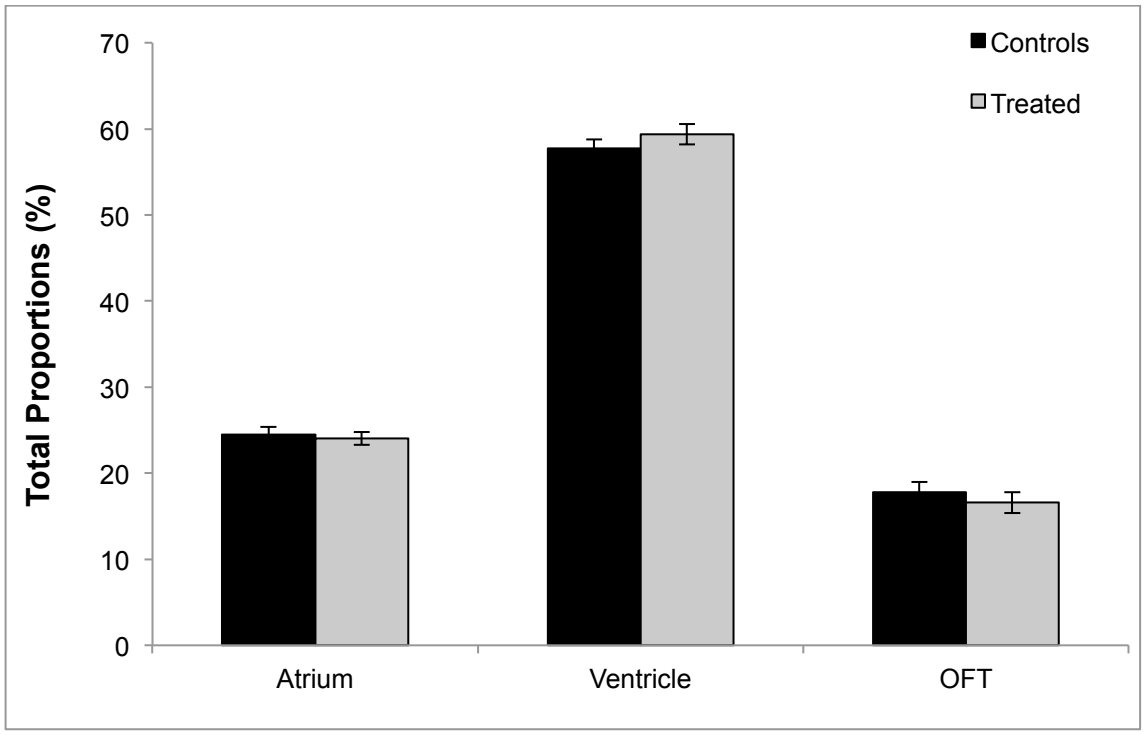

Figure 3.10 Stereological analysis revealed normal atrial, ventricular and outflow tract size in TPM1-treated hearts.

The proportion of atrium, ventricle and OFT contributing to each heart was calculated using stereological methods. No significant difference was seen between control and TPM1-treated hearts.

3.10 Stereology revealed changes in the ventricular components of TPM1-treated hearts

Stereological data was also obtained to look at the percentage the heart wall, ECM and lumen contributed to the atrium, ventricle and OFT of the heart. When the UT and SC groups were compared, no differences were seen in any of the regions tested (P>0.094) and the two groups were pooled. Similarly, no significant difference was seen in the regions of the atrium, ventricle and OFT when the TPM1-treated hearts with different phenotypes were compared (*P*>0.062). Therefore, these samples were pooled into one TPM1-treated group.

The pooled TPM1-treated group was compared against the control group and no significant differences were seen in the OFT wall (P=0.536), lumen (P=0.162) or ECM (*P*=0.064; Figure 3.12).

Similarly, in the atrium, no differences were seen in the lumen (P=0.775), ECM (0.795) or wall (*P*=0.507; Figure 3.11). However, the stereological data showed that the atrial septum represented 0.61±0.13% of the control hearts while in the TPM1-treated hearts it represented 0.42±0.11%, a 30.18% decrease in atrial septal myocardium compared to control groups. However, the number of points counted for the atrial septum was low (200 points required; 38 and 25 points counted for the control and TPM1-treated groups, respectively) and statistical analysis could not be completed.

Stereological analysis showed that the ventricular wall and trabeculae in control hearts represented 16.18±0.87% of the heart, while the TPM1-treated ventricular wall (including trabeculae) accounted for 12.68±0.60%; a decrease of 21.64% (*P*=0.003; Figure 3.11). Consistent with this, the ventricular lumen for the control and TPM1-treated hearts accounted for 20.17±2.72% and 28.90±2.37% respectively, an increase of 43.25% for the TPM1-treated groups (*P*=0.024; Figure 3.11).

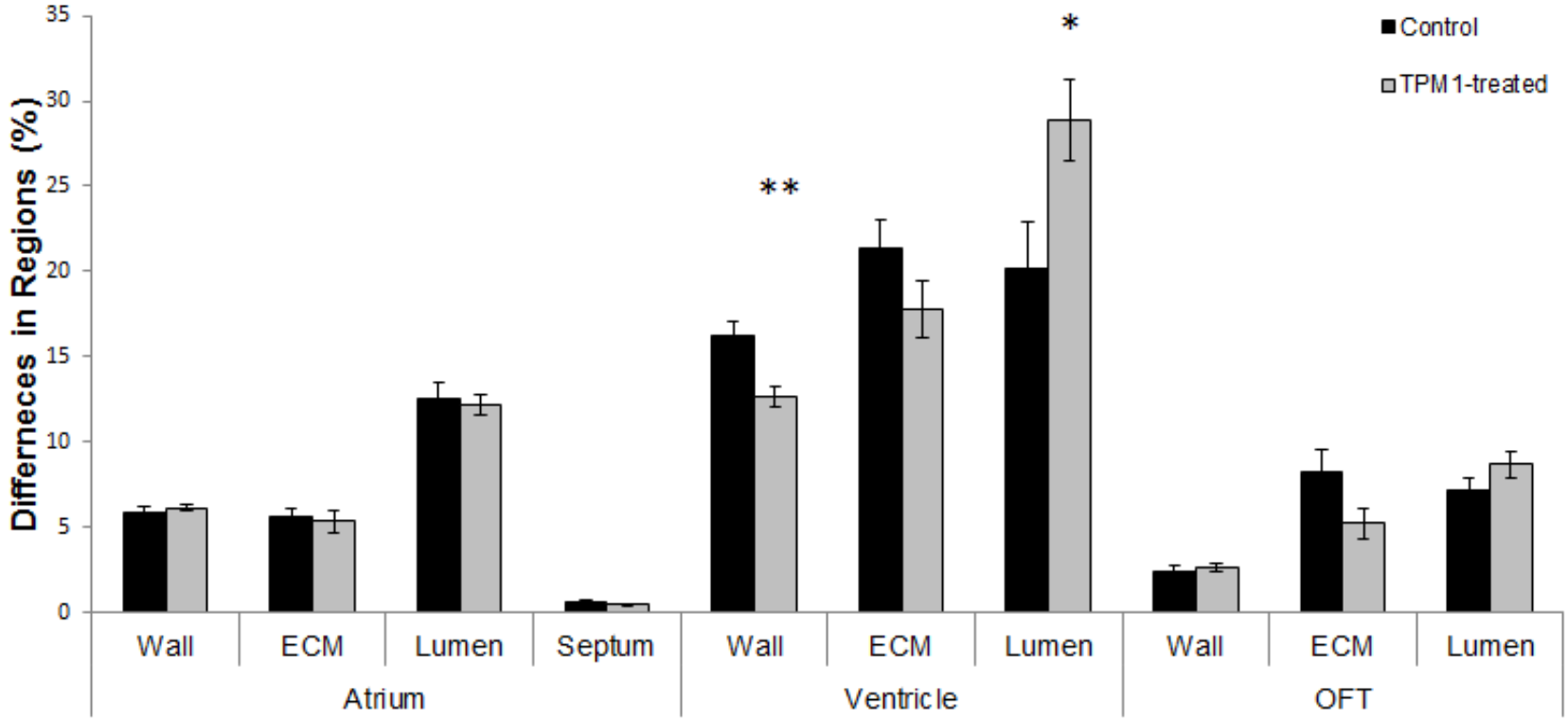

Figure 3.1Stereological analysis of tissue types within the atrium, ventricle and outflow tract.

Stereology revealed normal tissue proportions within the atrium and outflow tract. In the ventricle, although the ECM was normal, the ventricular was reduced and lumen increased in TPM1 treated hearts. ECM indicates extracellular matrix. * P=0.024, ** P=0.003.

3.11 TPM1 morpholino-treatment did not affect cell proliferation in the heart

Cell proliferation in the heart was detected using an antibody targeting Proliferating Cell Nuclear Antigen (PCNA), a protein expressed in the nucleus during the S-phase of the cell cycle and a co-factor of DNA polymerase delta (important for DNA replication and repair) (Kubben et al., 1994). PCNA positive cells were identified as cells containing dark brown nuclei (Figure 3.13A shows an example of sections stained for PCNA). Light brown nuclei were not considered positive for PCNA. DAPI was used as a counterstain to identify the total cell count. A total of 47,747 cells were counted as either PCNA positive or negative.

No significant differences in PCNA positive cells were seen between the SC and UT hearts (P>0.085) and therefore, these two groups were pooled. TPM1-treated hearts with normal (n=3) and abnormal (n=4) phenotypes were included in the study, and therefore, were tested for significant differences between the groups (P>0.433). Since no significant difference was seen between the TPM1-treated groups, they were also pooled.

In the atria of the control hearts, 31±1% (average percentage ± standard error of the mean) were PCNA positive, while in the TPM1-treated hearts 29±3% were positive for PCNA (P=0.702; Figure 3.12B).

In the septum, 26±2% of the control hearts were PCNA positive in comparison to 26±3% of the TPM1-treated heart (P=0.974; Figure 3.12B).

Finally, the ventricles of the control hearts had 37±1% proliferating cells and the TPM1-treated hearts had 33±3% PCNA positive cells (P=0.271; Figure 3.12B). Therefore, no significant differences in proliferation were seen between the control and TPM1-treated hearts in the atrium, septum or ventricles.

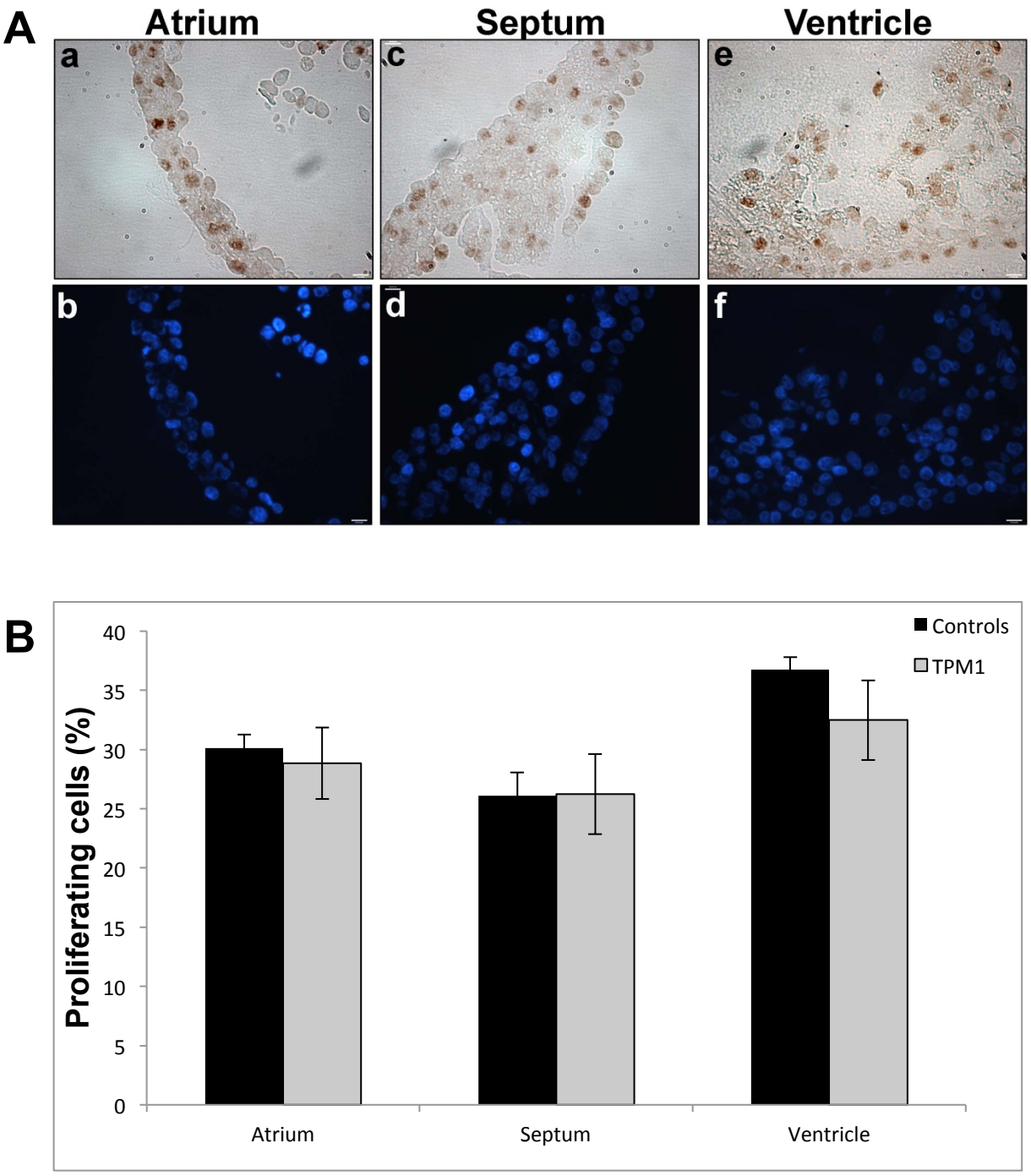

Figure 3.12 TPM1-treated hearts show normal proliferation.

A. An example of cells staining positive for a proliferation marker PCNA in the atrium, atrial septum and ventricles of control and TPM1-treated hearts using PCNA staining protocol. **B.** When TPM1-MO treated and control hearts were compared, no significant difference was seen between the groups in any regions examined ($P>0.271$).

3.12 TPM1 morpholino-treatment results in increased levels of apoptosis

Apoptosis was quantified in the chick heart by enzymatically labelling the free 3'-OH terminus of DNA with TdT. A total of 44,297 cells were identified as positive or negative for apoptosis. Cells positive for apoptosis were found isolated with no apoptotic foci observed (Figure 3.13A). No significant differences in apoptosis was seen between the UT and SC hearts and were therefore pooled into one control group (P>0.087). However, there were significant differences in apoptosis observed between TPM1-treated hearts with abnormal atrial septation/ventricular trabeculation (n=3) and TPM1-treated hearts with a normal gross morphology (n=4), hence these two groups were analysed separately against the controls.

In the atrial wall, 0.47±0.07% of the control cells, 0.43±0.08% of the normal phenotypic TPM1-treated hearts and 0.95±0.24% of the abnormal phenotypic TPM1-treated hearts were apoptotic (P=0.709 non-phenotype, P=0.179 with phenotype; no significant differences; Figure 3.13B).

In the atrial septum, apoptosis accounted for 0.49±0.06% of the control hearts and 0.37±0.04% of the normal phenotypic TPM1-treated hearts (P=0.224). However, apoptosis in the abnormal phenotypic TPM1-treated hearts accounted for 1.56±0.27% (P<0.001; significant difference; Figure 3.13B).

Finally in the ventricular wall (including trabeculae), 0.43±0.05% of the cells were apoptotic in the control hearts and 0.41±0.01% in the normal phenotype TPM1-treated hearts (P=0.775). For the TPM-treated hearts with an abnormal phenotype, apoptosis accounted for 0.68±0.05% of the cells (P=0.013; significant difference; Figure 3.13B). These results compliment the abnormal phenotypes observed from the internal phenotypic analysis (Section 3.6 and 3.7). An increase in apoptosis is observed in the ventricular wall and atrial septum, which are reduced in size in a subset of the TPM1-morpholino treated hearts, while normal levels of apoptosis is observed in TPM1-morpholino treated hearts which appear to have normal atrial septum and ventricular trabeculae development.

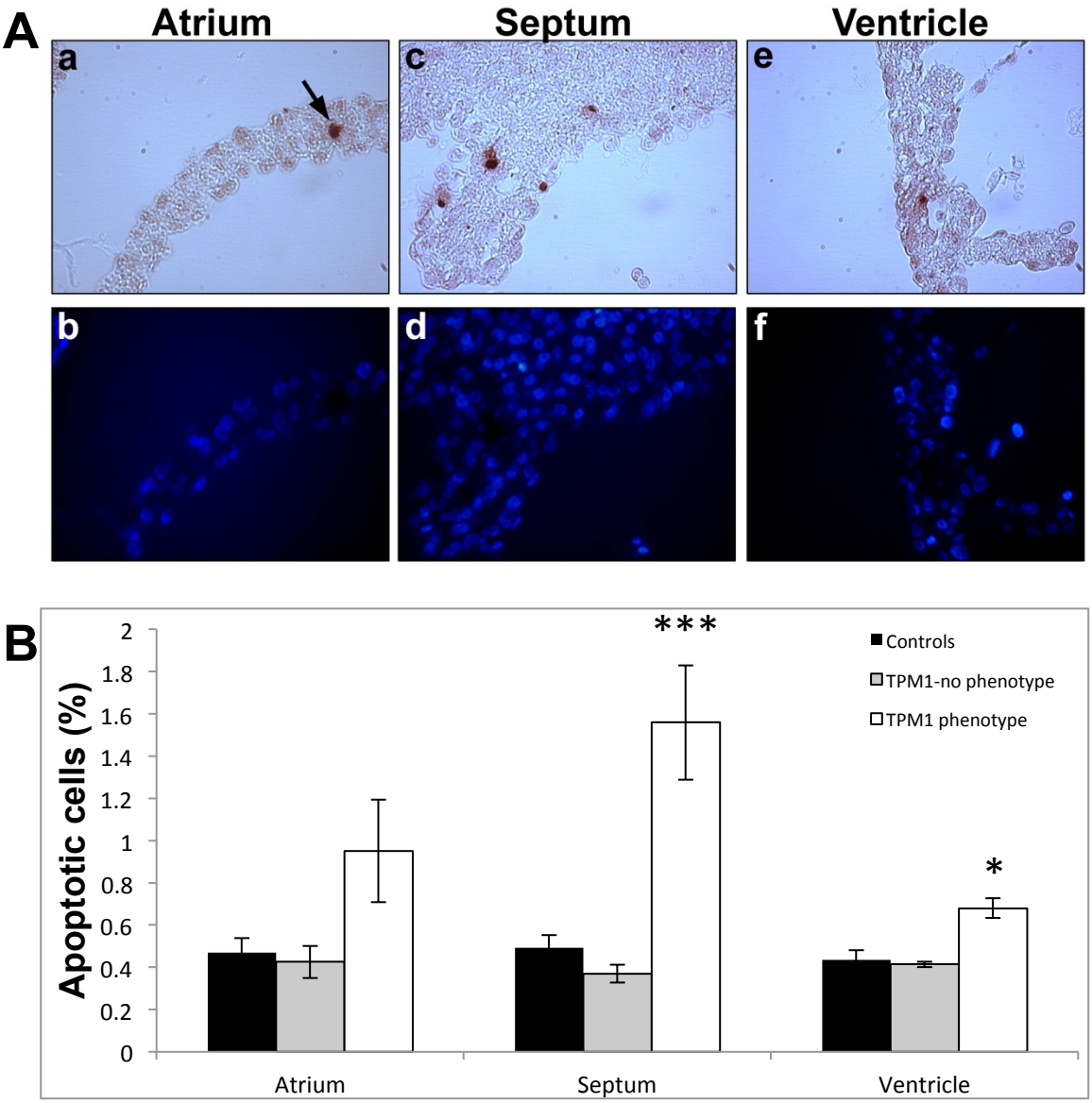

Figure 3.13Apoptosis is increased in the atrial septum and ventricular wall of TPM1-treated hearts.

A. An example of apoptotic cells detected in the atrium (a and b), septum (c and d) and ventricle (e and f) of a HH19 heart. An arrow indicates an apoptotic cell. **B.** Apoptosis was measured in untreated, standard control (pooled as controls), TPM1-treated hearts with a normal phenotype and TPM1-treated hearts with abnormal phenotypes. Apoptosis was normal in the normal phenotypic TPM1-treated hearts when compared with the controls (P>0.224). However, in the atrial septum and ventricles of the abnormal phenotypic hearts, apoptosis was significantly increased. *P<0.05 ***P<0.001.

3.13 Ultrastructural analysis

To investigate a potential cause of the internal abnormal phenotype observed in the HH11/19 hearts, morpholino treated hearts were examined at the ultrastructural level. Both the atrial and ventricular regions of the heart were analysed separately. Numerous cellular structures were observed, including sarcomere assembly into myofibrils to show maturation of the tissue, the presence of multiple mitochondria and the presence of desmosomes (an adherent junction that join neighbouring cells indicating good muscle integrity). Interestingly, these structures appeared normal upon comparison between the control (n=6) and TPM1-treated groups (n=9) in both the atrial and ventricular chambers, with normal myofibril formations, mitochondria and desmosomes present (Figure 3.14a-h). Intracellular spaces and cellular size within the tissue also appeared normal across the groups.

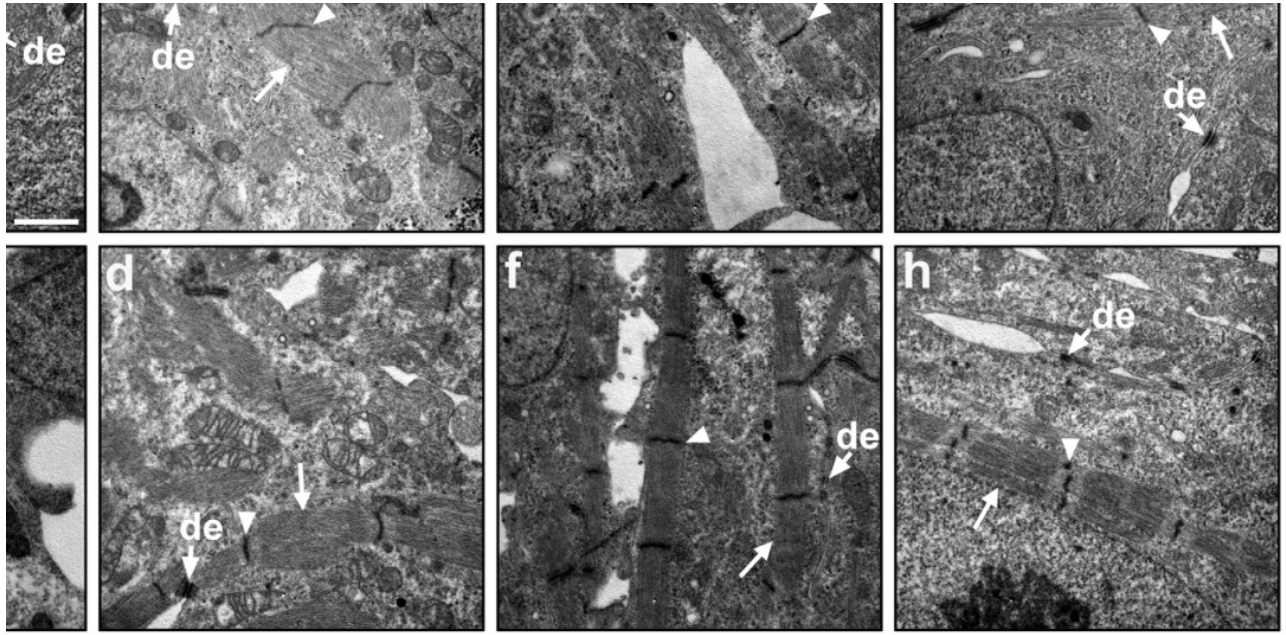

Figure 3.2Transmission electron microscopy reveals normal tissue integrity and structure.

The ultrastructure of the atrium and ventricles in control and TPM1-treated embryos was analysed to ensure normal tissue integrity. Numerous desmosomes and sarcomeres were apparent in the tissue and no differences could be seen between the untreated (a and b), standard control (c and d) and TPM1-treated (e-h) groups. De indicates desmosomes: arrow, sarcomere; arrowhead, Z-disc. Mag bar=1μm.

3.14 TPM1-morpholino treatment in culture results in sarcomere disarray and decreased sarcomeric maturity

The effect of TPM1-morpholino treatment on sarcomere assembly was investigated using cardiac cell micromass. Full embryonic hearts can be harvested and trypsinized to obtain beating cardiomyocytes surrounded by fibroblasts, endothelial cells and other cells present in the heart, in culture. Cardiomyocytes that actively uptake morpholino were studied and they can be distinguished due to the fluorescein tag present on the morpholino structure. Using an anti-TNNT2 antibody to detect the sarcomere, the cardiomyocytes were classified into one of four stages depending on its sarcomeric maturity (Figure 3.15Aa-d). Stage one consisted of cells with positive staining around the periphery of the cell but no sarcomeric structures could be clearly seen, especially around the nucleus (Figure 3.15Aa). Stage 2 cardiomyocytes contained assembled sarcomeres, however, they appeared thin and disorganised (Figure 3.15Ab). Stage 3 cardiomyocytes presented with organised sarcomeres that appear thin but were organised and run parallel to one-another (Figure 3.15Ac). Finally, stage 4 cardiomyocytes contained mature cardiomyocytes with thick bands running through the cell (Figure3.15Ad). More than 1000 cells were analysed in three independent experiments. Additionally, the classification was done blinded to avoid bias interpretation of results. Untreated and SC-treated cells had no significant difference between each other in any of the classifications and were pooled into one control group ($P>0.217$). When the control group was compared with the TPM1-treated group, the number of TPM1-treated cells at stage 1 and 2 were significantly increased ($P<0.001$ and $P=0.012$, respectively; Figure 3.15B). No significant difference was seen at stage 3 between the groups ($P=0.120$), however, the number of TPM1-treated cells that reached stage four was significantly reduced compared to the control group ($P<0.001$; Figure 3.15B). Therefore, TPM1-morpholino treatment *in vitro* results in decreased sarcomeric assembly and maturation in cardiomyocytes. These results may elucidate a possible cause for the abnormal structural defects observed in Sections 3.6 and 3.7.

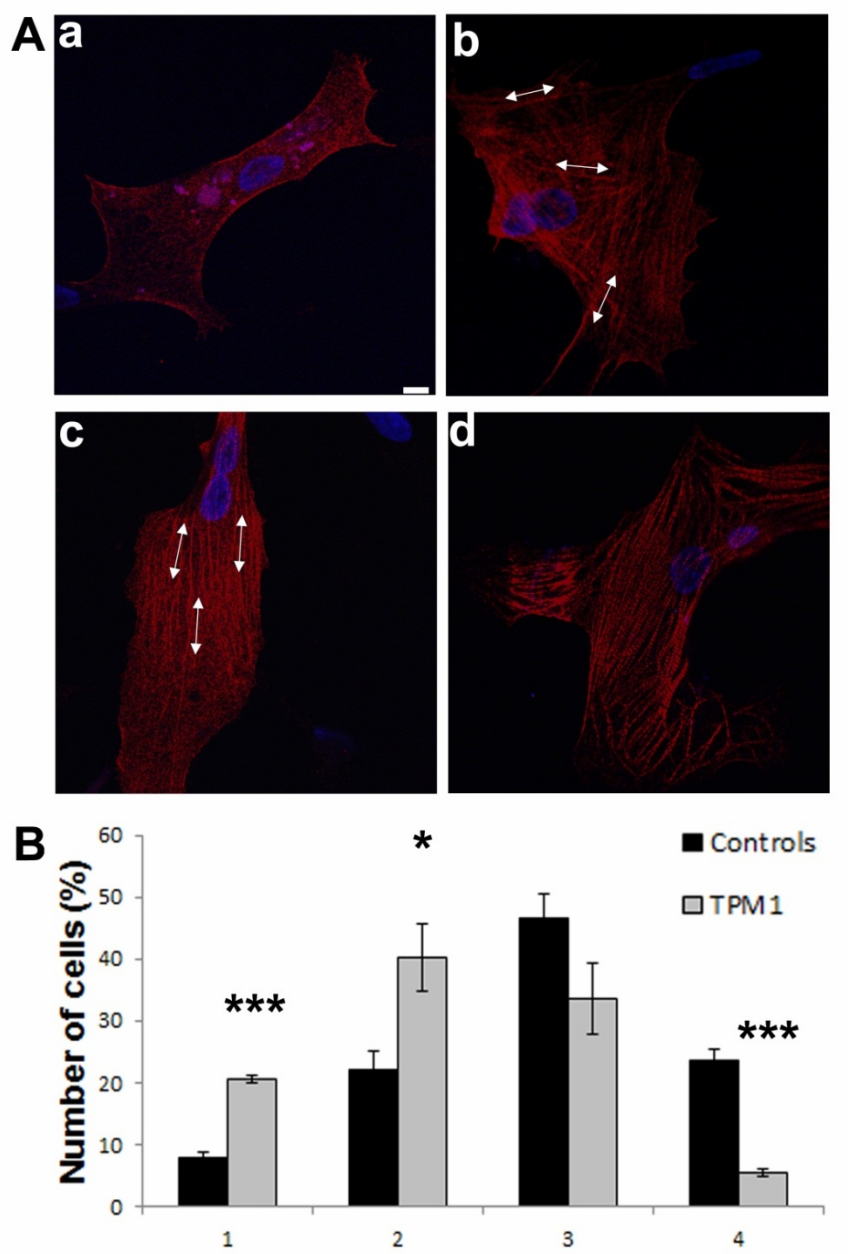

Figure 3.15 TPM1-morpholino treatment leads to immature sarcomere assembly.

A. Sarcomere assembly was categorized into 4 types: type 1 is immature myofibril assembling at the periphery of the cell with no fibril structures present (**a**); type 2 fibres are present in a disorganised fashion (**b**); type 3 has organised fibrils that are thin (**c**); type 4 has fully developed thick fibrils running across the cell (**d**). **B.** TPM1-treatment results in an increase in type 1 and type 2 immature cells, while there is a decrease in the number of type 4 cells. Type 3 appear reduced in the TPM1-treated group, but was not statistically significant. **P*<0.05 ****P*<0.001.

3.15 The molecular effect of TPM1-morpholino application

Western blot analysis was used to quantify the degree of protein knockdown in hearts treated with ATG start-site morpholino. This was performed on pooled hearts and later on single isolated hearts to confirm protein quantity.

3.15.1 Western blot using pooled hearts

TPM1-treated, SC and UT hearts were pooled in groups of three per sample. The optical density of the bands were measured for CH1 antibody detecting TPM1 and normalised against GAPDH (Figure 3.16A). No difference in optical density was seen between the SC (n=3) and UT (n=3) groups and they were pooled into one control group (P=0.622). No significant difference was seen between the control and TPM1-treated hearts (n=3; P=0.664) indicating no decrease in TPM1 protein after morpholino treatment (Figure 3.16B).

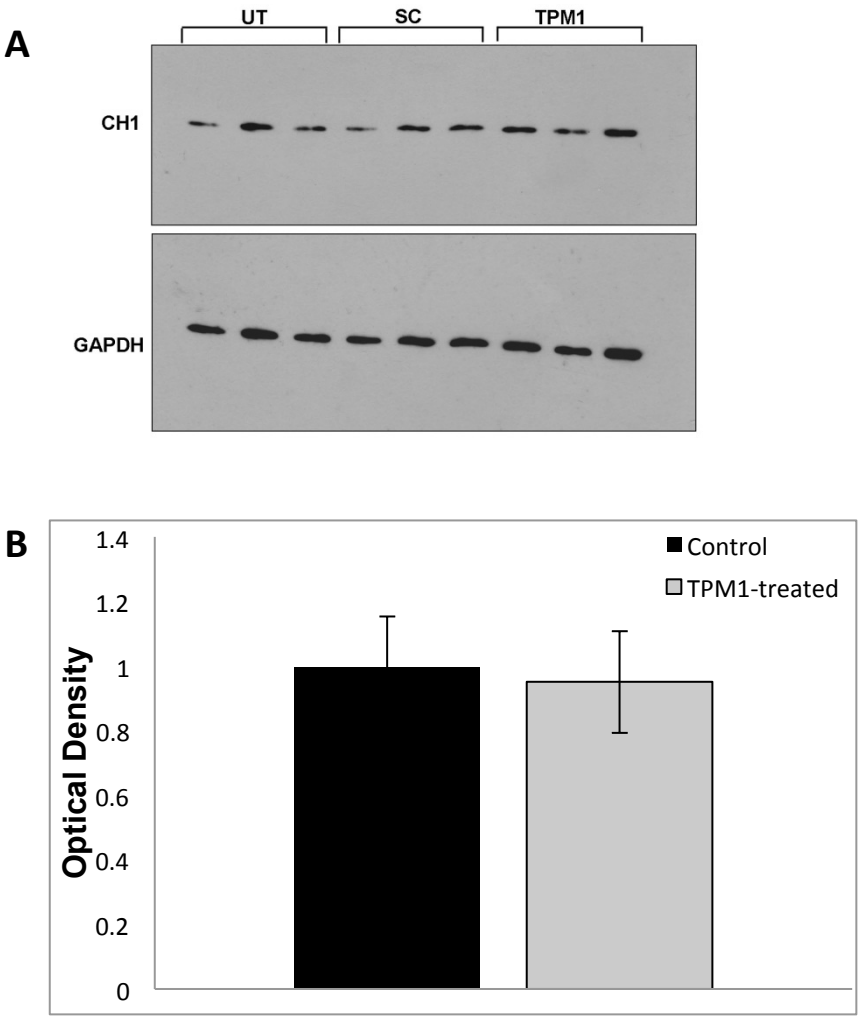

Figure 3.16 Western blotting to detect alterations in TPM1 after morpholino treatment in pooled hearts.

A. Three hearts of the same treatment were pooled into one sample to ensure there was enough protein for detection. **B.** No significant difference was seen between the control groups and the TPM1-morpholino treated group (P=0.664).

3.15.2 Western blot using individual embryonic hearts

As the penetrance of the phenotype of the TPM1-treated hearts was not 100%, it was postulated that the decrease in TPM1 protein may not be present in all of the morpholino treated hearts. Therefore, pooling the hearts in groups of three may dilute the decrease in TPM1, making it insignificant. Hence, individual TPM1-treated hearts were analysed. CH1 antibody detecting TPM1 was normalised using Histone H3 (Figure 3.17A). No significant difference between the UT and SC groups (n=4 for both UT and SC) was seen (P=0.403). Therefore, these two groups were pooled into one control group. When the control and TPM1-treated hearts (n=9) were compared, again no significant difference was seen in protein concentration (P=0.189; Figure 3.17B).

As no differences in protein concentrations were seen, a western blot was conducted using CH1 to test its specificity. TPM1 is expressed in the embryonic chick heart, however, after birth, it is replaced with TPM4 (Zajdel et al., 2003). A western was performed on HH19, HH34, neonatal and adult heart. CH1 antibody was positive in all the ages tested, including the adult heart, where TPM1 is known not to be expressed (Figure 3.17C). This data suggests that CH1 antibody is not only detecting TPM1, but also TPM4. Therefore, CH1 is not a suitable antibody to investigate a possible reduction of TPM1 after TPM1-morpholino treatment, since TPM4 expression may be increased due to compensatory effects.

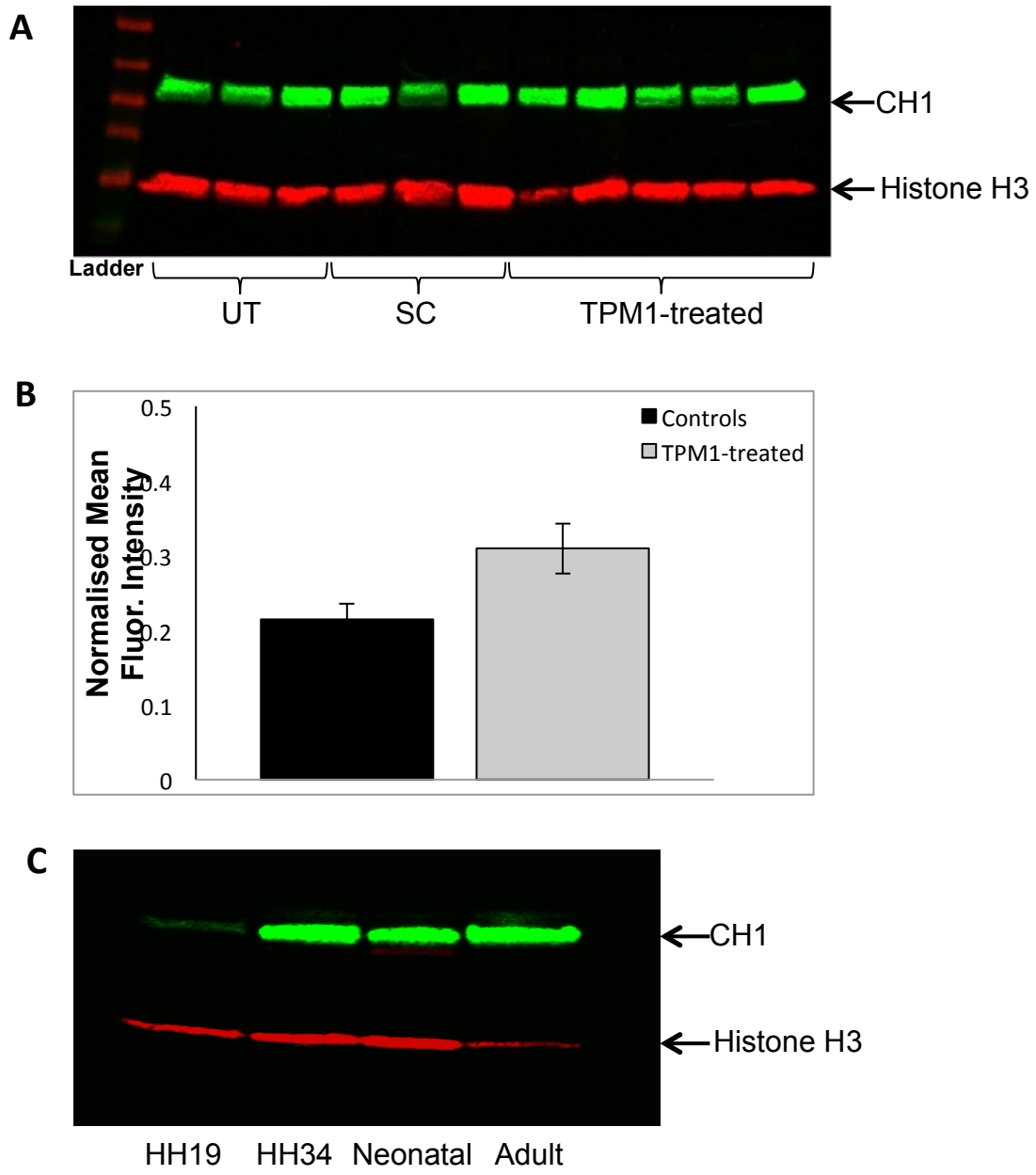

Figure 3.17 Western blot ting using individual hearts revealed no significant change in TPM1 protein after morpholino treatment.

A. Instead of pooling hearts together western blot was performed on individual hearts from each treatment group. **B.** Again, no significant difference in TPM1 protein was detected when compared with the control groups (*P*=0.189) although TPM1 appears to be increased. **C.** To check whether the antibody was specific to cardiac and skeletal TPM1, a western blot was done using embryonic heart (HH19 and 34) and neonatal and adult heart tissue which is known not to express TPM1. CH1 antibody was reactive in both the embryonic and postnatal tissues. CH1=38kDa, Histone H3=15kDa.

3.16 Optimizing the delivery of *GFP* containing construct directly to the developing chick heart in *ovo*

The delivery of plasmid mRNA and over expression its protein in the chick heart directly *in ovo* has been previously accomplished (Ishii et al., 2010). Ishii *et al*. microinjected plasmid containing *noggin* mRNA linked with *gfp* into the pericardial space of HH13-14 chick embryos. After harvesting at HH17, they found expression of the construct in the myocardium of the heart, but not in other tissues. The over-expression of genes in the myocardium would be ideal for doing a rescue after morpholino treatment. Utilizing their method, various modifications have been made to the protocol, including: microinjection at different ages, as well as amounts of transfection mixture injected into the pericardial space and amount of transfection reagent used.

3.16.1 Replication of the microinjection technique

Following Ishii et al.(Ishii et al., 2010), fifteen injections of 3nl of transfection mixture were injected into the pericardial sac of HH14 embryos. The transfection mixture contained 4µg pEGFP-C1 vector and 5µl of lipofectamine. Fast green was added to the transfection mixture so that the location of the injection could be visualized. Initially, 16 HH14 embryos were injected and all but one embryo survived (94%). From the surviving embryos, GFP fluorescence was checked and fluorescence, if present, was always observed in the heart and not in the surrounding tissues. The degree of fluorescence was classified using a star rating system, with 1-star (*) meaning a low level of fluorescence and 5-stars (*****) meaning a high level of fluorescence (see Figure 3.18A). From this initial experiment, two embryos scored 1-star (13.3%), one embryos scored 2-stars (6.6%), 7 scored 3-stars (46.7%) and five embryos scored 4-stars (33.3%; Table 3.2).

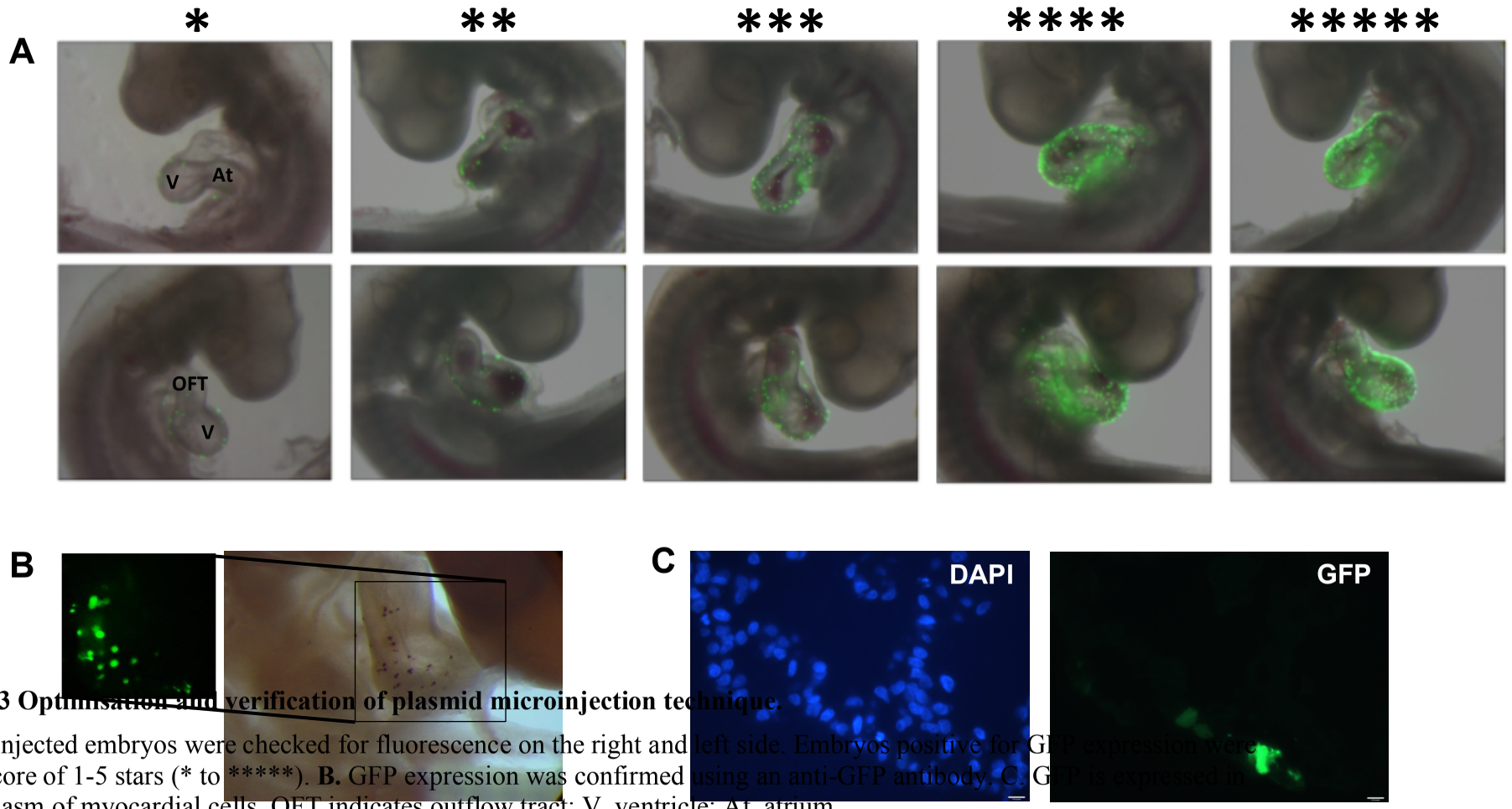

Figure 3.3 Optimisation and verification of plasmid microinjection technique.

A. Microinjected embryos were checked for fluorescence on the right and left side. Embryos positive for GFP expression were given a score of 1-5 stars (* to *****). **B.** GFP expression was confirmed using an anti-GFP antibody. C. GFP is expressed in the cytoplasm of myocardial cells. OFT indicates outflow tract; V, ventricle; At, atrium.

3.16.2 GFP expression confirmation using indirect detection method

Using an anti-GFP antibody, GFP expression was detected using whole mount immunohistochemistry. Upon 3,3`-diaminobenzidine reaction, GFP could be detected in the same areas as the fluorescent-GFP produced from the plasmid (Figure 3.18B). It also showed that all GFP fluorescent signals coming from the live embryonic heart could be detected by the anti-GFP antibody. Therefore, all translated *GFP* in each cell is visible using fluorescence.

3.16.3 Whole mount immunohistochemistry confirms location of GFP expression

In order to confirm the location of the GFP observed and the percentage of expression, immunohistochemistry was completed on 8µm sections through a 5-star chick heart. Consecutive sections were collected, stained for GFP and DAPI and imaged. The total number of cells per section were counted on every third section using the DAPI stain for all nuclei (Figure 3.18C). GFP could be seen in the cytoplasm of a small proportion of myocardial cells, but was generally seen on the outer myocardial layer of the heart and not internally (Figure 3.18C). The total number of cells with GFP expression was also counted. 7.2% of the myocardium was positive for GFP. This compares with 4% expressed observed by Ishii *et al*. (Ishii et al., 2010). Therefore, it may be possible to further increase the expression by optimizing the amount of construct, transfection reagent and volume of transfection mixture injected.

3.16.4 Microinjection technique is also possible at HH11 and HH19

To attempt microinjecting transfection mixtures directly to the myocardium of varying ages of embryos, HH11 and HH19 embryos were used. HH11 embryos have a very weak heart beat and can be difficult to visualize. However, the heart is only newly developed and very few structural processes have occurred compared to the HH19 heart. HH19 embryonic hearts are large relative to embryo and are clearly visible at 1.5X magnification. However, the heart beats powerfully and quickly at this stage, so in order to decrease the risk of damage to the heart, the embryos were left at room temperature 2hrs prior to injection in order to slow the heartbeat.

Firstly, 14 HH11 embryos were microinjected. Two embryos died (14%), and of the remaining survivals, all embryos were fluorescent. Six embryos scored 4-stars for fluorescence (50%), and six scored 5-stars (50%; see Table 3.2).

For the HH19 study, out of 29 embryos injected, 5 died (17%; see Table 3.2), while the remaining embryos displayed variable amounts of fluorescence. Four embryos scored 1-star (16.7%), one of the embryos scored 2-stars (4.2%), two embryos scored 3-stars (8.3%), seven embryos scored 4-stars (29.2%) and 10 embryos scored 5-stars (41.7%; see Table 3.2). This data suggests that microinjection is a viable technique at HH11 and HH19 and embryo survival and GFP expression is not adversely affected by the technique.

Embryo Age	**No. of Embryos Dead**	**No. of Embryos Alive**	**Fluorescence Scores**	**%**
HH14	1 (6%)	15	*2 **1 ***7 ****5	13.3% 6.6% 46.7% 33.3%
HH11	2 (14%)	12	****6 *****6	50% 50%
HH19	5 (17%)	24	*4 **1 ***2 ****7 *****10	16.7% 4.2% 8.3% 29.2% 41.7%

Table 3.2 Optimisation of the microinjecting technique at various stages of heart development.

To optimise the microinjection of 4µg DNA at different ages, HH14, HH11 and HH19 were attempted.

3.16.5 Increasing the incubation time from 24 to 48 hours does not increase GFP expression

The length of incubation time was also investigated for the HH11 and HH19 injected embryos. From the above results (Section 3.16.1 and 3.16.2) fluorescence is present after 24hr incubation. To see if increasing the incubation time resulted in an increase in fluorescence, HH11 and HH19 embryos were injected with the pEGFP-C1 transfection mixture fifteen times and left for 48hrs.

HH11 embryos left for 48hrs post-injection had a 14.3% death rate. Of the surviving embryos, 6 were negative for fluorescence (33.3%). Seven scored 1-star (38.9%), four scored 2-stars (22.2%) and one embryo scored 3-stars (5.6%; Table 3.3).

For the HH19 embryos the death rate was 50%, 33% of the embryos scored 1-star and 66% scored 3-stars (Table 3.3). Increasing the duration of incubation time does not increase the expression of GFP in the HH11 or HH19 heart.

Embryo Age	No. of Embryos Dead	No. of Embryos Alive	Fluorescence Scores	%
HH11	3 (14.2%)	18	*7 **4 ***1 None 6	38.9% 22.2% 5.6% 33.3%
HH19	3 (50%)	3	*1 ***2	33.3% 66.6%

Table 3.3 Leaving embryos for 48hrs post injection does not increase fluorescence.

3.16.6 Increasing the amount of transfection mixture delivered to the chick heart results in increased death rates

The amount of transfection mixture injected into the pericardial space was analyzed to see if increasing the volume injected would increase the degree of fluorescence in the myocardium. 20 and 25 injections of 3ηl were tested. Increasing the volume of transfection reagent delivered to the heart increased the death rate when compared to the 15 injections in Table 3.2. 28.6% and 55.6% of the embryos died when injected with 20 and 25 times, respectively (Table 3.4).

Of the embryos that survived after 20 injections, one embryo scored 2-stars (20%), three scored 3-stars (60%) and one scored 4-stars (20%). After 25 injections, one embryo scored 1-star (25%) and three scored 3-stars (75%). Therefore, increasing the number of transfection mixture, by increasing the number of injections to the pericardial space, results in increased deaths, possible due to the increased risk of damaging the embryo.

Embryo Age	Amount Injected	No. of Embryos Dead	No. of Embryos Alive	Fluorescence Scores	%
HH19	15x3ul	5 (17.2%)	24	*4 **1 ***2 ****7 *****10	16.7% 4.2% 8.3% 29.2% 41.7%
	20x3	2 (28.6%)	5	**1 ***3 ****1	20% 60% 20%
	25x3	5 (55.6%)	4	*1 ***3	25% 75%

Table 3.4 Increasing the volume of liquid delivered to the pericardium by increasing the number of injections results in increased deaths.

Increasing the number of injections into the pericardium from 15, 20 and 25 times results in increased deaths.

3.16.7 Increasing the amount of Lipofectamine does not increase fluorescence

The amount of transfection reagent, Lipofectamine, added to the transfection mixture was optimized in order to see if it increased transfection efficiency of the pEGFP-C1 construct. Results from embryos injected with 10µl of Lipofectamine can be seen in Table 3.2.

4µg of the construct was added to 10, 15 or 20µl of Lipofectamine, made up to 50µl with OptiMEM (see Table 3.5 for summary). The death rate for each group was 14.3%, 0% and 14.3%, respectively.

Embryos injected with 15µl Lipofectamine were all positive for GFP expression, with embryos scoring: one 1 star (5%), four 2-stars (20%), seven 3-stars (35%), seven 4-stars (35%) and one 5-star (5%).

Finally, embryos injected with 20µl Lipofectamine had one 1-star (16.7%), one 2-stars (16.7%) and four 3-stars (66.7%). This data infers that increasing to ration of Lipofectamine to construct does not increase the expression of GFP within the heart, suggesting it does not increase delivery of construct to the cells of the heart.

Embryo Age	Amount of lipofectamine	Amount of DNA	No. of Embryos Dead	No. of Embryos Alive	Fluorescence Scores	%
HH11	10µl	4µg	2 (14.3%)	12	****6 *****6	50% 50%
	15 µl	4 µg	-	20	*1 **4 ***7 ****7 *****1	5% 20% 35% 35% 5%
	20 µl	4 µg	1 (14.3%)	6	*1 **1 ***4	16.7% 16.7% 66.7%

Table 3.5 Increasing the amount of Lipofectamine does not increase transfection.

3.16.8 Increasing the concentration of construct to Lipofectamine ratio to increase fluorescence

As the 10µl Lipofectamine mixtures appeared most promising, that amount was used for future experiments. In order to increase expression further in the hearts, the amount of plasmid DNA to Lipofectamine was also optimized. 4, 6, 8 and 10µg of the pEGFP-C1 DNA was used (see Table 3.6). Data from the 4µg injections can be found in section 3.16.4 and Table 3.2. The death rate for the 6µg injections was 12.5%, while the surviving embryos were positive for fluorescence with 3 embryos scoring 2-stars (42.9%) and 4 scored 3-stars (57.1%). The 8µg injections were most similar to the 4µg injections (Table 3.2), with 4 embryos scoring 4-stars (44.4% and 5 embryos scoring 5-stars (55.6%). Finally, for the 10ug injections, 2 scored 3-stars (25%), 2 scored 4-stars (25%) and 4 scored 5-stars (50%).

Embryo Age	Amount of lipofectamine	Amount of DNA	No. of Embryos Dead	No. of Embryos Alive	Fluorescence Scores	%
HH11	10µl	4µg	2 (14.3%)	12	****6 *****6	50% 50%
		6 µg	1 (12.5%)	7	**3 ***4	42.9% 57.1%
		8 µg	-	9	****4 *****5	44.4% 55.6%
		10 µg	-	8	***2 ****2 *****4	25% 25% 50%

Table 3.6 Increasing the amount of DNA does not result in increased transfection compared to Table 3.2.

3.17 Summary

TPM1 is a gene that gives rise to alternative splicing isoforms some of which are expressed in the developing heart and not the neonatal and adult heart. After birth, there is a shift in expression to *TPM4*.

Using three antisense morpholino oligonucleotides targeting *TPM1*, *in ovo* manipulation was achieved leading to a range of cardiac defects. Externally, the heart of TPM1-treated embryos had dextral distortion of looping. Internally, the hearts developed sub-optimal septa in the atrial chambers, while trabeculation in the ventricles appeared reduced in size and number. Ultrastructurally, these hearts appeared normal, with good tissue integrity and the production of sarcomeres in the cardiomyocytes. However, apoptosis was increased in the abnormal phenotypic TPM1-treated hearts while proliferation remained unchanged.

Manipulation of cardiomyocytes *in vitro* revealed abnormal sarcomere assembly in that immature sarcomeres were significantly increased and mature sarcomeres, though present, were decreased in the treated cells. Although TPM1-treatment results in a wide range of phenotypes, quantitative analysis of protein changes caused by the morpholino were not detected due to the non-specificity of the anti-TPM1 antibody with data suggesting it also detects TPM4.

To amend this shortcoming we attempted to express plasmid DNA within the developing heart using microinjection technique into the pericardial cavity. This technique could potentially be used to perform a rescue if enough plasmid could be delivered to the developing organ. We found that upon changing concentrations of plasmid and transfection reagent, we could not get expression of GFP above ~7% in the cardiac cells. Adding to this, expression of the plasmid containing GFP was only seen on the outer periphery of the myocardium and did not penetrate the tissue to the inner cell layers. Therefore, the degree of transfection may not be adequate to perform a rescue.

Since it was not possible to detect a decrease in protein in the ATG start site TPM1-MO treated embryos and a TPM1 specific antibody is not available, other techniques, such as *in vitro* translation systems, may provide a solution (Taylor et al., 1996).

Chapter 4 Novel *TPM1* mutations found in patients with congenital heart defects

4.1 Overview

This chapter presents the results from the screening of the *TPM1* gene for rare variants that could predispose to congenital heart defects (CHDs). The objectives for this chapter were to:

- Analyse the novel identified variants using *in silico* techniques
- Determine whether a novel splice-site mutation of the donor site of intron 1-2 is functionally significant *in vitro*

Fifteen primer pairs were designed spanning the *TPM1* gene and its surrounding sequences. WAVE dHPLC (denaturing High Performance Liquid Chromatography) system was used to determine any amino acid substitutions, deletions or insertions. WAVE dHPLC works by denaturing double stranded DNA. As the DNA helix unwinds, it is eluted and flows across a matrix. It then becomes paired with the control (or unmutated) DNA. Where a mutation is present, the paired strands are heterozygous, forming hetroduplexes, which elute before homoduplexes, or homozygous strands of DNA. These hetroduplexes appear on an electropherogram as two or more peaks (Jongbloed et al., 2005). Samples traces with suggestive variations were obtained and these variations were re-amplified and sequenced. Potentially deleterious variants were screened by dHPLC in 380 individuals with a CHD and 384 ethnically matched control subjects. This work was completed by Dr. Javier Grandos-Riveron. To complement the work completed by Dr. Granados-Riveron, the novel variants were analysed *in silico* and the functional effect of the splice-site mutation was investigated.

4.2 Description of four novel *TPM1* mutations found in patients with congenital heart defects

The coding region of the human *TPM1* gene was sequenced in a cohort of 380 unrelated patients with a range of CHDs, while 384 healthy unrelated individuals were used as a control (completed by Dr. Javier Granados-Riveron). Four novel mutations of the human *TPM1* gene were identified in four separate samples of DNA. Two of these mutations were non-synonymous (a nucleotide substitution resulting in a change in amino acid) and named I130V

and S229F according to their amino acid substitution. Another mutation was found in the splice donor-site of intron1-2a, while a fourth mutation was found in the polyadenylation (poly-A) signal of exon 10. The following patient information, family history and identification of mutations were completed by Dr. Javier Granados-Riveron, while I completed the following *in silico* and *in vitro* analysis.

The I130V mutation was found in a British patient with pulmonary atresia, an atrial septal defect (ASD) and a patent ductus arteriosus. The family history of this patient reveals an unaffected mother who is not a carrier of the mutation, while a male dizygotic twin sibling of the patient also has an ASD, although it is unknown whether they are a carrier of the I130V mutation. The father was not tested (Figure 4.1A). In this case, an adenine in exon 4 (which is highly conserved) is replaced with a guanine nucleotide, resulting in an amino acid change from isoleucine to valine (Figure 4.1C,D and E). Both of these amino acids are non-polar at physiological pH. Interestingly, the amino acid substitution is located in the *d* position of the seven residue heptad repeats (see Figure 1.9). This *d* position, as mentioned previously, is important for interlocking with the *a* position, that gives TPMs their coiled-coil configuration (Crick, 1953), and therefore, interuptions in these binding regions may affect the coiled-coil stability (Monera et al., 1995).

The S229F mutation was also found in a British patient with a secundum ASD. Both parents of this proband are deceased and it remains unknown whether they were carriers. Interestingly, the mother's twin (also untested) has a child with a known ASD, but was not tested for the S229F mutation (Figure 4.2A). In this case, a cytosine in exon 7 is replaced with a thymine, resulting in an amino acid change from serine to phenylalanine (Figure 4.2C and D). Serine is a polar amino acid, while phenylalanine is non-polar. The S229F mutation occupies a conserved position through evolution, as shown by a multi-species alignment of TPM1 orthologues (Figure 4.2E), where serine or threonine residues exist in birds, fish, mammals, *X. tropicalis*, *Drosophila* and *C. intestinalis*. Both serine and threonine have a small, polar side chain. The S229F mutant allele encodes a protein in which a phenylalanine residue occupies this position. A molecular homology model of the S229F TPM1 protein predicts that the much bulkier, non-polar side chain of the phenylalanine residue would impair the binding of the two TPM1 peptide molecules that form the coiled-coil tropomyosin filament by steric hindrance (Figure. 4.2).

Another mutation was found in the essential splice site (the first or last two bases of an intron), where the second base thymine was replaced with a cytosine (IVS1+2T>C; Figure 4.3B and C). The location of the mutation was in the intron 1-2. This novel splice-site mutation was found in a British patient with Tetralogy of Fallot (TOF). In addition, a known nucleotide polymorphism was located in this proband on the opposite strand to the IVS1+2T>C mutation. This was a *tgt* insert (accession number RS34102093) located 185bp into intron1-2 (Figure 4.3).

The final mutation was found in the poly-A signal of exon 10. Both parents of the proband are untested and deceased (Figure 4.4A). The mutation presented in a patient with two ASDs and dilated right atrium and ventricle. The mutation resulted in a GATAAA/AATAAA change, in which an adenine is replaced for a guanine in the first position of the consensus. This mutation has been identified in three healthy individuals (present in dbSNP database; RS545752658). The functional effect of this mutation was not analysed in this thesis (Figure 4.4).

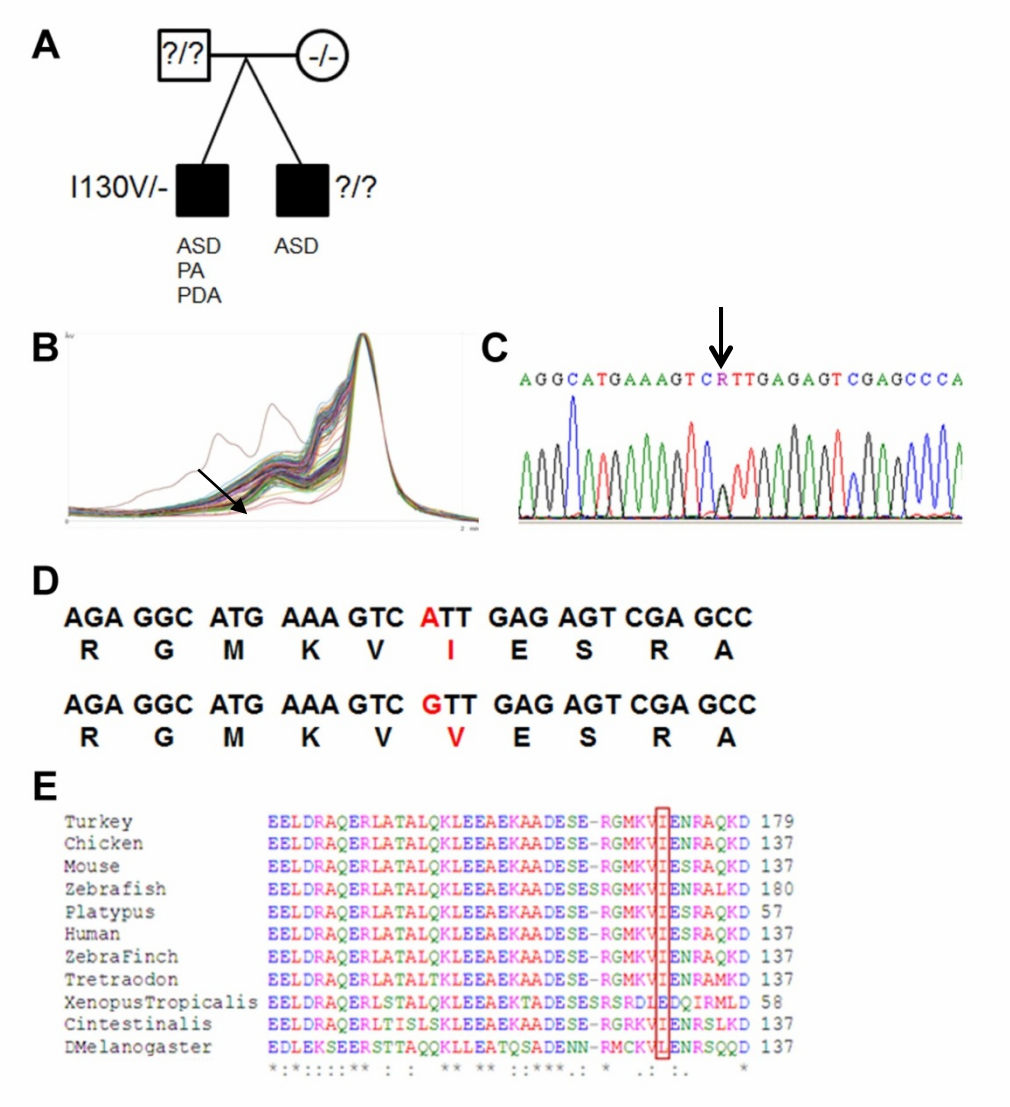

Figure 4.1 An overview of the data available regarding the I130V novel mutation found in a patient with pulmonary atresia, ASD and PDA.

A. This patient's mother is not a carrier of the I130V mutation and the father was not screened. A dizygotic twin of the patient also has an ASD, however, we were unable to screen this individual. **B.** An electropherogram from the analysis of the WAVE dHPLC. The arrow indicates the hetroduplexes released from the heterozygous DNA (DNA with mutation on one strand) from the patients. **C.** A chromatogram indicating the point of mutation (arrow). **D.** The nucleotide and amino acid sequence of normal (top sequence) and the I130V mutated *TPM1* (bottom sequence). **E.** This Isoleucine residue is highly conserved throughout species. This work was completed by Javier Granados-Riveron.

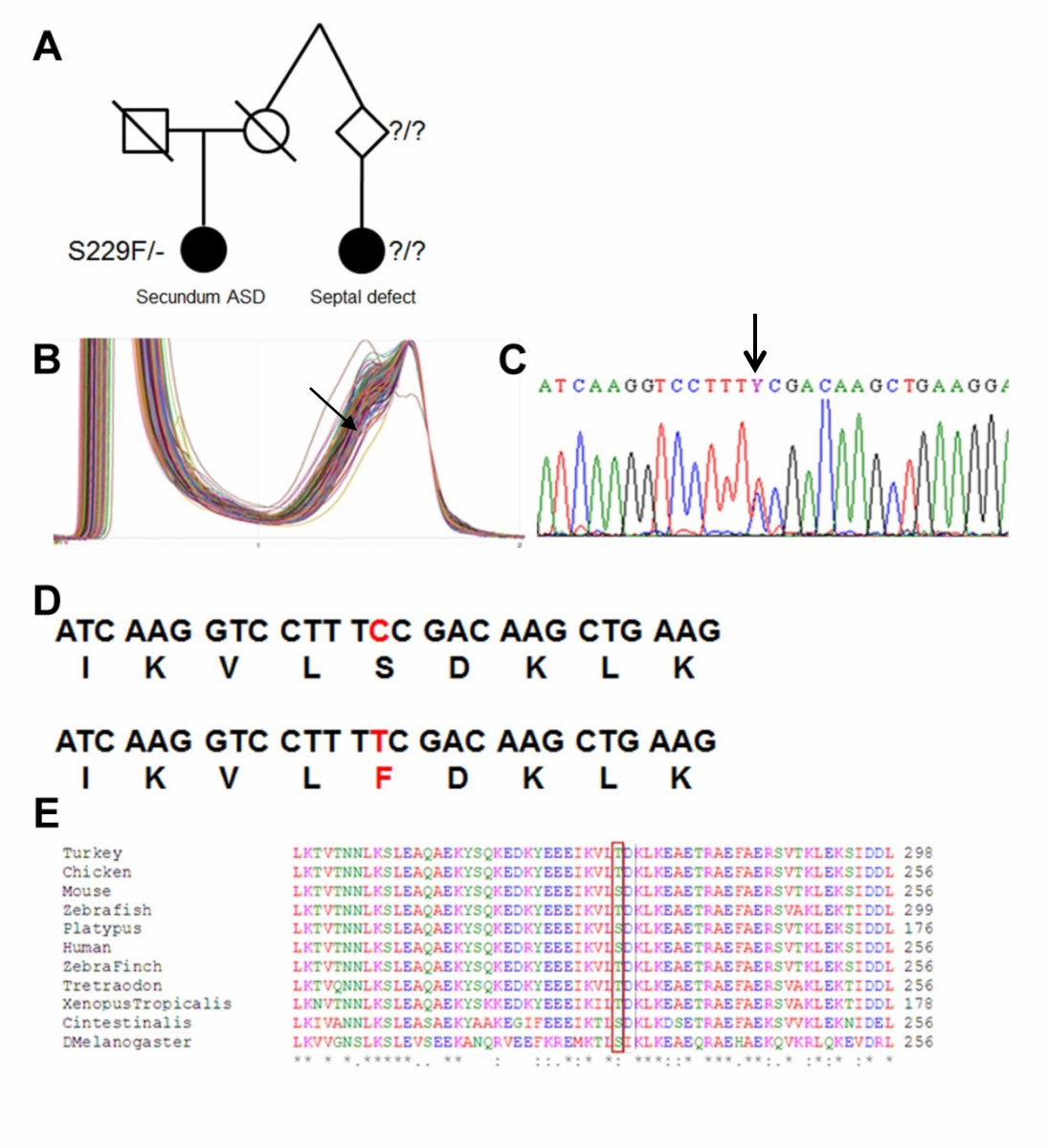

Figure 4.2 An overview of the data available regarding the S229F novel mutation found in a patient with an ASD.

A. The parents of this patient are both deceased and, therefore, were not screened. A dizygotic twin of the patients mother has a daughter with a septal defect. **B.** An electropherogram from the analysis of the WAVE dHPLC. The arrow indicates the hetroduplexes released from the heterozygous DNA. **C.** A chromatogram indicating the point of mutation (arrow). **D.** The nucleotide and amino acid sequence of normal (top sequence) and the S229F mutated *TPM1* (bottom sequence). **E.** Serine and threonine are both highly conserved polar amino acids at position 229 of TPM1. This work was completed by Javier Granados-Riveron.

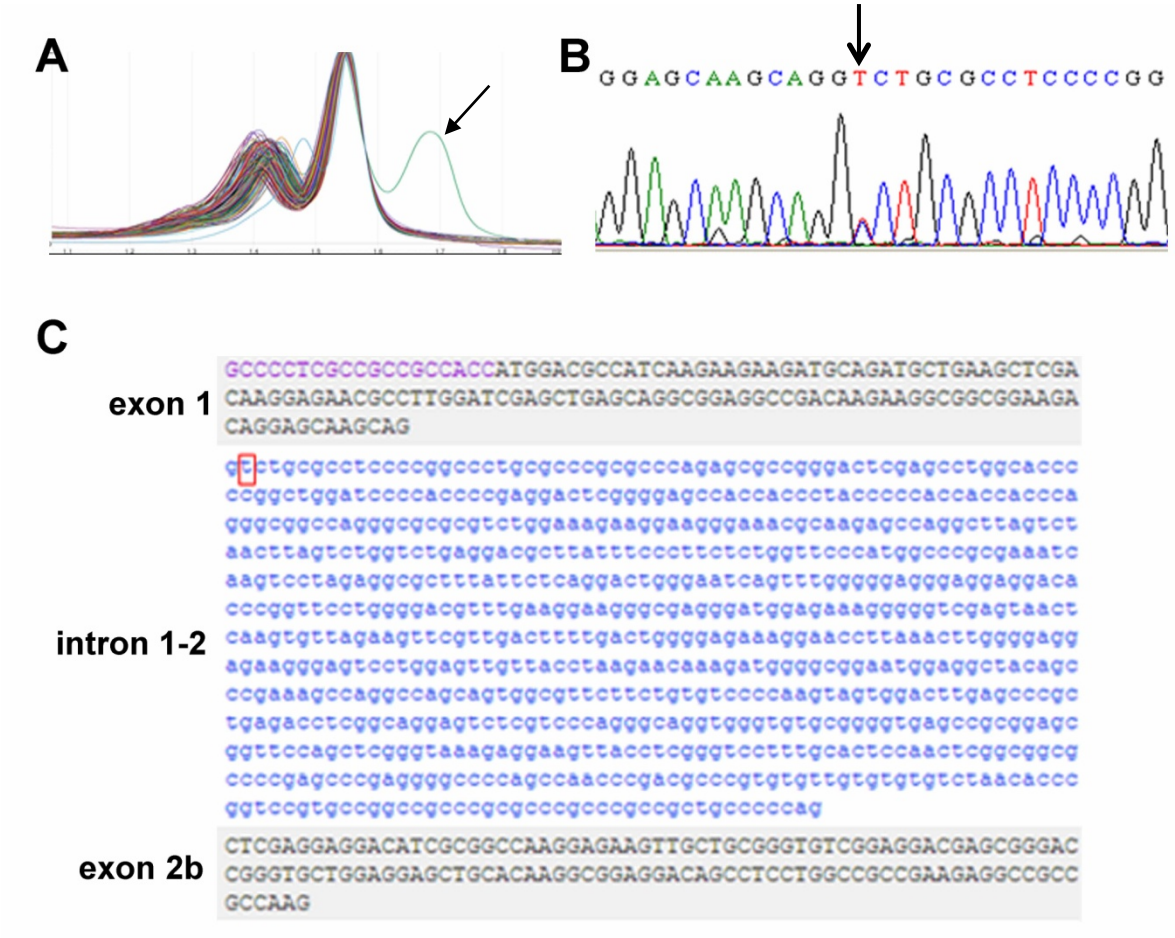

Figure 4.3 A splice site mutation was discovered at the splice donor site of a patient with tetralogy of Fallot.

A. An electropherogram from the analysis of the WAVE dHPLC. The arrow indicates the hetroduplexes released from the heterozygous DNA. **B.** A chromatogram resulting from sequencing indicating the point of mutation. C. The T>C nucleotide swap is located at the second base on inron1-2, the splice donor site of an intron. This work was completed by Javier Granados-Riveron.

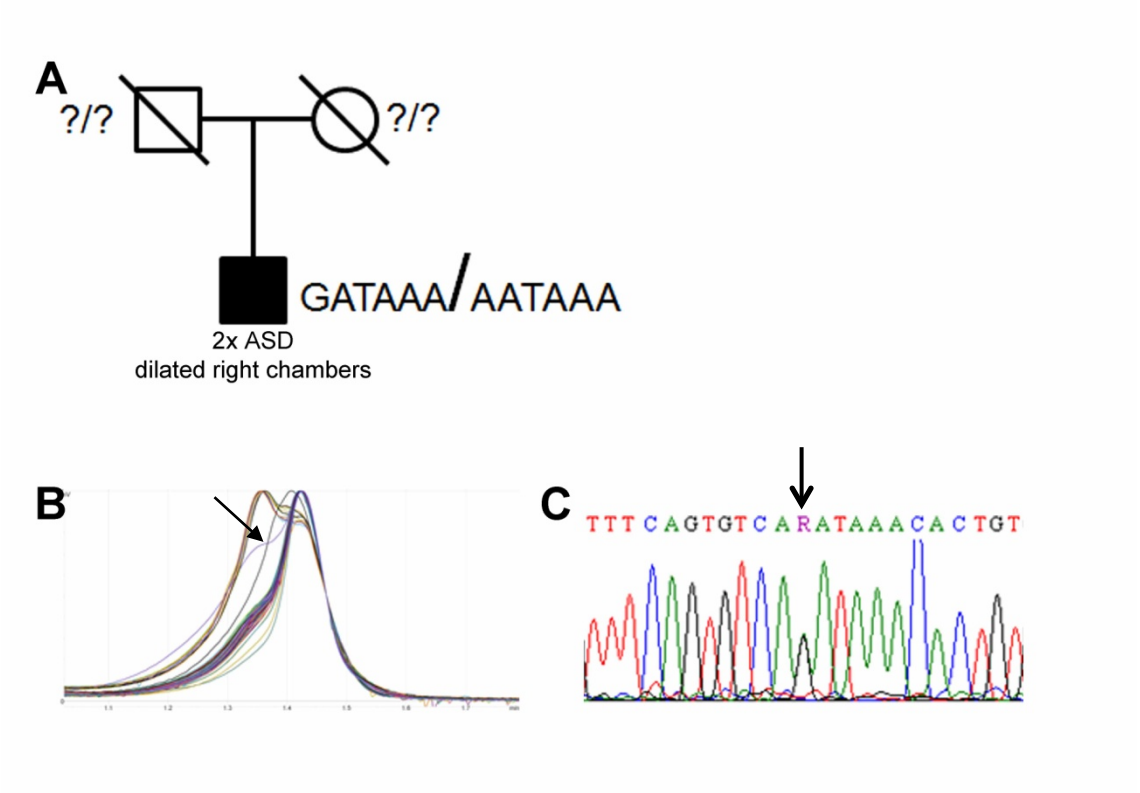

Figure 4.4 A mutation was discovered in the polyadenylation signal of a patient with two ASDs and dilated right chambers.

A. The parents of this patient are both deceased and, therefore, were not screened. **B.** An electropherogram from the analysis of the WAVE dHPLC. The arrow indicates the hetroduplexes released from the heterozygous DNA. **C.** A chromatogram resulting from sequencing indicating the point of mutation. This work was completed by Javier Granados-Riveron.

4.3 *In silico* analysis of the *TPM1* mutations

Non-synonymous single nucleotide mutations stand for more than 50% of the mutations known to be involved in human inherited diseases (Krawczak et al., 2000). For this reason, it is important to investigate the possible effect of these novel mutations. The 1000 Genomes Project provides the sequences of genomes of a large group of people from various populations in order to find genetic variants that have a frequency of at least 1% in the populations studied (Abecasis et al., 2010). This is important in the foundation for investigating the relationship between genotype and phenotype. The project contained three categories: 1) low-coverage (2-4X) sequencing of 180 whole genome samples; 2) high coverage (20-60X) sequencing of two mother-father-child trios; and 3) exon-targeted sequencing in 900 samples. This data now describes the location, allele frequency and local haplotype structure of approximately 15 million single nucleotide polymorphisms, one million short insertions and deletions, and 20,000 structural variants, most of which were previously undescribed. None of the mutations found in our mutational scan were present in the 1000 genome database (http://browser.1000genomes.org) and, therefore, still remain novel putative mutations with a probable frequency <1%.

In silico analysis of the four mutations was carried out to investigate the potential damaging effects these mutations may have. This was done using three online mutation-predicting programs, Polyphen-2 (http://genetics.bwh.harvard.edu/pph2/), SIFT (http://sift.jcvi.org/) and MutationTaster (http://www.mutationtaster.org/). Mutations within introns and untranslated regions cannot be analysis by PolyPhen or SIFT.

PolyPhen-2 (Polymorphism Phenotyping V2) predicts the possible impact of an amino acid substitution on the structure and function of a protein by using sequence and structural-based considerations (Adzhubei et al., 2010). It does this via a direct comparison of the normal allele (wild type) to the mutated (possible disease causing) allele. Results are graded on a score form 0-1, where 0 is less damaging and 1 is the most damaging.

SIFT on the other hand uses a sequence homology-based method in order to classify amino acid substitutions (Kumar et al., 2009). It uses the evolutionary conservation of amino acids within protein families to predict whether a substitution is likely to be damaging to the protein. So for highly conserved amino acid positions, a substitution would more likely be intolerant than an amino acid position with low degree of conservation. SIFT prediction

works differently in that the grading of the predictions run from 0-1 were 0 is the most damaging and 1 is the least. A mutation is predicted as damaging if the score is ≤0.05 and tolerated if >0.05.

MutationTaster has evolved from a large training set of known mutations (>40,000) and polymorphisms (>500,000). From these sets, and using the Bayes classifier of probability, it predicts if an alteration is a disease causing mutation or harmless polymorphism. The training sets contained different types of alterations, such as non-synonymous, mutations in introns, alterations that lead to substitution, insertion or deletion of an amino acid, or complex alterations such as introduction of a premature stop codon. It ranges its predictability score on the scale of 1 to 0, 1 indicating a high 'security' (not probability such as t-test statistics) of the given prediction.

The two non-synonymous mutations were entered into the PolyPhen-2 website server to predict any polymorphisms within the protein. The output from the software showed that the novel mutation I130V is predicted as benign with scores of 0.154, while the S229F mutation is predicted as possibly damaging with a score of 0.671 (Table 4.1).

Results in the SIFT server came back as damaging for both mutations, with an extremely low score of 0, unanimously. This is an expected result as SIFT works as a homology based system and both the I130 and S229 amino acids are conserved in *TPM1* (see Figure 4.1E and 4.2E).

All four mutations were analyzed by MutationTaster, as both protein and transcript sequences are accepted by this program. The two non-synonymous mutations are predicted as being disease causing with a high score of 0.971 and 0.888. The splice site and the poly-A signal mutations are predicted as harmless polymorphisms with good predictability scores of 0.729 and 0.711, respectively.

Variant	PolyPhen-2	Score	SIFT	Score	MutationTaster	Score
I130V	Benign	0.154	Damaging	0	Disease causing	0.971
S229F	Possible damaging	0.671	Damaging	0	Disease causing	0.888
IVS+2T>C	ND	ND	ND	ND	Benign Polymorphism	0.729
Poly-A signal AATAAA/GATAAA	ND	ND	ND	ND	Benign Polymorphism	0.711

Table 4.1 Prediction of the possible effects of four novel mutations by PolyPhen-2, SIFT and MutationTaster.
ND indicates not determined.

4.4 Investigating the effect of a novel splice-donor site mutation *in vitro*

To assess the functional consequence of a novel *TPM1* spice site mutation, three constructs were created, spanning the 5' upstream region of *TPM1* to exon 2a, using the patient and a control's genomic DNA (see Figure 4.5A). One construct contained the IVS1+2T>C splice site mutation, one contained the *tgt* insertion, and the final construct was a wild-type with no variations in the consensus. COS7 cells were transfected for 48 hours and harvested for analysis. RT-PCR showed that the wild-type and *tgt* insertion produced a transcribed *TPM1* product from the constructs of 370bps. However, no band was seen at this size for the splice-site mutation construct (n=3). Genomic bands could be seen for all transfected constructs indicating that transfection had occurred for all the samples (Figure 4.5B, top panel).

When the extension time of the PCR reaction was decreased, the genomic contamination disappears for the IVS1+2T>C and wild-type (Figure 4.5B, middle panel). No signal was detected for the splice-site mutation (T>C mutant) while the 370bp signal was detected for the wild-type. No signal was detected for the negative RT controls (-) or water controls (H_2O). The bottom PCR gel indicates *ACTB* (β-actin) which was used as a loading control (249bps; Figure 4.5B, bottom panel).

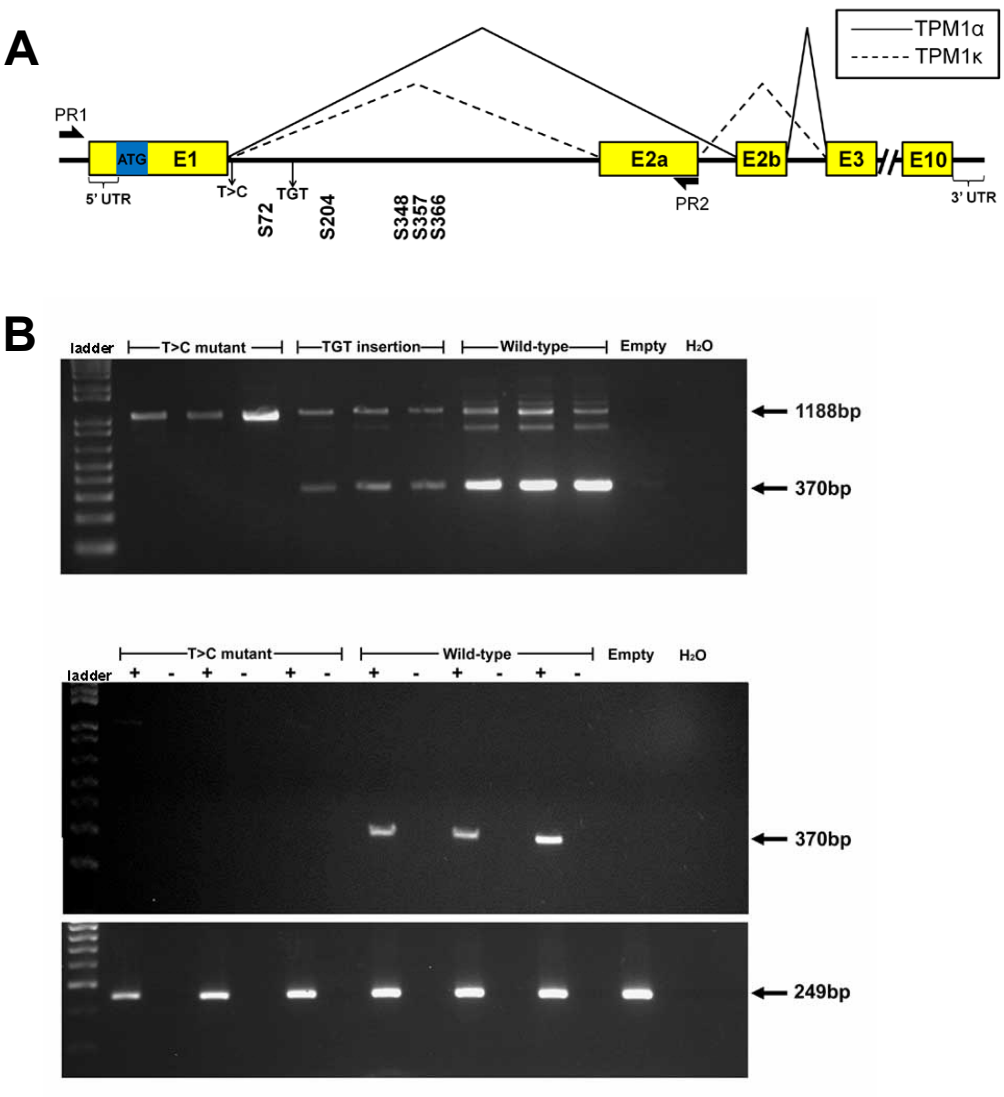

Figure 4.5 RT-PCR showing the splicing of *TPM1* containing a T>C mutation at the splice-donor site versus the *tgt* insert and the wild-type.

A. Schematic diagram showing the alternate splicing of *TPM1* and the regions to which the primers were designed. **Top panel.** The wild-type and *tgt* insert mRNA appears to have spliced normally, giving an expected band size of 370bps. On the other hand, the T>C mutants produce no splice product. However, genomic contamination is present for all three constructs. **Middle panel**. After decreasing the extension times of the PCR reaction, the genomic contamination disappears. A normal spliced product is present for the wild-type, but absent in the T>C construct. **Bottom panel**. *ACTB* (β-actin) was used as a loading control (247bp). The –ve RT, empty (transfection with empty vector) and –ve PCR controls were negative. + indicates RT; -, no RT; H_2O, water control.

4.5 Summary

Four novel variants of the TPM1 gene were discovered in a cohort of 380 patients with a range of CHDs. *In silico* analyses using SIFT and MutationTaster predicted both the non-synonymous mutations, I130V and S229F, to affect protein function. However, Polyphen-2 predicted only the S229F mutation to have a detrimental effect to function. Interestingly, mutation taster predicted the novel splice site mutation IVS+2T>C to be benign, even though the mutation is found in the donor site of the intron known to be important for splicing. This benign prediction was also found for the polyadenylation signal. *In vitro* analyses of the splice-site mutation showed that a mutation in the donor site of intron 1-2 resulted in failed splicing of the intron.

Chapter 5 Investigating a role for *TNNT2* in the developing chick heart

5.1 Overview

The chick embryo is a useful tool for studying heart development as the chick heart develops quickly after fertilisation. The chick can also be manipulated *in ovo*, allowing it to continue developing in its natural environment. This chapter describes the *in ovo* and *in vitro* role of TNNT2 in the developing heart.

The aims of these experiments were:

- To investigate a potential role for *TNNT2* in the developing chick heart by morpholino treatment *in ovo*. Using this method, the effect of TNNT2-morpholino treatment (TNNT2-MO) on 3-Dimensional structures that are developing the embryonic chick, such as the heart chambers, the atrial septum and ventricular trabeculae can be studied.
- Stereological analysis to detect any alterations not detectable by qualitative analysis.
- *In vitro* TNNT2-MO treatment in cell culture to investigate the effect on myofibril assembly.

Similarly to Chapter 3, an ATG start-site morpholino specific to *TNNT2* was designed to conduct *in ovo* and *in vitro* manipulation. The development of the heart was studied after morpholino treatment to investigate whether the morpholino had an effect. In cell culture, sarcomere assembly was monitored in cardiomyocytes positive for morpholino uptake.

5.2 Differential expression of *TNNT2* isoforms in the chick heart

A primer pair specific to *TNNT2* was designed to exon 1 and exon7/8, which are both present in the embryonic and adult isoforms of *TNNT2.* In addition the primer pair isvlocated around exon 5 which is absent in the adult isoform due to alternate splicing (Figure 5.1A). Therefore, designing a primer pair surrounding exon 5 would produce different band sizes by PCR, depending on whether the exon was present or absent in the transcript. cDNA was obtained from the heart tissue of different stages of embryonic development (HH12, HH14, HH19, HH22, HH24, HH26 and HH34) and from the neonatal and adult atrium and ventricles. Primer pairs were first optimised using HH24 whole embryo cDNA.

During embryonic stages of development, a high molecular weight band was present at all stages examined (235bp; Figure 5.1B top panel). A faint band was also present below the intense band at all stages (178bp).

In the neonatal atrium and ventricle, the faint band present in the embryonic hearts was now more intense and was expressed similar to the higher band that was originally present in the embryonic hearts (178bp; Figure 5.1B). In the adult atrium and ventricle, the upper band displayed a reduced signal, while the lower band remained and was intensely expressed (Figure 5.1B). This data shows the alternate splicing observed embryonically and postnatally. RT (-) and PCR (H_20) controls were negative and *Glyceraldehyde 3-phosphate dehydrogenase* (*GAPDH*) was utilised as a loading control (Figure 5.1B).

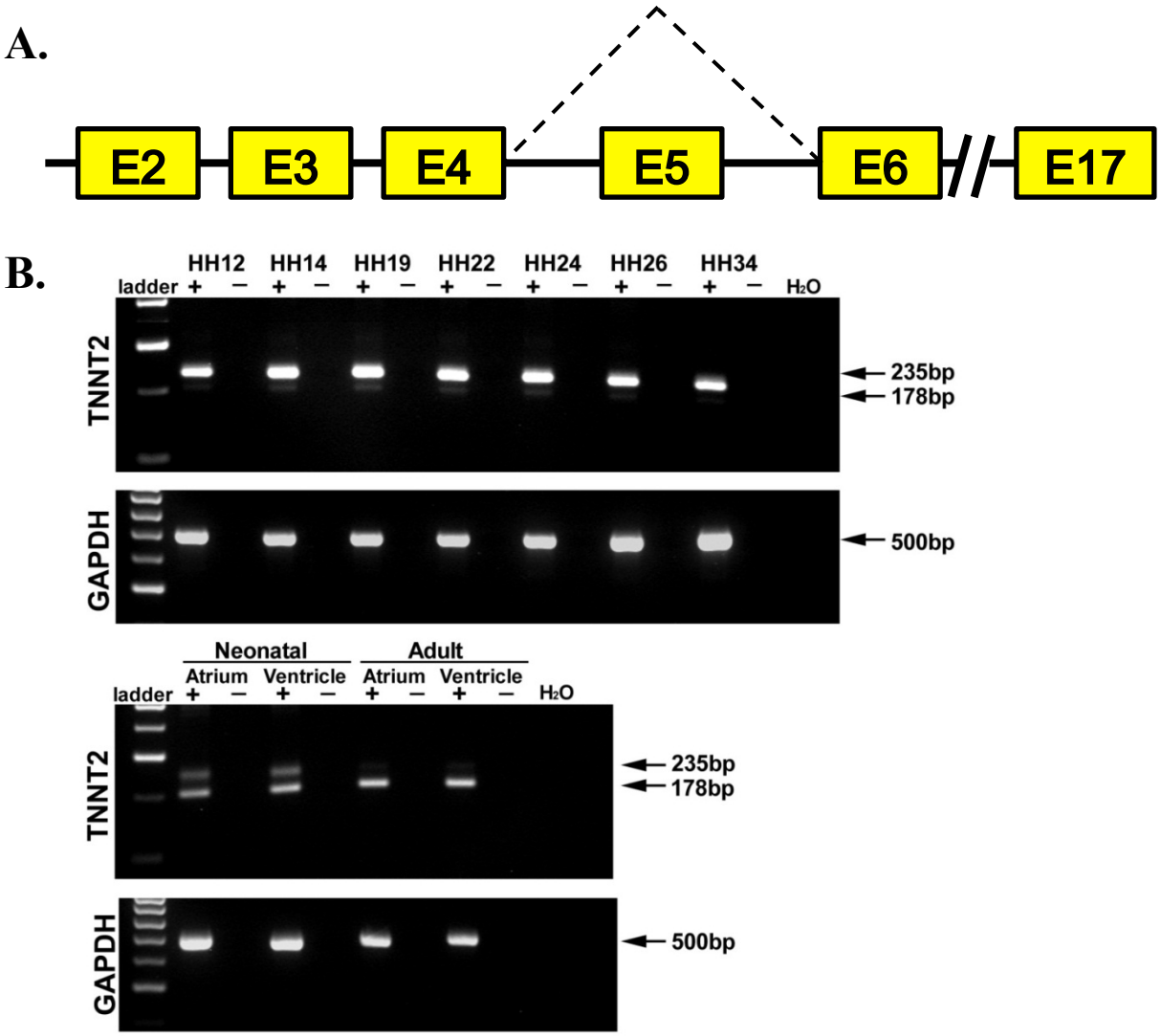

Figure 5.1 Expression profile of *TNNT2* showing the alternate splicing of *TNNT2* in the embryonic, neonatal and adult chick heart.

A. An illustration depicting the alternate splicing of exon 5 (57 base pairs) in the embryonic and adult heart. Exon 5 remains in the embryonic transcripts, while it is spliced postnatally.

B. A primer pair was designed to *TNNT2* around the alternately spiced exon 5. The top panel showed a 235bp expression of a TNNT2 isoform in the embryonic chick (HH12-34). A smaller 178bp band can be seen faintly expressed at those stages. In the neonatal heart (3rd panel) two bands can be seen in both the atrium and the ventricle. In the adult atrium and ventricle, the upper band is faintly expressed while the lower band has a strong signal. GAPDH was used as a loading control (2nd and 4th panels). +, RT; -, noRT; H_2O, PCR control; bp, base pairs.

5.3 Embryo grouping, survival and morpholino uptake

Two concentrations of TNNT2 morpholino, 250µM and 500µM, were initially used to optimise the required concentration needed to obtain a strong phenotype. HH11/19 represents morpholino treatment at HH10/11, and harvesting at HH19.

Survival rates were calculated for the 250µM and 500µM studies. For the 250µM study, the survival rates for UT (n=22), SC (n=30) and TNNT2-MO treated (n=22) embryos were 95.5%, 93.34% and 86.36%, respectively (P=0.171, no significant difference).

Survival rates for the 500µM study for UT chick embryos (n=35), SC group (n=45) and TNNT2-MO treated group (n=43) were 91.4%, 91.1% and 97.7%, respectively (P=0.761, no significant difference).

Surviving embryos were examined for 'morpholino uptake' determined by the degree of fluorescence. In the 250µM study, 39.3% and 47.4% of the SC and TNNT2-treated embryos were positive for morpholino uptake, respectively (P=0.59). For the 500µM study, 51.2% of the SC and 76.2% of the TNNT2-MO treated embryos were positive (P=0.123).

5.4 Quantification of the degree of protein 'knockdown' achieved by morpholino treatment

Western blot analysis was used on individual HH11/19 hearts treated with TNNT2-MO to quantify the degree of protein 'knockdown'. CT3 antibody, which is an anti-cTnT antibody, was normalised using GAPDH. No significant difference between the UT and SC groups (n=3 for both UT and SC) was seen (P=0.233). Therefore, these two groups were pooled into one control group. When the control and TNNT2-MO treated hearts (n=5) were compared, cTnT was significantly decreased by 32.8% in the TNNT2-MO treated hearts (P=0.016; Figure 5.2).

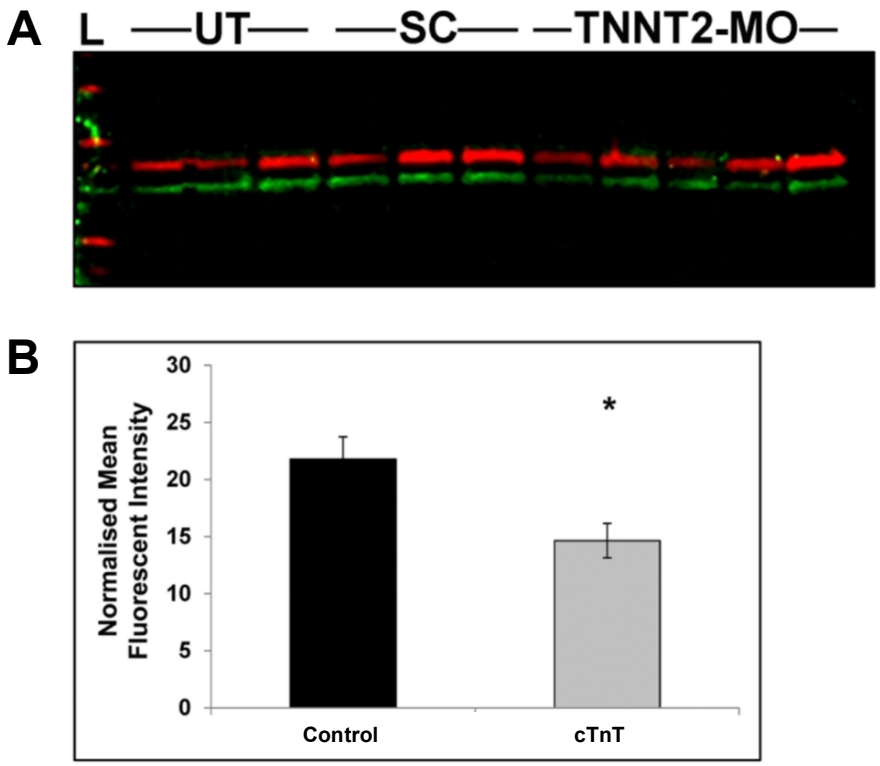

Figure 5.2Western blot using individual hearts revealed knockdown of cTnT in the morpholino treated hearts.

A. An example of a blot detecting cTnT (red) and GAPDH (green). **B.** TNNT2-treatment at HH11 results in significant reduction of cTnT in the chick hearts (*P*=0.016).

5.5 Development of the heart appears normal externally after TNNT2-morpholino treatment

Once embryos were confirmed positive for morpholino uptake, embryos were examined under low and high magnifications. Features such as looping; atrial and ventricular positioning and size; length and shape of the OFT were studied.

For the 500µM study all controls (n=54) and TNNT2-MO treated (n=43) embryos appeared to have a normal external phenotype (Figure 5.3; see Table 5.1 for a summary of TNNT2-MO experiments).

Similarly, no abnormal external phenotype was observed for the 250µM study for either the controls (n=20) or TNNT2-treated (n=22) embryos (Figure 5.3; Table 5.1).

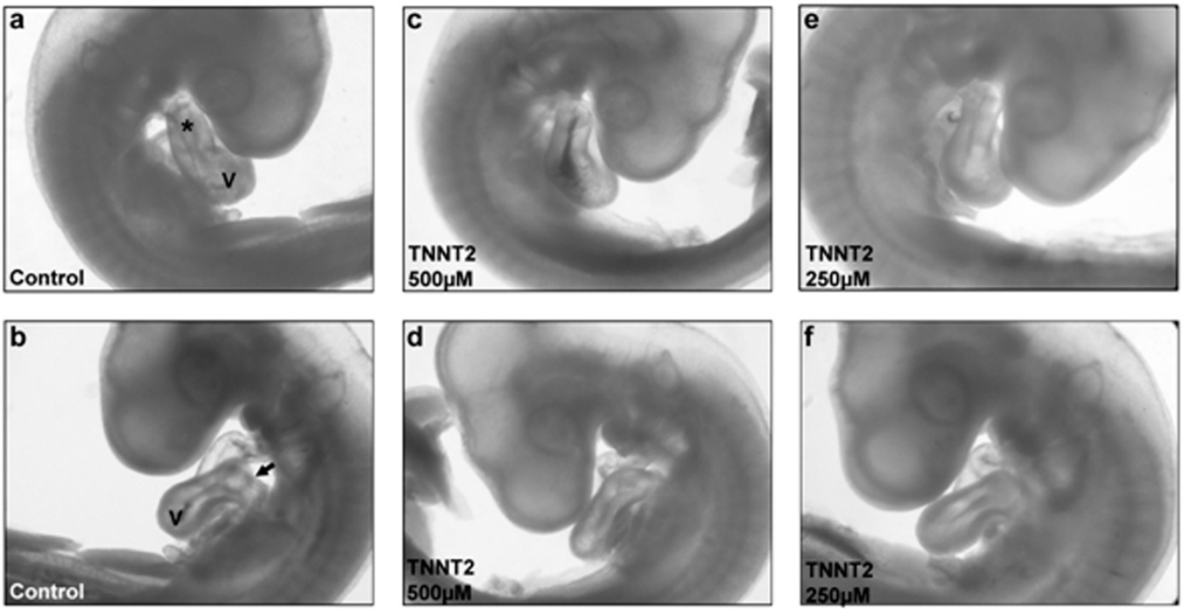

Figure 5.3 The external features of TNNT2-treated embryos appears normal.
At the time of harvesting, the external features of the embryos were studied. All of the control (a and b), 500µM (c and d) and 250µM TNNT2 treated embryos (e and f) display normal external shape and development. V indicates ventricle; *, outflow tract; arrow, atrium.

-	20	20	-	-	15	-	-	15	15
-	22	22	-	-	9	-	-	9	9

Table 5.1 Summary of phenotypic analysis after treatment with TNNT2 morpholino.

Assessment of heart shape based on qualitative analysis of gross morphological features.
Qualitative assessment of atrial septa and degree of trabeculation obtained from serial histological sections.
* Stage of development when knockdown/harvesting performed.
† Control embryos include standard control and untreated; TNNT2 denotes embryos treated with cardiac troponin 2 ATG morpholino.
‡ Total number of embryos analysed externally and internally.
Ab, abnormal; ext, externally; int, internally.

5.6 TNNT2-morpholino treatment results in abnormal atrial septation

HH11/19 embryos were serially sectioned in a transverse orientation to analyse internal structures of the developing atrium, such as development of the atrial septum from the roof of the common atrium; the presence and size of endocardial cushions protruding into the chamber; and the presence of cardiac jelly.

In the 500μM study, the atrial septa appear to develop normally in all the controls (n=38; Table 5.1; Figure 5.4a, b and a'). In the TNNT2-treated embryos, atrial septation is induced in all TNNT2-treated hearts. However, in 57.1% of the morpholino-treated embryos, the septum appeared small and resembled a knuckle shaped outgrowth from the atrial myocardium (n=12/21; Table 5.1; Figure 5.4c, d and c').

For the 250μM study, atrial septation was present in all control (n=15) and TNNT2-treated (n=9) embryos and all septa appeared have a normal size in all embryos (see Table 5.1 for summary).

The presence of cardiac jelly and normal endocardial cushions was observed in all hearts, including those treated with 500 and 250μM of TNNT2-morpholino (Figure 5.4a-d).

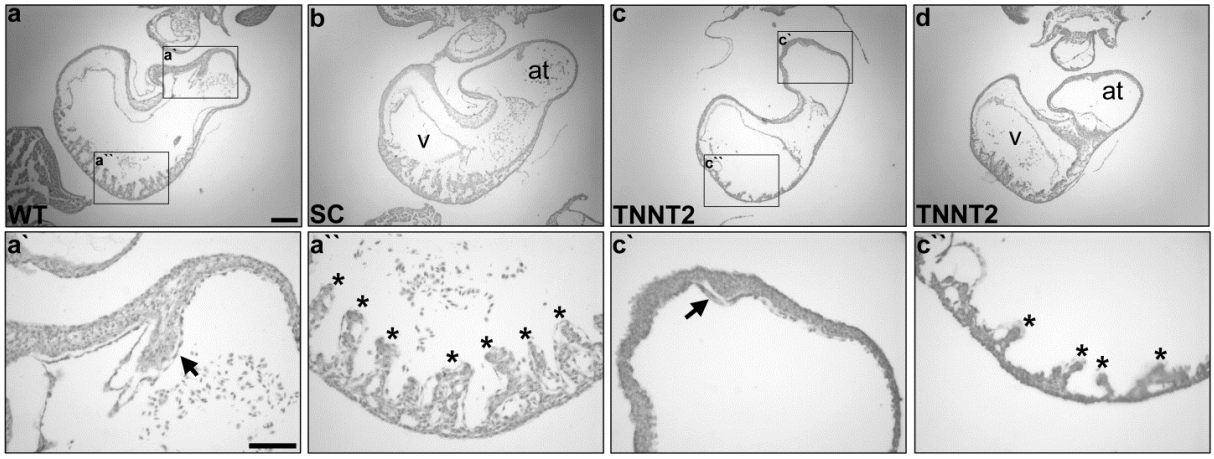

Figure 5.4 Internal examination of TNNT2-treated embryos revealed abnormal atrial septation and trabecular formation in the ventricles.

The internal appearance of the UT and SC hearts appeared normal (a and b), with initiation and growth of an atrial septum (a') and trabeculae (a''). TNNT2-treated hearts displayed atrial septation initiation, however, the atrial septa in these hearts appeared small and stunted in size (c, c' and d). The trabeculae were also affected in a subset of TNNT2-treated hearts with an atrial phenotype (c and c''). At indicates atrium; v, ventricle; *, trabeculae; arrow, septum. Mag bar=100µm.

5.7 Trabeculation of the ventricular myocardium appears normal for the majority of TNNT2-treated hearts

Similar to the TPM1-treated embryos in Chapter 3, the presence of trabeculae in the ventricular region of the developing heart was examined in TNNT2-treated embryos. These trabeculae appear as finger-like projections into the ventricular lumen. Trabeculation appears normal in the UT and SC groups in both the 500μM and 250μM studies (n=38 and n=15, respectively; Table 5.1; Figure 5.4) and appeared normal for the entire 250μM TNNT2-treated group (n=9).

In the 500μM study, almost all embryos appear to have normal trabeculation; however, a small proportion of the hearts appeared to have reduced number and size of trabeculae (2/21 or 9%; Figure 5.4). Interestingly, the hearts displaying the abnormal ventricular trabeculae also had a reduced atrial septum.

5.8 Stereological analysis reveals reduced atrial size in the TNNT2-treated hearts

Stereological analysis was completed on TNNT2-treated embryos in order to obtain information regarding tissue proportions compared to control hearts. This technique, as mentioned previously in chapter 3, involves placing a 96-point grid over every third tissue section of the heart, and counting the regions that the points hit. For the control hearts (UT n=3; SC n=4) 3978 points were counted, while 3922 points were counted for the TNNT2-treated hearts (n=4 with an atrial phenotype; n=5 with no internal phenotype).

The percentage proportion the atrium, ventricle and OFT contribute to the heart was first achieved by dividing the total number of counts per region by the total number of counts for that heart (Figure 5.4). No significant difference was seen between the UT and SC groups (P>0.567), so the two were pooled together. This also applied for the TNNT2-treated embryos with a normal and abnormal phenotype (P>0.283). No significant difference of proportions was seen in the ventricle or OFT between the control and TNNT2-treated hearts (Figure 5.5; P>0.062). However, there was a difference seen in the total proportion of the atrium, where the control and TNNT2-treated hearts contributes 24.8±1% and 22.3±0.5% of the total hearts (P=0.045).

The data collected here also confirms data collected for the TPM1 study of control hearts, where the ventricle makes up ~60% of the total heart, while the atrium and OFT contribute to ~25% and ~15%, respectively (Figure 3.10 and 5.5).

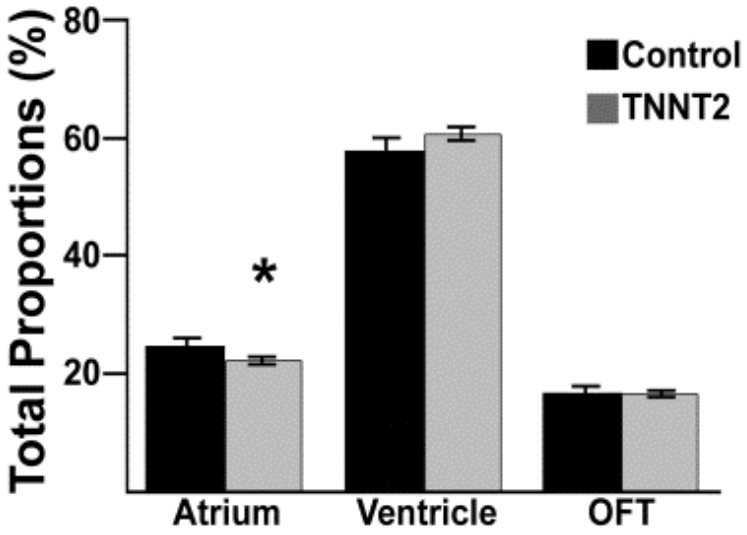

Figure 5.5 Stereological analysis reveals reduced atrial size.
The contributions of the ventricles and the OFT to the overall heart size remains constant between the controls and TNNT2-treated hearts (P>0.062). However, the atrial contribution to the heart is significantly decreased in the TNNT2-treated hearts (P=0.045).

5.9 Stereological analysis reveals normal tissue proportions

The percentage of lumen, myocardium and ECM within each region of the heart region (OFT, ventricle and atrium) was analysed using the stereological method from above. The UT and SC groups were first tested for any significant differences using an independent t-test. As no significant difference was seen, these two groups were pooled (P>0.091). A t-test was also used to check significance between the TNNT2-treated groups either with an atrial septal phenotype, or with no abnormal phenotype present. No significant difference was seen between the regions tested in the atrium and OFT, therefore the groups were pooled (P>0.076). However, a difference was seen in the ventricular ECM between the TNNT2-treated hearts with and without an abnormal phenotype (P=0.035). Therefore, the ventricular regions were analysed separately (Figure 5.6). This data suggests that there is an increase in the amount of ECM secreted by the cells of the developing heart. No differences were seen in the atrial or OFT regions tested between the controls and the TNNT2-treated hearts (P>0.217; Figure 5.6A).

In TNNT2-treated hearts with the atrial phenotype, ventricular ECM accounted for 21.67±2.35%, while the ventricular ECM in the normal phenotypic TNNT2-treated hearts accounted for 27.35±0.92%. However, when the TNNT2-treated groups are tested against the controls separately, no significant difference is seen in the ventricular ECM (P=0.856 normal phenotype; P=0.073 with abnormal phenotype; Figure 5.6B). No differences were seen in the ventricular lumen or wall proportion.

The variation observed between the TNNT2-morpolino treated hearts with and without the abnormal structural phenotypes, and the lack of variation observed when they are compared against the control group separately suggests that the number of hearts used should be increased to elucidate whether or not the ECM is increased in the non-phenotypic hearts.

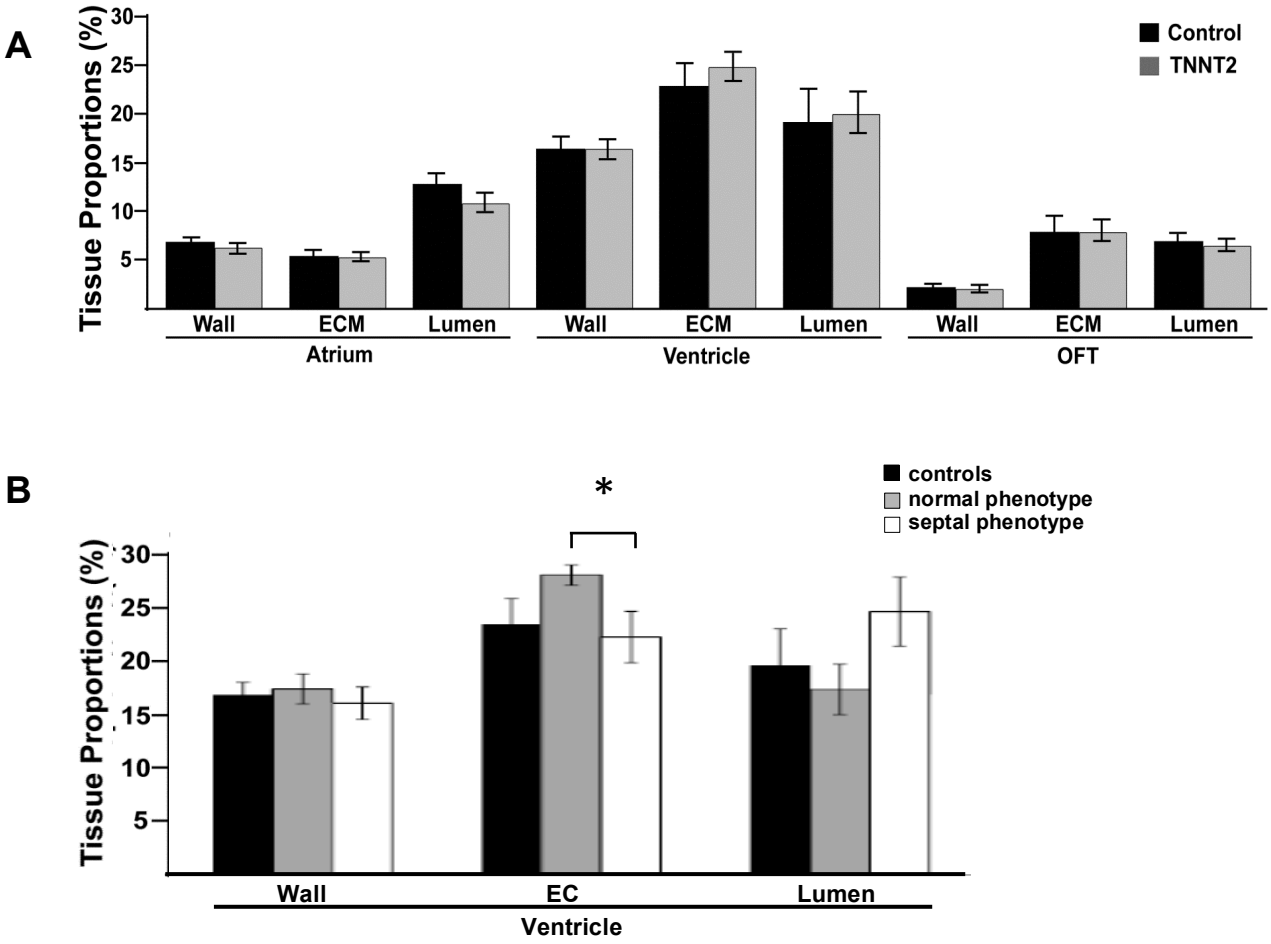

Figure 5.6 Stereological analysis reveals no differences in tissue proportions in the TNNT2-treated hearts when compared against the controls.

A. Differences in contributions of various cardiac tissue types to each region of the heart were examined. No differences were seen between the control and the pooled (normal and abnormal phenotypes) TNNT2-treated hearts (P>0.073). **B.** When the TNNT2-treated hearts with and without an abnormal phenotype were tested against each other, there was a significant difference in the proportions of ECM in the ventricular region (P=0.035). However, neither were significantly different from the control (P>0.073).

5.10 Morpholino treatment *in vitro* does not affect sarcomere assembly or maturity

Sarcomere assembly upon TNNT2-morpholino treatment was investigated *in vitro* using cardiac cell micromass. Using a TPM1 antibody to detect the sarcomere, we classified each cardiomyocyte into one of four stages depending on its sarcomeric maturity. Over 500 cells were analysed in this study. Stage 1 consisted of cells with positive staining around the periphery of the cell but no sarcomeric structures could be clearly seen, especially around the nucleus (Figure 5.7Aa). Stage 2 cardiomyocytes contained assembled sarcomeres, however, they appeared thin and disorganised (Figure 5.7Ab). Stage 3 cardiomyocytes presented with organised sarcomeres that appear thin but are organised and run parallel to one-another (Figure 5.7Ac). Finally, stage 4 cardiomyocytes contained mature cardiomyocytes with thick bands running through the cell (Figure 5.7Ad). Cardiomyocytes that actively uptake fluorescein-tagged morpholino were studied (Figure 5.7C). No significant difference was seen between UT and SC-treated cells, therefore these groups were pooled into one control group ($P>0.582$). When the control group was compared with the TNNT2-treated group, no significant difference was seen in sarcomere assembly in any of the groups ($P>0.180$; Figure 5.7C).

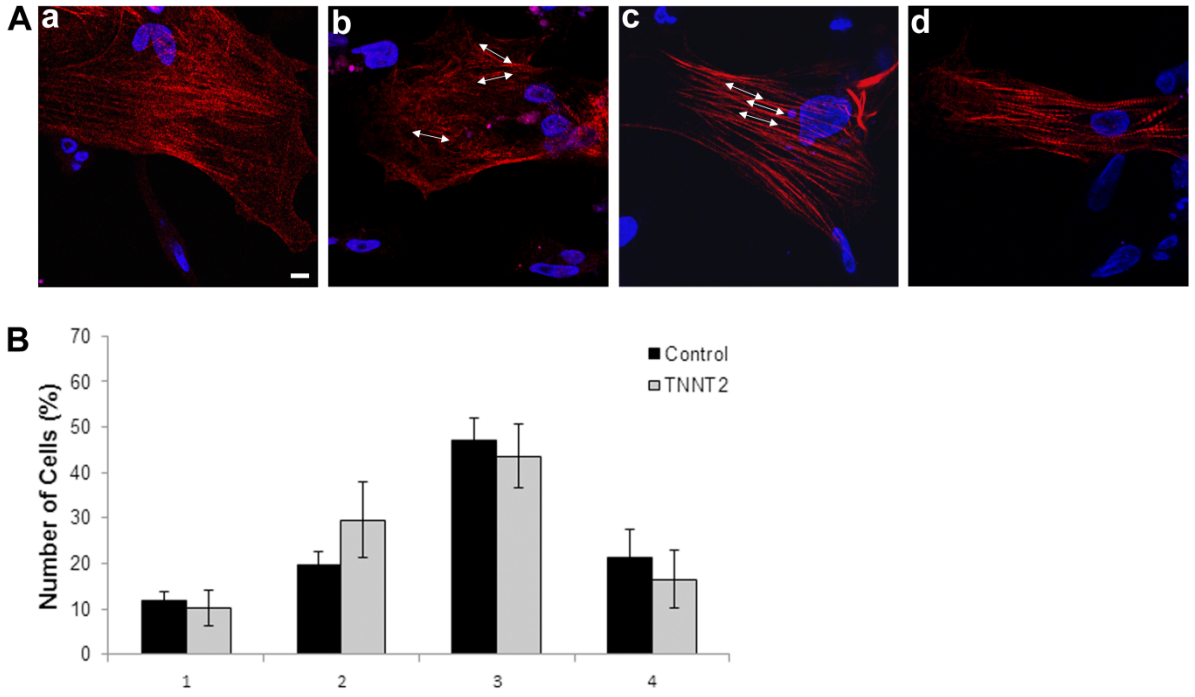

Figure 5.7 TNNT2-MO treatment does not lead to immature sarcomere assembly. **(A)** Sarcomere assembly was categorized into 4 types: type 1 is the immature myofibril that is assembling at the periphery of the cell and no fibril structures can be seen (a); type 2 when fibres are present but in a disorganised fashion (b); type 3 has organised fibrils but are still thin (c); and type 4 has fully developed thick fibrils running from one end of the cell to the other (d). **B.** TNNT2-treatment does not appear to affect sarcomere assembly or maturity.

5.11 Summary

Using antisense oligonucleotide morpholinos, knockdown of cTNT was achieved. This reduction in cTnT resulted in abnormal atrial septal development and ventricular trabeculation. Although no abnormal external phenotype was distinguishable by qualitative analysis, stereology revealed that the atrial chamber was reduced in size in the TNNT2-treated embryos. However, the atrial wall, lumen and ECM proportions similar to that of the controls. Furthermore, tissue proportions remained unchanged in each region quantified, except where the ECM in the ventricle was significantly different between the TNNT2-treated groups with and without an abnormal phenotype. Knockdown of cTnT *in vitro* revealed normal sarcomere assembly in cardiomyocytes extracted from 6 day old embryonic chick hearts.

Chapter 6 Discussion

6.1 Overview

This is the first study looking at a role for *TPM1* and *TNNT2* in the early developing chick heart. Using antisense oligonucleotide morpholino technology, targeted manipulation of both genes was conducted *in ovo* using pluronic gel as a transporter. The gross anatomical structures of the developing hearts were analysed to determine if the morpholino treatment resulted in any developmental abnormalities. Atrial septation and ventricular chamber maturation via the production of trabeculae were affected in both the TPM1 and TNNT2 morpholino groups. In addition, TPM1-morpholino treatment had a detrimental effect on myofibril assembly in vitro, as well as causing increased apoptosis in the developing heart.

In a cohort of 380 patients with a range of congenital heart anomalies, the *TPM1* gene, including introns, was sequenced. A total of four *de novo* genetic variants were identified by Dr. Javier Granados-Riveron; I130V, S229F, IVS1+2T>C and GATAAA/AATAAA in the polyadenylation signal. None of the novel mutations were found in the controls. Where possible the inheritance of the variants was determined. *In silico* analysis was completed for the four mutations revealing predictions to whether or not the mutations were detrimental to the protein and its function. *In vitro* functional analyses of IVS1+2T>C was carried out to investigate the effect of the mutation compared to the wild type. The principal novel finding of these studies was that the IVS1+2T>C mutation results in abnormal splicing of the *TPM1* pre-mRNA and may be a contributing factor to CHD in man.

6.2 TPM1 plays a number of roles during cardiogenesis

TPM1 is a α-helical coiled-coil double-stranded protein, which binds to itself from head to tail and sits in the long grooves of the helical filaments of actin (Brown et al., 2005). TPM1 functions in regulating actin and stabilising it, and also works with the troponin complex in response to Ca^{2+}, by blocking the actin-myosin interaction in its absence and exposing the myosin binding site on the actin filament to allow contraction in its presence (Jagatheesan et al., 2003, Brown et al., 2005). The *TPM1* homozygous knockout mouse has already been created, although these embryos died at ED9.5-13.5 (Blanchard et al., 1997). In turn, the phenotype of these embryos was not described prior to the commencement of this thesis.

TPM1 has been linked to cardiomyopathies in humans and animal models (Van Driest et al., 2003), yet, it has not previously been associated with CHDs.

Part of the aim of this thesis was to determine a role for tropomyosins in the developing heart. Therefore, an expression profile of different isoforms of *TPM1* and *TPM4* at different stages of development was initially completed. Isoforms *TPM1α* and *TPM1κ* were expressed throughout development in the chick heart up to HH34 (day 8 in development), while these isoforms were absent in the neonatal and adult heart. Instead, *TPM4* is expressed in both the embryonic and postnatal heart. This is consistent with the results from Wang *et al.* who looked at the expression of these genes and isoforms, but only in the HH12 and HH41 (15-day old embryo) and adult chick heart (Wang et al., 2008).

A protein expression profile was also conducted using an anti-TPM1 antibody, CH1. TPM1 appears to be restricted to the myocardium of the atrium, ventricle and OFT, and is not present in the ECM and endocardium in the embryonic and neonatal heart. The RT-PCR conducted showed *TPM1α* and *TPM1κ* were not expressed in the neonatal heart, however, the immunohistochemistry using the CH1 antibody stained positively in the neonatal heart indicating that is may be detecting TPM4 in addition to TPM1. Furthermore, TPM1 and TPM4 are highly homologous at the C-terminus. CH1 antibody is known to react within the C-terminus of TPM1, in the region of exon 9a, although the epitope for CH1 is not known. Therefore, it is likely that the CH1 antibody can detect TPM4 as well as TPM1. Regardless, this data shows the overall expression of tropomyosins in the developing heart, where it is restricted only to the myocardium of the atrium, ventricle and OFT, and absent from the ECM, endocardium and surrounding non-cardiac tissues.

Targeted manipulation of *TPM1* using antisense oligonucleotide morpholinos was performed at HH10/11 in the chick, just after the heart tube had formed, and at HH19, when atrial septation and trabeculation are well underway. For these studies, 500μM of morpholino was applied to the developing embryos. This concentration was previously optimised in the laboratory by an MRes student Diji Kuriakose. Upon TPM1 morpholino application, she observed abnormal atrial septation and trabeculae formation. In addition, she found that 500μM morpholino application gave the best phenotype penetrance (Kuriakose, 2008). In this current thesis, three morpholinos were designed to *TPM1*, one ATG-start site morpholino

targeting translation of mRNA, and two splice site morpholinos designed to either exon1-intron1 or exon4-intron4 which interferes with splicing of the pre-mRNA.

Upon external analysis of the TPM1-morpholino treated embryos, almost 4% (4 out of 96 embryos) presented with an abnormal external phenotype in which the heart was abnormally looped. Alterations in cardiac conductivity and contractility are known to have a morphological effect on cardiogenesis. Previous studies involving retinoic acid treatment of HH15 chick embryos resulted in abnormal looping of the heart. This in turn led to the misalignment of the ventricular septum and resulting in cardiac defects such a double outlet right ventricle (Bouman et al., 1995). Retinoic acid is thought to decrease cardiac contraction forces, therefore causing haemodynamic alterations leading to looping abnormalities (Broekhuizen et al., 1995). In the Connexin 40 deficient and null mouse, animals displayed VSD, double outlet right ventricle, TOF, endocardial cushion defects, bifid atrial appendage and aortic arch defects (Gu et al., 2003). Connexins are gap junction proteins responsible for the propagation of an action potential through the myocardium (Gros and Jongsma, 1996). The electrical conduction in those hearts was remarkably impaired (Tamaddon et al., 2000). It is possible, therefore, that alteration in haemodynamics of TPM1-treated heart results in abnormal looping.

Action potential recordings were obtained from TPM1-treated ventricular and atrial cardiomyocytes (unpublished data obtained in collaboration with Dr Luis Polo-Prada). Both cardiomyocyte groups exhibited shorter action potential durations and increased maximal rate of rise ($\delta v/\delta t$) when compared to the untreated control cells (Figure 6.1B and F). In addition, the ventricular cells that were treated with TPM1-morpholino had significantly reduced amplitudes (Figure 6.1A). Interestingly, 100% of the cells measured in the TPM1-treated group had an affected action potential (n=187 cells, $P<0.005$).

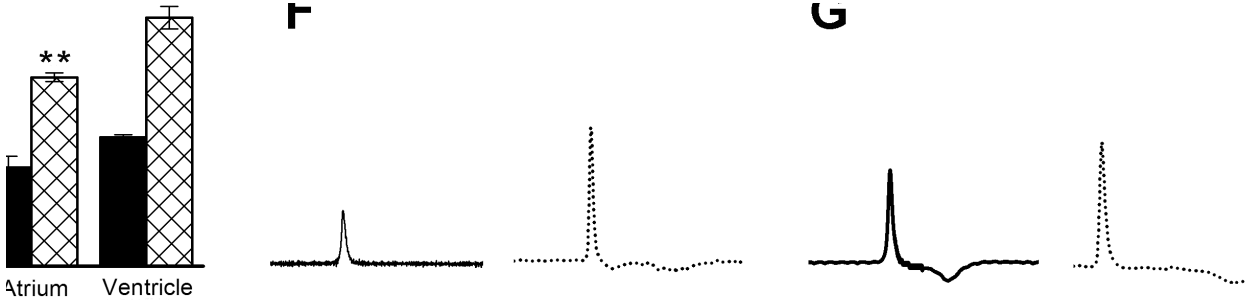

Figure 6.1 The action potentials and depolarisation of cardiomyocytes after TPM1-morpholino treatment.

A. This graph depicts the changes in the amplitude in the atrial and ventricular cardiomyocytes from TPM1-treated and control hearts. The amplitude is decreased in the TPM1-treated cardiomyocytes in the ventricle. **B.** The duration of the action potential in both the atrial and ventricular cardiomyocytes was significantly reduced in the TPM1 treated hearts. **C** and **D.** Representative traces of the action potentials from the atrial (C) and the ventricular (D) cardiomyocytes showing the change in the amplitude and duration of the action potentials. **E.** The rate of depolarisation (measured by $\delta v/\delta t$) in both the atrial and ventricular cardiomyocytes. **F** and **G.** Representative traces of the depolarisation in the atrial (F) and ventricular (G) cardiomyocytes. ** $P< 0.005$.

Considering 100% of the TPM1-morpholino treated cardiomyocytes had affected action potentials, only 58% of the hearts of the same treatment displayed gross morphological abnormalities (i.e. abnormal atrial septation and/or reduced ventricular trabeculae). This may indicate that the contractile mechanism may be more sensitive to the effect of the TPM1-treatment and the structural phenotype may be a secondary anomaly caused by the abnormal contraction in a form follows function paradigm (Midgett and Rugonyi, 2014, Granados-Riveron and Brook, 2012, Rutland et al., 2011). In other words, the abnormal physiology observed by the action potential recordings in turn cause abnormal development of anatomical structures such as the atrial septum and ventricular trabeculae.

It is thought, the increase in $\delta v/\delta t$ may indicate an increase in the number of active Na^{2+} channels which are opened at the initial stages of depolarisation (Pinnell et al., 2007). However, since the amplitude (only ventricular) and duration of the action potential was significantly reduced in TPM1-treated hearts, it may suggest that the number of L-type $I_{Ca}{}^{2+}$ channels are significantly decreased with an increase in the number of active $I_K{}^{+}$ channels, producing a rapid repolarisation effect (Pinnell et al., 2007).

In the eMHC knockdown chick heart, action potential recordings were also obtained and appeared different to the TPM1-treated hearts. While the amplitude of the action potentials were decreased in the eMHC knockdown hearts, the durations and depolarisations of the action potentials were significantly increased (Rutland et al., 2011). In addition, no obvious changes in the contraction patterns of the TPM1-treated cardiomyocytes were observed. In contrast, 75-80% of the eMHC knockdown cardiomyocytes had no action potential (Rutland et al., 2011). These differences in action potential between TPM1 and eMHC morpholino treated hearts may be down to the regulation of ion channels of the cardiomyocytes. Changes in the Ca^{2+} transients in the eMHC knockdown resulted in the extension of the plateau phase of the action potential, therefore, increasing the duration of the action potential (Rutland et al., 2011). Therefore, it may be worthwhile investigating Ca^{2+} in TPM1-treated hearts.

Serial sectioning through TPM1-treated hearts revealed an abnormal atrial septum and/or reduced trabeculae in 58% of the embryos (embryos treated and harvested at HH11/19). All of the embryos with the abnormal external phenotype had abnormal atrial septation and/or reduced trabeculae. Stereological analysis further complemented this qualitative phenotype and revealed reduced proportions of ventricular wall and trabeculae in morpholino treated

hearts (P=0.003). In addition, stereology also revealed increased ventricular lumen size in TPM1-treated embryos, including those TPM1-treated hearts that appeared to have no abnormal internal phenotype upon morphological analysis (P=0.024). This may be due to the method by which each heart was analysed, whereby the each serial section through the heart is studied. Perhaps those hearts that were marked as normal (with no abnormal phenotype) from the qualitative analysis may actually have reduced ventricular wall mass that is not obvious from visual examination as it is too minute to see on one section. In the recently described *Tpm1* homozygous knockout mouse, the ventricular myocardium appeared thin, and only one cell thick in places (McKeown et al., 2014). In addition, those hearts had fewer trabeculae which were thinner and wispier in appearance. This data fits with the thin myocardial wall and reduced trabeculae observed in the TPM1-morpholino treated hearts reported in this thesis.

Unfortunately, the stereological analysis was unable to back up the reduced atrial septum phenotype, as there were not enough counts to complete a statistical analysis. However, the trend did indicate a decrease in atrial septal proportions (Figure 3.11). In addition, although the atrial septum was abnormal in 41% of the hearts (n=28/69), the structure was never absent from the developing TPM1-treated hearts, suggesting a role for TPM1 in the growth and maintenance, and not initiation of atrial septation (Figure 3.7). This may be indicated by the presence of a double atrial septum observed in one of the TPM1-treated hearts. Instead of a normal single septum extending from the dorso-cranial wall of the atrial chamber, two septa were present and both appeared reduced in size. As we reach the most posterior part of these septa, they fuse together as they merge into the atrial wall. A similar phenotype was observed after knockdown of αMHC, where 97% of embryos had reduced or absent atrial septa (Rutland et al., 2009). Two of these embryos had either two or three atrial septa growing from the dorso-cranial atrial chamber. Therefore, structural sarcomeric proteins may play a role in the specification of myocardial processes such as atrial septation to ensure correct myocardial architecture.

The abnormal looping, abnormal atrial septum or reduce trabecular phenotypes were not seen in the HH19/24 TPM1-treated embryos. At HH10/11, formation of the myocardium and migration of cardiac cells is still underway, therefore, TPM1 may not be fully expressed in large amounts at this time. However, in the older HH19 heart, large quantities of TPM1 with

a long half-life (5.5 days) (Marston and Redwood, 2003) are already present in the heart. In addition, as the heart tissue is much denser at HH19 than HH10, it may be more difficult for the morpholino to penetrate into the inner layers of the heart tissue.

Apoptosis is an important event during development, by which tissues can be remodelled or removed. The level of apoptosis in the TPM1-treated hearts was quantified by enzymatically labelling the free 3'-OH terminus of DNA with TdT. Apoptosis was significantly increased in the ventricular myocardium when compared to the control hearts. Although apoptosis was unaffected in the atrial myocardium, apoptosis was increased in the atrial septum. This increase in apoptosis could explain the stunted atrial septum and reduced trabeculae that was seen in the TPM1-treated hearts. Increased apoptosis during development and in the adult has been associated with dilated cardiomyopathy in human and animal models (Das et al., 2010, Guerra et al., 1999, Tintu et al., 2009, Wencker et al., 2003). However, in this chick model, although the lumen size is increased and ventricular wall mass is decreased, the overall proportion of the ventricular chamber is comparable to that of the control heart. Therefore, in this study there is not a dilated cardiomyopathy phenotype that is characterised by dilated left and/or right ventricles with thinned ventricular wall (Towbin and Bowles, 2002). It has been postulated that apoptosis may be linked to CHDs as the arrest of a developmental process during cardiogenesis due to insufficient cell numbers required for that process (Fisher et al., 2000). Previous studies using teratogens such as glucocorticoids resulted in alterations in the timing and level of cell death in the OFT cushions (Pexieder, 1975). This was often associated with VSDs and malalignment of the great vessels. Altered haemodynamics also disrupts apoptosis in the heart (Pexieder, 1975). It was found that high sheer stress protects the heart from apoptosis, while low sheer stress and turbulent blood flow can result in increased apoptosis (Li et al., 2005). In addition, TPM1 may play a role in aiding cell survival in the developing heart, and increased apoptosis resulting from reduced TPM1 expression results in abnormal atrial septum development and reduced trabeculation in the ventricles.

Ultrastructural analysis of the TPM1-treated hearts revealed normal tissue integrity of the hearts compared to the controls. With this, myofibril presence, the size of intracellular spaces, cellular size, presence of mitochondria and the assembly of adherens junctions (desmosomes) were all analysed and appeared normal. In the *Tpm1* homozygous knockout mouse cardiomyocytes appeared enlarged with expanded intracellular spaces and extended cellular

processes, accounting for the enlarged heart phenotype (McKeown et al., 2014). No myofibrils appeared to have assembled, but instead disorganised thick filaments were interspersed with Z-body like thin filaments. Adherens junctions appeared small in the homozygous knockout heart (McKeown et al., 2014). These structures appeared normal in the heterozygous mouse (McKeown et al., 2014). One limitation of this paper is, however, that the embryos used for the ultrastructural analysis are embryonic lethal early in development (ED9.5), yet the analysis was carried out on ED9.5 embryos. If the embryo is dying and possibly undergoing absorption, then the ultrastructure of the tissue in these embryos is going to be poor. Therefore, the data may not be a true reflection of the tissue integrity in TPM1 homozygous knockout hearts.

TPM1-morpholino treatment of cardiomyocytes in cell culture revealed normal myofibril assembly, but the number of immature myofibrils was increased and mature myofibrils reduced in these cells when compared to the control. In the *Tpm1* homozygous knockout mouse, myofibril assembly was completely halted and the thick and thin filaments fail to interact (McKeown et al., 2014). Similarly, in the *cardiac* mutant axolotl heart, the reduction of Tpm1 resulted in the failure of myofibrils to assemble resulting in a non-contractile heart (Moore and Lemanski, 1982, Starr et al., 1989). However, sarcomeric structures were initiated and remained in the nascent stages of myofibrillogenesis (Zajdel et al., 2007). In the data described within this thesis, morpholino treatment is conducted after the initial heart tube has formed and therefore, TPM1 was already present in the heart. Conversely, in the homozygous knockout mouse and cardiac mutant axolotl, *Tpm1* is absent or diminished from the outset. From these studies, we can hypothesize that sufficient amounts of *TPM1* is required for normal myofibrillogenesis.

6.3 *In ovo* transfection may not be an appropriate method to perform a rescue in morpholino treated hearts

Since it was not possible to demonstrate the degree of protein knockdown in the TPM1 study in the chick, the development of a rescue was attempted to show that the phenotypes observed were due to specific targets of the morpholino and not non-specific effects. The over expression of protein in the chick heart *in ovo* was previously accomplished (Ishii et al., 2010). These investigators directly microinjected a construct containing a *Noggin* insert

linked with *Gfp* into the pericardium of HH13-14 chick embryos. When these embryos were harvested, they found expression of the GFP in the myocardium of the heart, with no expression observed in other tissues. They achieved a typical transfection efficiency of 4% expression of GFP. They also showed by real time PCR that the expression of *Noggin* was increased by 170-270 times in the injected hearts.

After the first attempt at microinjecting a GFP construct into the HH14 chick pericardium, survival rates in this study were much greater. A 94% (only one embryo died) survival rate was observed while Ishii et al. reported a survival of only 40-80% (Ishii et al., 2010). The studies in this thesis showed that microinjection was also possible at HH11 and HH19, where HH11 gave very high transfection, or 5 stars using the scoring system. Immunohistochemical analysis showed that there was GFP expression in about 7.2% of the myocardium after random sample counting.

The high levels of *Noggin* expression in the microinjected experiments by Ishii et al. is expected, since Noggin is a signally molecule, that may be secreted and have non-autonomous actions on surrounding cells. Since TPM1 is not a signally molecule and the purpose of this experiment was to complete a rescue in TPM1-morpholino treated hearts, an much larger amount of construct transfection would be required. To do this the amount of transfection reagent, concentration of the construct and incubation times were altered. However, none of these factors increased the level of GFP expression. In addition, the transfected cells were located in the outer myocardial layer of cells, with no transfection observed in the atrial septal tissue, trabeculae, or endocardial cushions. It was agreed that this level of expression would not be sufficient to conduct a rescue in morpholino treated embryos.

6.4 The functional consequence of TPM1 mutations in patients with CHDs

To determine a role for *TPM1* in human cardiogenesis, a cohort of 380 individuals with a range of CHD were screened. Four novel variants were detected, two non-synonymous, one splice-site mutation and one found in the polyadenylation site of *TPM1*. Non-synonymous single nucleotide mutations represent more than 50% of the mutations known to be involved

in human inherited diseases (Krawczak et al., 2000). For this reason, it is important to investigate the possible effect of these novel mutations.

The I130V mutation is located within the fourth α-zone of the TPM1 protein, which has been proposed, based on structural analysis, to interact with subdomains 1 and 3 of F-actin, in the context of the sarcomere (Brown et al., 2005). *In silico* analysis based on amino acid conservation predicted the mutation to be disease causing. This *d* position, as mentioned previously, is important for interlocking with the *a* position, that gives TPMs their coiled-coil configuration (Crick, 1953), and therefore, interruptions in these binding regions may affect the coiled-coil stability (Monera et al., 1995).The second non-synonymous mutation identified , S229F, was also predicted to be disease causing. In addition, the substitution of a small polar serine for a larger polar phenylalanine could possibly impair the binding, by steric hindrance, of the two TPM1 peptides that form the coiled-coil TPM1 filament (Mamidi et al., 2013).

In silico analysis was also completed on the IVS1+2T>C mutation found in a patient with Tetralogy of Fallot, a complex defect including: ventricular septal defect, overriding aorta, right ventricular outflow obstruction, and right ventricular hypertrophy. Surprisingly, the mutations was not predicted to be harmful.. However, this is not consistent with the literature. GT>GC substitutions in the splicing donor site of exon1-intron1 are known to cause human disease when present in other genes (Rossi and Superti-Furga, 2001, Verot et al., 2007). The most likely outcome of this donor-site mutation is: intron1-2 inclusion in the mature mRNA; the use of cryptic donor sites in the same intron or in the adjacent exon; or exon skipping (Talerico and Berget, 1990, Schwarze et al., 1999). In vitro analysis revealed a spliced mRNA product failed to be produced in COS7 cells transfected with the mutated transcript. Therefore, since no mRNA product was produced, a mutation in the first donor site does not result in the use of cryptic donor sites (first one seen 137 bases downstream of the donor-splice site). In addition, intron inclusion was not seen. Therefore, the donor-splice site in the first intron of *TPM1* is essential for the generation of normal RNA products. However, as the construct was designed to span exon1 to exon2a (see Figure 4.5), this experiment could not distinguish between three different possibilities; exon1 and/or exon2a could be absent from the mRNA product, a premature stop codon in intron1/2a may have been reached, or no product at all could be produced.

A mutation detected in the 3′ untranslated region of the gene modifies the first base of the sequence of the polyadenylation signal (AATAAA/GATAAA). This mutation has been identified in 3 healthy individuals in the general population with no known phenotype. Polyadenylation is important for the stability, translation efficiency and transportation of mRNA and mutations of the polyadenylation signal consensus can cause human disease (Bennett et al., 2001), and specifically, it has been shown that this particular substitution reduces the efficiency of the cleavage of the mRNA precursor at the polyadenylation site to approximately 30% of the wild-type sequence whereas the polyadenylation itself is reduced to 11% (Sheets et al., 1990), therefore, an increase of pre-mRNA degradation of *TPM1* may occur. Interestingly, this mutation is also located within an experimentally validated binding-site for microRNA-21 (Zhu et al., 2007). microRNAs are small non-coding RNAs that regulate gene expression by repressing their translation or cleavage (Pillai, 2005). In addition, microRNAs are believed to act as tumor suppressors or oncogenes, depending on their targeted gene. *TPM1* is a known tumor suppressor and binding of microRNA-21 to *TPM1* represses its expression, resulting in tumor growth. However, mutations within the microRNA-21 binding site, such as the one describe in this thesis, would reduce its suppression of *TPM1* resulting in tumor growth suppression and may be a promising future therapeutic target for tumor growth (Zhu et al., 2007).

To date, a range of genes have been associated with CHDs, from transcription factors, ligands and their receptors to structural proteins (England and Loughna, 2013, Wessels and Willems, 2010), with mutations in these structural proteins also associated with cardiomyopathies (Walsh et al., 2010, Morimoto, 2008). It is also of note that some mutations in these genes have been associated with a wide spectrum of CHDs which may be isolated or in combination, such as ASDs, transposition of the great arteries, TOF, VSD and conduction anomalies (Budde et al., 2007, Ching et al., 2005, Granados-Riveron et al., 2010). This study demonstrates that *TPM1* plays a crucial role in cardiogenesis, both structurally and physiologically. Functional analysis of novel human mutations has provided proof that *TPM1* is a candidate gene worthy of further screening for cardiovascular disorders.

Unfortunately, not much is known about the family trees of the patients in each case. For the I130V mutation, the affected male has a dizygotic twin, who also has an ASD. For the S229F, the parent of the affect individual has a dizygotic twin of unknown sex. This individual also

has a daughter with a septal defect. Clarifying the carriers within these complex family trees could provide some important information regarding the inheritance of these mutations. In addition, no family history was available for the IVS1+2T>C carrier. A follow up study with the families was attempted, however, without success.

6.5 *TNNT2* role in the developing heart

cTnT forms part of the troponin complex, in which it binds to tropomyosin regulating its movements around the actin filament. *TNNT2* is known to play a role in cardiomyopathies, with a large number of mutations identified in patients with cardiomyopathies. In addition, the *Tnnt2* homozygous knockout mouse has been described in the literature and the embryos are not viable beyond ED10 (Ahmad et al., 2008, Nishii et al., 2008).

One of the aims of this thesis was to show the expression of *TNNT2* through a number of embryonic stages and in the neonatal and adult heart. *TNNT2* is expressed in the heart throughout embryonic development and expression remains in the neonatal and adult heart. In addition, an isoformal shift of *TNNT2* between embryonic and neonatal life has been demonstrated. Taking advantage of the alternate spicing of exon 5 in *TNNT2*, primers were designed to demonstrate the inclusion and exclusion of this exon in the embryo and postnatally, respectively. The high molecular weight isoform of *TNNT2* is expressed as early as HH12 in the embryonic chick heart and is present through all the stages of development studied. The low molecular weight isoform of *TNNT2* is also detected as a faint band. In the neonatal heart, an isoformal shift occurs, where both the high and low molecular weight isoforms are present with both producing strong signals. In the adult heart, however, the high molecular weight isoform of *TNNT2* appears decreased with the predominant expression of low molecular weight one. Concurrent with the literature, *TNNT2* is detected in the embryonic chick heart at HH12, and even earlier at HH4 in the mesoderm (Antin et al., 2002). However, expression of cTnT, the protein produced by *TNNT2*, was not detected until HH9 (Antin et al., 2002). The isoformal shift of *TNNT2* is consistent with a study conducted looking at the expression of cTnT at the protein level. In the HH31 chick, the high molecular weight isoform is predominantly expressed, however, the expression of the low molecular

weight isoform increases as development continues, while the high molecular weight diminishes (Yonemura et al., 2002). By HH46 (or day 20-21; hatching stage) the expression of both isoforms appear equal. Throughout neonatal development and in the adult, the low molecular weight isoform becomes predominantly expressed, replacing the high molecular weight one (Yonemura et al., 2002).

Using a morpholino designed to the *TNNT2* ATG start-site, targeted manipulation was possible *in ovo*. Two different concentrations of morpholino were initially used, 250µM and 500µM to determine an effective knockdown to produce a phenotypic effect. Neither concentrations produced an abnormal external phenotype. However, another ATG start-site morpholino that was designed to *TNNT2* upstream of the ATG start site produced an abnormal external phenotype at a 500µM concentration (unpublished data, Kar-Lai Pang). This phenotype presented as a diverticulum (or outgrowth) from the primitive ventricle. Congenital ventricular diverticula have been reported in the literature, but as of yet, have not been linked to sarcomeric proteins (Jeserich et al., 2006, Ashraf et al., 1984, Kobza et al., 2003, Del Rio et al., 2005). The penetrance of this diverticulum is very low and only present in 2 out of 69 TNNT2-morpholino treated embryos. In addition, a diverticulum was never observed in our laboratory previously. It is thought that congenital ventricular diverticula occur in 0.04% of the general population. Although the diverticulum defect was not observed using the TNNT2-morpholino used in this thesis, the penetrance of the defect adds difficultly in assessing whether the defect is due to TNNT2 knockdown or independent of the treatment.

In the*Tnnt2* homozygous knockout mouse designed by Ahmad *et al.*, cardiac looping appeared normal (Ahmad et al., 2008) , which is consistent with the TNNT2-morpholino treated heart. However, in another *Tnnt2* homozygous knockout mouse model, abnormal looping was seen along with dilation of the heart tubes (Nishii et al., 2008). However, this abnormal looping was potentially due to the lack of heart beat in the knockout mouse. In this thesis, all TNNT2-morpholino treated embryos had a heartbeat, therefore, we would expect the phenotypes to vary between the two experimental models.

After serial sectioning through the 250µM and 500µM TNNT2-morpholino treated hearts, no abnormalities were obvious in the 250µM treated hearts. However, in 57.1% of the 500µM treated hearts, the atrial septum appeared reduced in size as it protrudes from the dorso-cranial wall of the atrial chamber, although it was never absent. There was no report of an

abnormal atrial septum in the homozygous knockout mouse, although the morphology of the atrial chamber as a whole was not assessed (Ahmad et al., 2008, Nishii et al., 2008). Stereological analysis revealed normal tissue proportions (myocardial wall and ECM) and lumen size in the TNNT2-treated hearts. Unfortunately, no statistical data could be collected for the atrial septum, as not enough counts were collected to complete the analysis.

Interestingly, in a subset of embryos with an abnormal atrial septum, reduced trabeculation was observed in the ventricular chamber (16.7% of embryos with a reduced atrial septum). Although stereological analysis of the TNNT2-morpholino treated hearts did not reveal reduced myocardium in the ventricular chamber, the hearts included in this study did not carry the ventricular phenotype as the penetrance was low. In the homozygous knockout mouse, the ventricular walls appeared thinner although the trabeculae were not mentioned in this study (Ahmad et al., 2008).

Stereological analysis has shown that the total proportion the atrium contributing to the hearts of TNNT2-morpholino treated embryos was reduced compared to the control hearts. The OFT and ventricular contributions remained normal when compared to the controls. It is unknown whether this reduction in size is due to underdevelopment of the chamber itself, or caused by reduced blood-flow through the chamber. To date, no report of a reduced atrial chamber size, independent of the ventricle, has been within the literature.

TNNT2-morpholino treatment of cardiomyocytes *in vitro* revealed normal myofibril assembly, with the number of immature and mature myofibrils consistent with the controls. In the homozygous knockout mouse, thick and thin filaments failed to assemble together into sarcomeres, however, the thin filaments did arrange into Z-body like structures (Nishii et al., 2008). This was not evident in the *sih* mutant zebrafish (null allele for *tnnt2*) where thin filaments did not assemble (Huang et al., 2009). The authors concluded that cTnt was required for the stability of the thin filament, which myofibril assembly relies on. However, other thin filament proteins such as Tpm1 and cTni (cardiac troponin I) were either diminished or undetectable, respectively, in this model and may contribute to the lack of myofibrils (Huang et al., 2009). Morpholino treatment was also completed by Huang et al., which resulted in a 98% decrease in ctnt and these embryos displayed the same phenotype as the *sih* mutant (Huang et al., 2009). TNNT2-morpholino treatment conducted in the chick in this study only resulted in a 33% decrease of protein. This may possibly explain the

differences in the severity of the phenotypes observed between the mouse, zebrafish and the chick. In addition, in the mouse and zebrafish, targeting manipulation of *Tnnt2* occurs prior to heart development, before a protein pool of cTnT is available, whereas in the chick, manipulation occurs after the heart tube is formed and after the initiation of cTnT expression.

6.6 Strengths and limitations of this work

ATG start site morpholinos are designed to decrease or 'knockdown' the amount of endogenous protein in the model organism (Nasevicius and Ekker, 2000). They achieve this by steric block, preventing the initiation of translation of the spliced RNA into protein. This knockdown can be detected and measured by western blot, whereby the protein band should be reduced in expression or absent from the blot. It was attempted to perform a western blot using an anti-TPM1 antibody, CH1. Unfortunately, it was not possible to detect any protein decrease using this antibody. However, when looking at TPM in the individual hearts, there appeared to be an increase in TPM protein in the morpholino treated hearts, although this was not significant. This may suggest an upregulation of *TPM4* induced by compensatory mechanisms (Izumo et al., 1988). It was shown by RT-PCR that *TPM1α* and *TPM1κ* were not expressed in the neonatal heart and *TPM4* was expressed. However, immunohistochemistry, using the anti-TPM1 antibody was positive in the neonatal heart, suggesting that it may also detect TPM4. To overcome this problem, three morpholinos were designed to the *TPM1* gene, one targeting the ATG start site, one targeting exon1-intron1 and another targeting exon4-intron4. The phenotypes obtained using these three morpholinos were similar and non-significantly different in penetrance, therefore, the morpholinos were not producing non-specific effects. Since there were also two splice-site targeting morpholinos, primers were designed around the exon1-intron1 and exon4-intron4 boundaries in the hope that an alternately spliced product could be detected. However, this was unsuccessful.

Of late, morpholinos themselves have been the subject of much criticism. In the zebrafish, countless studies have been published utilising this technology. However, due to the potential of non-specific effects caused by morpholinos, newly described phenotypes in zebrafish embryos treated with morpholinos (morphants, with the morpholino injected at the one cell stage) should be compared with a genetic mutant prior to describing it as a specific phenotype. In the zebrafish, a comparison was done between morpholino treated and nuclease

induced mutant embryos. 80% of the observed phenotypes in the morphants were not present in the mutant embryos indicating a high level of non-specific effects from the morpholino (Kok et al., 2015).

Another limiting factor when working with morpholinos in the chick is the method of application of the embryonic tissue. Pluronic gel is a cheap and effective way of internalising morpholino into developing embryonic tissue. However, it is unknown how much morpholino actually becomes internalised and bound to its target. Although the morpholinos are tagged with a fluorescent marker and their location can be visualised in the embryo, it is not possible to quantify how much is in the embryo. It is believed that it is the unbound morpholino that can lead to the non-specific binding to unintended targets (Eisen and Smith, 2008). However, careful bioinformatic analysis was performed during the morpholino design to reduce the chance of non-specific binding. In addition, morpholinos induce a temporary inhibition of gene function. Some morpholinos have shown remarkable similarities and appear to work specifically when compared to their mutant counterpart and therefore, this method should not be discarded as it is a valuable technique (Kok et al., 2015). Morpholinos are still invaluable tools in developmental biology and data can be rapidly obtained with their use, however, the investigator must be aware of the potential pitfalls.

Morpholinos are most commonly used in the Xenopus and zebrafish (Draper et al., 2001, Heasman et al., 2000, Nutt et al., 2001). The major advantage of these model organisms is that the embryos themselves develop externally, and therefore can be easily accessed for manipulation. This allows the microinjecting of morpholinos at the one cell stage of embryonic development. Morpholino can therefore, be passed to subsequent daughter cells after cell division of the blastula. In these studies, investigators have achieved almost 100% knockdown of the targeted gene with high efficiency as they are targeting manipulation prior to protein pools being produced (Sehnert et al., 2002, Nutt et al., 2001). However, this results in a more severe phenotype with a range of defects, and while embryonic death usually occurs in the early stages of heart development, it can be difficult (and sometimes impossible) to decipher the role that a protein plays in cardiogenic processes, such as atrial septation, ventricular trabeculation etc. (Rethinasamy et al., 1997, McKeown et al., 2014, Fritz-Six et al., 2003, Nishii et al., 2008, Chen et al., 1998). In the chick, this degree of knockdown cannot be achieved as morpholino application is not completed until just after the

heart tube has formed. Previous studies completed in this laboratory have shown a protein knockdown of 82.6% and 63% for eMYH and αMYH, respectively (Rutland et al., 2009, Rutland et al., 2011). In the cTnT study, there was a knockdown of 32.8%. This degree of knockdown can still, however, produce abnormal phenotypes in the developing chick heart. In addition, the chick heart resembles mammalian heart development much more than the Xenopus and zebrafish, as these models produce a three and two chambered heart, respectively (Warkman and Krieg, 2007, Lieschke and Currie, 2007). This means that certain developmental features such as atrial and/or ventricular septation cannot be studied in these models.

One major limitation of the microinjection transfection technique is that by using a plasmid and Lipofectamine as a means of transfection. Only ~7% of the cells within the heart appeared to express GFP 24 hours after microinjection. Although this is an improvement in the transfection efficiency achieved by Ishii and colleagues, this amount is most likely not sufficient to complete a rescue (Ishii et al., 2010). This limitation may be due to the expanding size of the heart tube as a result of second heart field cell addition (Soufan et al., 2006). Techniques such as electroporation along with plasmid microinjection may help solve the transfection efficiency, although may affect embryo survival due to increased risk of tissue damage (Norris and Streit, 2014).

6.7 Future directions

6.7.1 Potential functional effect of missense mutations found in TPM1

Due to time limitations, the functional analysis of the two missense mutations found in *TPM1* from the patient cohort was not completed. An experiment was designed to differentiate C2C12 cells, a myoblast cell line, which had been transfected with a construct containing *TPM1* mRNA containing the missense mutations. Using this method it would be possible to look at the effect the missense mutations have on sarcomeric assembly as the myoblasts differentiated into myocytes. Unfortunately, the C2C12 cells were detaching from the coverslips while differentiating, and I was unable to analyse the transfected cells. However, taking advantage of earlier experiments in this thesis using the microinjection technique, transfection of whole embryonic hearts with the TPM1 constructs may provide

information into the role of these mutations in the developing heart, such as myofibril incorporation and formation. These studies are currently ongoing.

6.7.2 Further investigation into the action potentials in the TPM1-treated heart

Patch clamp techniques revealed abnormal action potentials in cardiomyocytes treated with TPM1-morpholino. The action potentials in the TPM1-morpholino treated cells were more like those from an adult heart (Arguello et al., 1986, DeHann, 1967) and may suggest an increase in sodium channels activated on the cell surface. In addition, the reduced duration of action potentials may be due to an increase in calcium activated potassium or L-type calcium channels. Investigating the expression of sodium channels, such as $Na_v1.5$, using quantitative PCR may elucidate changes in their regulation (Lowe et al., 2008). Calcium transient markers, such as Fura-FF AM, would allow the quantification of the changes in intracellular calcium by detecting fluorescence intensities emitted by the dye by single cardiomyocytes in culture (Rutland et al., 2011).

6.7.3 Functional analysis of TNNT2-treated hearts

It is known that the T-box transcription factor, *TBX5*, is expressed in the myocardium and endocardium of the atrium and is necessary for normal atrial septal development (Bimber et al., 2007). Haploinsufficiency of *TBX5* leads to Holt-Oram syndrome in which the patients have limb and cardiac abnormalities, most commonly an ASD (Bruneau et al., 1999, Xie et al., 2012). It also plays a role in myocardial proliferation, where *Tbx5* mutants have a thinner compact myocardium (Xie et al., 2012). Using *in situ* hybridisation techniques, it might be interesting to look at the expression of transcription factors expressed in the atrial septum of the TPM1 and TNNT2-morpholino treated hearts. Transcription factors, such as *TBX5* and *NOTCH1*, which are known to play a role in atrial septation and ventricular maturation, respectively, may elucidate any alterations in the molecular signals in the morpholino treated embryos, thus leading to the abnormal phenotypes observed (Yi Li et al., 1997, Grego-Bessa et al., 2007).

Unlike the TPM1 study, it was not possible to make electrical recordings in the TNNT2-knockdown hearts. The presence of the abnormally small atrial septum and the lack of

ventricular trabeculae in a subset of these hearts may indicate some alterations in the haemodynamics of the heart (Groenendijk et al., 2007). *Endothelial Nitric oxide synthase* or *NOS3* is upregulated under high sheer stress (Groenendijk et al., 2005). Qualitative PCR (qPCR) may indicate if there are changes to sheer stress within the endocardium of TNNT2-knockdown hearts that are leading to abnormalities in the atrial septum and ventricular trabeculae. These studies are currently ongoing.

6.7.4 Screening of *TNNT2* gene in CHD patients

TPM1 has long been associated with cardiomyopathies, as has *MYH6*, *MYH7*, *ACTC1* and *TNNT2* (Morimoto, 2008). More recently, *MYH6*, *MYH7* and *ACTC1* have been linked to CHDs, where MYH6 has been linked to VSD and left ventricular non-compaction, while MYH7 and ACTC1 mutations have been found in patients with ASDs (Ching et al., 2005, Budde et al., 2007, Matsson et al., 2008). In this thesis, four *de novo* mutations in the *TPM1* gene have been described in patients with a range of CHDs, three of which were found in patients with ASDs. Targeted manipulation of TPM1 in the chick revealed several structural phenotypes, such as a reduced atrial septum (with a double septum identified in one heart), decreased trabeculae and abnormal looping, which may contribute to CHD like structural defects in the adult heart. These defects include double outlet right ventricle resulting from the abnormal looping, ASDs due to the shortened atrial septum unable to fuse to the endocardial cushions, or VSDs, as the lack of trabeculae will affect the compaction of the ventricular myocardium during ventricular septation. The atrial septum and ventricular trabecular phenotype was also observed after knockdown of cTnT in the chick heart, although at less penetrance. Regardless, screening of the *TNNT2* gene in a cohort of patients with CHDs may elucidate *de novo* mutations that cause CHDs.

6.7.5 New techniques for targeted gene manipulation

Although morpholinos have been extremely useful in targeting specific genes, their many pitfalls have been discussed above (Section 6.6). New methods of gene targeting or ‘genome editing’ use nucleases with a specific DNA-binding domain that can recognise any known sequence when the nuclease is fused to a DNA cleavage element (Urnov et al.,

2010). The nuclease can then induce specific and efficient double-stranded DNA breaks, which in turn stimulates the cellular DNA repair mechanisms. These mechanisms include error-prone non-homologous end joining and homology direct repair (Wyman and Kanaar, 2006). The CRISPR-Cas9 gene editing system would provide a cheaper and more effective method of gene knockout in the chick, rather than establishing transgenic chicks though conventional knockout models (Flemr and Buhler, 2015). However, the utilization of these technologies has not come to full fruition in the chick.

6.8 Conclusions

This study has shown that targeted manipulation of TPM1 in the developing heart can lead to structural abnormalities, such as a small atrial septum, reduced trabeculation and abnormal looping, and apoptosis, most likely a secondary defect caused by changes in the action potential of the cardiomyocytes within the myocardium. *In vitro* manipulation of the cardiomyocytes also showed decreased myofibril maturity within these cells.

In addition to this animal model of *TPM1* function, novel variants of the *TPM1* gene were found in a cohort of patients with a range of CHDs. The two non-synonymous mutations are highly conserved and predicted to be disease causing using *in silico* analysis. A novel splice site mutation although not predicted as damaging, led to abnormal splicing *in vitro*. As *TPM1* has not previously been linked to CHDs, this study could have implications for clinical practice and may possibly provide genetic counselling to patients regarding recurrence risk to their offspring in the future.

As well as *TPM1*, *TNNT2* has not been linked to CHDs and more historically associated with cardiomyopathies. However, in this animal model where cTnT was knocked down *in ovo*, atrial septation was affected and to some degree ventricular trabeculation. Although myofibril assembly was not affected, haemodynamic alterations may be a primary cause of the structural anomalies. Full gene sequencing of *TNNT2* in patients with CHDs should be considered in the future as a likely candidate gene.

Chapter 7 References

ABECASIS, G., ALTSHULER, D., AUTON, A., BROOKS, L., DURBIN, R., GIBBS, R., HURLES, M. & MCVEAN, G. 2010. A map of human genome variation from population-scale sequencing. *Nature,* 467**,** 1061-1073.

ABU-ISSA, R. & KIRBY, M. L. 2007. Heart Field: From Mesoderm to Heart Tube. *Annual Review of Cell and Developmental Biology,* 23**,** 45-68.

ADZHUBEI, I., S., S., L., P., RAMENSKY, V., GERASIMOVA, A., BORK, P., KONDRASHOV, A. & SUNYAEV, S. 2010. A method and server for predicting damaging missense mutations. *Nature Methods,* 7**,** 248-249.

AHMAD, F., BANERJEE, S. K., LAGE, M. L., HUANG, X. N., SMITH, S. H., SABA, S., RAGER, J., CONNER, D. A., JANCZEWSKI, A. M., TOBITA, K., TINNEY, J. P., MOSKOWITZ, I. P., PEREZ-ATAYDE, A. R., KELLER, B. B., MATHIER, M. A., SHROFF, S. G., SEIDMAN, C. E. & SEIDMAN, J. G. 2008. The Role of Cardiac Troponin T Quantity and Function in Cardiac Development and Dilated Cardiomyopathy. *PLoS ONE,* 3**,** e2642.

AN, F. S., ZHANG, Y., LI, D. Q., YANG, X. S., LI, L., ZHANG, C., YAN, M. L., WANG, Y. & AN, G. P. 2004. [A novel missense mutation, K124N, in the troponin T gene of Chinese populations with hypertrophic cardiomyopathy]. *Zhonghua Yi Xue Za Zhi,* 84**,** 1340-3.

ANDERSON, P. A., MALOUF, N. N., OAKELEY, A. E., PAGANI, E. D. & ALLEN, P. D. 1991. Troponin T isoform expression in humans. A comparison among normal and failing adult heart, fetal heart, and adult and fetal skeletal muscle. *Circulation Research,* 69**,** 1226-33.

ANDERSON, P. A. W., GREIG, A., MARK, T. M., MALOUF, N. N., OAKELEY, A. E., UNGERLEIDER, R. M., ALLEN, P. D. & KAY, B. K. 1995. Molecular Basis of Human Cardiac Troponin T Isoforms Expressed in the Developing, Adult, and Failing Heart. *Circulation Research,* 76**,** 681-686.

ANDERSON, R. H., BROWN, N. A. & WEBB, S. 2002. Development and structure of the atrial septum. *Heart,* 88**,** 104-110.

ANDERSON, R. H., WEBB, S., BROWN, N. A., LAMERS, W. & MOORMAN, A. 2003a. Development of the heart: (2) Septation of the atriums and ventricles. *Heart,* 89**,** 949-958.

ANDERSON, R. H., WEBB, S., BROWN, N. A., LAMERS, W. & MOORMAN, A. 2003b. Development of the heart: (3) Formation of the ventricular outflow tracts, arterial valves, and intrapericardial arterial trunks. *Heart,* 89**,** 1110-1118.

ANDREWS, R. E., FENTON, M. J., RIDOUT, D. A., BURCH, M. & ASSOCIATION, O. B. O. T. B. C. C. 2008. New-Onset Heart Failure Due to Heart Muscle Disease in Childhood: A Prospective Study in the United Kingdom and Ireland. *Circulation,* 117**,** 79-84.

ANTIN, P. B., BALES, M. A., ZHANG, W., GARRIOCK, R. J., YATSKIEVYCH, T. A. & BATES, M. A. 2002. Precocious expression of cardiac troponin T in early chick

embryos is independent of bone morphogenetic protein signaling. *Dev Dyn,* 225**,** 135-41.

ARGUELLO, C., ALANIS, J., PANTOJA, O. & VALENZUELA, B. 1986. Electrophysiological and ultrastructural study of the atrioventricular canal during the development of the chick embryo. *J Mol Cell Cardiol,* 18**,** 499-510.

ASHRAF, M. H., GINGELL, R., PIERONI, D., DHAR, N. & SUBRAMANIAN, S. 1984. Congenital diverticulum of the heart of biventricular origin. *Thorac Cardiovasc Surg,* 32**,** 389-91.

BAILLIARD, F. & ANDERSON, R. H. 2009. Tetralogy of Fallot. *Orphanet J Rare Dis,* 4**,** 2.

BAKKER, M. L., BOUKENS, B. J., MOMMERSTEEG, M. T. M., BRONS, J. F., WAKKER, V., MOORMAN, A. F. M. & CHRISTOFFELS, V. M. 2008. Transcription Factor Tbx3 Is Required for the Specification of the Atrioventricular Conduction System. *Circulation Research,* 102**,** 1340-1349.

BASSO, C., CORRADO, D., MARCUS, F. I., NAVA, A. & THIENE, G. 2009. Arrhythmogenic right ventricular cardiomyopathy. *Lancet,* 373**,** 1289-300.

BASSON, C. T., HUANG, T., LIN, R. C., BACHINSKY, D. R., WEREMOWICZ, S., VAGLIO, A., BRUZZONE, R., QUADRELLI, R., LERONE, M., ROMEO, G., SILENGO, M., PEREIRA, A., KRIEGER, J., MESQUITA, S. F., KAMISAGO, M., MORTON, C. C., PIERPONT, M. E., MULLER, C. W., SEIDMAN, J. G. & SEIDMAN, C. E. 1999. Different TBX5 interactions in heart and limb defined by Holt-Oram syndrome mutations. *Proc Natl Acad Sci U S A,* 96**,** 2919-24.

BECKER, A. E., CONNOR, M. & ANDERSON, R. H. 1975. Tetralogy of Fallot: a morphometric and geometric study. *Am J Cardiol,* 35**,** 402-12.

BELLAIRS, R. & OSMOND, M. 2005. *The Atlas of Chick Development,* London, Elsevier Academic Press.

BENNETT, C. L., BRUNKOW, M. E., RAMSDELL, F., O'BRIANT, K. C., ZHU, Q., FULEIHAN, R. L., SHIGEOKA, A. O., OCHS, H. D. & CHANCE, P. F. 2001. A rare polyadenylation signal mutation of the FOXP3 gene (AAUAAA-->AAUGAA) leads to the IPEX syndrome. *Immunogenetics,* 53**,** 435-9.

BERTRANOU, E. G., BLACKSTONE, E. H., HAZELRIG, J. B., TURNER, M. E. & KIRKLIN, J. W. 1978. Life expectancy without surgery in tetralogy of Fallot. *Am J Cardiol,* 42**,** 458-66.

BETTINELLI, A. L., MULDER, T. J., FUNKE, B. H., LAFFERTY, K. A., LONGO, S. A. & NIYAZOV, D. M. 2013. Familial ebstein anomaly, left ventricular hypertrabeculation, and ventricular septal defect associated with a MYH7 mutation. *Am J Med Genet A,* 161A**,** 3187-90.

BIMBER, B., DETTMAN, R. W. & SIMON, H.-G. 2007. Differential regulation of Tbx5 protein expression and sub-cellular localization during heart development. *Developmental biology,* 302**,** 230-242.

BLANCHARD, E. M., IIZUKA, K., CHRISTE, M., CONNER, D. A., GEISTERFER-LOWRANCE, A., SCHOEN, F. J., MAUGHAN, D. W., SEIDMAN, C. E. &

SEIDMAN, J. G. 1997. Targeted Ablation of the Murine α-Tropomyosin Gene. *Circulation Research,* 81**,** 1005-1010.

BLOUNT, S. G., BALCHUM, O. J. & GENSINI, G. 1956. The Persistent Ostium Primum Atrial Septal Defect. *Circulation,* 13**,** 499-509.

BOUMAN, H. G., BROEKHUIZEN, M. L., BAASTEN, A. M., GITTENBERGER-DE GROOT, A. C. & WENINK, A. C. 1995. Spectrum of looping disturbances in stage 34 chicken hearts after retinoic acid treatment. *Anat Rec,* 243**,** 101-8.

BOZZOLA, J. J. & RUSSELL, L. D. 1992. *Electron Microscopy,* Massachusetts, Jones and Bartlett Publishers, Inc.

BRAUNWALD, E. 2008. *Heart Disease: A textbook of cardiovascular medicine,* Phiadelphia, Saunders.

BRENNER, B. & YU, L. C. 1993. Structural changes in the actomyosin cross-bridges associated with force generation. *Proc Natl Acad Sci USA,* 90**,** 5252-5256.

BRIGGS, L. E., KAKARLA, J. & WESSELS, A. 2012. The pathogenesis of atrial and atrioventricular septal defects with special emphasis on the role of the dorsal mesenchymal protrusion. *Differentiation,* 84**,** 117-130.

BRITO, D., MILTENBERGER-MILTENYI, G., VALE PEREIRA, S., SILVA, D., DIOGO, A. N. & MADEIRA, H. 2012. Sarcomeric hypertrophic cardiomyopathy: genetic profile in a Portuguese population. *Rev Port Cardiol,* 31**,** 577-87.

BROEKHUIZEN, M. L., BOUMAN, H. G., MAST, F., MULDER, P. G., GITTENBERGER-DE GROOT, A. C. & WLADIMIROFF, J. W. 1995. Hemodynamic changes in HH stage 34 chick embryos after treatment with all-trans-retinoic acid. *Pediatr Res,* 38**,** 342-8.

BROWN, J. H., KIM, K.-H., JUN, G., GREENFIELD, N. J., DOMINGUEZ, R., VOLKMANN, N., HITCHCOCK-DEGREGORI, S. E. & COHEN, C. 2001. Deciphering the design of the tropomyosin molecule. *Proceedings of the National Academy of Sciences,* 98**,** 8496-8501.

BROWN, J. H., ZHOU, Z., RESHETNIKOVA, L., ROBINSON, H., YAMMANI, R. D., TOBACMAN, L. S. & COHEN, C. 2005. Structure of the mid-region of tropomyosin: Bending and binding sites for actin. *Proceedings of the National Academy of Sciences of the United States of America,* 102**,** 18878-18883.

BRUNEAU, B. G. 2008. The developmental genetics of congenital heart disease. *Nature,* 451**,** 943-948.

BRUNEAU, B. G., LOGAN, M., DAVIS, N., LEVI, T., TABIN, C. J., SEIDMAN, J. G. & SEIDMAN, C. E. 1999. Chamber-specific cardiac expression of Tbx5 and heart defects in Holt-Oram syndrome. *Dev Biol,* 211**,** 100-8.

BUCKINGHAM, M., MEILHAC, S. & ZAFFRAN, S. 2005. Building the mammalian heart from two sources of myocardial cells. *Nat Rev Genet,* 6**,** 826-837.

BUDDE, B. S., BINNER, P., WALDMÜLLER, S., HÖHNE, W., BLANKENFELDT, W., HASSFELD, S., BRÖMSEN, J., DERMINTZOGLOU, A., WIECZOREK, M., MAY, E., KIRST, E., SELIGNOW, C., RACKEBRANDT, K., MÜLLER, M., GOODY, R.

S., VOSBERG, H.-P., NÜRNBERG, P. & SCHEFFOLD, T. 2007. Noncompaction of the Ventricular Myocardium Is Associated with a De Novo Mutation in the β-Myosin Heavy Chain Gene. *PLoS ONE,* 2**,** e1362.

CAHILL, T. J., ASHRAFIAN, H. & WATKINS, H. 2013. Genetic cardiomyopathies causing heart failure. *Circ Res,* 113**,** 660-75.

CAI, C.-L., LIANG, X., SHI, Y., CHU, P.-H., PFAFF, S. L., CHEN, J. & EVANS, S. 2003. Isl1 Identifies a Cardiac Progenitor Population that Proliferates Prior to Differentiation and Contributes a Majority of Cells to the Heart. *Developmental Cell,* 5**,** 877-889.

CALESHU, C., SAKHUJA, R., NUSSBAUM, R. L., SCHILLER, N. B., URSELL, P. C., ENG, C., DE MARCO, T., MCGLOTHLIN, D., BURCHARD, E. G. & RAME, J. E. 2011. Furthering the link between the sarcomere and primary cardiomyopathies: restrictive cardiomyopathy associated with multiple mutations in genes previously associated with hypertrophic or dilated cardiomyopathy. *Am J Med Genet A,* 155A**,** 2229-35.

CARNIEL, E., TAYLOR, M. R., SINAGRA, G., DI LENARDA, A., KU, L., FAIN, P. R., BOUCEK, M. M., CAVANAUGH, J., MIOCIC, S., SLAVOV, D., GRAW, S. L., FEIGER, J., ZHU, X. Z., DAO, D., FERGUSON, D. A., BRISTOW, M. R. & MESTRONI, L. 2005. Alpha-myosin heavy chain: a sarcomeric gene associated with dilated and hypertrophic phenotypes of cardiomyopathy. *Circulation,* 112**,** 54-9.

CASSELS, D. E. 1973. *The Ductus Arteriosus*, Thomas.

CHANG, A. N., HARADA, K., ACKERMAN, M. J. & POTTER, J. D. 2005. Functional consequences of hypertrophic and dilated cardiomyopathy-causing mutations in alpha-tropomyosin. *J Biol Chem,* 280**,** 34343-9.

CHANG, B., NISHIZAWA, T., FURUTANI, M., FUJIKI, A., TANI, M., KAWAGUCHI, M., IBUKI, K., HIRONO, K., TANEICHI, H., UESE, K., ONUMA, Y., BOWLES, N. E., ICHIDA, F., INOUE, H., MATSUOKA, R. & MIYAWAKI, T. 2011. Identification of a novel TPM1 mutation in a family with left ventricular noncompaction and sudden death. *Mol Genet Metab,* 102**,** 200-6.

CHEN, H., ZHANG, W., SUN, X., YOSHIMOTO, M., CHEN, Z., ZHU, W., LIU, J., SHEN, Y., YONG, W., LI, D., ZHANG, J., LIN, Y., LI, B., VANDUSEN, N. J., SNIDER, P., SCHWARTZ, R. J., CONWAY, S. J., FIELD, L. J., YODER, M. C., FIRULLI, A. B., CARLESSO, N., TOWBIN, J. A. & SHOU, W. 2013. Fkbp1a controls ventricular myocardium trabeculation and compaction by regulating endocardial Notch1 activity. *Development,* 140**,** 1946-1957.

CHEN, J., KUBALAK, S. W., MINAMISAWA, S., PRICE, R. L., BECKER, K. D., HICKEY, R., ROSS, J. & CHIEN, K. R. 1998. Selective Requirement of Myosin Light Chain 2v in Embryonic Heart Function. *Journal of Biological Chemistry,* 273**,** 1252-1256.

CHENARD, J., SAMSON, M. & BEAULIEU, M. 1965. Embryonal sinusoids in the myocardium: Report of a casse sucessfully treated surgically. *Can Med Assoc J,* 92**,** 1356-9.

CHING, Y.-H., GHOSH, T. K., CROSS, S. J., PACKHAM, E. A., HONEYMAN, L., LOUGHNA, S., ROBINSON, T. E., DEARLOVE, A. M., RIBAS, G., BONSER, A. J., THOMAS, N. R., SCOTTER, A. J., CAVES, L. S. D., TYRRELL, G. P., NEWBURY-ECOB, R. A., MUNNICH, A., BONNET, D. & BROOK, J. D. 2005. Mutation in myosin heavy chain 6 causes atrial septal defect. *Nat Genet,* 37**,** 423-428.

CHRISTOFFELS, V. M., HABETS, P. E. M. H., FRANCO, D., CAMPIONE, M., DE JONG, F., LAMERS, W. H., BAO, Z.-Z., PALMER, S., BIBEN, C., HARVEY, R. P. & MOORMAN, A. F. M. 2000. Chamber Formation and Morphogenesis in the Developing Mammalian Heart. *Developmental Biology,* 223**,** 266-278.

CHRISTOFFELS, V. M. & MOORMAN, A. F. M. 2009. Development of the Cardiac Conduction System: Why Are Some Regions of the Heart More Arrhythmogenic Than Others? *Circulation: Arrhythmia and Electrophysiology,* 2**,** 195-207.

CHRISTOFFELS, V. M., SMITS, G. J., KISPERT, A. & MOORMAN, A. F. 2010. Development of the pacemaker tissues of the heart. *Circ Res,* 106**,** 240-54.

COHEN, C. & PARRY, D. 1990. Alpha-helical coiled coils and bundles: how to design an alpha-helical protein. *Proteins,* 7**,** 1-15.

COHEN, J. S. 1993. *Phosphorothioate Oligodeoxynucleotides,* Boca Raton, CRC press.

CRICK, F. 1953. The packing of α-helices: Simple coiled coils. *Acta Crystallogr.,* 6**,** 689-697.

CURILA, K., BENESOVA, L., PENICKA, M., MINARIK, M., ZEMANEK, D., VESELKA, J., WIDIMSKY, P. & GREGOR, P. 2009. Low prevalence and variable clinical presentation of troponin I and troponin T gene mutations in hypertrophic cardiomyopathy. *Genet Test Mol Biomarkers,* 13**,** 647-50.

D'CRUZ, L. G., BABOONIAN, C., PHILLIMORE, H. E., TAYLOR, R., ELLIOTT, P. M., VARNAVA, A., DAVISON, F., MCKENNA, W. J. & CARTER, N. D. 2000. Cytosine methylation confers instability on the cardiac troponin T gene in hypertrophic cardiomyopathy. *J Med Genet,* 37**,** E18.

DAEHMLOW, S., ERDMANN, J., KNUEPPEL, T., GILLE, C., FROEMMEL, C., HUMMEL, M., HETZER, R. & REGITZ-ZAGROSEK, V. 2002. Novel mutations in sarcomeric protein genes in dilated cardiomyopathy. *Biochemical and Biophysical Research Communications,* 298**,** 116-120.

DAS, S., BABICK, A. P., XU, Y. J., TAKEDA, N., RODRIGUEZ-LEVYA, D. & DHALLA, N. S. 2010. TNF-alpha-mediated signal transduction pathway is a major determinant of apoptosis in dilated cardiomyopathy. *J Cell Mol Med,* 14**,** 1988-97.

DE JONG, F., OPTHOF, T., WILDE, A., JANSE, M., CHARLES, R., LAMERS, W. & MOORMAN, A. 1992. Persisting zones of slow impulse conduction in developing chicken hearts. *Circulation Research,* 71**,** 240-250.

DE LANGE, F. J., MOORMAN, A. F. M., ANDERSON, R. H., MÄNNER, J., SOUFAN, A. T., VRIES, C. D. G.-D., SCHNEIDER, M. D., WEBB, S., VAN DEN HOFF, M. J. B. & CHRISTOFFELS, V. M. 2004. Lineage and Morphogenetic Analysis of the Cardiac Valves. *Circulation Research,* 95**,** 645-654.

DE VLAMING, A., SAULS, K., HAJDU, Z., VISCONTI, R. P., MEHESZ, A. N., LEVINE, R. A., SLAUGENHAUPT, S. A., HAGÈGE, A., CHESTER, A. H., MARKWALD, R. R. & NORRIS, R. A. 2012. Atrioventricular valve development: New perspectives on an old theme. *Differentiation,* 84**,** 103-116.

DEHANN, R. L. 1967. Regulation of spontaneous activity and growth of embryonic chick heart cells in tissue culture. *Dev Biol,* 16**,** 216-49.

DEL MONTE, G., GREGO-BESSA, J., GONZÁLEZ-RAJAL, A., BOLÓS, V. & DE LA POMPA, J. L. 2007. Monitoring Notch1 activity in development: Evidence for a feedback regulatory loop. *Developmental Dynamics,* 236**,** 2594-2614.

DEL RIO, M., MARTINEZ, J. M., BENNASAR, M., PALACIO, M., FIGUERAS, F., PUERTO, B., MORTERA, C. & CARARACH, V. 2005. Prenatal diagnosis of a right ventricular diverticulum complicated by pericardial effusion in the first trimester. *Ultrasound Obstet Gynecol,* 25**,** 409-11.

DELIC, S., STREIF, S., DEUSSING, J. M., WEBER, P., UEFFING, M., HOLTER, S. M., WURST, W. & KUHN, R. 2008. Genetic mouse models for behavioral analysis through transgenic RNAi technology. *Genes Brain Behav,* 7**,** 821-30.

DENZ, C. R., NARSHI, A., ZAJDEL, R. W. & DUBE, D. K. 2004. Expression of a novel cardiac-specific tropomyosin isoform in humans. *Biochemical and Biophysical Research Communications,* 320**,** 1291-1297.

DOBRZYNSKI, H., NIKOLSKI, V. P., SAMBELASHVILI, A. T., GREENER, I. D., YAMAMOTO, M., BOYETT, M. R. & EFIMOV, I. R. 2003. Site of Origin and Molecular Substrate of Atrioventricular Junctional Rhythm in the Rabbit Heart. *Circulation Research,* 93**,** 1102-1110.

DODDS, G. A., 3RD, WARNES, C. A. & DANIELSON, G. K. 1997. Aortic valve replacement after repair of pulmonary atresia and ventricular septal defect or tetralogy of Fallot. *J Thorac Cardiovasc Surg,* 113**,** 736-41.

DOMÍNGUEZ, J. N., MEILHAC, S. M., BLAND, Y. S., BUCKINGHAM, M. E. & BROWN, N. A. 2012. Asymmetric Fate of the Posterior Part of the Second Heart Field Results in Unexpected Left/Right Contributions to Both Poles of the Heart. *Circulation Research,* 111**,** 1323-1335.

DRAPER, B. W., MORCOS, P. A. & KIMMEL, C. B. 2001. Inhibition of zebrafish fgf8 pre-mRNA splicing with morpholino oligos: a quantifiable method for gene knockdown. *Genesis,* 30**,** 154-6.

DU, A., SANGER, J. M. & SANGER, J. W. 2008. Cardiac myofibrillogenesis inside intact embryonic hearts. *Developmental Biology,* 318**,** 236-246.

DU, C.-K., MORIMOTO, S., NISHII, K., MINAKAMI, R., OHTA, M., TADANO, N., LU, Q.-W., WANG, Y.-Y., ZHAN, D.-Y., MOCHIZUKI, M., KITA, S., MIWA, Y., TAKAHASHI-YANAGA, F., IWAMOTO, T., OHTSUKI, I. & SASAGURI, T. 2007. Knock-In Mouse Model of Dilated Cardiomyopathy Caused by Troponin Mutation. *Circulation Research,* 101**,** 185-194.

DUBE, S., PANEBIANCO, L., MATOQ, A. A., CHIONUMA, H. N., DENZ, C. R., POIESZ, B. J. & DUBE, D. K. 2014. Expression of TPM1kappa, a Novel Sarcomeric

Isoform of the TPM1 Gene, in Mouse Heart and Skeletal Muscle. *Mol Biol Int,* 2014**,** 896068.

EBASHI, S., ENDO, M. & OHTSUKI, I. 1969. Control of muscle contraction. *Quarterly Reviews of Biophysics,* 2**,** 351-384.

EICHNA, L. W. & DEHAAN, R. L. 1961. Differentiation of the Atrioventricular Conducting System of the Heart. *Circulation,* 24**,** 458-470.

EISEN, J. S. & SMITH, J. C. 2008. Controlling morpholino experiments: don't stop making antisense. *Development,* 135**,** 1735-1743.

EISENBERG, E. & HILL, T. L. 1985. Muscle contraction and free energy transduction in biological systems. *Science,* 227**,** 999-1006.

ENGELFRIET, P. M., DUFFELS, M. G. J., MÖLLER, T., BOERSMA, E., TIJSSEN, J. G. P., THAULOW, E., GATZOULIS, M. A. & MULDER, B. J. M. 2007. Pulmonary arterial hypertension in adults born with a heart septal defect: the Euro Heart Survey on adult congenital heart disease. *Heart,* 93**,** 682-687.

ENGLAND, J. & LOUGHNA, S. 2013. Heavy and light roles: myosin in the morphogenesis of the heart. *Cellular and Molecular Life Sciences***,** 1-19.

ERDMANN, J., DAEHMLOW, S., WISCHKE, S., SENYUVA, M., WERNER, U., RAIBLE, J., TANIS, N., DYACHENKO, S., HUMMEL, M., HETZER, R. & REGITZ-ZAGROSEK, V. 2003. Mutation spectrum in a large cohort of unrelated consecutive patients with hypertrophic cardiomyopathy. *Clinical Genetics,* 64**,** 339-349.

ERGINEL-UNALTUNA, N., DUBE, D. K., ROBERTSON, D. R. & LEMANSKI, L. F. 1995. In vivo protein synthesis in developing hearts of normal and cardiac mutant axolotls (Ambystoma mexicanum). *Cellular & molecular biology research,* 41**,** 181-187.

EROGLU, A. G., OZTUNC, F., SALTIK, L., BAKARI, S., DEDEOGLU, S. & AHUNBAY, G. 2003. Evolution of ventricular septal defect with special reference to spontaneous closure rate, subaortic ridge and aortic valve prolapse. *Pediatr Cardiol,* 24**,** 31-5.

FATKIN, D. 2011. Guidelines for the diagnosis and management of familial dilated cardiomyopathy. *Heart Lung Circ,* 20**,** 691-3.

FINSTERER, J., STOLLBERGER, C. & BONNER, E. 2010. Acquired noncompaction associated with coronary heart disease and myopathy. *Heart Lung,* 39**,** 240-1.

FISHER, S. A., LANGILLE, B. L. & SRIVASTAVA, D. 2000. Apoptosis During Cardiovascular Development. *Circulation Research,* 87**,** 856-864.

FISHMAN, M. C. & CHIEN, K. R. 1997. Fashioning the vertebrate heart: earliest embryonic decisions. *Development,* 124**,** 2099-2117.

FLACK, K. 1907. The form and nature of the muscular connections between the primary divisions of the vertebrate heart. *J Anat Physiol.,* 41**,** 172-189.

FLEENOR, D. E., HICKMAN, K. H., LINDQUESTER, G. J. & DEVLIN, R. B. 1992. Avian cardiac tropomyosin gene produces tissue-specific isoforms through alternative RNA splicing. *Journal of Muscle Research and Cell Motility,* 13**,** 55-63.

FLEMR, M. & BUHLER, M. 2015. Single-Step Generation of Conditional Knockout Mouse Embryonic Stem Cells. *Cell Rep,* 12**,** 709-16.

FOKSTUEN, S., MUNOZ, A., MELACINI, P., ILICETO, S., PERROT, A., OZCELIK, C., JEANRENAUD, X., RIEUBLAND, C., FARR, M., FABER, L., SIGWART, U., MACH, F., LERCH, R., ANTONARAKIS, S. E. & BLOUIN, J. L. 2011. Rapid detection of genetic variants in hypertrophic cardiomyopathy by custom DNA resequencing array in clinical practice. *J Med Genet,* 48**,** 572-6.

FORISSIER, J. F., CARRIER, L., FARZA, H., BONNE, G., BERCOVICI, J., RICHARD, P., HAINQUE, B., TOWNSEND, P. J., YACOUB, M. H., FAURE, S., DUBOURG, O., MILLAIRE, A., HAGEGE, A. A., DESNOS, M., KOMAJDA, M. & SCHWARTZ, K. 1996. Codon 102 of the cardiac troponin T gene is a putative hot spot for mutations in familial hypertrophic cardiomyopathy. *Circulation,* 94**,** 3069-73.

FORRY-SCHAUDIES, S., GRUBER, C. & HUGHES, S. 1990. Chicken cardiac tropomyosin and a low-molecular-weight nonmuscle tropomyosin are related by alternative splicing. *Cell Growth Differ,* 1**,** 473-481.

FRANKLIN, A. J., BAXLEY, T., KOBAYASHI, T. & CHALOVICH, J. M. 2012. The C-terminus of troponin T is essential for maintaining the inactive state of regulated actin. *Biophys J,* 102**,** 2536-44.

FRANSEN, M. E. & LEMANSKI, L. F. 1989. Studies of heart development in normal and cardiac lethal mutant axolotls: a review. *Scanning microscopy,* 3**,** 1101-15; discussion 1115-6.

FRAZIER, A. H., RAMIREZ-CORREA, G. A. & MURPHY, A. M. 2011. Molecular mechanisms of sarcomere dysfunction in dilated and hypertrophic cardiomyopathy. 31**,** 29-33.

FRISSO, G., LIMONGELLI, G., PACILEO, G., DEL GIUDICE, A., FORGIONE, L., CALABRÒ, P., IACOMINO, M., DETTA, N., DI FONZO, L. M., MADDALONI, V., CALABRÒ, R. & SALVATORE, F. 2009. A child cohort study from southern Italy enlarges the genetic spectrum of hypertrophic cardiomyopathy. *Clinical Genetics,* 76**,** 91-101.

FRITZ-SIX, K. L., COX, P. R., FISCHER, R. S., XU, B., GREGORIO, C. C., ZOGHBI, H. Y. & FOWLER, V. M. 2003. Aberrant myofibril assembly in tropomodulin1 null mice leads to aborted heart development and embryonic lethality. *The Journal of Cell Biology,* 163**,** 1033-1044.

GARG, V., KATHIRIYA, I. S., BARNES, R., SCHLUTERMAN, M. K., KING, I. N., BUTLER, C. A., ROTHROCK, C. R., EAPEN, R. S., HIRAYAMA-YAMADA, K., JOO, K., MATSUOKA, R., COHEN, J. C. & SRIVASTAVA, D. 2003. GATA4 mutations cause human congenital heart defects and reveal an interaction with TBX5. *Nature,* 424**,** 443-7.

GIMENO, J. R., MONSERRAT, L., PEREZ-SANCHEZ, I., MARIN, F., CABALLERO, L., HERMIDA-PRIETO, M., CASTRO, A. & VALDES, M. 2009. Hypertrophic cardiomyopathy. A study of the troponin-T gene in 127 Spanish families. *Rev Esp Cardiol,* 62**,** 1473-7.

GOMES, A. V., GUZMAN, G., ZHAO, J. & POTTER, J. D. 2002. Cardiac Troponin T Isoforms Affect the Ca2+Sensitivity and Inhibition of Force Development: INSIGHTS INTO THE ROLE OF TROPONIN T ISOFORMS IN THE HEART. *Journal of Biological Chemistry,* 277**,** 35341-35349.

GORDON, A. M., REGNIER, M. & HOMSHER, E. 2001. Skeletal and Cardiac Muscle Contractile Activation: Tropomyosin "Rocks and Rolls". *Physiology,* 16**,** 49-55.

GOUJON, M., MCWILLIAM, H., WEIZHONG, L., FRANCK, V., SQUIZZATO, S., PAERM, J. & LOPEZ, R. 2010. A new bioinformatics analysis tools framework at EMBL–EBI. *Nucleic Acids Res.,* 38**,** W695-699.

GOURDIE, R. G., HARRIS, B. S., BOND, J., JUSTUS, C., HEWETT, K. W., O'BRIEN, T. X., THOMPSON, R. P. & SEDMERA, D. 2003. Development of the cardiac pacemaking and conduction system. *Birth Defects Research Part C: Embryo Today: Reviews,* 69**,** 46-57.

GRANADOS-RIVERON, J. T. & BROOK, J. D. 2012. The Impact of Mechanical Forces in Heart Morphogenesis. *Circulation: Cardiovascular Genetics,* 5**,** 132-142.

GRANADOS-RIVERON, J. T., GHOSH, T. K., POPE, M., BU'LOCK, F., THORNBOROUGH, C., EASON, J., KIRK, E. P., FATKIN, D., FENELEY, M. P., HARVEY, R. P., ARMOUR, J. A. L. & DAVID BROOK, J. 2010. α-Cardiac myosin heavy chain (MYH6) mutations affecting myofibril formation are associated with congenital heart defects. *Human Molecular Genetics,* 19**,** 4007-4016.

GREASER, M. L. & GERGELY, J. 1971. Reconstitution of troponin activity from three protein components. *J Biol Chem,* 246**,** 4226-33.

GREENWAY, S. C., MCLEOD, R., HUME, S., ROSLIN, N. M., ALVAREZ, N., GIUFFRE, M., ZHAN, S. H., SHEN, Y., PREUSS, C., ANDELFINGER, G., JONES, S. J. & GERULL, B. 2014. Exome sequencing identifies a novel variant in ACTC1 associated with familial atrial septal defect. *Can J Cardiol,* 30**,** 181-7.

GREGO-BESSA, J., LUNA-ZURITA, L., DEL MONTE, G., BOLÓS, V., MELGAR, P., ARANDILLA, A., GARRATT, A. N., ZANG, H., MUKOUYAMA, Y.-S., CHEN, H., SHOU, W., BALLESTAR, E., ESTELLER, M., ROJAS, A., PÉREZ-POMARES, J. M. & DE LA POMPA, J. L. 2007. Notch Signaling Is Essential for Ventricular Chamber Development. *Developmental Cell,* 12**,** 415-429.

GREGORIO, C. C. & ANTIN, P. B. 2000. To the heart of myofibril assembly. *Trends in Cell Biology,* 10**,** 355-362.

GROENENDIJK, B. C., HIERCK, B. P., VROLIJK, J., BAIKER, M., POURQUIE, M. J., GITTENBERGER-DE GROOT, A. C. & POELMANN, R. E. 2005. Changes in shear stress-related gene expression after experimentally altered venous return in the chicken embryo. *Circ Res,* 96**,** 1291-8.

GROENENDIJK, B. C. W., VAN DER HEIDEN, K., HIERCK, B. P. & POELMANN, R. E. 2007. *The Role of Shear Stress on ET-1, KLF2, and NOS-3 Expression in the Developing Cardiovascular System of Chicken Embryos in a Venous Ligation Model*.

GROS, D. B. & JONGSMA, H. J. 1996. Connexins in mammalian heart function. *BioEssays,* 18**,** 719-730.

GU, H., SMITH, F. C., TAFFET, S. M. & DELMAR, M. 2003. High Incidence of Cardiac Malformations in Connexin40-Deficient Mice. *Circulation Research,* 93**,** 201-206.

GUERRA, S., LERI, A., WANG, X., FINATO, N., DI LORETO, C., BELTRAMI, C. A., KAJSTURA, J. & ANVERSA, P. 1999. Myocyte death in the failing human heart is gender dependent. *Circ Res,* 85**,** 856-66.

GUNNING, P. W., SCHEVZOV, G., KEE, A. J. & HARDEMAN, E. C. 2005. Tropomyosin isoforms: divining rods for actin cytoskeleton function. *Trends in Cell Biology,* 15**,** 333-341.

HAMBURGER, V. & HAMILTON, H. L. 1951. A series of normal stages in the development of the chick embryo. *Journal of Morphology,* 88**,** 49-92.

HAMBURGER, V. & HAMILTON, H. L. 1992. A series of normal stages in the development of the chick embryo. *Developmental Dynamics,* 195**,** 231-272.

HANSON, E. L., JAKOBS, P. M., KEEGAN, H., COATES, K., BOUSMAN, S., DIENEL, N. H., LITT, M. & HERSHBERGER, R. E. 2002. Cardiac troponin T lysine 210 deletion in a family with dilated cardiomyopathy. *Journal of Cardiac Failure,* 8**,** 28-32.

HARVEY, R. P. 2002. Patterning the vertebrate heart. *Nat Rev Genet,* 3**,** 544-556.

HEASMAN, J., KOFRON, M. & WYLIE, C. 2000. Beta-catenin signaling activity dissected in the early Xenopus embryo: a novel antisense approach. *Dev Biol,* 222**,** 124-34.

HERSHBERGER, R. E., NORTON, N., MORALES, A., LI, D., SIEGFRIED, J. D. & GONZALEZ-QUINTANA, J. 2010. Coding Sequence Rare Variants Identified in MYBPC3, MYH6, TPM1, TNNC1, and TNNI3 From 312 Patients With Familial or Idiopathic Dilated Cardiomyopathy. *Circulation: Cardiovascular Genetics,* 3**,** 155-161.

HERSHBERGER, R. E., PARKS, S. B., KUSHNER, J. D., LI, D., LUDWIGSEN, S., JAKOBS, P., NAUMAN, D., BURGESS, D., PARTAIN, J. & LITT, M. 2008. Coding sequence mutations identified in MYH7, TNNT2, SCN5A, CSRP3, LBD3, and TCAP from 313 patients with familial or idiopathic dilated cardiomyopathy. *Clinical and translational science,* 1**,** 21-26.

HILL, L. E., MEHEGAN, J. P., BUTTERS, C. A. & TOBACMAN, L. S. 1992. Analysis of troponin-tropomyosin binding to actin. Troponin does not promote interactions between tropomyosin molecules. *Journal of Biological Chemistry,* 267**,** 16106-13.

HITCHCOCK-DEGREGORI, S. E., SONG, Y. & GREENFIELD, N. J. 2002. Functions of Tropomyosin's Periodic Repeats†. *Biochemistry,* 41**,** 15036-15044.

HO, C. Y., CARLSEN, C., THUNE, J. J., HAVNDRUP, O., BUNDGAARD, H., FARROHI, F., RIVERO, J., CIRINO, A. L., ANDERSEN, P. S., CHRISTIANSEN, M., MARON, B. J., ORAV, E. J. & KOBER, L. 2009. Echocardiographic strain imaging to assess early and late consequences of sarcomere mutations in hypertrophic cardiomyopathy. *Circ Cardiovasc Genet,* 2**,** 314-21.

HOEDEMAEKERS, Y. M., CALISKAN, K., MICHELS, M., FROHN-MULDER, I., VAN DER SMAGT, J. J., PHEFFERKORN, J. E., WESSELS, M. W., TEN CATE, F. J., SIJBRANDS, E. J., DOOIJES, D. & MAJOOR-KRAKAUER, D. F. 2010. The

importance of genetic counseling, DNA diagnostics, and cardiologic family screening in left ventricular noncompaction cardiomyopathy. *Circ Cardiovasc Genet,* 3**,** 232-9.

HOFF, E. C., KRAMER, T. C., DUBOIS, D. & PATTEN, B. M. 1939. The development of the electrocardiogram of the embryonic heart. *American Heart Journal,* 17**,** 470-488.

HOFFMAN, J. I. E. & KAPLAN, S. 2002. The incidence of congenital heart disease. *Journal of the American College of Cardiology,* 39**,** 1890-1900.

HOGERS, B., DERUITER, M. C., GITTENBERGER-DE GROOT, A. C. & POELMANN, R. E. 1999. *Extraembryonic venous obstructions lead to cardiovascular malformations and can be embryolethal*.

HOOGAARS, W. M. H., TESSARI, A., MOORMAN, A. F. M., DE BOER, P. A. J., HAGOORT, J., SOUFAN, A. T., CAMPIONE, M. & CHRISTOFFELS, V. M. 2004. *The transcriptional repressor Tbx3 delineates the developing central conduction system of the heart*.

HOOK, J., LEMCKERT, F., QIN, H., SCHEVZOV, G. & GUNNING, P. 2004. Gamma Tropomyosin Gene Products Are Required for Embryonic Development. *Mol. Cell. Biol.,* 24**,** 2318-2323.

HUANG, W., ZHANG, R. & XU, X. 2009. Myofibrillogenesis in the developing zebrafish heart: A functional study of tnnt2. *Developmental Biology,* 331**,** 237-249.

HUMPHREY, R. R. 1972. Genetic and experimental studies on a mutant gene (c) determining absence of heart action in embryos of the Mexican axolotl (Ambystoma mexicanum). *Developmental Biology,* 27**,** 365-375.

ICARDO, J. M. & FERNANDEZ-TERAN, A. 1987. Morphologic study of ventricular trabeculation in the embryonic chick heart. *Acta Anat (Basel),* 130**,** 264-74.

ICHIDA, F. 2009. Left ventricular noncompaction. *Circ J,* 73**,** 19-26.

IKEDA, U., MINAMISAWA, M. & KOYAMA, J. 2014. Isolated left ventricular non-compaction cardiomyopathy in adults. *Journal of Cardiology,* 65**,** 91-97.

ISHII, Y., GARRIOCK, R. J., NAVETTA, A. M., COUGHLIN, L. E. & MIKAWA, T. 2010. BMP signals promote proepicardial protrusion necessary for recruitment of coronary vessel and epicardial progenitors to the heart. *Dev Cell.,* 2**,** 307-316.

IZUMO, S., NADAL-GINARD, B. & MAHDAVI, V. 1988. Protooncogene induction and reprogramming of cardiac gene expression produced by pressure overload. *Proceedings of the National Academy of Sciences,* 85**,** 339-343.

JAGATHEESAN, G., RAJAN, S., PETRASHEVSKAYA, N., SCHWARTZ, A., BOIVIN, G., VAHEBI, S., DETOMBE, P., SOLARO, R. J., LABITZKE, E., HILLIARD, G. & WIECZOREK , D. F. 2003. Functional Importance of the Carboxyl-terminal Region of Striated Muscle Tropomyosin. *Journal of Biological Chemistry,* 278**,** 23204-23211.

JANUSZEWSKA, K., MALEC, E., JUCHEM, G., KACZMAREK, I., SODIAN, R., UBERFUHR, P. & REICHART, B. 2009. Heart-lung transplantation in patients with pulmonary atresia and ventricular septal defect. *J Thorac Cardiovasc Surg,* 138**,** 738-43.

JESERICH, M., MERKLE, N., GOBEL, H., HEILMANN, C. & BEYERSDORF, F. 2006. Congenital left ventricular apical aneurysm or diverticulum mimicking infarct aneurysm and a right ventricular diverticulum in an adult. *Clin Res Cardiol,* 95**,** 373-8.

JIN, J.-P., ZHANG, Z. & BAUTISTA, J. A. 2008. Isoform Diversity, Regulation, and Functional Adaptation of Troponin and Calponin. 18**,** 93-124.

JIN, J. P. & CHONG, S. M. 2010. Localization of the two tropomyosin-binding sites of troponin T. *Archives of Biochemistry and Biophysics,* 500**,** 144-150.

JIN, J. P., WANG, J. & ZHANG, J. 1996. Expression of cDNAs encoding mouse cardiac troponin T isoforms: characterization of a large sample of independent clones. *Gene,* 168**,** 217-21.

JONGBLOED, R. J., MARCELIS, C. L., DOEVENDANS, P. A., SCHMEITZ-MULKENS, J. M., VAN DOCKUM, W. G., GERAEDTS, J. P. & SMEETS, H. J. 2003. Variable clinical manifestation of a novel missense mutation in the alpha-tropomyosin (TPM1) gene in familial hypertrophic cardiomyopathy. *J Am Coll Cardiol,* 41**,** 981-6.

JONGBLOED, R. J., SMEETS, H., DOEVENDANS, P. A. & VAN DEN WIJNGAARD, A. 2005. Methods in molecular cardiology: DHPLC mutation detection analysis. *Neth Heart J,* 13**,** 11-17.

KAMISAGO, M., SHARMA, S. D., DEPALMA, S. R., SOLOMON, S., SHARMA, P., MCDONOUGH, B., SMOOT, L., MULLEN, M. P., WOOLF, P. K., WIGLE, E. D., SEIDMAN, J. G., JARCHO, J., SHAPIRO, L. R. & SEIDMAN, C. E. 2000. Mutations in Sarcomere Protein Genes as a Cause of Dilated Cardiomyopathy. *New England Journal of Medicine,* 343**,** 1688-1696.

KANZLER, B. T., HAAS-ASSENBAUM, A., HAAS, I., MORAWIEC, L., HUBER, E. & BOEHM, T. 2003. Morpholino oligonucleotide-triggered knockdown reveals a role for maternal E-cadherin during early mouse development. *Mechanisms of Development,* 120**,** 1423-1432.

KARIBE, A., TOBACMAN, L. S., STRAND, J., BUTTERS, C., BACK, N., BACHINSKI, L. L., ARAI, A. E., ORTIZ, A., ROBERTS, R., HOMSHER, E. & FANANAPAZIR, L. 2001. Hypertrophic cardiomyopathy caused by a novel alpha-tropomyosin mutation (V95A) is associated with mild cardiac phenotype, abnormal calcium binding to troponin, abnormal myosin cycling, and poor prognosis. *Circulation,* 103**,** 65-71.

KASKI, J. P., SYRRIS, P., BURCH, M., TOME-ESTEBAN, M. T., FENTON, M., CHRISTIANSEN, M., ANDERSEN, P. S., SEBIRE, N., ASHWORTH, M., DEANFIELD, J. E., MCKENNA, W. J. & ELLIOTT, P. M. 2008. Idiopathic restrictive cardiomyopathy in children is caused by mutations in cardiac sarcomere protein genes. *Heart,* 94**,** 1478-84.

KAZMOUZ, S., KENNY, D., CAO, Q. L., KAVINSKY, C. J. & HIJAZI, Z. M. 2013. Transcatheter closure of secundum atrial septal defects. *J Invasive Cardiol,* 25**,** 257-64.

KELLY, R. G., BROWN, N. A. & BUCKINGHAM, M. E. 2001. The Arterial Pole of the Mouse Heart Forms from Fgf10-Expressing Cells in Pharyngeal Mesoderm. *Developmental Cell,* 1**,** 435-440.

KIRBY, M., GALE, T. & STEWART, D. 1983. Neural crest cells contribute to normal aorticopulmonary septation. *Science,* 220**,** 1059-1061.

KIRBY, M. L. & WALDO, K. L. 1990. Role of neural crest in congenital heart disease. *Circulation,* 82**,** 332-40.

KIRBY, M. L. & WALDO, K. L. 1995. Neural Crest and Cardiovascular Patterning. *Circulation Research,* 77**,** 211-215.

KIRK, E. P., SUNDE, M., COSTA, M. W., RANKIN, S. A., WOLSTEIN, O., CASTRO, M. L., BUTLER, T. L., HYUN, C., GUO, G., OTWAY, R., MACKAY, J. P., WADDELL, L. B., COLE, A. D., HAYWARD, C., KEOGH, A., MACDONALD, P., GRIFFITHS, L., FATKIN, D., SHOLLER, G. F., ZORN, A. M., FENELEY, M. P., WINLAW, D. S. & HARVEY, R. P. 2007. Mutations in cardiac T-box factor gene TBX20 are associated with diverse cardiac pathologies, including defects of septation and valvulogenesis and cardiomyopathy. *Am J Hum Genet,* 81**,** 280-91.

KLAASSEN, S., PROBST, S., OECHSLIN, E., GERULL, B., KRINGS, G., SCHULER, P., GREUTMANN, M., HÜRLIMANN, D., YEGITBASI, M., PONS, L., GRAMLICH, M., DRENCKHAHN, J.-D., HEUSER, A., BERGER, F., JENNI, R. & THIERFELDER, L. 2008. Mutations in Sarcomere Protein Genes in Left Ventricular Noncompaction. *Circulation,* 117**,** 2893-2901.

KOBZA, R., OECHSLIN, E., PRETRE, R., KURZ, D. J. & JENNI, R. 2003. Enlargement of the right atrium--diverticulum or aneurysm? *Eur J Echocardiogr,* 4**,** 223-5.

KODO, K. & YAMAGISHI, H. 2011. A Decade of Advances in the Molecular Embryology and Genetics Underlying Congenital Heart Defects. *Circulation Journal,* 75**,** 2296-2304.

KOK, FATMA O., SHIN, M., NI, C.-W., GUPTA, A., GROSSE, ANN S., VAN IMPEL, A., KIRCHMAIER, BETTINA C., PETERSON-MADURO, J., KOURKOULIS, G., MALE, I., DESANTIS, DANA F., SHEPPARD-TINDELL, S., EBARASI, L., BETSHOLTZ, C., SCHULTE-MERKER, S., WOLFE, SCOT A. & LAWSON, NATHAN D. 2015. Reverse Genetic Screening Reveals Poor Correlation between Morpholino-Induced and Mutant Phenotypes in Zebrafish. *Developmental Cell,* 32**,** 97-108.

KONNO, T., SHIMIZU, M., INO, H., YAMAGUCHI, M., TERAI, H., UCHIYAMA, K., OE, K., MABUCHI, T., KANEDA, T. & MABUCHI, H. 2004. Diagnostic value of abnormal Q waves for identification of preclinical carriers of hypertrophic cardiomyopathy based on a molecular genetic diagnosis. *Eur Heart J,* 25**,** 246-51.

KORESSAAR, T. & REMM, M. 2007. Enhancements and modifications of primer design program Primer3. *Bioinformatics,* 23**,** 1289-1291.

KOSTYUKOVA, A. S., TIKTOPULO, E. I. & MAÉDA, Y. 2001. Folding Properties of Functional Domains of Tropomodulin. *Biophysical Journal,* 81**,** 345-351.

KRAWCZAK, M., BALL, E. V., FENTON, I., STENSON, P. D., ABEYSINGHE, S., THOMAS, N. & COOPER, D. N. 2000. Human Gene Mutation Database—A biomedical information and research resource. *Human Mutation,* 15**,** 45-51.

KREUZBERG, M. M., WILLECKE, K. & BUKAUSKAS, F. F. 2006. Connexin-Mediated Cardiac Impulse Propagation: Connexin 30.2 Slows Atrioventricular Conduction in Mouse Heart. *Trends in Cardiovascular Medicine,* 16**,** 266-272.

KUBBEN, F. J., PEETERS-HAESEVOETS, A., ENGELS, L. G., BAETEN, C. G., SCHUTTE, B., ARENDS, J. W., STOCKBRÜGGER, R. W. & BLIJHAM, G. H. 1994. Proliferating cell nuclear antigen (PCNA): a new marker to study human colonic cell proliferation. *Gut,* 35**,** 530-535.

KUMAR, P., HENIKOFF, S. & NG, P. 2009. Predicting the effects of coding non-synonymous variants on protein function using the SIFT algorithm. *Nat Protoc.,* 4**,** 1073-1081.

KURIAKOSE, D. 2008. *A role for Tropomyosin 1 during chick heart development.* Masters of Research, University of Nottingham.

KUSHWAHA, S. S., FALLON, J. T. & FUSTER, V. 1997. Restrictive cardiomyopathy. *N Engl J Med,* 336**,** 267-76.

LAKDAWALA, N. K., DELLEFAVE, L., REDWOOD, C. S., SPARKS, E., CIRINO, A. L., DEPALMA, S., COLAN, S. D., FUNKE, B., ZIMMERMAN, R. S., ROBINSON, P., WATKINS, H., SEIDMAN, C. E., SEIDMAN, J. G., MCNALLY, E. M. & HO, C. Y. 2010. Familial Dilated Cardiomyopathy Caused by an Alpha-Tropomyosin Mutation: The Distinctive Natural History of Sarcomeric Dilated Cardiomyopathy. *Journal of the American College of Cardiology,* 55**,** 320-329.

LAKDAWALA, N. K., FUNKE, B. H., BAXTER, S., CIRINO, A. L., ROBERTS, A. E., JUDGE, D. P., JOHNSON, N., MENDELSOHN, N. J., MOREL, C., CARE, M., CHUNG, W. K., JONES, C., PSYCHOGIOS, A., DUFFY, E., REHM, H. L., WHITE, E., SEIDMAN, J. G., SEIDMAN, C. E. & HO, C. Y. 2012. Genetic testing for dilated cardiomyopathy in clinical practice. *J Card Fail,* 18**,** 296-303.

LAMERS, W. H. & MOORMAN, A. F. M. 2002. Cardiac Septation: A late contribution of the embryonic primary myocardium to heart morphogenesis. *Circulation Research,* 91**,** 93-103.

LAMERS, W. H., WESSELS, A., VERBEEK, F. J., MOORMAN, A. F., VIRAGH, S., WENINK, A. C., GITTENBERGER-DE GROOT, A. C. & ANDERSON, R. H. 1992. New findings concerning ventricular septation in the human heart. Implications for maldevelopment. *Circulation,* 86**,** 1194-205.

LARKIN, M. A., BLACKSHIELDS, G., BROWN, N. P., CHENNA, R., MCGETTIGAN, P. A., MCWILLIAM, H., VALENTIN, F., WALLACE, I. M., WILM, A., LOPEZ, R., THOMPSON, J. D., GIBSON, T. J. & HIGGINS, D. G. 2007. Clustal W and Clustal X version 2.0. *Bioinformatics,* 23**,** 2947-2948.

LAZZARINI, E., JONGBLOED, J. D. H., PILICHOU, K., THIENE, G., BASSO, C., BIKKER, H., CHARBON, B., SWERTZ, M., VAN TINTELEN, J. P. & VAN DER ZWAAG, P. A. 2015. The ARVD/C Genetic Variants Database: 2014 Update. *Human Mutation,* 36**,** 403-410.

LEES-MILLER, J. P. & HELFMAN, D. M. 1991. The molecular basis for tropomyosin isoform diversity. *BioEssays,* 13**,** 429-437.

LEHMAN, W., CRAIG, R. & VIBERT, P. 1994. Ca2+-induced tropomyosin movement in Limulus thin filaments revealed by three-dimensional reconstruction. *Nature,* 368**,** 65-67.

LEHRER, S. S. 1994. The regulatory switch of the muscle thin filament: Ca²⁺ or myosin heads? *Journal of Muscle Research and Cell Motility,* 15**,** 232-236.

LI, D., CZERNUSZEWICZ, G. Z., GONZALEZ, O., TAPSCOTT, T., KARIBE, A., DURAND, J. B., BRUGADA, R., HILL, R., GREGORITCH, J. M., ANDERSON, J. L., QUINONES, M., BACHINSKI, L. L. & ROBERTS, R. 2001. Novel cardiac troponin T mutation as a cause of familial dilated cardiomyopathy. *Circulation,* 104**,** 2188-93.

LI, Y. S., HAGA, J. H. & CHIEN, S. 2005. Molecular basis of the effects of shear stress on vascular endothelial cells. *J Biomech,* 38**,** 1949-71.

LIESCHKE, G. J. & CURRIE, P. D. 2007. Animal models of human disease: zebrafish swim into view. *Nat Rev Genet,* 8**,** 353-67.

LOPEZ-SANCHEZ, C. & GARCIA-MARTINEZ, V. 2011. Molecular determinants of cardiac specification. *Cardiovasc Res,* 91**,** 185-95.

LOWE, J. S., PALYGIN, O., BHASIN, N., HUND, T. J., BOYDEN, P. A., SHIBATA, E., ANDERSON, M. E. & MOHLER, P. J. 2008. Voltage-gated Nav channel targeting in the heart requires an ankyrin-G–dependent cellular pathway. *The Journal of Cell Biology,* 180**,** 173-186.

MAMIDI, R., MUTHUCHAMY, M. & CHANDRA, M. 2013. Instability in the Central Region of Tropomyosin Modulates the Function of Its Overlapping Ends. *Biophysical Journal,* 105**,** 2104-2113.

MANASEK, F. J. 1968. Embryonic development of the heart. I. A light and electron microscopic study of myocardial development in the early chick embryo. *Journal of Morphology,* 125**,** 329-365.

MÄNNER, J. 2000. Cardiac looping in the chick embryo: A morphological review with special reference to terminological and biomechanical aspects of the looping process. *The Anatomical Record,* 259**,** 248-262.

MÄNNER, J. 2004. On rotation, torsion, lateralization, and handedness of the embryonic heart loop: New insights from a simulation model for the heart loop of chick embryos. *The Anatomical Record Part A: Discoveries in Molecular, Cellular, and Evolutionary Biology,* 278A**,** 481-492.

MÄNNER, J. 2009. The anatomy of cardiac looping: A step towards the understanding of the morphogenesis of several forms of congenital cardiac malformations. *Clinical Anatomy,* 22**,** 21-35.

MANNING, E. P., TARDIFF, J. C. & SCHWARTZ, S. D. 2011. A model of calcium activation of the cardiac thin filament. *Biochemistry,* 50**,** 7405-13.

MARIAN, A. J., ZHAO, G., SETA, Y., ROBERTS, R. & YU, Q. T. 1997. Expression of a mutant (Arg92Gln) human cardiac troponin T, known to cause hypertrophic cardiomyopathy, impairs adult cardiac myocyte contractility. *Circ Res,* 81**,** 76-85.

MARMIGERE, F. & ERNFORS, P. 2007. Specification and connectivity of neuronal subtypes in the sensory lineage. *Nat Rev Neurosci,* 8**,** 114-127.

MARON, B. J., GARDIN, J. M., FLACK, J. M., GIDDING, S. S., KUROSAKI, T. T. & BILD, D. E. 1995. Prevalence of hypertrophic cardiomyopathy in a general population of young adults. Echocardiographic analysis of 4111 subjects in the CARDIA Study. Coronary Artery Risk Development in (Young) Adults. *Circulation,* 92**,** 785-9.

MARON, B. J., SATO, N., ROBERTS, W. C., EDWARDS, J. E. & CHANDRA, R. S. 1979. Quantitative analysis of cardiac muscle cell disorganization in the ventricular septum. Comparison of fetuses and infants with and without congenital heart disease and patients with hypertrophic cardiomyopathy. *Circulation,* 60**,** 685-96.

MARON, B. J., TOWBIN, J. A., THIENE, G., ANTZELEVITCH, C., CORRADO, D., ARNETT, D., MOSS, A. J., SEIDMAN, C. E. & YOUNG, J. B. 2006. Contemporary Definitions and Classification of the Cardiomyopathies: An American Heart Association Scientific Statement From the Council on Clinical Cardiology, Heart Failure and Transplantation Committee; Quality of Care and Outcomes Research and Functional Genomics and Translational Biology Interdisciplinary Working Groups; and Council on Epidemiology and Prevention. *Circulation,* 113**,** 1807-1816.

MAROTO MONEDERO, C., CAMINO LÓPEZ, M., GIRONA, J. M. & MALO CONCEPCIÓN, P. 2001. Clinical practice guidelines of the Spanish Society of Cardiology in congenital heart disease in newborns *Spanish Society of Cardiology,* 54**,** 49-66.

MARSTON, S. B. & REDWOOD, C. S. 2003. Modulation of Thin Filament Activation by Breakdown or Isoform Switching of Thin Filament Proteins. *Circulation Research,* 93**,** 1170-1178.

MARTINSEN, B. J. 2005. Reference guide to the stages of chick heart embryology. *Developmental Dynamics,* 233**,** 1217-1237.

MATSSON, H., EASON, J., BOOKWALTER, C. S., KLAR, J., GUSTAVSSON, P., SUNNEGÅRDH, J., ENELL, H., JONZON, A., VIKKULA, M., GUTIERREZ, I., GRANADOS-RIVERON, J., POPE, M., BU'LOCK, F., COX, J., ROBINSON, T. E., SONG, F., BROOK, D. J., MARSTON, S., TRYBUS, K. M. & DAHL, N. 2008. Alpha-cardiac actin mutations produce atrial septal defects. *Human Molecular Genetics,* 17**,** 256-265.

MAUGHAN, D. 2005. Kinetics and Energetics of The Crossbridge Cycle. *Heart Failure Reviews,* 10**,** 175-185.

MCKENNA, W., DEANFIELD, J., FARUQUI, A., ENGLAND, D., OAKLEY, C. & GOODWIN, J. 1981. Prognosis in hypertrophic cardiomyopathy: role of age and clinical, electrocardiographic and hemodynamic features. *Am J Cardiol,* 47**,** 532-8.

MCKEOWN, C. R., NOWAK, R. B., GOKHIN, D. S. & FOWLER, V. M. 2014. Tropomyosin is required for cardiac morphogenesis, myofibril assembly, and

formation of adherens junctions in the developing mouse embryo. *Developmental Dynamics,* 243**,** 800-817.

MIDGETT, M. & RUGONYI, S. 2014. Congenital heart malformations induced by hemodynamic altering surgical interventions. *Frontiers in Physiology,* 5**,** 287.

MILANO, A., VERMEER, A. M. C., LODDER, E. M., BARC, J., VERKERK, A. O., POSTMA, A. V., VAN DER BILT, I. A. C., BAARS, M. J. H., VAN HAELST, P. L., CALISKAN, K., HOEDEMAEKERS, Y. M., LE SCOUARNEC, S., REDON, R., PINTO, Y. M., CHRISTIAANS, I., WILDE, A. A. & BEZZINA, C. R. 2014. HCN4 Mutations in Multiple Families With Bradycardia and Left Ventricular Noncompaction Cardiomyopathy. *Journal of the American College of Cardiology,* 64**,** 745-756.

MILIOU, A., ANASTASAKIS, A., D'CRUZ, L. G., THEOPISTOU, A., RIGOPOULOS, A., RIZOS, I., STAMATELOPOULOS, S., TOUTOUZAS, P. & STEFANADIS, C. 2005. Low prevalence of cardiac troponin T mutations in a Greek hypertrophic cardiomyopathy cohort. *Heart,* 91**,** 966-967.

MINETTE, M. S. & SAHN, D. J. 2006. Ventricular Septal Defects. *Circulation,* 114**,** 2190-2197.

MITCHELL, S. C., KORONES, S. B. & BERENDES, H. W. 1971. Congenital heart disease in 56,109 births. Incidence and natural history. *Circulation,* 43**,** 323-32.

MJAATVEDT, C. H., NAKAOKA, T., MORENO-RODRIGUEZ, R., NORRIS, R. A., KERN, M. J., EISENBERG, C. A., TURNER, D. & MARKWALD, R. R. 2001. The outflow tract of the heart is recruited from a novel heart-forming field. *Dev Biol,* 238**,** 97-109.

MOGENSEN, J., MURPHY, R. T., SHAW, T., BAHL, A., REDWOOD, C., WATKINS, H., BURKE, M., ELLIOTT, P. M. & MCKENNA, W. J. 2004. Severe disease expression of cardiac troponin C and T mutations in patients with idiopathic dilated cardiomyopathy. *Journal of the American College of Cardiology,* 44**,** 2033-2040.

MONERA, O. D., SEREDA, T. J., ZHOU, N. E., KAY, C. M. & HODGES, R. S. 1995. Relationship of sidechain hydrophobicity and alpha-helical propensity on the stability of the single-stranded amphipathic alpha-helix. *J Pept Sci,* 1**,** 319-29.

MONSERRAT, L., HERMIDA-PRIETO, M., FERNANDEZ, X., RODRÍGUEZ, I., DUMONT, C., CAZÓN, L., CUESTA, M. G., GONZALEZ-JUANATEY, C., PETEIRO, J., ÁLVAREZ, N., PENAS-LADO, M. & CASTRO-BEIRAS, A. 2007. Mutation in the alpha-cardiac actin gene associated with apical hypertrophic cardiomyopathy, left ventricular non-compaction, and septal defects. *European Heart Journal,* 28**,** 1953-1961.

MOODY, W. J. 1995. Critical periods of early development created by the coordinate modulation of ion channel properties. *Perspect Dev Neurobiol,* 2**,** 309-15.

MOOLMAN, J. C., CORFIELD, V. A., POSEN, B., NGUMBELA, K., SEIDMAN, C., BRINK, P. A. & WATKINS, H. 1997. Sudden death due to troponin T mutations. *J Am Coll Cardiol,* 29**,** 549-55.

MOORE, P. & LEMANSKI, L. 1982. Quantification of tropomyosin by radioimmunoassay in developing hearts of cardiac mutant axolotls,Ambystoma mexicanum. *Journal of Muscle Research & Cell Motility,* 3**,** 161-167.

MOORMAN, A., WEBB, S., BROWN, N. A., LAMERS, W. & ANDERSON, R. H. 2003. Development of the heart: (1) Formation of the cardiac chambers and atrial trunks. *Heart,* 89**,** 806-814.

MOORMAN, A. F. M. & CHRISTOFFELS, V. M. 2003. Cardiac Chamber Formation: Development, Genes, and Evolution. *Physiological Reviews,* 83**,** 1223-1267.

MOORMAN, A. F. M. & LAMERS, W. H. 1994. Molecular anatomy of the developing heart. *Trends in Cardiovascular Medicine,* 4**,** 257-264.

MORALES, A., PINTO, J. R., SIEGFRIED, J. D., LI, D., NORTON, N., HOFMEYER, M., VALLIN, M., MORALES, A. R., POTTER, J. D. & HERSHBERGER, R. E. 2010. Late onset sporadic dilated cardiomyopathy caused by a cardiac troponin T mutation. *Clin Transl Sci,* 3**,** 219-26.

MORIMOTO, S. 2008. Sarcomeric proteins and inherited cardiomyopathies. *Cardiovascular Research,* 77**,** 659-666.

MORITA, H., REHM, H. L., MENESSES, A., MCDONOUGH, B., ROBERTS, A. E., KUCHERLAPATI, R., TOWBIN, J. A., SEIDMAN, J. G. & SEIDMAN, C. E. 2008. Shared genetic causes of cardiac hypertrophy in children and adults. *N Engl J Med,* 358**,** 1899-908.

MORRIS, E. P. & LEHRER, S. S. 1984. Troponin-tropomyosin interactions. Fluorescence studies of the binding of troponin, troponin T, and chymotryptic troponin T fragments to specifically labeled tropomyosin. *Biochemistry,* 23**,** 2214-20.

MOSKOWITZ, I. P. G., KIM, J. B., MOORE, M. L., WOLF, C. M., PETERSON, M. A., SHENDURE, J., NOBREGA, M. A., YOKOTA, Y., BERUL, C., IZUMO, S., SEIDMAN, J. G. & SEIDMAN, C. E. 2007. A Molecular Pathway Including Id2, Tbx5, and Nkx2-5 Required for Cardiac Conduction System Development. *Cell,* 129**,** 1365-1376.

MURAKAMI, C., NAKAMURA, S., KOBAYASHI, M., MAEDA, K., IRIE, W., WADA, B., HAYASHI, M., SASAKI, C., NAKAMARU, N., FURUKAWA, M. & KURIHARA, K. 2010. Analysis of the sarcomere protein gene mutation on cardiomyopathy – Mutations in the cardiac troponin I gene. *Legal Medicine,* 12**,** 280-283.

MUTHUCHAMY, M., PAJAK, L., HOWLES, P., DOETSCHMAN, T. & WIECZOREK, D. F. 1993. Developmental analysis of tropomyosin gene expression in embryonic stem cells and mouse embryos. *Molecular and Cellular Biology,* 13**,** 3311-3323.

NAKAJIMA-TANIGUCHI, C., MATSUI, H., FUJIO, Y., NAGATA, S., KISHIMOTO, T. & YAMAUCHI-TAKIHARA, K. 1997. Novel missense mutation in cardiac troponin T gene found in Japanese patient with hypertrophic cardiomyopathy. *J Mol Cell Cardiol,* 29**,** 839-43.

NASEVICIUS, A. & EKKER, S. C. 2000. Effective targeted gene 'knockdown' in zebrafish. *Nat Genet,* 26**,** 216-20.

NEEDHAM, J. 1959. *A History of Embryology,* New York, Abelard-Schuman.

NIIMURA, H., PATTON, K. K., MCKENNA, W. J., SOULTS, J., MARON, B. J., SEIDMAN, J. G. & SEIDMAN, C. E. 2002. Sarcomere Protein Gene Mutations in Hypertrophic Cardiomyopathy of the Elderly. *Circulation,* 105**,** 446-451.

NISHIBATAKE, M., KIRBY, M. L. & VAN MIEROP, L. H. 1987. Pathogenesis of persistent truncus arteriosus and dextroposed aorta in the chick embryo after neural crest ablation. *Circulation,* 75**,** 255-64.

NISHII, K., MORIMOTO, S., MINAKAMI, R., MIYANO, Y., HASHIZUME, K., OHTA, M., ZHAN, D.-Y., LU, Q.-W. & SHIBATA, Y. 2008. Targeted disruption of the cardiac troponin T gene causes sarcomere disassembly and defects in heartbeat within the early mouse embryo. *Developmental Biology,* 322**,** 65-73.

NORRIS, A. & STREIT, A. 2014. Morpholinos: studying gene function in the chick. *Methods (San Diego, Calif.),* 66**,** 454-465.

NUTT, S. L., BRONCHAIN, O. J., HARTLEY, K. O. & AMAYA, E. 2001. Comparison of morpholino based translational inhibition during the development of Xenopus laevis and Xenopus tropicalis. *Genesis,* 30**,** 110-3.

OHTSUKI, I. & NAGANO, K. 1982. Molecular arrangement of troponin-tropomyosin in the thin filament. *Adv Biophys,* 15**,** 93-130.

OLIVOTTO, I., GIROLAMI, F., ACKERMAN, M. J., NISTRI, S., BOS, J. M., ZACHARA, E., OMMEN, S. R., THEIS, J. L., VAUBEL, R. A., RE, F., ARMENTANO, C., POGGESI, C., TORRICELLI, F. & CECCHI, F. 2008. Myofilament Protein Gene Mutation Screening and Outcome of Patients With Hypertrophic Cardiomyopathy. *Mayo Clinic Proceedings,* 83**,** 630-638.

OLSON, T. M., KISHIMOTO, N. Y., WHITBY, F. G. & MICHELS, V. V. 2001. Mutations that Alter the Surface Charge of Alpha-tropomyosin are Associated with Dilated Cardiomyopathy. *Journal of Molecular and Cellular Cardiology,* 33**,** 723-732.

OTSUKA, H., ARIMURA, T., ABE, T., KAWAI, H., AIZAWA, Y., KUBO, T., KITAOKA, H., NAKAMURA, H., NAKAMURA, K., OKAMOTO, H., ICHIDA, F., AYUSAWA, M., NUNODA, S., ISOBE, M., MATSUZAKI, M., DOI, Y. L., FUKUDA, K., SASAOKA, T., IZUMI, T., ASHIZAWA, N. & KIMURA, A. 2012. Prevalence and distribution of sarcomeric gene mutations in Japanese patients with familial hypertrophic cardiomyopathy. *Circ J,* 76**,** 453-61.

PALM, T., GREENFIELD, N. J. & HITCHCOCK-DEGREGORI, S. E. 2003. Tropomyosin Ends Determine the Stability and Functionality of Overlap and Troponin T Complexes. *Biophysical Journal,* 84**,** 3181-3189.

PARRY, D. 1975. Analysis of the primary sequence of alpha-tropomyosin from rabbit skeletal muscle. *J Mol Biol.,* 98**,** 519-5535.

PARVATIYAR, M. S., LANDSTROM, A. P., FIGUEIREDO-FREITAS, C., POTTER, J. D., ACKERMAN, M. J. & PINTO, J. R. 2012. A Mutation in TNNC1-encoded Cardiac Troponin C, TNNC1-A31S, Predisposes to Hypertrophic Cardiomyopathy and Ventricular Fibrillation. *Journal of Biological Chemistry,* 287**,** 31845-31855.

PEARLSTONE, J. R. & SMILLIE, L. B. 1982. Binding of troponin-T fragments to several types of tropomyosin. Sensitivity to Ca2+ in the presence of troponin-C. *J Biol Chem,* 257**,** 10587-92.

PEARLSTONE, J. R. & SMILLIE, L. B. 1983. Effects of troponin-I plus-C on the binding of troponin-T and its fragments to alpha-tropomyosin. Ca2+ sensitivity and cooperativity. *J Biol Chem,* 258**,** 2534-42.

PEDDY, S. B., VRICELLA, L. A., CROSSON, J. E., OSWALD, G. L., COHN, R. D., CAMERON, D. E., VALLE, D. & LOEYS, B. L. 2006. Infantile restrictive cardiomyopathy resulting from a mutation in the cardiac troponin T gene. *Pediatrics,* 117**,** 1830-3.

PENNY, D. J. & VICK, G. W., 3RD 2011. Ventricular septal defect. *Lancet,* 377**,** 1103-12.

PERRY, S. V. 2001. Vertebrate tropomyosin: distribution, properties and function. *Journal of Muscle Research and Cell Motility,* 22**,** 5-49.

PEXIEDER, T. 1975. Cell Death and the Morphogenesis of the Heart. *Cell death in the morphogenesis and teratogenesis of the heart.* Springer Berlin Heidelberg.

PHILLIPS, G. N., FILLERS, J. P. & COHEN, C. 1986. Tropomyosin crystal structure and muscle regulation. *Journal of Molecular Biology,* 192**,** 111-127.

PILLAI, R. S. 2005. MicroRNA function: multiple mechanisms for a tiny RNA? *RNA,* 11**,** 1753-61.

PINNELL, J., TURNER, S. & HOWELL, S. 2007. Cardiac muscle physiology. *Continuing Education in Anaesthesia, Critical Care & Pain,* 7**,** 85-88.

POSCH, M. G., WALDMULLER, S., MULLER, M., SCHEFFOLD, T., FOURNIER, D., ANDRADE-NAVARRO, M. A., DE GEETER, B., GUILLAUMONT, S., DAUPHIN, C., YOUSSEFF, D., SCHMITT, K. R., PERROT, A., BERGER, F., HETZER, R., BOUVAGNET, P. & OZCELIK, C. 2011. Cardiac alpha-myosin (MYH6) is the predominant sarcomeric disease gene for familial atrial septal defects. *PLoS One,* 6**,** e28872.

POSTMA, A. V., VAN ENGELEN, K., VAN DE MEERAKKER, J., RAHMAN, T., PROBST, S., BAARS, M. J., BAUER, U., PICKARDT, T., SPERLING, S. R., BERGER, F., MOORMAN, A. F., MULDER, B. J., THIERFELDER, L., KEAVNEY, B., GOODSHIP, J. & KLAASSEN, S. 2011. Mutations in the sarcomere gene MYH7 in Ebstein anomaly. *Circ Cardiovasc Genet,* 4**,** 43-50.

PROBST, S., OECHSLIN, E., SCHULER, P., GREUTMANN, M., BOYE, P., KNIRSCH, W., BERGER, F., THIERFELDER, L., JENNI, R. & KLAASSEN, S. 2011. Sarcomere gene mutations in isolated left ventricular noncompaction cardiomyopathy do not predict clinical phenotype. *Circ Cardiovasc Genet,* 4**,** 367-74.

RAJAN, S., JAGATHEESAN, G., KARAM, C. N., ALVES, M. L., BODI, I., SCHWARTZ, A., BULCAO, C. F., D'SOUZA, K. M., AKHTER, S. A., BOIVIN, G. P., DUBE, D. K., PETRASHEVSKAYA, N., HERR, A. B., HULLIN, R., LIGGETT, S. B., WOLSKA, B. M., SOLARO, R. J. & WIECZOREK, D. F. 2010. Molecular and Functional Characterization of a Novel Cardiac-Specific Human Tropomyosin Isoform. *Circulation,* 121**,** 410-418.

RAMACIOTTI, C., VETTER, J. M., BORNEMEIER, R. A. & CHIN, A. J. 1995. Prevalence, relation to spontaneous closure, and association of muscular ventricular septal defects with other cardiac defects. *Am J Cardiol,* 75**,** 61-5.

RANI, D. S., DHANDAPANY, P. S., NALLARI, P., NARASIMHAN, C. & THANGARAJ, K. 2014. A Novel Arginine to Tryptophan (R144W) Mutation in Troponin T (cTnT) Gene in an Indian Multigenerational Family with Dilated Cardiomyopathy (FDCM). *PLoS ONE,* 9**,** e101451.

RANI, D. S., NALLARI, P., DHANDAPANI, P. S., TAMILARASI, S., NARASIMHAN, C., RAKSHAK, D., SINGH, L. & THANGARAJ, K. 2008. Genomics of complex disorders I. *Genomic Med.,* 2**,** 303-30.

REGITZ-ZAGROSEK, V., ERDMANN, J., WELLNHOFER, E., RAIBLE, J. & FLECK, E. 2000. Novel mutation in the alpha-tropomyosin gene and transition from hypertrophic to hypocontractile dilated cardiomyopathy. *Circulation,* 102**,** E112-6.

RETHINASAMY, P., MUTHUCHAMY, M., HEWETT, T., BOIVIN, G., WOLSKA, B. M., EVANS, C., SOLARO, R. J. & WIECZOREK, D. F. 1997. Molecular and Physiological Effects of α-Tropomyosin Ablation in the Mouse. *Circulation Research,* 82**,** 116-123.

RHEE, D., SANGER, J. M. & SANGER, J. W. 1994. The premyofibril: Evidence for its role in myofibrillogenesis. *Cell Motility and the Cytoskeleton,* 28**,** 1-24.

RICHARD, P., CHARRON, P., CARRIER, L., LEDEUIL, C., CHEAV, T., PICHEREAU, C., BENAICHE, A., ISNARD, R., DUBOURG, O., BURBAN, M., GUEFFET, J.-P., MILLAIRE, A., DESNOS, M., SCHWARTZ, K., HAINQUE, B., KOMAJDA, M. & PROJECT, F. T. E. H. F. 2003. Hypertrophic Cardiomyopathy: distribution of disease genes, spectrum of mutations, and implications for a molecular diagnosis strategy. *Circulation,* 107**,** 2227-2232.

ROSS, M. H., KAYE, G. I. & PAWLINA, W. 2003. *Histology: a text and atlas,* Philadelphia.

ROSSI, A. & SUPERTI-FURGA, A. 2001. Mutations in the diastrophic dysplasia sulfate transporter (DTDST) gene (SLC26A2): 22 novel mutations, mutation review, associated skeletal phenotypes, and diagnostic relevance. *Hum Mutat,* 17**,** 159-71.

RUGH, R. 1962. *Experimental Embryology,* Minneapolis, Burgess Publishing Company.

RUTLAND, C., WARNER, L., THORPE, A., ALIBHAI, A., ROBINSON, T., SHAW, B., LAYFIELD, R., BROOK, J. D. & LOUGHNA, S. 2009. Knockdown of alpha myosin heavy chain disrupts the cytoskeleton and leads to multiple defects during chick cardiogenesis. *Journal of Anatomy,* 214**,** 905-915.

RUTLAND, C. S., POLO-PARADA, L., EHLER, E., ALIBHAI, A., THORPE, A., SUREN, S., EMES, R. D., PATEL, B. & LOUGHNA, S. 2011. Knockdown of embryonic myosin heavy chain reveals an essential role in the morphology and function of the developing heart. *Development,* 138**,** 3955-3966.

RYCHTER, Z. & OSTADAL, B. 1971. Fate of "sinusoidal" intertrabecular spaces of the cardiac wall after development of the coronary vascular bed in chick embryo. *Folia Morphol (Praha),* 19**,** 31-44.

SAKABE, M., MATSUI, H., SAKATA, H., ANDO, K., YAMAGISHI, T. & NAKAJIMA, Y. 2005. Understanding heart development and congenital heart defects through developmental biology: A segmental approach. *Congenital Anomalies,* 45**,** 107-118.

SAXENA, S., JONSSON, Z. O. & DUTTA, A. 2003. Small RNAs with imperfect match to endogenous mRNA repress translation. Implications for off-target activity of small inhibitory RNA in mammalian cells. *J Biol Chem,* 278**,** 44312-9.

SCHOTT, J.-J., BENSON, D. W., BASSON, C. T., PEASE, W., SILBERBACH, G. M., MOAK, J. P., MARON, B. J., SEIDMAN, C. E. & SEIDMAN, J. G. 1998. Congenital Heart Disease Caused by Mutations in the Transcription Factor NKX2-5. *Science,* 281**,** 108-111.

SCHWARZE, U., STARMAN, B. J. & BYERS, P. H. 1999. Redefinition of exon 7 in the COL1A1 gene of type I collagen by an intron 8 splice-donor-site mutation in a form of osteogenesis imperfecta: influence of intron splice order on outcome of splice-site mutation. *Am J Hum Genet,* 65**,** 336-44.

SEDMERA, D. & THOMAS, P. S. 1996. Trabeculation in the embryonic heart. *BioEssays,* 18**,** 607-607.

SEHNERT, A. J., HUQ, A., WEINSTEIN, B. M., WALKER, C., FISHMAN, M. & STAINIER, D. Y. R. 2002. Cardiac troponin T is essential in sarcomere assembly and cardiac contractility. *Nat Genet,* 31**,** 106-110.

SEIDMAN, J. G. & SEIDMAN, C. 2001. The Genetic Basis for Cardiomyopathy: from Mutation Identification to Mechanistic Paradigms. *Cell,* 104**,** 557-567.

SFERRAZZA, G. F., ZHANG, C., JIA, P., LEMANSKI, S. L., ATHAUDA, G., STASSI, A., HALAGER, K., MAIER, J. A., RUEDA-DE-LEON, E., GUPTA, A., DUBE, S., HUANG, X., PRENTICE, H. M., DUBE, D. K. & LEMANSKI, L. F. 2007. Role of myofibril-inducing RNA in cardiac TnT expression in developing Mexican axolotl. *Biochemical and Biophysical Research Communications,* 357**,** 32-37.

SHAMS, A., FOWLER, R. S., TRUSLER, G. A., KEITH, J. D. & MUSTARD, W. T. 1971. PULMONARY ATRESIA WITH INTACT VENTRICULAR SEPTUM: REPORT OF 50 CASES. *Pediatrics,* 47**,** 370-377.

SHEETS, M. D., OGG, S. C. & WICKENS, M. P. 1990. Point mutations in AAUAAA and the poly (A) addition site: effects on the accuracy and efficiency of cleavage and polyadenylation in vitro. *Nucleic Acids Res,* 18**,** 5799-805.

SIDDALL, L. S., BARCROFT, L. C. & WATSON, A. J. 2002. Targeting gene expression in the preimplantation mouse embryo using morpholino antisense oligonucleotides. *Mol Reprod Dev,* 63**,** 413-21.

SIEDNER, S., KRÜGER, M., SCHROETER, M., METZLER, D., ROELL, W., FLEISCHMANN, B. K., HESCHELER, J., PFITZER, G. & STEHLE, R. 2003. Developmental changes in contractility and sarcomeric proteins from the early embryonic to the adult stage in the mouse heart. *The Journal of Physiology,* 548**,** 493-505.

SILVA, G. V. 2014. Patent Foramen Ovale. *Tex Heart Inst J,* 3**,** 306-308.

SIMÕES-COSTA, M. & BRONNER, M. E. 2013. Insights into neural crest development and evolution from genomic analysis. *Genome Research,* 23**,** 1069-1080.

SNARR, B. S., KERN, C. B. & WESSELS, A. 2008. Origin and fate of cardiac mesenchyme. *Developmental Dynamics,* 237**,** 2804-2819.

SOLARO, R. J., POWERS, F. M., LIZHU, G. & GWATHMEY, J. K. 1993. Control of myofilament activation in heart failure. *Circulation,* 87**,** 38-43.

SOTO, B., BECKER, A. E., MOULAERT, A. J., LIE, J. T. & ANDERSON, R. H. 1980. Classification of ventricular septal defects. *British Heart Journal,* 43**,** 332-343.

SOUFAN, A. T., VAN DEN BERG, G., RUIJTER, J. M., DE BOER, P. A., VAN DEN HOFF, M. J. & MOORMAN, A. F. 2006. Regionalized sequence of myocardial cell growth and proliferation characterizes early chamber formation. *Circ Res,* 99**,** 545-52.

SPITZER, N. C. 1991. A developmental handshake: Neuronal control of ionic currents and their control of neuronal differentiation. *Journal of Neurobiology,* 22**,** 659-673.

STARR, C. M., DIAZ, J. G. & LEMANSKI, L. F. 1989. Analysis of actin and tropomyosin in hearts of cardiac mutant axolotls by two-dimensional gel electrophoresis, western blots, and immunofluorescent microscopy. *J Morphol,* 201**,** 1-10.

STEFANCSIK, R., JHA, P. K. & SARKAR, S. 1998. Identification and mutagenesis of a highly conserved domain in troponin T responsible for troponin I binding: potential role for coiled coil interaction. *Proc Natl Acad Sci U S A,* 95**,** 957-62.

STERN, C. D. 2005. The chick; a great model system becomes even greater. *Dev Cell,* 8**,** 9-17.

STEVENS, A. & LOWE, J. 2005. *Human Histology,* Philadelphia, Elsevier Mosby.

STOLLBERGER, C., KELLER, H. & FINSTERER, J. 2007. Disappearance of left ventricular hypertrabeculation/noncompaction after biventricular pacing in a patient with polyneuropathy. *J Card Fail,* 13**,** 211-4.

STÖLLBERGER, C., WINKLER-DWORAK, M., BLAZEK, G. & FINSTERER, J. 2006. Prognosis of left ventricular hypertrabeculation/noncompaction is dependent on cardiac and neuromuscular comorbidity. *International Journal of Cardiology,* 121**,** 189-193.

SUMMERTON, J. 1989. *Uncharged Nucleic Acid Analogs for Therapeutic and Diagnostic Applications: Oligomers Assembled from Ribose-Derived Subunits,* The Woodlands, Portfolio Publishing Company.

SUMMERTON, J. 2007. Morpholino, siRNA, and S-DNA Compared: Impact of Structure and Mechanism of Action on Off-Target Effects and Sequence Specificity *curr Top Med Chem,* 7**,** 651-660.

SUMMERTON, J. & WELLER, D. 1997. Morpholino Antisense Oligomers: Design, Preparation and Properties. *Antisense Nucleic Acid Drug Dev.,* 7**,** 187-195.

SUMMERTON, J. E. & WELLER, D. D. 1993. *Uncharged Morpholino-based polymers having phosphorous containing chiral intersubunit linkages*. US patent application 5,185,444.

SUNG, L. A. & LIN, J. J. C. 1994. Erythrocyte Tropomodulin Binds to the N-Terminus of hTM5, a Tropomyosin Isoform Encoded by the γ-Tropomyosin Gene. *Biochemical and Biophysical Research Communications,* 201**,** 627-634.

SUZUKI, H., KOMIYAMA, M., KONNO, A. & SHIMADA, Y. 1998. Exchangeability of actin in cardiac myocytes and fibroblasts as determined by fluorescence photobleaching recovery. *Tissue and Cell,* 30**,** 274-280.

SZTAJZEL, R., GENOUD, D., ROTH, S., MERMILLOD, B. & LE FLOCH-ROHR, J. 2002. Patent foramen ovale, a possible cause of symptomatic migraine: a study of 74 patients with acute ischemic stroke. *Cerebrovasc Dis.,* 2**,** 102-106.

TABER, L. A. 2006. Biophysical mechanisms of cardiac looping. *Int J Dev Biol.,* 50**,** 323-332.

TAKEDA, S., YAMASHITA, A., MAEDA, K. & MAEDA, Y. 2003. Structure of the core domain of human cardiac troponin in the Ca(2+)-saturated form. *Nature,* 424**,** 35-41.

TALERICO, M. & BERGET, S. 1990. Effect of 5' splice site mutations on splicing of the preceding intron. *Mol Cell Biol.,* 10**,** 6299-6305.

TAM, P. P. L. & BEHRINGER, R. R. 1997. Mouse gastrulation: the formation of a mammalian body plan. *Mechanisms of Development,* 68**,** 3-25.

TAMADDON, H. S., VAIDYA, D., SIMON, A. M., PAUL, D. L., JALIFE, J. & MORLEY, G. E. 2000. High-resolution optical mapping of the right bundle branch in connexin40 knockout mice reveals slow conduction in the specialized conduction system. *Circ Res,* 87**,** 929-36.

TARDIFF, J. C., FACTOR, S. M., TOMPKINS, B. D., HEWETT, T. E., PALMER, B. M., MOORE, R. L., SCHWARTZ, S., ROBBINS, J. & LEINWAND, L. A. 1998. A truncated cardiac troponin T molecule in transgenic mice suggests multiple cellular mechanisms for familial hypertrophic cardiomyopathy. *The Journal of Clinical Investigation,* 101**,** 2800-2811.

TARDIFF, J. C., HEWETT, T. E., PALMER, B. M., OLSSON, C., FACTOR, S. M., MOORE, R. L., ROBBINS, J. & LEINWAND, L. A. 1999. Cardiac troponin T mutations result in allele-specific phenotypes in a mouse model for hypertrophic cardiomyopathy. *The Journal of Clinical Investigation,* 104**,** 469-481.

TAYLOR, M. F., PAULAUSKIS, J. D., WELLER, D. D. & KOBZIK, L. 1996. In Vitro Efficacy of Morpholino-modified Antisense Oligomers Directed against Tumor Necrosis Factor-α mRNA. *Journal of Biological Chemistry,* 271**,** 17445-17452.

THIENE, G., NAVA, A., CORRADO, D., ROSSI, L. & PENNELLI, N. 1988. Right ventricular cardiomyopathy and sudden death in young people. *N Engl J Med,* 318**,** 129-33.

THIERFELDER, L., WATKINS, H., MACRAE, C., LAMAS, R., MCKENNA, W., VOSBERG, H. P., SEIDMAN, J. G. & SEIDMAN, C. E. 1994. Alpha-tropomyosin and cardiac troponin T mutations cause familial hypertrophic cardiomyopathy: a disease of the sarcomere. *Cell,* 77**,** 701-12.

TINTU, A., ROUWET, E., VERLOHREN, S., BRINKMANN, J., AHMAD, S., CRISPI, F., VAN BILSEN, M., CARMELIET, P., STAFF, A. C., TJWA, M., CETIN, I.,

GRATACOS, E., HERNANDEZ-ANDRADE, E., HOFSTRA, L., JACOBS, M., LAMERS, W. H., MORANO, I., SAFAK, E., AHMED, A. & LE NOBLE, F. 2009. Hypoxia induces dilated cardiomyopathy in the chick embryo: mechanism, intervention, and long-term consequences. *PLoS One,* 4**,** e5155.

TOKUYASU, K. T. & MAHER, P. A. 1987. Immunocytochemical Studies of Cardiac Myofibrillogenesis in Early Chick Embryos. I. Presence of Immunofluorescent Titin Spots in Premyofibril Stages. *Journal of Cell Biology,* 105**,** 2781-2793.

TORRICELLI, F., GIROLAMI, F., OLIVOTTO, I., PASSERINI, I., FRUSCONI, S., VARGIU, D., RICHARD, P. & CECCHI, F. 2003. Prevalence and clinical profile of troponin T mutations among patients with hypertrophic cardiomyopathy in tuscany. *Am J Cardiol,* 92**,** 1358-62.

TOWBIN, J. A. 2010. Left ventricular noncompaction: a new form of heart failure. *Heart Fail Clin,* 6**,** 453-69, viii.

TOWBIN, J. A. 2014. Inherited cardiomyopathies. *Circ J,* 78**,** 2347-56.

TOWBIN, J. A. & BOWLES, N. E. 2002. The failing heart. *Nature,* 415**,** 227-233.

TREVISAN, P., ZEN, T. D., ROSA, R. F. M., DA SILVA, J. N., KOSHIYAMA, D. B., PASKULIN, G. A. & ZEN, P. R. G. 2013. Chromosomal Abnormalities in Patients with Congenital Heart Disease. *Arquivos Brasileiros de Cardiologia,* 101**,** 495-501.

TURNACIOGLU, K. K., MITTAL, B., DABIRI, G. A., SANGER, J. M. & SANGER, J. W. 1997. An N-terminal fragment of titin coupled to green fluorescent protein localizes to the Z-bands in living muscle cells: overexpression leads to myofibril disassembly. *Molecular Biology of the Cell,* 8**,** 705-17.

UNTERGASSER, A., CUTCUTACHE, I., KORESSAAR, T., YE, J., FAIRCLOTH, B. C., REMM, M. & ROZEN, S. G. 2012. Primer3—new capabilities and interfaces. *Nucleic Acids Research,* 40**,** e115.

URNOV, F. D., REBAR, E. J., HOLMES, M. C., ZHANG, H. S. & GREGORY, P. D. 2010. Genome editing with engineered zinc finger nucleases. *Nat Rev Genet,* 11**,** 636-46.

VAN DE MEERAKKER, J. B. A., CHRISTIAANS, I., BARNETT, P., LEKANNE DEPREZ, R. H., ILGUN, A., MOOK, O. R. F., MANNENS, M. M. A. M., LAM, J., WILDE, A. A. M., MOORMAN, A. F. M. & POSTMA, A. V. 2013. A novel alpha-tropomyosin mutation associates with dilated and non-compaction cardiomyopathy and diminishes actin binding. *Biochimica et Biophysica Acta (BBA) - Molecular Cell Research,* 1833**,** 833-839.

VAN DEN BERG, G., ABU-ISSA, R., DE BOER, B. A., HUTSON, M. R., DE BOER, P. A. J., SOUFAN, A. T., RUIJTER, J. M., KIRBY, M. L., VAN DEN HOFF, M. J. B. & MOORMAN, A. F. M. 2009. A Caudal Proliferating Growth Center Contributes to Both Poles of the Forming Heart Tube. *Circulation Research,* 104**,** 179-188.

VAN DEN HOFF, M. J. B., MOORMAN, A. F. M., RUIJTER, J. M., LAMERS, W. H., BENNINGTON, R. W., MARKWALD, R. R. & WESSELS, A. 1999. Myocardialization of the Cardiac Outflow Tract. *Developmental Biology,* 212**,** 477-490.

VAN DER VEN, P. F. M., EHLER, E., PERRIARD, J.-C. & FÜRST, D. O. 1999. Thick filament assembly occurs after the formation of a cytoskeletal scaffold. *Journal of Muscle Research and Cell Motility,* 20**,** 569-579.

VAN DRIEST, S. L., ELLSWORTH, E. G., OMMEN, S. R., TAJIK, A. J., GERSH, B. J. & ACKERMAN, M. J. 2003. Prevalence and spectrum of thin filament mutations in an outpatient referral population with hypertrophic cardiomyopathy. *Circulation,* 108**,** 445-51.

VARNAVA, A., BABOONIAN, C., DAVISON, F., DE CRUZ, L., ELLIOTT, P. M., DAVIES, M. J. & MCKENNA, W. J. 1999. A new mutation of the cardiac troponin T gene causing familial hypertrophic cardiomyopathy without left ventricular hypertrophy. *Heart,* 82**,** 621-4.

VARNAVA, A. M., ELLIOTT, P. M., BABOONIAN, C., DAVISON, F., DAVIES, M. J. & MCKENNA, W. J. 2001. Hypertrophic cardiomyopathy: histopathological features of sudden death in cardiac troponin T disease. *Circulation,* 104**,** 1380-4.

VEROT, L., CHIKH, K., FREYDIERE, E., HONORE, R., VANIER, M. T. & MILLAT, G. 2007. Niemann-Pick C disease: functional characterization of three NPC2 mutations and clinical and molecular update on patients with NPC2. *Clin Genet,* 71**,** 320-30.

VIBERT, P., CRAIG, R. & LEHMAN, W. 1997. Steric-model for activation of muscle thin filaments. *Journal of Molecular Biology,* 266**,** 8-14.

WALDO, K., MIYAGAWA-TOMITA, S., KUMISKI, D. & KIRBY, M. L. 1998. Cardiac Neural Crest Cells Provide New Insight into Septation of the Cardiac Outflow Tract: Aortic Sac to Ventricular Septal Closure. *Developmental Biology,* 196**,** 129-144.

WALDO, K., ZDANOWICZ, M., BURCH, J., KUMISKI, D. H., STADT, H. A., GODT, R. E., CREAZZO, T. L. & KIRBY, M. L. 1999. A novel role for cardiac neural crest in heart development. *The Journal of Clinical Investigation,* 103**,** 1499-1507.

WALLIS, J. W., AERTS, J., GROENEN, M. A., CROOIJMANS, R. P., LAYMAN, D., GRAVES, T. A., SCHEER, D. E., KREMITZKI, C., FEDELE, M. J., MUDD, N. K., CARDENAS, M., HIGGINBOTHAM, J., CARTER, J., MCGRANE, R., GAIGE, T., MEAD, K., WALKER, J., ALBRACHT, D., DAVITO, J., YANG, S. P., LEONG, S., CHINWALLA, A., SEKHON, M., WYLIE, K., DODGSON, J., ROMANOV, M. N., CHENG, H., DE JONG, P. J., OSOEGAWA, K., NEFEDOV, M., ZHANG, H., MCPHERSON, J. D., KRZYWINSKI, M., SCHEIN, J., HILLIER, L., MARDIS, E. R., WILSON, R. K. & WARREN, W. C. 2004. A physical map of the chicken genome. *Nature,* 432**,** 761-4.

WALSH, R., RUTLAND, C., THOMAS, R. & LOUGHNA, S. 2010. Cardiomyopathy: A Systematic Review of Disease-Causing Mutations in Myosin Heavy Chain 7 and Their Phenotypic Manifestations. *Cardiology,* 115**,** 49-60.

WANG, J., THURSTON, H., ESSANDOH, E., OTOO, M., HAN, M., RAJAN, A., DUBE, S., ZAJDEL, R. W., SANGER, J. M., LINASK, K. K., DUBE, D. K. & SANGER, J. W. 2008. Tropomyosin expression and dynamics in developing avian embryonic muscles. *Cell Motility and the Cytoskeleton,* 65**,** 379-392.

WANG, Q., REITER, R. S., HUANG, Q.-Q., JIN, J.-P. & LIN, J. J.-C. 2001. Comparative studies on the expression patterns of three troponin T genes during mouse development. *The Anatomical Record,* 263**,** 72-84.

WARKMAN, A. S. & KRIEG, P. A. 2007. Xenopus as a model system for vertebrate heart development. *Semin Cell Dev Biol,* 18**,** 46-53.

WARRICK, H. M. & SPUDICH, J. A. 1987. Myosin Structure and Function in Cell Motility. *Annual Review of Cell Biology,* 3**,** 379-421.

WATKINS, H., MCKENNA, W. J., THIERFELDER, L., SUK, H. J., ANAN, R., O'DONOGHUE, A., SPIRITO, P., MATSUMORI, A., MORAVEC, C. S., SEIDMAN, J. G. & SEIDMAN, C. E. 1995. Mutations in the Genes for Cardiac Troponin T and α-Tropomyosin in Hypertrophic Cardiomyopathy. *New England Journal of Medicine,* 332**,** 1058-1065.

WEBB, G. & GATZOULIS, M. A. 2006. Atrial Septal Defects in the Adult. *Circulation,* 114**,** 1645-1653.

WEBB, S., BROWN, N. A., WESSELS, A. & ANDERSON, R. H. 1998. Development of the murine pulmonary vein and its relationship to the embryonic venous sinus. *The Anatomical Record,* 250**,** 325-334.

WEBB, S., QAYYUM, S. R., ANDERSON, R. H., LAMERS, W. H. & K. RICHARDSON, M. 2003. Septation and separation within the outflow tract of the developing heart. *Journal of Anatomy,* 202**,** 327-342.

WENCKER, D., CHANDRA, M., NGUYEN, K., MIAO, W., GARANTZIOTIS, S., FACTOR, S. M., SHIRANI, J., ARMSTRONG, R. C. & KITSIS, R. N. 2003. A mechanistic role for cardiac myocyte apoptosis in heart failure. *J Clin Invest,* 111**,** 1497-504.

WESSELS, M. W., HERKERT, J. C., FROHN-MULDER, I. M., DALINGHAUS, M., VAN DEN WIJNGAARD, A., DE KRIJGER, R. R., MICHELS, M., DE COO, I. F., HOEDEMAEKERS, Y. M. & DOOIJES, D. 2015. Compound heterozygous or homozygous truncating MYBPC3 mutations cause lethal cardiomyopathy with features of noncompaction and septal defects. *Eur J Hum Genet,* 23**,** 922-8.

WESSELS, M. W. & WILLEMS, P. J. 2010. Genetic factors in non-syndromic congenital heart malformations. *Clin Genet,* 78**,** 103-23.

WEXLER, R. K., ELTON, T., PLEISTER, A. & FELDMAN, D. 2009. Cardiomyopathy: an overview. *Am Fam Physician,* 79**,** 778-84.

WIECZOREK, D. F., JAGATHEESAN, G. & RAJAN, S. 2008. The Role of Tropomyosin in Heart Disease. *In:* GUNNING, P. (ed.) *Tropomyosin.* Springer New York.

WILMSHURST, P. T., BYRNE, J. C. & WEBB-PEPLOE, M. M. Relation between interatrial shunts and decompression sickness in divers. *The Lancet,* 334**,** 1302-1306.

WYMAN, C. & KANAAR, R. 2006. DNA double-strand break repair: all's well that ends well. *Annu Rev Genet,* 40**,** 363-83.

XIE, L., HOFFMANN, A. D., BURNICKA-TUREK, O., FRIEDLAND-LITTLE, J. M., ZHANG, K. & MOSKOWITZ, I. P. 2012. Tbx5-Hedgehog Molecular Networks Are

Essential in the Second Heart Field for Atrial Septation. *Developmental cell,* 23**,** 280-291.

XU, C., WEI, M., SU, B., HUA, X. W., ZHANG, G. W., XUE, X. P., PAN, C. M., LIU, R., SHENG, Y., LU, Z. G., JIN, L. R. & SONG, H. D. 2008. Ile90Met, a novel mutation in the cardiac troponin T gene for familial hypertrophic cardiomyopathy in a Chinese pedigree. *Genet Res (Camb),* 90**,** 445-50.

XU, H., MORISHIMA, M., WYLIE, J. N., SCHWARTZ, R. J., BRUNEAU, B. G., LINDSAY, E. A. & BALDINI, A. 2004. Tbx1 has a dual role in the morphogenesis of the cardiac outflow tract. *Development,* 131**,** 3217-3227.

YA, J., VAN DEN HOFF, M. J. B., DE BOER, P. A. J., TESINK-TAEKEMA, S., FRANCO, D., MOORMAN, A. F. M. & LAMERS, W. H. 1998. Normal Development of the Outflow Tract in the Rat. *Circulation Research,* 82**,** 464-472.

YAMAUCHI-TAKIHARA, K., NAKAJIMA-TANIGUCHI, C., MATSUI, H., FUJIO, Y., KUNISADA, K., NAGATA, S. & KISHIMOTO, T. 1996. Clinical implications of hypertrophic cardiomyopathy associated with mutations in the alpha-tropomyosin gene. *Heart,* 76**,** 63-5.

YANG, X., DORMANN, D., MÜNSTERBERG, A. E. & WEIJER, C. J. 2002. Cell Movement Patterns during Gastrulation in the Chick Are Controlled by Positive and Negative Chemotaxis Mediated by FGF4 and FGF8. *Developmental Cell,* 3**,** 425-437.

YI LI, Q., NEWBURY-ECOB, R. A., TERRETT, J. A., WILSON, D. I., CURTIS, A. R. J., HO YI, C., GEBUHR, T., BULLEN, P. J., ROBSON, S. C., STRACHAN, T., BONNET, D., LYONNET, S., YOUNG, I. D., RAEBURN, J. A., BUCKLER, A. J., LAW, D. J. & BROOK, J. D. 1997. Holt-Oram syndrome is caused by mutations in TBX5, a member of the Brachyury (T) gene family. *Nat Genet,* 15**,** 21-29.

YONEMURA, I., MITANI, Y., NAKADA, K., AKUTSU, S. & MIYAZAKI, J.-I. 2002. Developmental Changes of Cardiac and Slow Skeletal Muscle Troponin T Expression in Chicken Cardiac and Skeletal Muscles. *Zoological Science,* 19**,** 215-223.

YOSHIDA, T., VIVATBUTSIRI, P., MORRISS-KAY, G., SAGA, Y. & ISEKI, S. 2008. Cell lineage in mammalian craniofacial mesenchyme. *Mechanisms of Development,* 125**,** 797-808.

ZAJDEL, R., MCLEAN, M., DUBE, S. & DUBE, D. 2013. Expression of tropomyosin in relation to myofibrillogenesis in axolotl hearts. *Regenerative Medicine Research,* 1**,** 1-10.

ZAJDEL, R. W., DENZ, C. R., LEE, S., DUBE, S., EHLER, E., PERRIARD, E., PERRIARD, J.-C. & DUBE, D. K. 2003. Identification, characterization, and expression of a novel α-tropomyosin isoform in cardiac tissues in developing chicken. *Journal of Cellular Biochemistry,* 89**,** 427-439.

ZAJDEL, R. W., MCLEAN, M. D., LEMANSKI, S. L., MUTHUCHAMY, M., WIECZOREK, D. F., LEMANSKI, L. F. & DUBE, D. K. 1998. Ectopic expression of tropomyosin promotes myofibrillogenesis in mutant axolotl hearts. *Dev Dyn,* 213**,** 412-20.

ZAJDEL, R. W., THURSTON, H., PRAYAGA, S., DUBE, S., POIESZ, B. J. & DUBE, D. K. 2007. A reduction of tropomyosin limits development of sarcomeric structures in cardiac mutant hearts of the Mexican axolotl. *Cardiovasc Toxicol,* 7**,** 235-46.

ZAMECNIK, P. C. & STEPHENSON, M. L. 1978. Inhibition of Rous sarcoma virus replication and cell transformation by a specific oligodeoxynucleotide. *Proceedings of the National Academy of Sciences,* 75**,** 280-284.

ZELLER, R., IVANDIC, B. T., EHLERMANN, P., MUCKE, O., ZUGCK, C., REMPPIS, A., GIANNITSIS, E., KATUS, H. A. & WEICHENHAN, D. 2006. Large-scale mutation screening in patients with dilated or hypertrophic cardiomyopathy: a pilot study using DGGE. *J Mol Med (Berl),* 84**,** 682-91.

ZHU, S., SI, M. L., WU, H. & MO, Y. Y. 2007. MicroRNA-21 targets the tumor suppressor gene tropomyosin 1 (TPM1). *J Biol Chem,* 282**,** 14328-36.

Chapter 8 Appendix

Appendix 1: Amino acid abbreviations

Amino Acid	Abbreviation (1 letter)	Abbreviation (3 letter)
Alanine	A	Ala
Arginine	R	Arg
Asparagine	N	Asn
Aspartate	D	Asp
Cysteine	C	Cys
Glutamate	E	Glu
Glutamine	Q	Gln
Glycine	G	Gly
Histidine	H	His
Isoleucine	I	Ile
Leucine	L	Leu
Lysine	K	Lys
Methionine	M	Met
Phenylalanine	F	Phe
Proline	P	Pro
Serine	S	Ser
Threonine	T	Thr
Tryptophan	W	Trp
Tyrosine	Y	Tyr
Valine	V	Val